Department of Precision and Microsystems Engineering

On Lightweight Design of Submarine Pressure Hulls

Stanley I. Wong

Report no : EM 2012.021
Coach : Dr.ir. J.R. MacKay
Professor : Prof.dr.ir. A. Van Keulen
Specialisation : Structural Optimization and Computational Mechanics
Type of report : MSc Thesis
Date : 1 October 2012

Abstract

Pressure hulls are, especially for manned vehicles, one of the key structures of a submarine. Contributing roughly one third to the total submarine weight, these hulls provide a watertight envelope that must bear the hydrostatic external load. The design of such a structure can be complex as the whole submarine has to reach neutral buoyancy. Hence, the addition of structural hydrostatic load bearing capacity is not a straightforward operation. Increase of structural weight is not an option as it decreases the weight budget of the payload, engine and other performance related features. Obviously, the use of a lightweight pressure hull opens the door to a performance increase.

In the search of a lightweight pressure hull, it is found that use of composite materials can be a solution. However, a composite pressure hull design encapsulates the design of the composite itself. For this reason, pressure hull finite element models are created that include the composite related material mechanics. Suitable weight minimization techniques are performed on these models and results were compared to the conventional heavyweight pressure hull. As a result, it is demonstrated that pressure hulls made of sandwich-constructed composite offer a promising weight reduction of 28% with respect to the conventional reference design.

Contents

Chapter 1

Introduction

Pressure hulls are, especially for manned vehicles, one of the key structures of a submarine. Contributing roughly one third to the total submarine weight [1], these hulls provide a watertight envelope that must bear the hydrostatic external load. The design of such a structure can be complex as the whole submarine has to reach neutral buoyancy. Hence, the addition of structural hydrostatic load bearing capacity is not a straightforward operation. Increasing the structural weight as a (very possible) result of this operation decreases the weight budget of the payload, engine and other performance related features. Obviously, reduction of the structural weight opens the door to performance increase.

To accomplish such weight reductions one has to consider the whole pressure hull design. With the mechanical analysis and functional knowledge of the these hulls, concepts in weight reduction can be made. It can be said that the utilization of lightweight materials is one of the most promising concepts. Similar to aerospace development, composite materials can play a key role in lightweight pressure hull design. But as the design of a composite structure comprises the design of the actual composite material itself, understanding the mechanics of such a material is crucial. However, mechanical behavior of composites is more complex than the conventionally applied metals. The inherent anisotropic properties of composites can, if applied correctly, cause an increase of the (specific) structural mechanical performance. On the other hand, when wrongly applied, numerous failure mechanisms can cause unwanted collapse of the structure. Hence, the weight reduction process for a composite structure deals with these mechanics. Ultimately, the composite is tailored such that it provides enough strength to bear the structural loads. In this field, optimization algorithms are powerful tools to accomplish the latter while the weight is reduced. But as a composite laminate consists of many plies, this optimization can be quite a challenge, especially in a finite element (FE) formulation. The use of lamination parameters in a FE description of the structure decreases this computational intensity because of their higher level (or homogenized sectional) description of the material. In the present thesis, these parameters are used in a framework that minimizes the weight of the composite pressure

hull. Subsequently, with the knowledge of the optimal lamination parameters, a lay-up for the hull can be found in a computational extensive manner.

The conventional pressure hull is handled as a reference throughout the present work. Results for weight reduced designs are compared with this reference in order to get an idea of the reduction. Collapse of these ring-stiffened cylinders can originate from different mechanical sources such as geometrical imperfections or material yielding. The influence of these mechanisms on the overall collapse are elaborated. Ultimately, a FE model of a experimentally tested pressure hull is constructed that accounts for these effects. This model is validated and its limit in weight reduction is estimated by means of an optimization. Results in weight reduction are compared to the composite pressure hull optimization outputs and conclusions are drawn.

To summarize, in the present master's thesis the author focuses on the potential of composite pressure hulls with respect to the conventional pressure hull. At first, a brief journey into pressure hull history is treated in Section (2.1). Hereafter, an overview of the submarines found nowadays is provided in Section (2.2). Subsequently, the general aspects of a pressure hull are treated in Section (2.3) and the motivation for a weight reduced design and the focus for the present thesis is presented in Section (2.4). Before the composite pressure hulls are treated, it is important to understand the mechanics of an conventional pressure hull. These mechanical aspects are treated in Section (3). As mentioned earlier, the knowledge of the mechanical behavior for a composite material is crucial. Hence, Section (4) elaborates the most important mechanical topics for composites. The use of lamination parameters and the framework for a structural composite optimization process in FE are treated in Section (4.3). Along with the reference model, FE models of composite pressure hulls are described and optimized according to this framework in Section (5). At last, conclusions and recommendations are presented in Section (6).

Chapter 2

General description of submarines

This chapter has the purpose to give a concise background description of the present thesis. As a brief journey in time the historical background of submarines is treated in Section (2.1). Additionally, various submarine vehicles that are found nowadays are presented in Section (2.2). The hydrostatic pressure bearing structure that is found in the majority of submarine vehicles, the pressure hull, is introduced in Section (2.3). Next, the effect of structural weight reductions and the possibilities for weight reduction are discussed in Section (2.4). As an important note, the general purpose for the present thesis is proposed in Section (2.5). Finally, important conclusions of this chapter are found in Section (2.6).

2.1 Historical background

In the following a concise historical background for the pressure hull is provided. The present author has chosen to pick a few important events from the past for the sake of brevity.

The Drebbel

The first steerable submersible was built in 1620 by Cornelis Jacobszoon Drebbel. This Dutchman created the vehicle with the standards outlined by an earlier design from the English mathematician William Bourne. The hull of the so-called "Drebbel" was made of leather and reinforced by an internal structure of wood. Negative buoyancy was accomplished by letting in water through holes in the sides that flooded water tight compartments between orloppes (i.e. decks). To return to the surface, bellows-pistons operated by large wooden screws forced the water back out through holes in the hull, a technique suggested earlier by William Bourne [2].

Drebbel presented the submersible to the English Royal Navy at the river Thames in 1620.

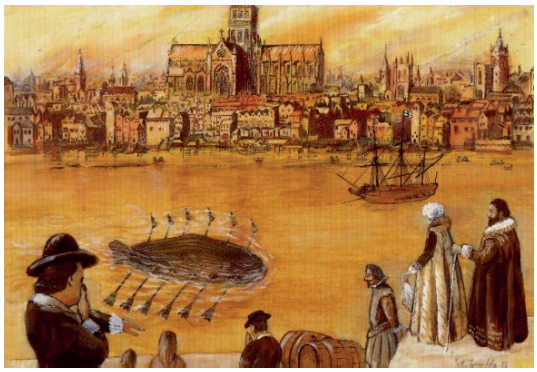

Figure 2.1: Artist impression of the Drebbel in the Thames, the figure is in the public domain.

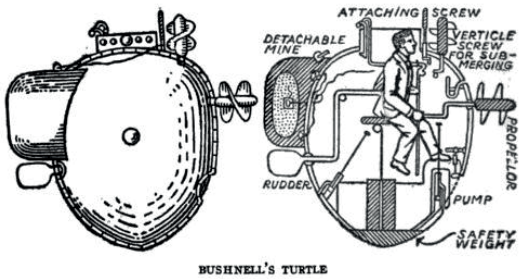

Figure 2.2: Diagram of David Bushnell's Turtle submarine from [3]

The vehicle was powered by 6 oars and was able to carry 16 persons. At the time, the provision of oxygen was the main issue. He managed to create oxygen with the help of potassium nitrate or sodium nitrate. By heating these substances oxygen is emitted. Although the Drebbel was submerged successfully for three hours with an average cruising depth of 4-5 meters, the Royal Navy was not convinced that submersibles were applicable in naval warfare. This event is illustrated in Fig. (2.1).

The American Turtle

Ironically, the first military submersible was build by David Bushnell, an American Patriot that designed it for use against the British Royal Navy during the American Revolutionary War in 1775. The vehicle which was called the Turtle (or American Turtle) had only place for one person. It was about 10 feet long, 6 feet tall and 3 feet wide and was named after its shape. Two tar covered wooden shells were reinforced with steel to form the hull. The craft's propulsion was hand and feet powered with horizontal and vertical Archimedean screw propellers. It could stay submerged for about 30 minutes because of the amount of air contained in the vessel. As Fig. (2.2) illustrates, there was a detachable mine at the back of the submersible.

With an mechanically timed mine explosion the stealthy submersible was the first submersible

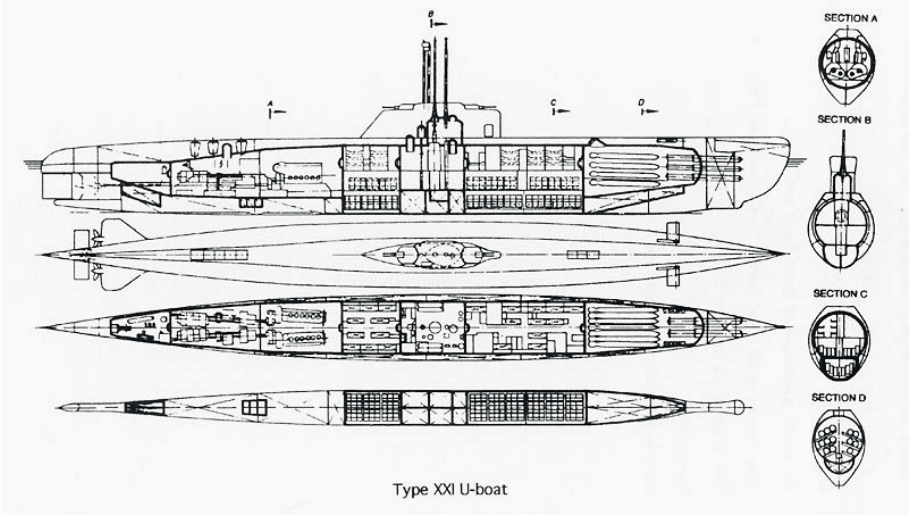

Figure 2.3: Diagram of a German Type XXI U-boat class submarine, from the U.S. government documentation found in [5]

that was used in combat and was specially designed to eliminate warships. It was able to move rapidly for 20 feet underwater while carrying and attach the 2000 pounds of gunpowder to the hull of a enemy ship. Unfortunately for Bushnell, all attempts to sink the British warships failed. Moreover, in 1776 Bushnell tried to transport the Turtle on a sloop; but the British discovered him, and with a few well-placed cannonballs sank the vessel and its precious cargo [4].

XXI U-Boat

During World War II the Germans developed a XXI U-Boat class submarine (displayed in Fig.(2.3)) primarily designed for submerged performance. Unlike the surface ships that could submerge once in danger, these electric powered boats were able to travel submerged at about 5 knots for two or three days before recharging. By the use of a snorkel the batteries were re-charged within five hours. The design also decreased its appearance on marine or airborne radar when surfaced. As a result the XXI U-boat was more stealthy and less in danger from aircraft which sank about 56% of all U-boats lost in the war [6]. Because of the streamlined design and the increased battery power these boats were able to outrun many surface ships at a speed over 17 knots, while submerged.

The Trieste

In 1960 Jacques Piccard and U.S. Navy Lieutenant Don Walsh were the first that have reached the bottom of the Challenger deep at Mariana Trench, i.e. the deepest known point in the Earths ocean floor. By reaching a depth of about 10,890 meters the vehicle, bathyscaphe "Trieste", was able to withstand over 110 MPa hydrostatic pressure. Due to the over-dimensioned nickel-molybdenum alloyed steel pressure sphere with a thickness of 12.7 centimeters a float was needed

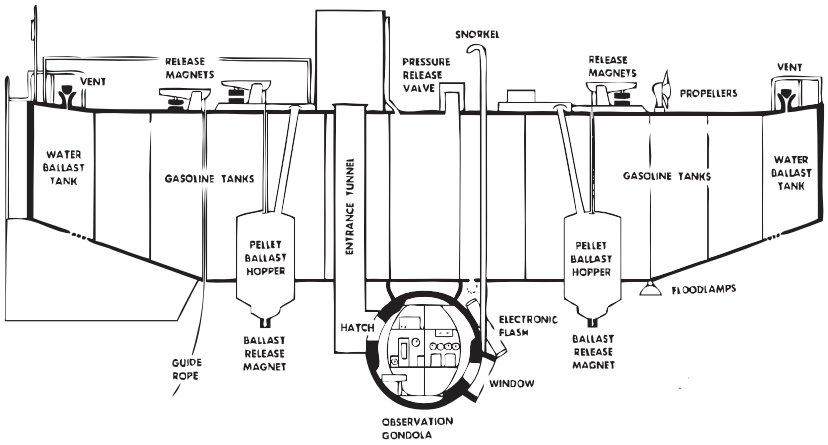

Figure 2.4: Cutaway of Trieste, adapted from [7]

to attain neutral buoyancy. This float was made of thin steel (about 0.5 centimeter) and was filled with 85,000 liters of aviation gasoline, a liquid with a specific gravity of approximately 0.7. Since this gasoline is more compressible than water, the rigid steel float has to be pressure-compensated during the descent. By allowing sea water to flow in via a two way valve located in the float, the pressure difference is compensated during the trip. As a result from this compressibility, every descending 900 meters 1 ton ballast must be dropped to maintain neutral buoyancy [7]. An illustration of the Trieste is displayed in Fig.(2.4).

2.2 Submarines: State of the art

Submarine vehicles that are found nowadays are treated in the following. A division is made between military submarines, Section (2.2.1), and submersibles in the commercial field, in Section (2.2.2).

2.2.1 Military submarines

Advanced modern day military submarines never need to refuel throughout their life spans of about 25 years because of their nuclear powered propulsion [8]. Being even faster submerged than surfaced, supply in food, other payload and maintenance of the vehicle are the only limiting factor in terms of submerged time. A part of the electricity provided by the nuclear reactor is used to produce oxygen by electrolysis of water. The only major loss of stealth is that the nuclear power plant is noisier than a battery powered submarine. The use of pumps in active cooling systems and steam turbine generators brings the noise to an unwanted higher level. However, recent developments in noise isolation and damping have made nuclear submarines quieter and hence notorious.

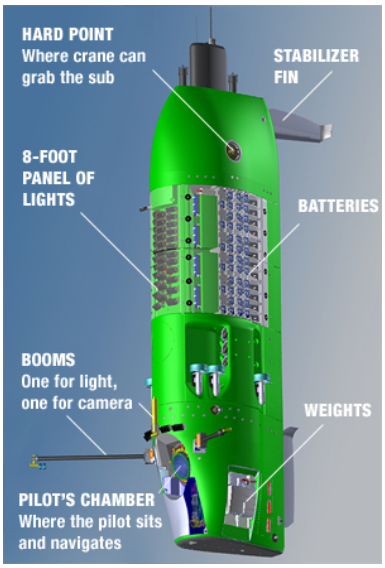

Figure 2.5: Impression of the "Deepsea Challenger", illustration is adapted from Acheron Project Pty Ltd Deepsea Challenger

Another modern day trend is the use of a so-called swimmer or seal delivery vehicle (SDV) to serve as a clandestine special forces transport [9]. This relatively small submarine vehicle, commutes between the larger main submarine and the hostile shores. It is able to carry 4 Special Forces and their equipment over a distance of a nautical mile. An example of such a vehicle is the Sivercrest Marine SDV which is constructed from glass fiber reinforced plastic attached to a marine grade aluminium frame. The vehicle serve can operate at depths up to 50 meters.

2.2.2 Submersibles

Recently, in 2012 the Canadian film director James Cameron piloted the deep-diving submersible named "Deepsea Challenger" to reach the bottom of the Challenger Deep. Remarkably, this was the second manned dive ever to dive the Challenger Deep, 52 years after the Trieste (see Section (2.1)). The submersible, displayed in Fig.(2.5) had a pilot sphere of steel with a 64 mm wall thickness. It was tested successfully to withstand 114 MPa of pressure. At its decent, the vehicle carried 500 kg of ballast weight that was released at the ocean floor to be able to rise to the surface. Cameron equipped the craft with cameras and recording devices, his aim is create a movie with the recorded material.

Apart manned submersibles, major development of unmanned vehicles such as remotely operated vehicles (ROVs) and autonomous underwater vehicles (AUVs) has taken during the last decades. ROVs are tethered to a ship and could for instance be used in deep water industries such as offshore oil and gas industries. In this field, ROVs are required to perform versatile tasks ranging from inspection to the connecting underwater pipelines. Hence it is no surprise that these

vehicles are highly maneuverable and are well equipped in terms of sensors and mechanical tools.

The AUV, which is the autonomous variant of the latter, is mainly found in fields where underwater research needs to be performed. Oceanographers use these vehicles to study the water by performing measurements with equipped sensors. Furthermore, ocean floors can be mapped with AUVs cost efficiently in for instance oil and gas industries. Because of their autonomic character these vehicles are mainly powered by batteries with a sufficiently large capacity with respect to the operation requirements.

2.3 Pressure hull description

The concept of a pressure hull is treated in this section. A basic description is given in Section 2.3.1. In the succeeding section the emphasis is on requirements, in Section 2.3.2.

2.3.1 Basic description

Pressure hulls are structures found in most of the submarines nowadays. The function of these structures is to form a watertight envelope which forms the barrier between the hydrostatic external pressure and the desired internal pressure. According to the actual submarine design, the pressure hull could be exposed on the outer envelope of the hull or hidden behind a light hull. All forms in between are of course also possible.

AUVs and UAVs carry equipment that needs to operate in a dry and atmospheric environment, therefore a pressure hull is required for fulfilling this task. For manned vehicles, the inside of the pressure hull is where the pilot (and crew) are located. Designing a pressure hull is a challenging task. Requirements like depth, fatigue life and impact can result in a pressure hull that is negatively buoyant due to the increase structural weight. Hence, as a designer it is important to understand the mechanics behind different pressure hull concepts that arise from particular requirements. In the next, a selection of these concepts is treated.

Conventional submarines are equipped with ring stiffened pressure hulls. Contrarily, pressure hulls in deep diving submersibles are in general spherical. Since there are lot of different pressure hull concepts, a selection is presented in Appendix A. Note that the the ring stiffened pressure hull is treated as a reference in the present thesis. The mechanics and capabilities of this concept are explored and elaborated, with the idea to understand and ultimately improve this concept.

2.3.2 Operational requirements

The aforementioned applications in Section (2.2) are considered to be the most fundamental appearances of a pressure hull found nowadays. In order to come up with various pressure hull concepts for a particular application, the operational requirements must be formulated. For

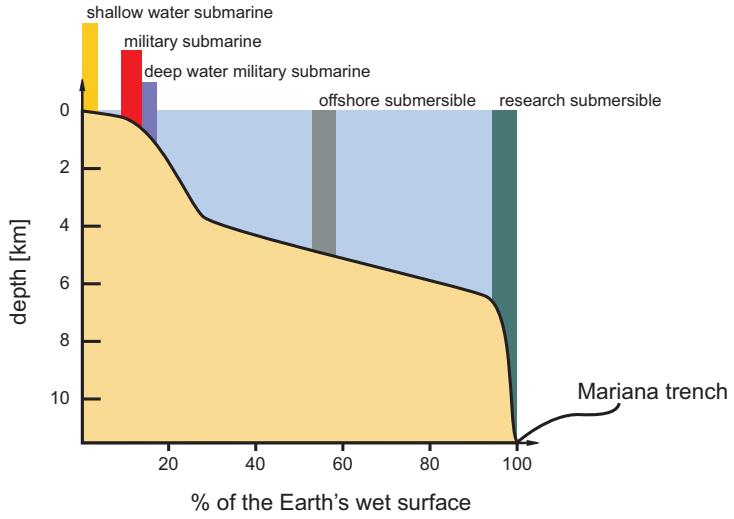

Figure 2.6: Hypsometric curve of the Earth's wet surface with operation depth indicators for various types of submarines

each individual application a list of basic requirements can be created. The requirements listed in the next are presented in a minimal form. More specific and precise requirements are not in the scope of the present thesis.

Diving depth

To start with the discussion on submarine diving depth capabilities, the earth's ocean floor is considered. In Fig.(2.6) an cumulative graph is shown for the earth's ocean floor depth distribution. In this figure, maximum diving depths are indicated for several sorts of submarines. As indicated, military submarines usually dive 300-450 meters at max. Since it is important for a military submarine to remain undetected and with acoustic detection as the primary form of detection, the submarine has to travel silent. A solution other than adding damping to e.g. noise producing equipment is the increase of the diving capabilities. Sound waves rarely travel in straight lines in sea water, the variations in temperature and salinity causing their refraction. This phenomenon can often result in a surface duct in which sound waves initiated, by active acoustic detection from surface units, are refracted back up to the surface along a curved path of only limited depth penetration. The surface duct depth will vary depending on ocean climatic conditions, but it is clearly advantageous to a submarine to be able to get below this depth where it can avoid detection from surface surveillance [1].

For these and other types of submarines such as offshore ROVs, estimated maximum diving depths are listed in Table (2.1). In this table one can see that for non-military purpose submarines, the diving depths maximal diving depths are relatively large. But because of the

Category	Maximum diving depth $[m]$
Shallow water submarine	$50^{[1]}$
Military submarine	$400^{[1]}$
Deep water military submarine	$750^{[10]}$
Offshore submersible	$5000^{[11]}$
Research submersible	$11000^{[11]}$

Table 2.1: List of diving depth requirements

increasing threat in anti-submarine warfare, depth performance is becoming more important for military applications [11].

Performance

In Appendix B a typical list of general requirements for a military submarine is presented. For the sake of briefness, only this list is added to the present thesis. Requirements related to for instance research submersibles are much alike; of course apart from e.g. load requirements due to weapon effects and stealth requirements.

The focus for the present thesis will be on the depth induced hydrostatic pressure requirement. To form an actual pressure hull performance with respect to overall weight of the structure is considered to be of great importance. This important aspect of the current research is elaborated in Section (2.4), which is the next section.

2.4 Design for weight reduction

In general, a submarine is a weight-sensitive structure in which the buoyancy and weight have to reach an equilibrium state. For a given enveloped volume, reducing the structural weight of the submarine has positive effects, e.g. larger payload capability, increase of engine size or even additional structural reinforcement which can ultimately result in even larger depths [12]. The weight of the pressure hull is an important part of the overall weight. For a conventional submarine the steel pressure hull represents roughly one third of the submerged displacement [9]. Hence, the application of lightweight materials as a replacement for the conventional steel in pressure hulls can improve the overall performance of the vehicle [13]. In the search of such materials, the focus is in the first place on materials that show large specific (normalized w.r.t. density) properties in compressive strength and stiffness. This search is performed in Appendix C. From this search it is observed that construction in composite materials is promising. For the present thesis, the composite and composite sandwich cylindrical pressure hull are considered. Of course, the idea of such composite pressure hulls is not new and has been researched intensively (e.g. by [14], [13],[15] and [12]). Furthermore, a comprehensive cost based study is performed [11] in the light of these pressure hulls which indicates that the use composites of composite should definitely be considered in future pressure hull design. It is proposed that unstiffened

cylindrical composite cylinders are the optimal choice when the submarine operates in deep water regimes. Additionally, sandwich pressure hulls are found to be superior in shallow design depths. However, the author indicated that a more accurate description, e.g. a FE model, is needed to analyze and investigate an actual design. Additionally, it is important to note that composites are already successfully applied in pressure hulls. In fact, the first submersible (built by Vickers-Slingsby) for commercial operation with a glass fiber reinforced plastic (GRP) pressure hull is the so called *L.2*. This submersible, has a maximum operating depth of over 350 meter, successfully made its first dive in 1975 in Loch Linnhe in Scotland. The former is described by [16] and indicates that this submersible is found to be extremely successful during operations.

2.5 Purpose of the present work

As indicated earlier, much research is performed in the field of composite pressure hulls. In the search of a composite laminate design, [17] used an linearized analytical buckling model coupled to a genetic algorithm to determine numerically optimized stacking sequences. However, the investigated model was prone to buckling and material failure effects did not had major influence on the collapse. Moreover, the found optimum was modeled in FE but due to computational intensity this model was not optimized and only used for the purpose of validation.

The optimum design of filament-wound multi-layer sandwich pressure hulls is treated in [18]. Analogous to the previous, a genetic algorithm is used which is coupled to an analytical linearized buckling model in order to find an optimum. Although material failure is taken into account general accuracy is still comparable with [17].

The ultimate purpose of this thesis is to formulate a basis for a lightweight design framework that uses composite and composite sandwich pressure hull FE models to accomplish an optimization procedure. If applied correctly, more realistic modeling can be performed with the use of FE. In order to do this, at first, the fundamentals of pressure hull mechanics needs to be assessed and together with an accurate mechanical composite and sandwich material description, FE models need to be created. Second, optimization can be performed to obtain the preferred goal, e.g. weight minimization or maximization of collapse pressure. Resulting designs from this procedure are treated and in order to quantify the improvement of such a lightweight pressure hull, the conventional ring stiffened cylindrical pressure hull is treated as a reference.

2.6 Conclusion

From the very first documented steerable submarine to present time, pressure hulls form one of the most important parts of submarine vehicles. Section (2.4) states that the appliance of lightweight materials in pressure hulls holds the key for the gain in performance increase. In

this field, much research is performed but the optimal laminate design is only treated in a low fidelity mechanical description.

To the author's best knowledge, the use of FE pressure hull models in a thorough composite laminate optimization context has not been investigated. Hence, the ultimate purpose of this thesis is to formulate a basis for a lightweight design framework that uses composite and composite sandwich pressure hull FE models to accomplish an optimization procedure. Besides, it is important to elaborate the related mechanics within a pressure hull, the methods laminate design and composite related mechanics. Resulting designs from this procedure are treated and in order to quantify the improvement of such a lightweight pressure hull, the conventional ring stiffened cylindrical pressure hull is treated as a reference.

Chapter 3

Pressure hull mechanics

For the search of a lightweight pressure hull, it is important to describe the actual mechanics of such a structure. A rough first order description is given in Section (3.1). Because the conventional ring stiffened cylinder is treated as a reference, a mechanical description is elaborated in Section (3.2). Furthermore, buckling of these cylinders is specifically treated in Section (3.3). Because differences in nominal structural geometry can affect the overall ability to resist the external pressure tremendously, it cannot be neglected in the present thesis. Therefore, Section (3.4) describes this important effect.

3.1 Boiler formulae approach

A first approach to understand the basic mechanics of a hull under external pressure is analogous to the approach discussed in [12]. It makes use of the boiler formula and despite the simplicity it is a good start in the process of pressure hull mechanics. This approach considers an infinite cylinder under external pressure. The so-called boiler formulae yield:

$$\sigma_\theta = \frac{pd}{2t}\,, \tag{3.1}$$

$$\sigma_x = \frac{pd}{4t}\,. \tag{3.2}$$

For simplicity the longitudinal stresses σ_x are ignored. Now, the formula for the circumferential stress remains in this section. Giving that σ_θ is the circumferential stress, which is compressive in case of an external pressure p. Further, d stands for the inner diameter and the thickness is denoted by t. From here, the formula can be written in terms of the external pressure. By introduction of the compressive yield strength σ_{yc}, the critical pressure for the concerned material can be found. Hence,

$$p_{cm} = \frac{2\sigma_{yc}t}{d}\,. \tag{3.3}$$

Here, p_{cm} is the critical pressure related to compressive yield of the material. Unfortunately, another big failure mechanism for these structures is buckling. Again, by assuming the infinite cylinder and ignoring the longitudinal effects, a critical pressure related to circumferential buckling is given by [19]:

$$p_{cb} = \frac{\left(n^2 - 1\right) D_{shell}}{r^3} \,. \tag{3.4}$$

In this formula, p_{cb} is the critical pressure related to buckling failure. The number of circumferential buckling waves is given by n. The inner radius is denoted by r. The flexural shell rigidity D_{shell} is given by:

$$D_{shell} = 1/12\, Et^3 \,. \tag{3.5}$$

In this expression, E is the Young's modulus or stiffness. If one writes Eq. (3.4) in terms of the inner diameter d, one will easily find that:

$$p_{cb} = \frac{2Et^3}{d^3} \,. \tag{3.6}$$

Note that collapse in the so-called ovalizing mode ($n = 2$) is assumed in this equation. In hydromechanics, an important measure for any hull is its weight to displacement ratio. It can be interpreted as an indication of buoyancy. If this ratio is smaller or larger than unity, the structure will float or sink, respectively. For neutral buoyancy this ratio is equal to unity. To express this ratio for a cylinder the expressions for weight (W) and displacement (Δ) are given by:

$$W = \rho\, g\pi\, dt \,, \tag{3.7}$$

$$\Delta = 1/4\, \rho_w g\pi\, d^2 \,, \tag{3.8}$$

where in Eq. (3.7) the ρ denotes the (average) hull density and the gravitational acceleration is g. And where in Eq. (3.8) the density of water is ρ_w. The weight to displacement ratio can now be expressed as:

$$\frac{W}{\Delta} = \frac{4\rho\, t}{d\rho_w} \,. \tag{3.9}$$

From here Eq. (3.3) and Eq. (3.6) are written as function of this ratio.

$$p_{cm} = \frac{\sigma_{yc}\rho_w}{2\rho} \frac{W}{\Delta} \,, \tag{3.10}$$

$$p_{cb} = \frac{E}{32} \left(\frac{\rho_w W}{\rho \Delta} \right)^3 \,. \tag{3.11}$$

Additionally, the critical pressure can be translated through Eq. (3.12) to a collapse depth of the hull. In this equation, p_c is the collapse pressure, i.e. collapse due to either buckling or material failure. The equation yields

$$H_c = \frac{p_c}{g\rho_w} \,. \tag{3.12}$$

Material	E [Gpa]	σ_{yc} [MPa]	ρ $[kg/m^3]$
Steel - HY80[a]	207	550	7800
CFRP (epoxy / HS carbon unidirectional)[a]	210	1200	1700
GRP (epoxy / S-glass filament wound)[a]	50	1000	2100
Titanium (6-4 STOA alloy)[a]	110	830	4500
Reinforced concrete[b]	28	87	1950

Table 3.1: List of material properties. Properties indicated with [a],[b] are adopted from [12],[20] respectively.

Note that in this equation g is the gravitational acceleration. With this expression, Eq. (3.10) and Eq. (3.11) can be written in terms of the collapse depth:

$$H_{cm} = \frac{\sigma_{yc}}{2\rho g}\frac{W}{\Delta}\,, \tag{3.13}$$

$$H_{cb} = \frac{E{\rho_w}^2}{32\rho^3 g}\left(\frac{W}{\Delta}\right)^3\,. \tag{3.14}$$

With the knowledge about the density ρ, Young's modulus E and compressive yield strength σ_{yc} of a material, a collapse depth vs. weight to displacement ratio graph can be constructed. This list of material properties is found in Table (3.1).

In the following, Eq. (3.13) and Eq. (3.14) are visualized, using the materials listed in Table (3.1). The result is shown in Fig. (3.1) for a range of 0 - 11 km in depth. For each material there is a dashed line yielding the material failure collapse depth. The buckling collapse is indicated with a solid line, which is curved because of the cubic relation between collapse depth and the weight to displacement ratio. Clearly, for large depths, CFRP (Carbon Fiber Reinforced Plastic) is in this approach superior. The performance of GRFP (Glass Fiber Reinforced Plastic) is also quite surprising. The performance of titanium is still better than steel. Also, steel still performs better than the reinforced concrete for large weight to displacement ratios. The same formulae are used for a shallow water application, i.e. 0 - 1000 m depth. The result is given in Fig. (3.2). Given the previous assumptions, steel performs the worst in this region. Titanium comes second, followed by reinforced concrete and GFRP. Like the deep-water submersible, CFRP performs the best of all the selected materials. It is clear that from the treated calculations one can deduce that CFRP and GFRP are promising pressure hull materials. But one must not forget the simplicity of the model, i.e. the infinite cylinder with circumferential collapse due to buckling and material failure.

3.2 Basics of stiffened cylinders

To observe the mechanical behavior of a stiffened cylinder, which is in the present work considered as the reference model, the method treated in [21] is elaborated in the following. Going back to the boiler formulae, i.e. Eq. (3.1) and Eq. (3.2), the internal forces per unit length can

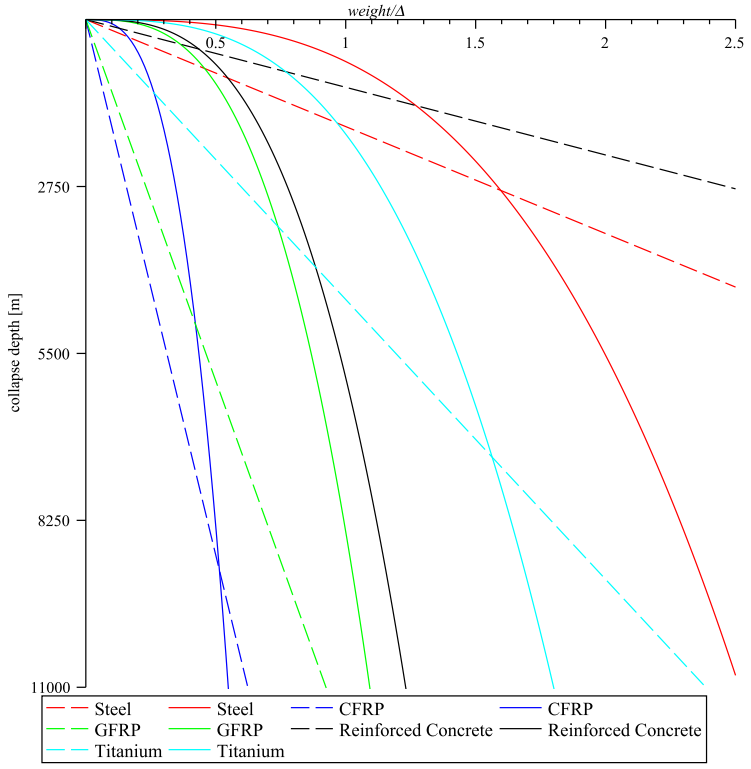

Figure 3.1: Critical collapse depths (0 - 11 km) for material failure (dashed lines) and buckling (solid lines) as a function of the weight to displacement ratio.

be deduced. When a slice of length Δx is cut of the shell, the hoop force is given by:

$$N_\theta = pr\,. \tag{3.15}$$

And the longitudinal force per unit length yields:

$$N_x = \frac{pr}{2}\,. \tag{3.16}$$

The values of N_θ and N_x, in the unstiffened case, are simply found by multiplying σ_θ and σ_x with t, respectively. But if we now define the effective thicknesses as:

$$t_\theta = t + \frac{A_R}{l}\,, \tag{3.17}$$

$$t_x = t\,. \tag{3.18}$$

With t_θ as the effective thickness in the circumferential direction. In this stiffened case there are ring-stiffeners in the circumferential direction, each at a distance l apart from each other. Further, the cross section of the ring stiffener is A_R. The effective thickness in the longitudinal

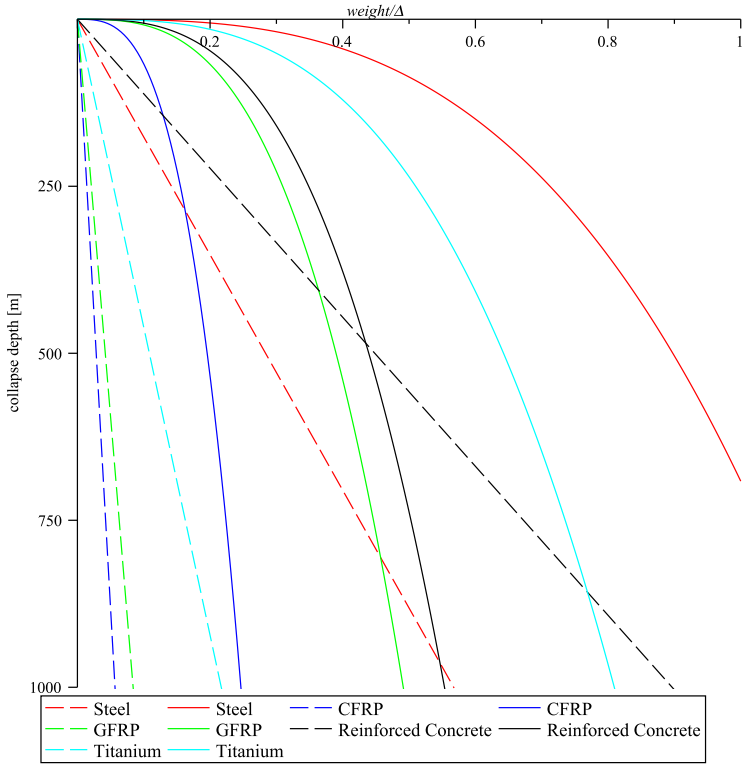

Figure 3.2: Critical collapse depths (0 - 1000 m) for material failure (dashed lines) and buckling (solid lines) as a function of the weight to displacement ratio.

direction is t_x. The axial and hoop stress for the unstiffened cylinder is found by division of the hoop force per unit length and the shell thickness. But since there are ring stiffeners that share the same hoop strain and with the assumption that there is a plane-stress condition in the shell, Hooke's law can be applied:

$$E\epsilon_\theta = \sigma_\theta - \nu\sigma_x = \sigma_R\,, \tag{3.19}$$

Where σ_R is the stress in the ring stiffeners. Likewise, the stress in shell in longitudinal direction is given by σ_x and the hoop stress is σ_θ. The Poisson's ratio is given by ν. Given that the internal forces are calculated as:

$$N_\theta = t\sigma_\theta + \frac{A_R}{l}\sigma_R\,, \tag{3.20}$$

$$N_x = t\sigma_x\,. \tag{3.21}$$

The three equations, Eq. (3.19), Eq. (3.20) and Eq. (3.21) can now give information about the stresses:

$$\sigma_\theta = \frac{pr}{2}\frac{2\,t + \nu\,t_\theta - \nu\,t}{t_\theta t}\,, \tag{3.22}$$

$$\sigma_x = \frac{pr}{2t}\,, \tag{3.23}$$

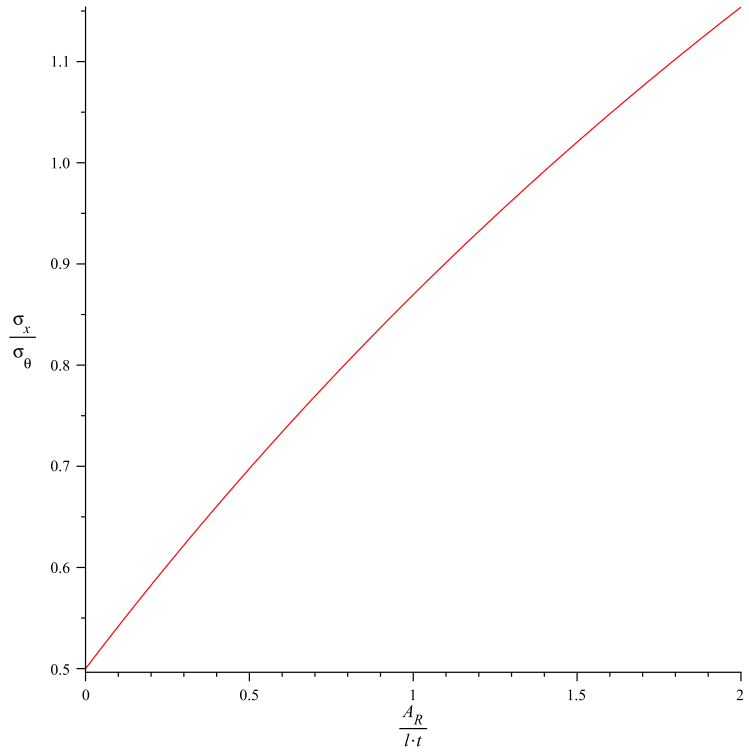

Figure 3.3: The ratio between longitudinal and circumferential hull stress as a function of the ring stiffener density

$$\sigma_R = \frac{pr}{2} \frac{2 - 4\,\nu^2 + \nu}{t_\theta}\,. \tag{3.24}$$

Notice that Eq. (3.23) is the same as obtained in the boiler formula approach (see Section 3.1). The ratio (σ_x/σ_θ) for a varying quantity which can be seen as a ring stiffener density (A_R/lt) is shown in Fig. (3.3) for a typical value for the Poisson's ratio $\nu = 0.3$. In this figure it can be observed that this ratio changes significantly when the ring density is increased. Notice that for a situation where no ring stiffeners are present, i.e. $A_R/lt = 0$, the well-known 2:1 stress relation for unstiffened shells straightforwardly appears. Obviously, the circumferential stress is lowered by ring application. This is desirable since there is not much over-all bending of the hull due to hydrodynamic forces.

The stress situation in a ring stiffened cylinder, which is the common form of a pressure hull, is explored and explained more precisely. For a given cylinder with internal ring stiffeners, as illustrated in Fig.(3.4a), the hull and ring structure deforms due to the (uniform) external pressure. Increasing radial stiffness at specific locations, i.e. ring stiffeners, means less local deformation. Halfway between the rings the hull experiences the largest displacement in radial direction. It is straightforward that due to this behavior, being the periodical mismatch in radial position of the hull, the hull experiences longitudinal bending. At the stiffener the hull

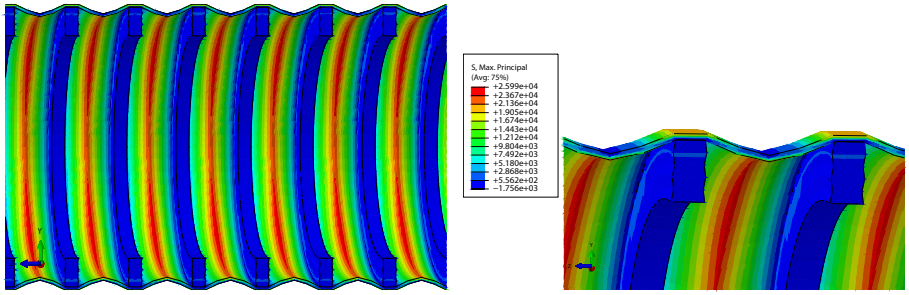

(a) ring stiffened cylinder

(b) close up of ring stiffened cylinder

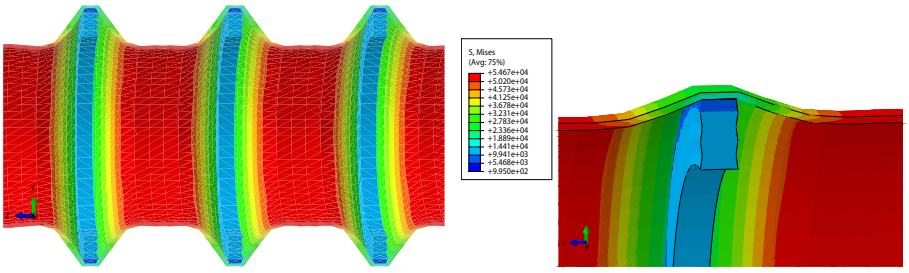

(c) over-spaced ring stiffened cylinder

(d) close up of over-spaced ring stiffened cylinder

Figure 3.4: The Von Mises stress in a stiffened structure

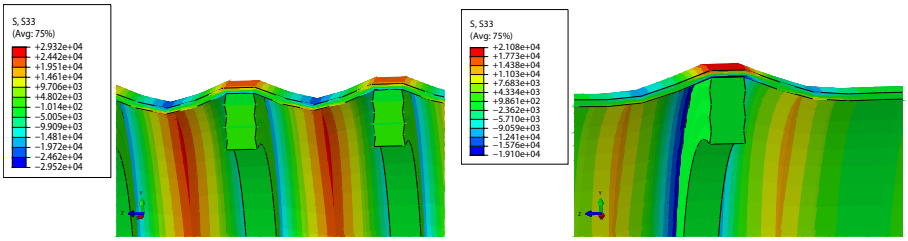

(a) ring stiffened specimen

(b) over-spaced ring stiffened specimen

Figure 3.5: Close-up of the out-of-plane stress

experiences a compressive stress at the inside and tensile stress on the outside Fig.(3.4b). The stress situation inverses halfway between the ring stiffeners, as indicated in the figure. If there is too much space between the stiffeners the use of stiffeners is inappropriate. This phenomenon is displayed in Fig.(3.4c). It can be observed that the infinite cylinder solution, at the right of the figure, for the radial displacement and stress also occurs between the stiffeners. This is not desired since the hull (partially) still behaves in the same way as in the unstiffened case.

As mentioned earlier, the axial compressive stress σ_x induced by the hydrostatic stress on the end domes can be superimposed on the other axial stresses in the hull. For the part of the hull which is in axial tension this rather positive, but for the part in the compressive state this is not quite nice. Furthermore, due to this axial stress the structure could collapse in a concertina-like mode. The out-of-plane stress, which is for instance important when construct-

ing with composite plies or in weldments, is illustrated in Fig.(3.5). It is important to note that the interface between the stiffener and hull experiences compression. If one places the stiffeners outside the hull, there will be tension at this interface. For composite plies and also for weldments this is potentially unwanted.

Failure or material yielding can be described by means of a failure or yield criterion, respectively. Generally, these criteria can be imagined as curves or surfaces in stress or strain space. Within the contour of the criterion the material shows no failure or yielding. If the stress or strain state in the material has reached the contour, the yield point is reached. For the conventional metal ring stiffened cylinder, the well-known von Mises yield criterion is commonly used to indicate yielding. The von Mises stress (or equivalent tensile stress) is described by

$$\sigma_{cr} = \sqrt{3J_2}\,, \tag{3.25}$$

where J_2 is the second invariant of the deviatoric stress tensor. This invariant is found by matter of solving the the characteristic equation for λ, i.e:

$$|\mathbf{S} - \lambda\mathbf{I}| = \lambda^3 - J_1\lambda^2 + J_2\lambda - J_3 = 0\,, \tag{3.26}$$

where the determinant is indicated by $|...|$, $\mathbf{I}$ is de identity tensor, J_n is the n-th deviatoric invariant and $\mathbf{S}$ is the deviatoric stress tensor defined as

$$\mathbf{S} = \boldsymbol{\sigma} - \frac{1}{3}\,\mathrm{tr}\,(\boldsymbol{\sigma})\,, \tag{3.27}$$

with $\boldsymbol{\sigma}$ as the Cauchy stress tensor. To be complete, Eq.(3.25) can be elaborated for a description in stress tensor element space:

$$\sigma_{cr} = \sqrt{\left[\frac{(\sigma_{11}-\sigma_{22})^2 + (\sigma_{22}-\sigma_{33})^2 + (\sigma_{33}-\sigma_{11})^2 + 6\left(\sigma_{12}^2 + \sigma_{31}^2 + \sigma_{23}^2\right)}{2}\right]}\,, \tag{3.28}$$

or in principle stress space:

$$\sigma_{cr} = \sqrt{\left[\frac{(\sigma_1-\sigma_2)^2 + (\sigma_2-\sigma_3)^2 + (\sigma_3-\sigma_1)^2}{2}\right]}\,. \tag{3.29}$$

By taking the von Mises stress equal to the tensile yield strength of the material, e.g. 690MPa for HY100 steel (see Appendix C), the criterion can be visualized. The result is shown for a two dimensional principle stress $(\sigma_1, \sigma_2, 0)$ space in Fig.(3.6). Notice that the intersections with the principle stress axes correspond to the yield strength of the material.

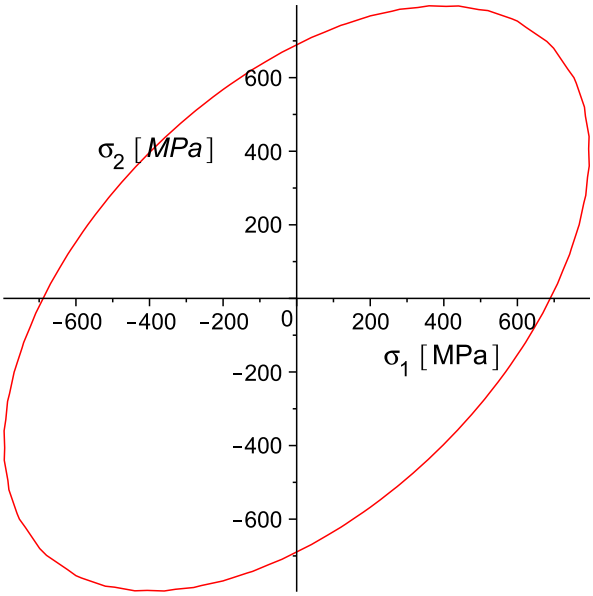

Figure 3.6: The von Mises yield criterion for HY100 steel in principle stress state.

3.3 Buckling of ring stiffened pressure hulls

In general, pressure hulls are prone to buckling. For the conventional ring stiffened pressure hull, these non-linear effects occur in different modes. In the next the most common modes, which ultimately result in collapse, are treated. For a well designed stiffened pressure hull, full advantage of the material strength is taken when the critical failure mode is the elasto-plastic interframe collapse [22]. In this mode, which is relatively predictable [1], shell yielding takes place before buckling occurs. This concertina-type pleat mode can be observed from Fig.(3.7(a)). It should be noted that this collapse mode can occur partially or fully about the circumference.

Another typical collapse mode is elastic interframe buckling. This mode, which is also known as elastic lobar buckling, occurs in shell sections between adjacent ring stiffeners. Small lobes are formed between the stiffeners, with a size proportional to the (characteristic) shell length between these stiffeners. Because of this relative small length, multiple lobes occur in circumferential direction as can be observed from Fig.(3.7(b)).

Thirdly, general instability of the stiffened cylinder can occur. This unwanted collapse mode is characterized by a insufficiently stiffened shell. To be precise, the radial stiffness of the ring stiffeners is not enough to prevent this overall collapse. Increasing the cross-sectional area and/or inertia of the stiffeners is needed, so that the support against this general instability is increased. This type of collapse can arise in compartments between rigid bulkheads, or spread over the entire structure. An example of this mode is shown in Fig.(3.7(c)).

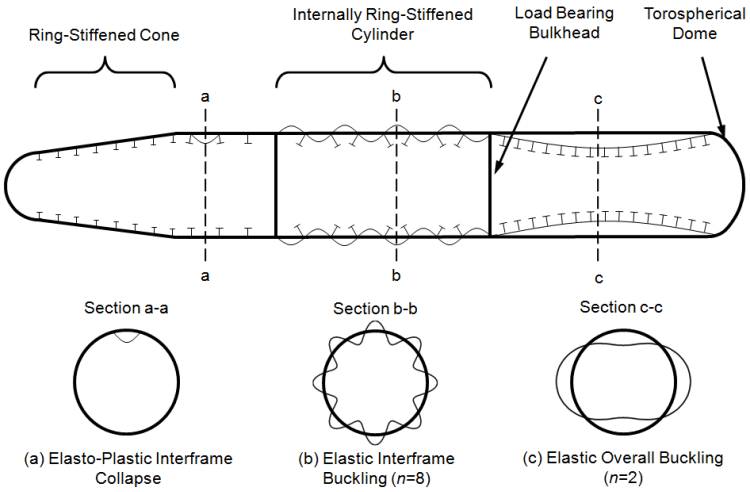

Figure 3.7: Compartmentalized pressure hull structure with inelastic interframe buckling (a), elastic interframe buckling in (b) and overall elastic buckling in (c). This figure is adapted from [22]

.

Classical solutions for the corresponding collapse pressures are generally used for stiffened cylindrical shells [23]. For the elasto-plastic interframe collapse the pressure is given by

$$P_{cr} = \frac{\sigma_y (t/R)}{(A-B)^{1/2}}\,, \tag{3.30}$$

where

$$A = \frac{3}{4} + \alpha^2 \left[F_2^2 + F_2 F_4 \left(1-2\nu\right) \sqrt{\frac{0.91}{1-\nu^2}} + F_4^2 \left(1-\nu+\nu^2\right) \left(\frac{0.91}{1-\nu^2}\right) \right]\,, \tag{3.31}$$

$$B = \frac{3}{2}\,\alpha \left[F_2 - \nu F_4 \sqrt{\frac{0.91}{1-\nu^2}} \right] \tag{3.32}$$

and

$$\alpha = \frac{A_S}{t L_S} \tag{3.33}$$

In these equations, σ_y is the yield strength of the material, t is the shell thickness and R is the mean shell radius. The Poisson's ratio is ν, the cross-sectional area of the ring-stiffeners is A_S and the frame spacing is denoted by L_S. These expressions where derived from the consideration of a point on the shell outer surface midway between adjacent rings [24]. Accordingly, the Huber-von Mises-Hencky yield criterion is applied to the point's biaxial stress field to derive the collapse pressure. The coefficients F_i are found via a graphical or iterative method. This method is not treated in the present thesis and hence the reader is advised to read [25] for further details.

Next, interframe buckling collapse occurs if the pressure is

$$P_{cr} = \frac{2.42E\left(t/2R\right)^{5/2}}{\left(1-(\nu)^2\right)^{0.75}\left[(L_S/2R)-0.447(t/2R)^{1/2}\right]}\,, \tag{3.34}$$

and the overall buckling collapse pressure yields

$$P_{cr} = \frac{m^4 Et}{R\left(n^2-1+\frac{m^2}{2}\right)\left(n^2+m^2\right)} + \frac{EI_{xx}\left(n^2-1\right)}{R^3 L_S}\,, \tag{3.35}$$

where

$$R_f = R - Y_S - \frac{t}{2}\,, \text{ and } m = \frac{\pi R}{L}\,. \tag{3.36}$$

In Eq.(3.35) n and m denote the number of circumferential and longitudinal buckling lobes, respectively. E is the Young's modulus of the material and I_{xx} is the moment of inertia of the shell-stiffener geometry.

Because elastic buckling in thick shell plating will occur at a high pressures, a more precise collapse prediction with the account for plasticity effects is needed. The well-known Johnson-Ostenfeld formula is used to describe this elasto-plastic behavior.

$$\sigma_{cr} = \sigma_e \text{ for } \sigma_e \leq \frac{\sigma_y}{2}\,, \tag{3.37}$$

$$\sigma_{cr} = \sigma_y\left(1-\frac{\sigma_y}{4\sigma_e}\right) \text{ for } \sigma_e > \frac{\sigma_y}{2}\,, \tag{3.38}$$

where the critical buckling strength σ_{cr} is a function of the yield strength σ_y and the elastic buckling strength σ_e. Of course, the latter can be estimated from the classical solutions previously treated. To be complete, an example of this inelastic correction is graphically shown in Fig.(3.8). It can be observed from the figure that the curves has two asymptotes being the elastic and plastic solutions.

3.4 The effect of shape imperfections

Previous formulations only described ideal or perfect geometric pressure hulls. However, in a real structure all sorts of non-ideal features can be found due to for instance fabrication aspects. These features can greatly affect the load-carrying capabilities of the pressure hull. Initial or residual stresses are known to cause early yielding of the pressure hull. Although the author is aware of the significance these residual stresses, the present thesis will only consider the geometric imperfections. Geometric imperfections, which are shape deviations from the nominal perfect dimensioned pressure hull, are known to lower the critical buckling pressure considerably [24]. In Fig.(3.9) a typical load displacement curve is illustrated. It can be observed from the figure that the collapse pressure is considerably lower for the imperfect shell compared to the

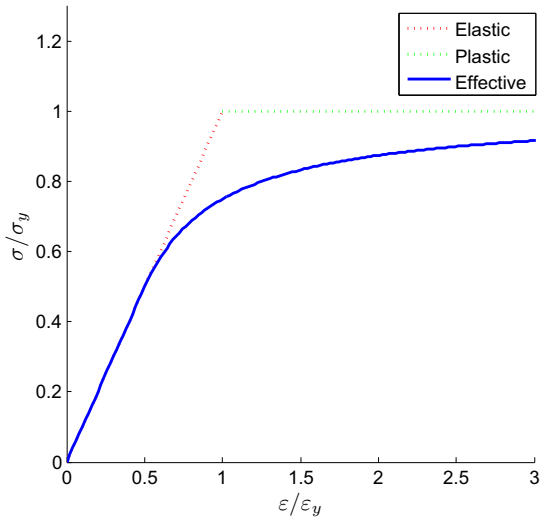

Figure 3.8: Impression of the critical strength according to the Johnson-Ostenfeld formula

bifurcation point pressure P_c for the perfect shell.

As indicated before, initial geometric imperfections are likely to arise from fabrication processes and hence their nature is not completely random. It is demonstrated in [26] that, indeed, one can associate characteristic initial imperfection distributions with different fabrication processes. Vital information about the shape and magnitude of these imperfections can be gathered by measurements. The use of a chord gauge device at equally spaced intervals around the circumference of the cylinder for measuring the out of circularity (OOC) was first described by Kendrick [27]. Accordingly, the use of this device is probably the only practical method to measure the OOC for large cylinders. Especially for pressure hulls with internal structures where measurement can only take place at the outer shell surface. Earlier, Kendrick [28] showed a way to express the measured imperfections mathematically. This method uses a double Fourier series:

$$w_0(x,\theta) = \sum_{m=1}^{\infty}\sum_{n=1}^{\infty} C_{0mn}\cos n\theta \sin\left(m\pi x/L\right) \ , \tag{3.39}$$

where the deviation or imperfection is denoted by w_0, C_{0mn} is the magnitude of the imperfection for a particular mode (m,n) and (θ,x) are the shell coordinates. For the measured imperfection data, the magnitudes have to be calculated in order to obtain a correct mathematical shape representation of the imperfect structure.

The imperfect state of the pressure hull can give rise to localized bending effects due to the externally applied pressure. These effects will cause high stresses and early yielding in the structure. Secondly, they can cause the structure to fail in the elastic range through contribu-

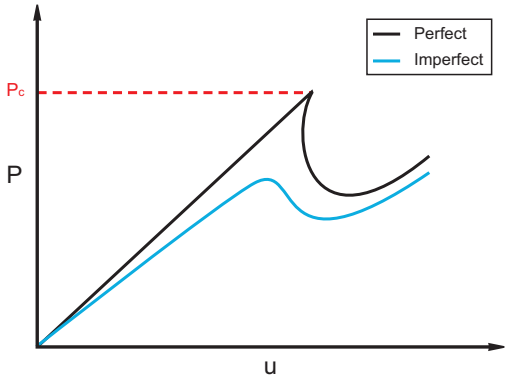

Figure 3.9: The load displacement curve for a geometrically perfect and imperfect shell

.

tion to the nonlinear large-displacement effects [29]. These imperfection induced phenomena can be captured in a FE analysis, or, can be accounted for in analytical descriptions.

For the analytical description (first described by Kendrick), the displacement effects are captured in

$$w = \left(\frac{P}{P_e - P} \right) w_0 \,, \tag{3.40}$$

where w is the displacement, P the applied pressure and P_e is the overall elastic buckling pressure. The initial OOC w_0 can be expressed as

$$w_0 = C_0 \cos n\theta \sin \left(m\pi x / L \right) \,, \tag{3.41}$$

which is one specific (m, n) mode corresponding term of the Fourier series of Eq.(3.39). This approach shows that the imperfect shape is amplified if the pressure increases. Straightforwardly, when the applied pressure in Eq.(3.40) tends to the overall perfect elastic collapse pressure, the equation has a root which will result in large displacements.

Stresses due to bending effects can be related to curvature changes that occur due to the previously described displacements. For a stiffener flange, Kendrick found that

$$\sigma = \sigma_0 + \frac{\left(n^2 - 1 \right) E e_f w}{a^2} \tag{3.42}$$

where σ_0 is the axisymmetric stress, a is the radial coordinate, e_f the combined section neutral axis to the frame flange and w is the normal displacement already described in Eq.(3.40).

3.5 Conclusion

The fundamental mechanics of a pressure hull are treated with the help of the boiler formulae. It is found in this approach that in contrast to an unstiffened steel pressure hull, large weight savings can be obtained if construction is performed with lightweight materials as CFRP.

Because this approach is simplistic and the fact that conventional pressure hulls are generally ring-stiffened cylinders, the mechanics of such a structure is also elaborated. Hence, the most important causes of collapse are treated. Starting with the effect of frame spacing on the stress distribution in the shell, the importance of appropriate stiffener design is indicated. Because adding stiffeners also increases the number of mechanisms of the structure to fail, various buckling effects are described and corresponding collapse pressures are analytically quantified.

In the last part of this chapter, the effect of shape imperfections is briefly discussed. Because imperfections can be deleterious to the structural integrity, the measurement and mathematical representations of these geometric deviations is important. Furthermore, approaches to estimate the collapse pressure for this imperfect structural state were presented.

Chapter 4

Composite pressure hulls

The goal of the present chapter is to describe the mechanical background needed in order to design a composite lightweight pressure hull. Since designing a composite structure includes the design of the composite material itself, aspects as for instance lamination theory and failure prediction of composites are crucial in such a design process. Therefore, these and other important composite related topics are described in Section (4.1). Because a composite pressure hull can also fail due to buckling effects, an analytic method to derive these collapse pressures are treated in Section (4.2). At last, Section (4.3) describes the way to design a composite structure such that the total weight is minimized.

4.1 Composite mechanics and material behavior

Starting with the actual basics of a composite, Section (4.1.1) shows how macro-mechanical material properties can be estimated with the help of simple formulae. The mechanical response of composite plies and laminates is elaborated in Section (4.1.2) and ply stacking guidelines concerning the latter is treated in Section (4.1.3). Because the prediction of material failure in a composite is a complex story but of great importance, strength prediction is treated in Section (4.1.4). In Section (4.1.6) failure functions are introduced.

4.1.1 Basics of a composite material

A composite material, as the words imply, is composed of two or more materials and is therefore heterogenous. Composites are made up of two or more individual materials which are later in this work referred to as constituents. In case of two constituents, one material embeds the other and hence it is called matrix (or resin). The other constituent functions as reinforcement for this matrix. For the present thesis, a composite material is a fiber reinforced plastic consisting of two different materials. That is, a plastic representing the matrix which is generally a polymer, reinforced by a fibrous material which forms the skeleton of the composite. Composites are anisotropic materials that, if applied and designed correctly, are superior to metals due to their

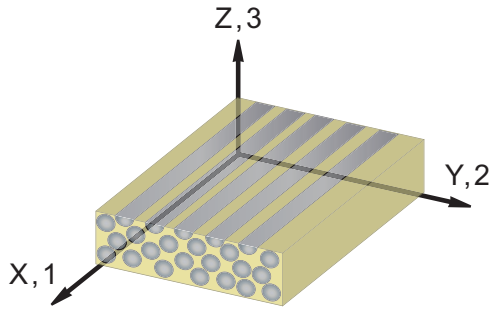

Figure 4.1: Composite fibrous ply with the applied coordinate systems

.

mechanical properties with respect to weight. Hence, in aerospace and other weight critical industries composites are widely applied. In the following a short mechanical description is given of algebraic methods to determine the properties of composite materials. The rule or method of mixtures is a very basic algebraic description of a composite, but is a good starting point for estimations of its properties. Only suitable for uni-directional (UD) plies, i.e. a single orientation for the inherent fibers, this rule uses the fiber volume fraction, V_f together with the properties of the constituents to estimate properties of the composite. For the density of the composite this yields [30]

$$\rho = V_f \rho_f + (1 - V_f)\rho_m, \tag{4.1}$$

where ρ, ρ_f and ρ_m are the composite, fiber and matrix densities, respectively. Similar equations are used to estimate the properties in fiber direction, that is X-direction (see Fig.(4.1) for an impression) for the estimated Young's modulus of the composite, E_X, that is [30]

$$E_X = V_f E_f + (1 - V_f)E_m, \tag{4.2}$$

and for the composite tensile strength σ^{XT} in fiber direction one obtains [30]

$$\sigma^{XT} = V_f \sigma_f^T + (1 - V_f)\sigma_m^T. \tag{4.3}$$

Likewise, the longitudinal Poisson's ratio ν_{XY} is defined as [30],

$$\nu_{XY} = \nu_f V_f + \nu_m(1 - V_f). \tag{4.4}$$

In this equation ν_f and ν_m are the Poissons ratios for the fiber and matrix, respectively. Of course, it is assumed here that both constituents are isotropic.

The properties of an UD composite ply can be predicted by analytical and practical methods. These can then be used in a macro-mechanical analysis of the considered structure. But

micro-mechanical effects are also important to mention. For instance, if there is poor bonding between matrix and fiber on a micro-mechanical level, this will also affect the macro-mechanical properties.

For the rule of mixtures and the following listed methods, a few assumptions are made: The matrix and the fiber are both homogenous and isotropic. The fiber is nicely dispersed in the matrix and perfectly aligned with regular spacing. The UD ply is macroscopically homogeneous and transverse isotropic, which is a special case of orthotropy. There is a perfect bond between the fibers and matrix. And it behaves in a linear elastic manner. Further the effect of thermal shrinkage on the stress state is not considered, the ply is assumed to be initially stress free.

Different from the previous, there is not a single analytical formula for the transverse modulus i.e. E_Y. A selection is made among those formulae and later the behavior for different fiber volume fractions is displayed graphically. The considered methods are:
The Jones [31] method:

$$E_Y = \frac{E_f E_m}{E_f\,(1 - V_f) + E_m V_f}. \tag{4.5}$$

The Förster/Knappe [32] method:

$$E_Y = \frac{E_m^0}{(1 - V_f)^{1.45} + V_f\,E_m^0/E_f}. \tag{4.6}$$

With E_m^0 defined as

$$E_m^0 = \frac{E_m}{1 - {\nu_m}^2}. \tag{4.7}$$

The Schneider [33] method:

$$E_Y = \frac{E_m^0\left(1 + {V_f}^3\right)}{(1 - V_f)^{0.75} + 6V_f\,E_m^0/E_f}, \tag{4.8}$$

with E_m^0 defined as in 4.7.
The Puck [34] method:

$$E_Y = \frac{E_m^0\left(1 + 0.85\,{V_f}^2\right)}{(1 - V_f)^{1.25} + V_f\,E_m^0/E_f}, \tag{4.9}$$

again, with E_m^0 defined as in 4.7. As mentioned earlier, the behavior of these methods under varying fiber volume fraction V_f is graphically illustrated in 4.2. The transverse Poisson's ratio ν_{YX} is defined as,

$$\nu_{YX} = \nu_{XY}\frac{E_Y}{E_X}, \tag{4.10}$$

where ν_{XY} is defined earlier in 4.4.

Again, for transverse shear modulus G_{XY} a selection is made among various methods and

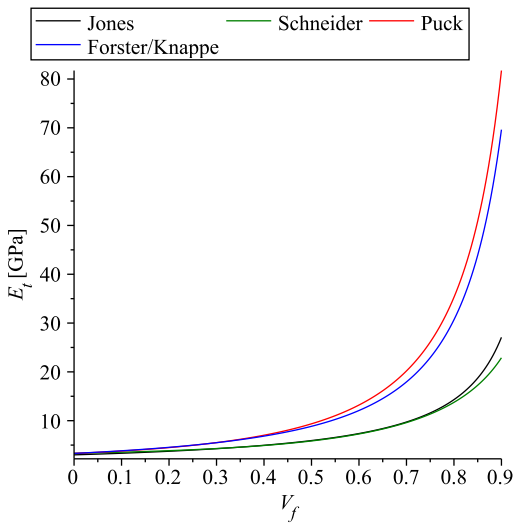

Figure 4.2: The transverse stiffness for different methods as functions of the fiber volume fraction. Note that $E_f = 250GPa$, $E_m = 3000MPa$ and $\nu_m = 0.3$, which are typical values for a carbon/epoxy composite.

.

later the behavior for different fiber volume fractions is displayed graphically. The considered methods are: The Jones [31] method is derived from a representative volume element:

$$G_{XY} = \frac{G_f G_m}{G_f\,(1+V_f) + G_m V_f}. \tag{4.11}$$

The Förster/Knappe [32] method is based on semi-empirical glass/epoxy experiments:

$$G_{XY} = G_m \frac{1+0.4\,\sqrt{V_f}}{(1-V_f)^{1.45} + V_f\,G_m/G_f}. \tag{4.12}$$

Schneider [33] also formulated a semi-empirical method with carbon/epoxy experiments:

$$G_{XY} = G_m \frac{1+0.25\,\sqrt{V_f}}{(1-V_f)^{1.25} + 1.25V_f\,G_m/G_f}. \tag{4.13}$$

The Puck [34] method, which is semi-empirically derived from glass/epoxy experiments:

$$G_{XY} = G_m \frac{1+0.4\,\sqrt{V_f}}{(1-V_f)^{1.45} + V_f\,G_m/G_f}. \tag{4.14}$$

From a constructing point of view, these UD properties by themselves offer the basis to calculate

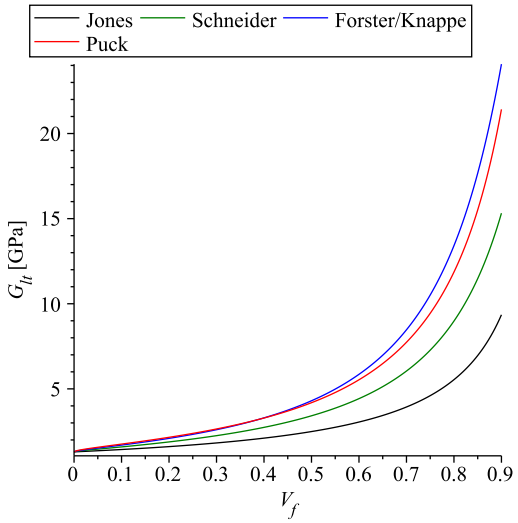

Figure 4.3: The transverse shear modulus for different methods as functions of the fiber volume fraction. Note that $G_f = 30$ GPa and $E_m = 1300$ MPa which are typical values for a carbon/epoxy composite.

.

the laminate properties. For an orthotropic UD ply Hooke's law can now be formulated as:

$$\begin{bmatrix} \varepsilon_1 \\ \varepsilon_2 \\ \varepsilon_3 \\ \varepsilon_4 \\ \varepsilon_5 \\ \varepsilon_6 \end{bmatrix} = \begin{bmatrix} \frac{1}{E_1} & -\frac{\nu_{21}}{E_2} & -\frac{\nu_{31}}{E_3} & 0 & 0 & 0 \\ -\frac{\nu_{12}}{E_1} & \frac{1}{E_2} & -\frac{\nu_{32}}{E_3} & 0 & 0 & 0 \\ -\frac{\nu_{13}}{E_1} & -\frac{\nu_{23}}{E_2} & \frac{1}{E_3} & 0 & 0 & 0 \\ 0 & 0 & 0 & \frac{1}{G_{23}} & 0 & 0 \\ 0 & 0 & 0 & 0 & \frac{1}{G_{13}} & 0 \\ 0 & 0 & 0 & 0 & 0 & \frac{1}{G_{12}} \end{bmatrix} \begin{bmatrix} \sigma_1 \\ \sigma_2 \\ \sigma_3 \\ \sigma_4 \\ \sigma_5 \\ \sigma_6 \end{bmatrix} \tag{4.15}$$

and because this compliance matrix is symmetric one obtains

$$-\frac{\nu_{12}}{E_1} = -\frac{\nu_{21}}{E_2}, \quad -\frac{\nu_{13}}{E_1} = -\frac{\nu_{31}}{E_3}, \quad -\frac{\nu_{23}}{E_2} = -\frac{\nu_{32}}{E_3}\,. \tag{4.16}$$

Furthermore, the previously assumed transverse isotropy implies that $E_2 = E_3 = E_Y$ and hence Hooke's law can be simplified as

$$\begin{bmatrix} \varepsilon_1 \\ \varepsilon_2 \\ \varepsilon_3 \\ \varepsilon_4 \\ \varepsilon_5 \\ \varepsilon_6 \end{bmatrix} = \begin{bmatrix} \frac{1}{E_X} & -\frac{\nu_{YX}}{E_Y} & -\frac{\nu_{YX}}{E_Y} & 0 & 0 & 0 \\ -\frac{\nu_{XY}}{E_X} & \frac{1}{E_Y} & -\frac{\nu_Y}{E_Y} & 0 & 0 & 0 \\ -\frac{\nu_{XY}}{E_X} & -\frac{\nu_Y}{E_Y} & \frac{1}{E_Y} & 0 & 0 & 0 \\ 0 & 0 & 0 & \frac{2(1+\nu_Y)}{E_Y} & 0 & 0 \\ 0 & 0 & 0 & 0 & \frac{1}{G_{XY}} & 0 \\ 0 & 0 & 0 & 0 & 0 & \frac{1}{G_{XY}} \end{bmatrix} \begin{bmatrix} \sigma_1 \\ \sigma_2 \\ \sigma_3 \\ \sigma_4 \\ \sigma_5 \\ \sigma_6 \end{bmatrix}, \tag{4.17}$$

note that symmetry of this matrix can be checked with Eq.(4.10).

Multiple layers of plies form a so called laminate. The laminate can be tailored such that the properties are an outcome of the design. Each ply has a thickness and one or more fiber directions. A single ply can, as mentioned earlier be an unidirectional composite if all fibers in a laminate are in one specific direction. On the other hand, fabrics are multidirectional plies and consist of fibers which are woven together. Mechanical properties of a composite lay-up could also be estimated via algebraic methods. This is performed in Section (4.1.2).

4.1.2 Classical laminate theory

The laminate theory is developed to obtain the stiffness and strength properties of a laminate, according to the composition and properties of each individual layer. In this theory, the Kirchhoff-Love hypothesis is active. Therefore it is assumed that a material line perpendicular to the mid-plane of the laminate, remains straight and perpendicular in the deformed configuration. Shear stresses in the out-of-plane direction are therefore neglected. Additionally, the out-of-plane stress will be neglected such that a plane stress situation arises. The result is that the deformation of the plate will now be completely described by the deformation of the mid-plane.
For this theory, thin plates are considered with a constant thickness. The xy-plane is located at the mid-plane of the plate. Straightforwardly, the z-axis is perpendicular to the plate. The deformation can be expressed by means of the displacement vector

$$\mathbf{u} = u\mathbf{i} + v\mathbf{j} + w\mathbf{k}. \tag{4.18}$$

Where $\mathbf{i}$,$\mathbf{j}$ and $\mathbf{k}$ are the unit vectors corresponding to the x, y and z coordinates and u,v and w are the components of the displacement vector. The components of the strain vector are described by

$$\begin{aligned} \varepsilon_x &= \frac{\partial u}{\partial x}, & \varepsilon_y &= \frac{\partial v}{\partial y}, & \varepsilon_z &= \frac{\partial w}{\partial z}, \\ \gamma_{yz} &= \frac{\partial v}{\partial z} + \frac{\partial w}{\partial y}, & \gamma_{xz} &= \frac{\partial u}{\partial z} + \frac{\partial w}{\partial x}, & \gamma_{xy} &= \frac{\partial u}{\partial y} + \frac{\partial v}{\partial x}. \end{aligned} \tag{4.19}$$

It is important to say that the strains are assumed to be small, since there are only first-order derivatives in Eq.(4.19). The length of the material line perpendicular to the mid-plane is unchanged after the deformation, hence:

$$w(x, y) = w^0(x, y). \tag{4.20}$$

Note that the superscripted zero refers to the mid-plane. The angle β, which is illustrated in Fig.(4.4), is the same as the slope of the plate, thus:

$$\beta = \frac{\partial w^0}{\partial x}. \tag{4.21}$$

The displacement in the x direction can be described by the displacement of the mid-plane and a term related to the bending described in Eq.(4.21), i.e.

$$u = u^0 - \beta z. \tag{4.22}$$

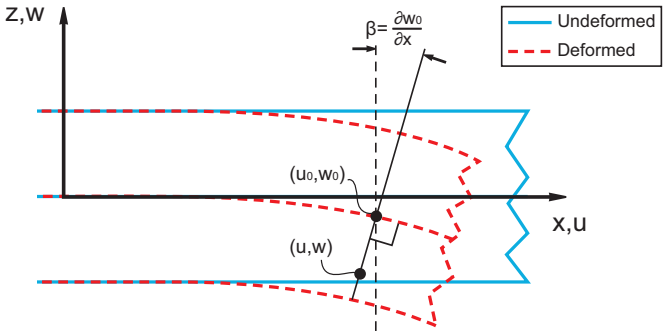

Figure 4.4: Deformation of a plate with the Kirchhoff-Love hypothesis, notice that in this situation $\beta < 0$

In this equation the z denotes the distance to the mid-plane. More general, the displacement in the x direction is given by

$$u(x, y, z) = u^0(x, y) + z\frac{\partial w^0}{\partial x}. \tag{4.23}$$

Analogously, the displacement in the y direction yields

$$v(x, y, z) = v^0(x, y) + z\frac{\partial w^0}{\partial y}. \tag{4.24}$$

Since all displacements are described, the strains from Eq.(4.19) can be expressed as

$$\begin{aligned} &\varepsilon_x = \frac{\partial u^0}{\partial x} - z\frac{\partial^2 w^0}{\partial x^2}, \quad \varepsilon_y = \frac{\partial v^0}{\partial y} - z\frac{\partial^2 w^0}{\partial y^2}, \quad \varepsilon_z = 0, \\ &\gamma_{yz} = 0, \quad \gamma_{xz} = 0, \quad \gamma_{xy} = \frac{\partial u^0}{\partial y} + \frac{\partial v^0}{\partial x} - 2z\frac{\partial^2 w^0}{\partial x \partial y}. \end{aligned} \tag{4.25}$$

The extensional strains and the shear strain of the mid-plane are simply described by:

$$\varepsilon_x^0 = \frac{\partial u^0}{\partial x}, \quad \varepsilon_y^0 = \frac{\partial v^0}{\partial y}, \quad \gamma_{xy}^0 = \frac{\partial u^0}{\partial y} + \frac{\partial v^0}{\partial x}. \tag{4.26}$$

The definition of curvature κ_x^0 is

$$\kappa_x^0 = -\frac{\frac{\partial^2 w^0}{\partial x^2}}{\left(1 + \left(\frac{\partial w^0}{\partial x}\right)^2\right)^{\frac{3}{2}}} \approx -\frac{\partial^2 w^0}{\partial x^2}. \tag{4.27}$$

Similarly the curvature in y-direction of the mid-plane is:

$$\kappa_y^0 \approx -\frac{\partial^2 w^0}{\partial y^2}. \tag{4.28}$$

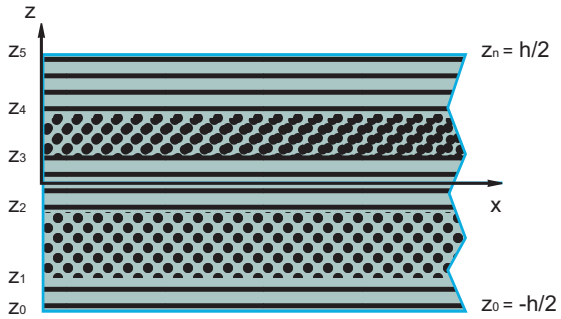

Figure 4.5: Schematic representation of a laminate with $n = 5$ plies

The twisting of a plate is described by the (technical) curvature

$$\kappa_{xy}^0 \approx -2\frac{\partial^2 w^0}{\partial x \partial y}. \tag{4.29}$$

With the definitions of the extensional strains for the midplane and the midplane curvatures the strain vector (for the plane stress situation) is given in a compact manner:

$$\begin{aligned} \varepsilon_x &= \varepsilon_x^0 + z\kappa_x^0, \\ \varepsilon_y &= \varepsilon_y^0 + z\kappa_y^0, \\ \gamma_{xy} &= \gamma_{xy}^0 + z\kappa_{xy}^0. \end{aligned} \tag{4.30}$$

Notice that Eq.(4.30) can be written as the system:

$$\boldsymbol{\varepsilon} = \boldsymbol{\varepsilon}^0 + z\boldsymbol{\kappa}^0, \tag{4.31}$$

with

$$\begin{bmatrix} \varepsilon_x \\ \varepsilon_y \\ \gamma_{xy} \end{bmatrix} = \begin{bmatrix} \varepsilon_x^0 \\ \varepsilon_y^0 \\ \gamma_{xy}^0 \end{bmatrix} + z \begin{bmatrix} \kappa_x^0 \\ \kappa_y^0 \\ \kappa_{xy}^0 \end{bmatrix}. \tag{4.32}$$

Hooke's law can be applied to describe the stress-strain relationship:

$$\begin{bmatrix} \sigma_x \\ \sigma_y \\ \tau_{xy} \end{bmatrix} = \begin{bmatrix} Q_{11} & Q_{12} & Q_{16} \\ & Q_{22} & Q_{26} \\ & & Q_{66} \end{bmatrix} \begin{bmatrix} \varepsilon_x \\ \varepsilon_y \\ \gamma_{xy} \end{bmatrix}. \tag{4.33}$$

Consider a laminate with n plies, each with an orthogonal coordinate system that has a xy-plane that coincides with the ply's mid-plane as illustrated in Fig.(4.5). For the k-th ply within

the laminate Hooke's law can be formulated:

$$\begin{bmatrix} \sigma_x \\ \sigma_y \\ \tau_{xy} \end{bmatrix}_k = \begin{bmatrix} Q_{11} & Q_{12} & Q_{16} \\ & Q_{22} & Q_{26} \\ & & Q_{66} \end{bmatrix}_k \begin{bmatrix} \varepsilon_x \\ \varepsilon_y \\ \gamma_{xy} \end{bmatrix}_k . \tag{4.34}$$

If each coordinate system $(x, y, z)_k$ is rotated such that the x-axis is aligned with the fibers, one obtains $(x', y', z')_k$. Each rotation is measured clockwise, with angle ϕ_k as the orientation of the k-th ply. With respect to the stresses, the following relation holds in the k-th ply:

$$\begin{bmatrix} \sigma_x \\ \sigma_y \\ \tau_{xy} \end{bmatrix}_k = \begin{bmatrix} c^2 & s^2 & 2\,sc \\ s^2 & c^2 & -2\,sc \\ -sc & sc & c^2 - s^2 \end{bmatrix}_k \begin{bmatrix} \sigma'_x \\ \sigma'_y \\ \tau'_{xy} \end{bmatrix}_k . \tag{4.35}$$

In this relation $c = cos\phi_k$ and $s = sin\phi_k$. In short Eq.(4.35) can be written as:

$$\boldsymbol{\sigma}'_k = \boldsymbol{T}_k \boldsymbol{\sigma}_k \tag{4.36}$$

Where $\mathbf{T_k}$ is the transformation matrix and $\boldsymbol{\sigma}'_k$ is the stress in the k-th ply according to coordinate system $(x', y', z')_k$. Further, a similar relation holds for the strains:

$$\boldsymbol{\varepsilon}'_k = \boldsymbol{T}_k \boldsymbol{\epsilon}_k \tag{4.37}$$

Now with the help of Eq.(4.34) there is enough information to express the stress-strain relations in the (x,y,z) coordinate system:

$$\boldsymbol{\sigma}_k = \boldsymbol{T}_k^{-1} \boldsymbol{\sigma}'_k = \boldsymbol{T}_k^{-1} \boldsymbol{Q}_k \boldsymbol{\varepsilon}'_k = \boldsymbol{T}_k^{-1} \boldsymbol{Q}_k \boldsymbol{T}_k \boldsymbol{\varepsilon}_k. \tag{4.38}$$

The following substitution can be made:

$$\boldsymbol{Q}_k{}' = \boldsymbol{T}_k^{-1} \boldsymbol{Q}_k \boldsymbol{T}_k. \tag{4.39}$$

After some algebra, the following is found:

$$\begin{aligned}
Q'_{11} &= Q_{11}c^4 + 2(Q_{12} + 2Q_{66})s^2c^2 + Q_{22}s^4\,, \\
Q'_{22} &= Q_{11}s^4 + 2(Q_{12} + 2Q_{66})s^2c^2 + Q_{22}c^4\,, \\
Q'_{12} &= (Q_{11} + Q_{22} - 4Q_{66})s^2c^2 + Q_{12}(s^4 + c^4)\,, \\
Q'_{16} &= (Q_{11} - Q_{12} - 2Q_{66})sc^3 + (Q_{12} - Q_{22} + 2Q_{66})s^3c\,, \\
Q'_{26} &= (Q_{11} - Q_{12} - 2Q_{66})s^3c + (Q_{12} - Q_{22} + 2Q_{66})sc^3\,, \\
Q'_{66} &= (Q_{11} + Q_{22} - 2Q_{12} - 2Q_{66})s^2c^2 + Q_{66}(s^4 + c^4)\,.
\end{aligned} \tag{4.40}$$

where $c = cos\phi_k$, $s = sin\phi_k$, $Q' = Q'_k$ and $Q = Q_k$ are used for the description of the k-th ply. With the transformed reduced stiffness matrix $\boldsymbol{Q}'$ Eq.(4.38) is rewritten into:

$$\boldsymbol{\sigma}_k = \boldsymbol{Q}'_k \boldsymbol{\varepsilon}_k. \tag{4.41}$$

This relation is important for laminate stress-strain calculations. Now, the k-th ply is considered with distance z corresponding too the ply's midplane. With Eq.(4.31) it is clear that

$$\boldsymbol{\varepsilon}_k = \boldsymbol{\varepsilon}^0 + z\boldsymbol{\kappa}^0, \qquad z_{k-1} \leq z \leq z_k. \tag{4.42}$$

Again with Hooke's law returns:

$$\boldsymbol{\sigma}_k = \boldsymbol{Q}'_k \boldsymbol{\varepsilon}^0 + z\boldsymbol{Q}'_k \boldsymbol{\kappa}^0, \qquad z_{k-1} \leq z \leq z_k. \tag{4.43}$$

The normal forces per unit length N_x,N_y and the shear force N_{xy} per unit length are directed in-plane. These forces per unit length are related to the stress at a cross section of a ply by:

$$\begin{aligned} (N_x)_k &= \int_{z_{k-1}}^{z_k} (\sigma_x)_k \, dz, \\ (N_y)_k &= \int_{z_{k-1}}^{z_k} (\sigma_y)_k \, dz, \\ (N_{xy})_k &= \int_{z_{k-1}}^{z_k} (\tau_{xy})_k \, dz. \end{aligned} \tag{4.44}$$

The total forces per unit length in the laminate are found by summation over the individual plies, i.e.:

$$\begin{aligned} N_x &= \sum_{k=1}^{n} \int_{z_{k-1}}^{z_k} (\sigma_x)_k \, dz, \\ N_y &= \sum_{k=1}^{n} \int_{z_{k-1}}^{z_k} (\sigma_y)_k \, dz, \\ N_{xy} &= \sum_{k=1}^{n} \int_{z_{k-1}}^{z_k} (\tau_{xy})_k \, dz. \end{aligned} \tag{4.45}$$

Or, more compact:

$$\boldsymbol{N} = \sum_{k=1}^{n} \int_{z_{k-1}}^{z_k} \boldsymbol{\sigma}_k \, dz. \tag{4.46}$$

Analogously, the bending and torsional moments per unit length are found by:

$$\begin{aligned} M_x &= \sum_{k=1}^{n} \int_{z_{k-1}}^{z_k} (\sigma_x)_k \, z \, dz, \\ M_y &= \sum_{k=1}^{n} \int_{z_{k-1}}^{z_k} (\sigma_y)_k \, z \, dz, \\ M_{xy} &= \sum_{k=1}^{n} \int_{z_{k-1}}^{z_k} (\tau_{xy})_k \, z \, dz. \end{aligned} \tag{4.47}$$

Or, more compact:

$$\boldsymbol{M} = \sum_{k=1}^{n} \int_{z_{k-1}}^{z_k} \boldsymbol{\sigma}_k \, z \, dz. \tag{4.48}$$

With Eq.(4.43) it is found that the total forces and moments per unit length are:

$$\begin{aligned} \boldsymbol{N} &= \sum_{k=1}^{n} \int_{z_{k-1}}^{z_k} \boldsymbol{Q}'_k \boldsymbol{\varepsilon}^0 + z \boldsymbol{Q}'_k \boldsymbol{\kappa}^0 \, dz = \left(\sum_{k=1}^{n} (z_k - z_{k-1}) \boldsymbol{Q}'_k \right) \boldsymbol{\varepsilon}^0 + \left(\frac{1}{2} \sum_{k=1}^{n} (z_k^2 - z_{k-1}^2) \boldsymbol{Q}'_k \right) \boldsymbol{\kappa}^0, \\ \boldsymbol{M} &= \sum_{k=1}^{n} \int_{z_{k-1}}^{z_k} z \boldsymbol{Q}'_k \boldsymbol{\varepsilon}^0 + z^2 \boldsymbol{Q}'_k \boldsymbol{\kappa}^0 \, dz = \left(\frac{1}{2} \sum_{k=1}^{n} (z_k^2 - z_{k-1}^2) \boldsymbol{Q}'_k \right) \boldsymbol{\varepsilon}^0 + \left(\frac{1}{3} \sum_{k=1}^{n} (z_k^3 - z_{k-1}^3) \boldsymbol{Q}'_k \right) \boldsymbol{\kappa}^0. \end{aligned} \tag{4.49}$$

Now define the extensional stiffness matrix $\mathbf{A}$ as

$$\mathbf{A} = \sum_{k=1}^{n} (z_k - z_{k-1}) \boldsymbol{Q}'_k, \tag{4.50}$$

the coupling stiffness matrix $\mathbf{B}$ as

$$\mathbf{B} = \frac{1}{2} \sum_{k=1}^{n} (z_k^2 - z_{k-1}^2) \boldsymbol{Q}'_k \tag{4.51}$$

and the bending stiffness matrix $\mathbf{D}$ as

$$\mathbf{D} = \frac{1}{3} \sum_{k=1}^{n} (z_k^3 - z_{k-1}^3) \boldsymbol{Q}'_k. \tag{4.52}$$

The last three equations form a system that governs the response of a laminate to forces and moments. To illustrate:

$$\begin{bmatrix} \mathbf{N} \\ \mathbf{M} \end{bmatrix} = \begin{bmatrix} \mathbf{A} & \mathbf{B} \\ \mathbf{B} & \mathbf{D} \end{bmatrix} \begin{bmatrix} \boldsymbol{\varepsilon}^0 \\ \boldsymbol{\kappa}^0 \end{bmatrix} \tag{4.53}$$

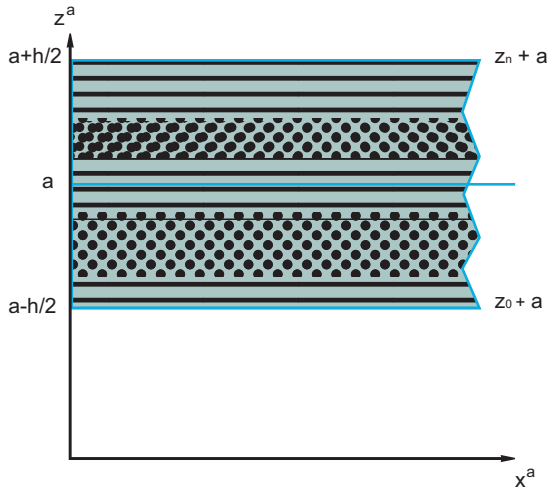

Figure 4.6: Schematic representation of a laminate with distance a offset between the midplane and the coordinate system

With the symmetric properties of $\mathbf{Q}'_k$ it is straightforward that matrices $\mathbf{A}$,$\mathbf{B}$ and $\mathbf{D}$ are also symmetric. Therefore the system can be written as:

$$\begin{bmatrix} \mathrm{N_x} \\ \mathrm{N_y} \\ \mathrm{N_{xy}} \\ \mathrm{M_x} \\ \mathrm{M_y} \\ \mathrm{M_{xy}} \end{bmatrix} = \begin{bmatrix} \mathrm{A_{11}} & \mathrm{A_{12}} & \mathrm{A_{13}} & \mathrm{B_{11}} & \mathrm{B_{12}} & \mathrm{B_{13}} \\ & \mathrm{A_{22}} & \mathrm{A_{23}} & & \mathrm{B_{22}} & \mathrm{B_{23}} \\ & & \mathrm{A_{33}} & & & \mathrm{B_{33}} \\ & & & \mathrm{D_{11}} & \mathrm{D_{12}} & \mathrm{D_{13}} \\ & & & & \mathrm{D_{22}} & \mathrm{D_{23}} \\ & & & & & \mathrm{D_{33}} \end{bmatrix} \begin{bmatrix} \varepsilon_x^0 \\ \varepsilon_y^0 \\ \gamma_{xy}^0 \\ \kappa_x^0 \\ \kappa_y^0 \\ \kappa_{xy}^0 \end{bmatrix}. \tag{4.54}$$

An inverted expression of the system can be produced when there are no singularities. The strains and curvatures are in this case equal to:

$$\begin{aligned} \boldsymbol{\varepsilon}^0 &= (\mathbf{A} - \mathbf{B}\mathbf{D}^{-1}\mathbf{B})^{-1}\mathbf{N} + (\mathbf{B} - \mathbf{D}\mathbf{B}^{-1}\mathbf{A})^{-1}\mathbf{M}, \\ \boldsymbol{\kappa}^0 &= (\mathbf{B} - \mathbf{A}\mathbf{B}^{-1}\mathbf{D})^{-1}\mathbf{N} + (\mathbf{D} - \mathbf{B}\mathbf{A}^{-1}\mathbf{B})^{-1}\mathbf{M}. \end{aligned} \tag{4.55}$$

Again, this is a system of equations, hence:

$$\begin{bmatrix} \boldsymbol{\varepsilon}^0 \\ \boldsymbol{\kappa}^0 \end{bmatrix} = \begin{bmatrix} \mathbf{a} & \mathbf{b} \\ \mathbf{b}^T & \mathbf{d} \end{bmatrix} \begin{bmatrix} \mathbf{N} \\ \mathbf{M} \end{bmatrix} \tag{4.56}$$

It is important to mention that the CLPT can be formulated such that the reference plane, which was the laminate midplane in the treated case, can have an offset of a to the midplane.

In such a situation, as illustrated in Fig.(4.6), Eq.(4.46) and (4.48) change in:

$$\boldsymbol{N}^a = \sum_{k=1}^{n} \int_{a-z_{k-1}}^{a+z_k} \boldsymbol{\sigma}_k \, dz^a = \sum_{k=1}^{n} \int_{z_{k-1}}^{z_k} \boldsymbol{\sigma}_k \, dz = \boldsymbol{N}, \tag{4.57}$$

$$\boldsymbol{M}^a = \sum_{k=1}^{n} \int_{a-z_{k-1}}^{a+z_k} \boldsymbol{\sigma}_k \, z^a \, dz^a = \sum_{k=1}^{n} \int_{z_{k-1}}^{z_k} \boldsymbol{\sigma}_k \, (a+z) \, dz = \boldsymbol{M} + a\boldsymbol{N}. \tag{4.58}$$

Furthermore, the strain description throughout the laminate simply becomes

$$\boldsymbol{\varepsilon} = \boldsymbol{\varepsilon}^a + z\boldsymbol{\kappa}^a, \tag{4.59}$$

where the ^{a} represents strain and curvature changes at the reference plane. Multiplication with the reduced stiffness matrix ultimately results in

$$\begin{bmatrix} \mathbf{N}^a \\ \mathbf{M}^a \end{bmatrix} = \begin{bmatrix} \mathbf{A}^a & \mathbf{B}^a \\ \mathbf{B}^a & \mathbf{D}^a \end{bmatrix} \begin{bmatrix} \boldsymbol{\varepsilon}^a \\ \boldsymbol{\kappa}^a \end{bmatrix} \tag{4.60}$$

where the translated stiffness matrices are:

$$\begin{aligned} \mathbf{A}^a &= \mathbf{A}\,, \\ \mathbf{B}^a &= \mathbf{B} + a\mathbf{A}\,, \\ \mathbf{D}^a &= \mathbf{D} + 2a\mathbf{B} + a^2\mathbf{A}\,. \end{aligned} \tag{4.61}$$

Notice that change in reference plane does not affect the extensional stiffness matrix $\mathbf{A}$.
A shortcoming in the CLPT is the absence of out of plane shear effects, deformations are solely caused by the internal bending resultants. Especially for sandwich structures these effects cannot be neglected. This theory over-estimates the stiffness of such a structure. The first order shear deformation theory (FSDT) includes the effect of transverse shear deformations. With the assumption that the displacement components are expanded in series of powers of the thickness coordinate z [35]. For an N-th order theory, the displacement u can be written as

$$u(x,y,z) = u^0(x,y) + \sum_{n=1}^{N} z^n {\theta_x}^{(n)}(x,y)\,, \tag{4.62}$$

note that all coordinates refer to the midplane and the coefficients ${\theta_x}^{(n)}(x,y)$ are

$${\theta_x}^{(n)}(x,y) = \left.\frac{d^n u}{dz^n}\right|_{z=0} \quad \text{for } n = 0, 1, 2, ... \tag{4.63}$$

By doing the same for v, the displacements are found for $(N = 1)$ i.e. first order:

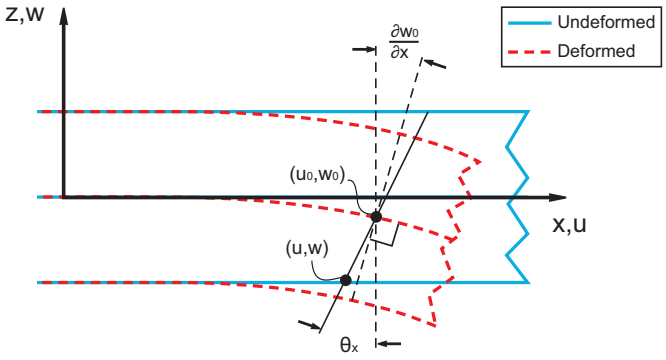

Figure 4.7: Deformation of a plate according to the FSDT

$$
\begin{aligned}
u(x,y,z) &= u^0(x,y) + z\theta_x(x,y),\\
v(x,y,z) &= v^0(x,y) + z\theta_y(x,y),\\
w(x,y,z) &= w^0(x,y).
\end{aligned}
\tag{4.64}
$$

One can clearly see from the equations and Fig.(4.7) that the shearing angle θ_i is assumed to be constant in the z-direction. The principle of minimum total potential energy can be used to find five equilibrium equations in terms of u^0, v^0, w^0, θ_x and θ_y. The expressions for the strains are for this first order theory:

$$
\begin{aligned}
\varepsilon_x &= \frac{\partial u^0}{\partial x} + z\frac{\partial \theta_x}{\partial x},\\
\varepsilon_y &= \frac{\partial v^0}{\partial y} + z\frac{\partial \theta_y}{\partial y},\\
\varepsilon_z &= 0,\\
\gamma_{yz} &= \frac{\partial w_0}{\partial y} + \theta_y,\\
\gamma_{xz} &= \frac{\partial w_0}{\partial x} + \theta_x,\\
\gamma_{xy} &= \frac{\partial u^0}{\partial y} + \frac{\partial v^0}{\partial x} + z\left(\frac{\partial \theta_y}{\partial x} + \frac{\partial \theta_x}{\partial y}\right).
\end{aligned}
\tag{4.65}
$$

The extensional strains and in-plane shear strain of the mid-plane are the same as in Eq.(4.26). The definitions for the curvatures changes, i.e.:

$$
\begin{aligned}
\kappa_x &= \frac{\partial \theta_x}{\partial x},\\
\kappa_y &= \frac{\partial \theta_y}{\partial y},\\
\kappa_{xy} &= \frac{\partial \theta_x}{\partial y} + \frac{\partial \theta_y}{\partial x}.
\end{aligned}
\tag{4.66}
$$

$$\begin{bmatrix} \mathrm{N_x} \\ \mathrm{N_y} \\ \mathrm{N_{xy}} \\ \mathrm{M_x} \\ \mathrm{M_y} \\ \mathrm{M_{xy}} \end{bmatrix} = \begin{bmatrix} \mathrm{A_{11}} & \mathrm{A_{12}} & \mathrm{A_{13}} & \mathrm{B_{11}} & \mathrm{B_{12}} & \mathrm{B_{13}} \\ & \mathrm{A_{22}} & \mathrm{A_{23}} & & \mathrm{B_{22}} & \mathrm{B_{23}} \\ & & \mathrm{A_{33}} & & & \mathrm{B_{33}} \\ & & & \mathrm{D_{11}} & \mathrm{D_{12}} & \mathrm{D_{13}} \\ & & & & \mathrm{D_{22}} & \mathrm{D_{23}} \\ & & & & & \mathrm{D_{33}} \end{bmatrix} \begin{bmatrix} \varepsilon_x^0 \\ \varepsilon_y^0 \\ \gamma_{xy}^0 \\ \kappa_x \\ \kappa_y \\ \kappa_{xy} \end{bmatrix}. \tag{4.67}$$

The forces and moments per unit length in this equation as functions of the ply stresses are already elaborated in Eq.(4.45) and (4.47), respectively. The transverse shear forces per unit length due to the transverse shears are:

$$\begin{bmatrix} V_x \\ V_y \end{bmatrix} = \begin{bmatrix} \tilde{S}_{11} & \tilde{S}_{12} \\ \tilde{S}_{21} & \tilde{S}_{22} \end{bmatrix} \begin{bmatrix} \gamma_{xz} \\ \gamma_{yz} \end{bmatrix} \tag{4.68}$$

Where $\tilde{\mathbf{S}}$ is the transverse shear stiffness matrix. As a function of stress, the transverse forces per unit length (V_x, V_y) are given by the integrals:

$$\begin{aligned} V_x &= \sum_{k=1}^{n} \int_{z_{k-1}}^{z_k} (\tau_{xz})_k \, dz, \\ V_y &= \sum_{k=1}^{n} \int_{z_{k-1}}^{z_k} (\tau_{yz})_k \, dz. \end{aligned} \tag{4.69}$$

Or, more compact:

$$\boldsymbol{V} = \sum_{k=1}^{n} \int_{z_{k-1}}^{z_k} \boldsymbol{\tau}_k \, dz. \tag{4.70}$$

Because of the assumption that all layers behave in the same manner, the equivalent single layer (ESL) theory, a sandwich material is can be described even more accurate. Multi-layer theories are developed to solve this problem. For the sake of briefness these are not treated in the present work.

4.1.3 Lay-up guidelines

In a search for an actual laminate it is important to look at existing guidelines. NASA reviewed design guidelines for composite laminates [36]. Because of the large amount of relevancy in this work, the most appropriate guidelines concerning the present thesis are treated in the next.

1.Design for uncoupled membrane and bending response
In 4.1.2 the coupling stiffness matrix **B** is introduced. For a laminate, this matrix governs the coupling between membrane and bending response (see Eq.4.60). In practice this means that membrane loading results in bending and bending moments induce membrane strains. These coupling effects increase the complexity of the laminate behavior. In most practical cases, a zero coupling stiffness matrix is desired [30]. Furthermore, uncoupling laminate bending and membrane response also eliminates warping due to changes in temperature [36]. Hence the relation

$$\mathbf{B} = \frac{1}{2}\sum_{k=1}^{n}(z_k^2 - z_{k-1}^2)\boldsymbol{Q}'_k = 0 \tag{4.71}$$

has to be satisfied. This uncoupled state of the laminate can be obtained by a symmetric lay-up with respect to the middle surface. This is proved in the following for a laminate with n plies: Let the laminate be defined as illustrated in Fig.(4.5). Furthermore, for two identical and equal orientated plies of the same thickness, located oppositely with respect to the laminate midplane (in the following referred to as a symmetric pair), Eq.(4.71) can be obtained. First, because of the equality in orientation and engineering properties of each ply pair, the transformed reduced stiffness matrix $\boldsymbol{Q}'$ is equal. For n layers this means that

$$\boldsymbol{Q}'_k = \boldsymbol{Q}'_{n+1-k} \tag{4.72}$$

is satisfied. For the z-coordinate a similar equation is found, because of the geometric symmetry:

$$\begin{aligned} z_k &= -z_{n-k}\,, \\ z_{k-1} &= -z_{n+1-k}\,. \end{aligned} \tag{4.73}$$

These equalities result in

$$z_k^2 - z_{k-1}^2 = z_{n-k}^2 - z_{n+1-k}^2 = -(z_{n+1-k}^2 - z_{n-k}^2). \tag{4.74}$$

With this result it easily seen that summation of the two plies in a symmetric pair result in a zero coupling stiffness matrix **B**. Consequently, for a symmetric lay-up Eq.(4.71) is satisfied.

2. Design for balanced laminates
Balance in a laminate is obtained when the angle plies ($+\theta$ or $-\theta$), other than 90° and 0°, only occur in $\pm\theta$ pairs in the lay-up. The individual $+\theta$ and $-\theta$ layers are not necessarily adjacent to each other [31], but as the balanced laminate has to be symmetric about the mid-plane there

will be two $\pm\theta$ pairs per angle ply θ required. A balanced laminate zeroes the shear extension coupling coefficients in the extensional stiffness matrix A as described in Eq.(4.50). With help from Eq.(4.40) it is found that:

$$\begin{aligned} A_{16} &= \sum_{k=1}^{n} [Q'_{16}]_k (z_k - z_{k-1}) \\ &= \sum_{k=1}^{n} [(Q_{11} - Q_{12} - 2Q_{66})sc^3 + (Q_{12} - Q_{22} + 2Q_{66})s^3c]_k (z_k - z_{k-1}) \,, \\ A_{26} &= \sum_{k=1}^{n} [Q'_{26}]_k (z_k - z_{k-1}) \\ &= \sum_{k=1}^{n} [(Q_{11} - Q_{12} - 2Q_{66})s^3c + (Q_{12} - Q_{22} + 2Q_{66})sc^3]_k (z_k - z_{k-1}) \,, \end{aligned} \tag{4.75}$$

where $c = cos\,\theta$ and $s = sin\,\theta$. Notice that plies in the 0° and 90° direction do not contribute to A_{16} and A_{26}. It is easily observed from Eq.(4.75) that there are only odd powers of $cos\theta$ and $sin\theta$ in the equation and since $cos(\theta) = cos(-\theta)$ and $sin(\theta) = -sin(-\theta)$ the equations A_{16} and A_{26} equal zero for a $\pm\theta$ pair with equal thickness.

It has to be mentioned that the bending-twisting coupling still exists in balanced laminates since D_{16} and D_{26} are always nonzero for symmetric laminates with angle plies other than 0° and 90°. Because the angle plies occur in pairs through the laminate, these coupling coefficients will be relatively small.

3. 10% rule

This guideline has no formal documentation regarding the validity but it is has been followed with great success on a number of production programs [36]. To increase the fiber domination, a laminate should have at least 10% of plies in each of the 0°,±45° and 90° directions. The robustness is increased when this rule is satisfied and unpredicted deviations in load directions are accounted for.

4. The four contiguous ply rule

The interlaminar shear effects that occur at the edges of the laminate can be critical if the number of neighboring UD layers with the same fiber orientation is too large. Also, effects like matrix cracking can occur due to the (now) large influence of the Poisson effect. Stacking not more than four contiguous plies at the same orientation angle prevents these effects.

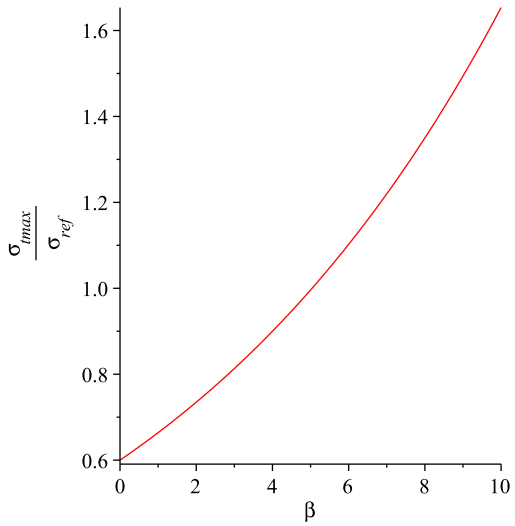

Figure 4.8: Response of the statistical determined tensile strength of an UD composite, with β as a material property.

4.1.4 Composite strength prediction

This section describes the most common used static strength formulae of composites. A composite material shows numerous failure mechanisms, an approach is performed to describe the most important of these.

Fiber failure is one of the most important failure mechanisms of a composite. Fiber failure due to tensile forces is one of the simplest failure mechanisms to identify and quantify, and occurs when the loads applied to a composite structure cause fracture in the fibers [37]. Similar fibers under stress do not all have the same fracture strength nor do they fracture in the same place [38]. Therefore the tensile strength of an UD composite is statistically studied. For instance it has been found on basis of statistical analysis that for commercial E-glass fibers the average of fiber strength is about 1.42 that of the bundle strength [39]. By use of statistical analysis, Dow and Rosen [40] obtained:

$$\sigma_{tmax} = \sigma_{ref} V_f \left(\frac{\sqrt{1-\nu_f}}{\sqrt{\nu_f}} \right)^{-1/2\,\beta} . \tag{4.76}$$

The parameter σ_{ref} indicates the reference tensile strength level and β is a statistical parameter in the Weibull distribution of fiber strength ($\beta = 7.7$ for E-Glass) [38]. The response of Eq.(4.76) is plotted in Fig.(4.8).

The fibers in a composite are the load carrying constituents, both in tension as in compression. This capability is only possible due to fiber stabilization induced by the matrix. Since this stabilization is not always performed in an ideal way, fiber micro buckling (Fig.(4.9)) can occur in a composite under compression [41]. Fiber buckling can also take place when thermal shrinkage is developed during the cure process of a composite. The author is aware of this but these effects are beyond the scope of the present thesis. In composites with very low fiber volume

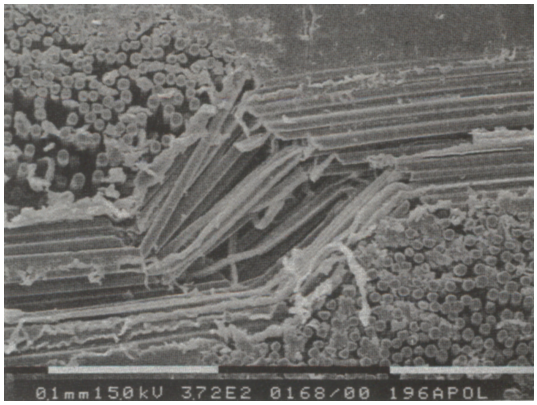

Figure 4.9: SEM-capture of fiber buckling due to compressive loading, adapted from [41]

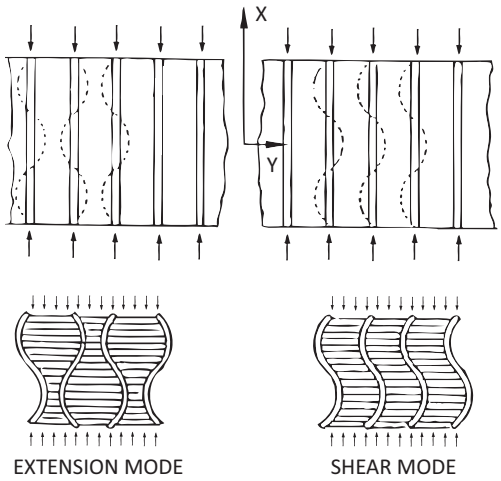

Figure 4.10: Buckling modes of fibers under compression, adapted from [38]

content, fiber buckling may occur even when the matrix stresses are in the elastic range. But for higher volume fractions ($V_f > 0.4$) fiber buckling is generally preceded by matrix yield and/or constituent debonding and matrix microcracking [38].

There are two modes in fiber buckling: The (symmetric) extension mode and the (asymmetric) shear mode. A schematic drawing of these modes is shown in Fig.(4.10). The extension mode buckling of the fiber is characterized by fibers deforming out-of-phase with one another. The matrix compressed and extended transverse to the fibers. This is only possible when the inter-fiber distance is quite large, i.e. for a small fiber volume fraction (V_f) [38]. The more common fiber buckling mode is the shear mode. Here the matrix shows shear strain due to the in-phase displacement of the fibers. In this mode the initial separation of the fibers is unchanged. The Rosen theory describes the two modes of buckling. The main assumption for this theory is that the fibers are regarded as being much stiffer than the matrix ($G_f >> G_m$). Hence fiber-shearing

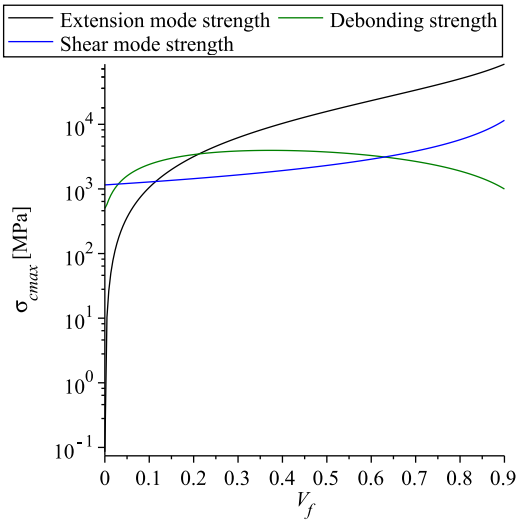

Figure 4.11: The longitudinal compressive strength of a composite for debonding, extension mode and shear mode failure

deformations are negligible [38]. In the following the Rosen theory is elaborated for extension and shear mode buckling. For extension mode buckling the critical stress in the composite is:

$$\sigma_{cmax} = 2\,V_f \sqrt{\frac{V_f E_m E_f}{3(1-V_f)}}. \tag{4.77}$$

For shear mode buckling the critical stress in the composite is:

$$\sigma_{cmax} = \frac{G_m}{1-V_f}. \tag{4.78}$$

The observation that transverse splitting or debonding might be the initiating failure event is formulated in [38]. The expression for the maximum composite compressive strength for a debonding type of failure is:

$$\sigma_{cmax} = \frac{\left(E_f V_f + E_m\left(1-V_f\right)\right)\left(1-\sqrt[3]{V_f}\right)\varepsilon_{mu}}{\nu_f V_f + \nu_m\left(1-V_f\right)}. \tag{4.79}$$

The value of the maximum compressive strength is displayed in Fig.(4.11) for Eq.(4.77),(4.78) and (4.79). It is important to note that typical values for the composite are used, being $E_f = 250\,GPa$, $E_m = 3\,GPa$, $\nu_f = 0.4$, $\nu_m = 0.3$ and the maximum strain of the matrix $\varepsilon_{mu} = 0.05$. Generally, the properties in strength in the fiber direction for UD composites are good. However, for the transverse direction the properties are matrix dominated. In this case it is the matrix that carries the main load. In this case the fibers can be seen as defects in the matrix. Increasing V_f means the addition of more defects in the matrix, which has a negative effect on the transverse strength of the UD. To illustrate that [38] describes the transverse strength in tension for an

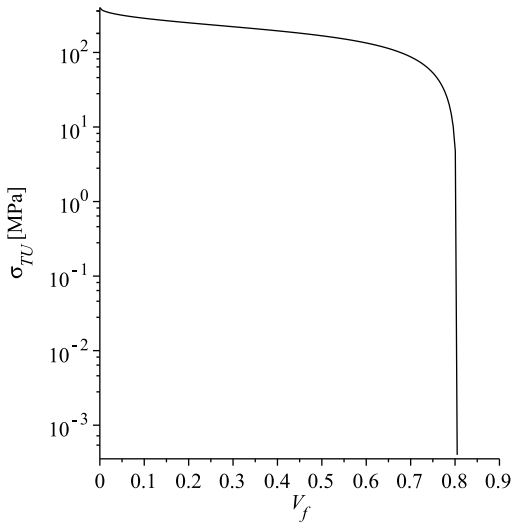

Figure 4.12: The transverse strength of an UD composite with an increasing fiber volume fraction V_f.

UD ply by:

$$\sigma_{TU} = \frac{\sigma_{mu}}{S}. \tag{4.80}$$

In this equation, σ_{mu} is the strength of the matrix in a tensile state and S is the strength reduction factor. The latter is described by:

$$S = \frac{1 - V_f\left(1 - \frac{E_m}{E_f}\right)}{1 - \sqrt{\frac{4\,V_f}{\pi}}\left(1 - \frac{E_m}{E_f}\right)} \tag{4.81}$$

It is important to show how V_f affects the transverse strength σ_{TU}. From Fig.(4.12) it can be observed that especially for high fiber volume contents (V_f) the transverse strength is diminished. The material properties to create this figure are $E_f = 250\,GPa$, $E_m = 3\,GPa$, $\nu_f = 0.4$ and $\sigma_{mu} = 400MPa$. Of course, in a proper laminate, the transverse strength can be made fiber dominated.

For compression, the same effect as the treated transverse tensile strength is active. The failure mechanism for this type of strength is mainly based on matrix shear effects that occur at an angle of (around) 45° relative to the axis of compression [30].

4.1.5 Sandwich strength

Since a general sandwich structure consists of a compliant core material between two strong and stiff skin layers, the mechanical complexity increases with respect to the previous. Apart from of the skins, the core and bonding material can show failure effects. In the next an approach to describe the most common failure mechanisms is elaborated. A division is made between global

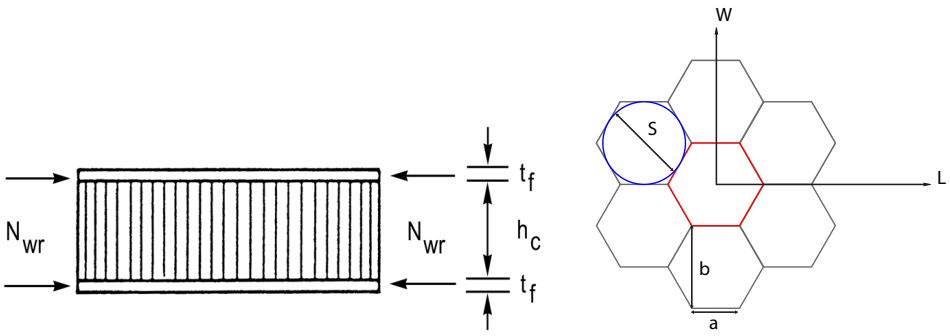

(a) (b)

Figure 4.13: Loads and dimensions of a sandwich plate (a), from [42]. The directions and dimensions for a honeycomb core are indicated in (b)

and local failure modes.

For the global modes, failure of the facings can occur. This event can be the result of e.g. insufficient thickness for the applied loads. Also, the core can show failure with shear dominated failure as the most common mechanism. When the adhesive has insufficient strength in shear or tension debonding occurs.

An important local failure mechanism is face wrinkling. This can for instance occur if a sandwich panel is subjected to out-of-plane bending and/or in-plane compression. The face wrinkling stress can be found by means of the solution for a plate on a elastic foundation. For isotropic cores this stress [38] is

$$\sigma_{fw} = Q \sqrt[3]{\frac{E_c E_f G_c}{(1-\nu_f^2)}}\,, \tag{4.82}$$

for orthotropic cores, such as honeycombs, the face wrinkling stress [38] is found by

$$\sigma_{fw} = Q \sqrt{\frac{E_c E_f t_f}{(1-\nu_f^2) t_c}}\,. \tag{4.83}$$

In these equations, E_f refers to the Young's modulus of the face in the compressive direction and $\nu_f = \sqrt{\nu_x \nu_y}$ is the Poisson's modulus. For the isotropic and orthotropic core the Young's modulus is E_c. Note that for the latter the modulus refers to the through-the-thickness direction. The t_f and t_c refer to the face and core thickness, respectively, as indicated in Fig.(4.13a). Because the equations are related to perfect plates, the factor $Q < 1$ has to be applied for realistic imperfect sandwich structures.

For honeycomb and other discontinuously face supporting cores, a more local buckling effect can occur. This so-called dimpling of the face is a buckling effect that is dependent of the

unsupported area of the face. With the assumption that the face can be modeled as a simply supported plate with orthotropic properties, the "Norris" formula [38] can be used to calculate the critical buckling stress:

$$\sigma_d = \frac{K_d E_x}{(1 - \nu_{xy}\nu_{yx})} \left(\frac{t_f}{S}\right)^2 . \tag{4.84}$$

With K_d as an empirical factor, which is usually 2 to 2.25. The characteristic plate length S, i.e. the cell size, see Fig.(4.13b) is for a honeycomb defined as the diameter of the inscribed circle.

Because this "Norris" formula is conservative with respect to the buckling stress, an improved (but still conservative) formula [38] for the dimpling stress is developed:

$$\sigma_d = \frac{K_d D_{22}}{t_f b^2} , \tag{4.85}$$

where

$$K_d = \pi^2 \left[\frac{D_{11}}{D_{22}} \left(\frac{b}{a}\right)^2 + \frac{8}{3}\frac{(D_{12} + 2D_{66})}{D_{22}} + \frac{16}{3}\left(\frac{a}{b}\right)^2\right] . \tag{4.86}$$

The elements D_{ij} belong to the bending stiffness matrix of the face. The dimension of the honeycomb cells i.e. a and b is illustrated in Fig.(4.13b). It is important to note that this formula showed a 15% lower critical dimpling stress than in experiments, which is indeed conservative. Further, b is equal to the cell size S which is used earlier.

4.1.6 Failure criteria

For composite materials it is appropriate to describe failure with a so-called failure function. As a yield criterion for metals, this failure function represents a surface in stress or strain space. Sometimes, this surface is described piecewise, this is a result of multiple failure criterion each capturing a specific failure mechanism of the composite. The description of all failure mechanisms of a composite is beyond the scope of the present thesis. However, the most important failure mechanisms in a composite are briefly described before, this section describes the corresponding failure functions.

The (static) stress state of an isotropic material can be described as a point in a six-dimensional stress space. Here, the origin of the space is equivalent to the unstressed condition. Therefore, as the stress state moves further away from the origin, the chance that the material fails will increase. The purpose of a failure criterion is to describe a surface in this stress space which envelopes the 'safe area' where the material is undamaged. If a stress point is located outside this envelope, the function will indicate material failure. At first, the failure criteria in a plane-stress space are treated. Because of the (assumed) in plane loaded orthotropic UD composite ply the components σ_{33}, σ_{13} and σ_{23} are considered to be equal to zero.
The most simplistic failure criteria are the independent criteria. The main assumption for these criteria is that there is no interaction between the six stress components. For each of the components there is a lower and upper bound, independent from the state of the other components.

The maximum stress criterion is described by:

$$\begin{aligned} \sigma_{11} &= X_t \text{ or } X_c\,, \\ \sigma_{22} &= Y_t \text{ or } Y_c\,, \\ |\sigma_{12}| &= Q\,, \end{aligned} \tag{4.87}$$

where X_t and X_c are the composite tensile and compressive strengths in 1-direction, respectively. Y_t and Y_c refer to the strengths transverse direction and Q is the shear strength. It is important to note that failure is said to occur if any one of the stresses σ_{11}, σ_{22} and σ_{12} reaches the allowable value in Eq.(4.88).

The second independent failure criterion is described by strains. The so called maximum strain criterion. The criterion is described by:

$$\begin{aligned} \varepsilon_{11} &= \varepsilon_{X_t} \text{ or } \varepsilon_{X_c}, \\ \varepsilon_{22} &= \varepsilon_{Y_t} \text{ or } \varepsilon_{Y_c}, \\ |\varepsilon_{12}| &= \varepsilon_{Q}. \end{aligned} \tag{4.88}$$

This criterion has the same format as the maximum stress criterion, i.e. strains become critical when reaching maximal strains. Both the maximum stress and strain criteria can be for instance used as an indication of fiber failure, but due to the non-interactive their correspondence with the true nature of failure is limited. Note that the tensorial description is used for the stresses and strains.

The simple Puck criterion separates the fiber and matrix failure. The former is assumed to originate solely by σ_{11} (with the fibers aligned in the 1-direction), the latter from a combination of σ_{22} and σ_{12}. To illustrate, the simple Puck criterion is given by:

$$\begin{aligned} &\sigma_{11} = X_1 \text{ or } X_c, \\ &\text{or } \left(\frac{\sigma_{22}}{Y_t}\right)^2 + \left(\frac{\sigma_{12}}{Q}\right)^2 = 1, \\ &\text{or } \left(\frac{\sigma_{22}}{Y_c}\right)^2 + \left(\frac{\sigma_{12}}{Q}\right)^2 = 1. \end{aligned} \tag{4.89}$$

The part related to matrix failure is plotted in Fig.(4.14). The figure is created with the maximum transverse tensile and compressive strength $Y_t = 200$ and $Y_c = 450$ and shear strength $Q = 100$. In the modified Puck criterion describes the matrix failure as a single ellipse. This is more convenient when there is a large difference between the tensile and compressive strength,

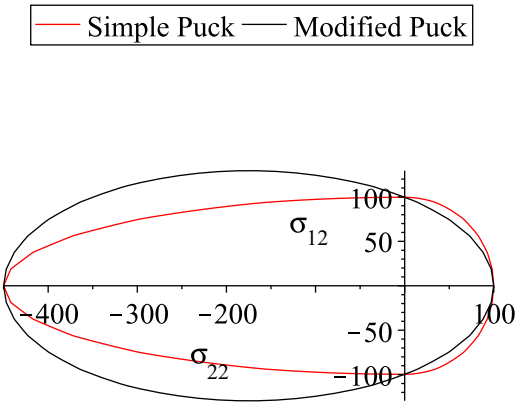

Figure 4.14: The simple and modified Puck matrix failure criteria.

according to [38]. The modified Puck criterion for both fiber failure and matrix failure yields:

$$\begin{aligned} &\sigma_{11} = X_1 \text{ or } X_c, \\ &\text{or } \frac{{\sigma_{22}}^2}{Y_t Y_c} + \sigma_{22}\left(\frac{1}{Y_t} - \frac{1}{Y_c}\right) + \left(\frac{\sigma_{12}}{Q}\right)^2 = 1 \end{aligned} \tag{4.90}$$

The modified Puck criterion for matrix failure is shown in Fig.(4.14). The same strengths are used as the simple Puck criterion, in order to plot this matrix failure criterion.

An anisotropic generalization of the von Mises criteria, with taking interaction into account between different components of the stress tensor, are the quadratic criteria. The most used quadratic failure criterion is the Tsai-Wu [43] criterion, that is, for plane stress described by

$$\boldsymbol{\sigma}^T : \mathbf{F} : \boldsymbol{\sigma} + \mathbf{f} : \boldsymbol{\sigma} = 1\,, \tag{4.91}$$

where $\boldsymbol{\sigma}$ is the Cauchy stress tensor and $\mathbf{F}$ and $\mathbf{f}$ are the symmetric strength tensors of fourth and second order, respectively. In a plane-stress situation the criterion can be written as

$$F_{11}\sigma_{11}^2 + F_{22}\sigma_{22}^2 + 2F_{12}\sigma_{11}\sigma_{22} + F_{66}\sigma_{12}^2 + f_1\sigma_{11} + f_2\sigma_{22} = 1\,, \tag{4.92}$$

with

$$F_{11} = \frac{1}{X_t X_c}, \quad F_{22} = \frac{1}{Y_t Y_c}, \quad F_{66} = \frac{1}{Q^2}, \quad F_{12} = F_{12}^* \sqrt{F_{11}F_{22}} \tag{4.93}$$

and

$$f_1 = \frac{1}{X_t} + \frac{1}{X_c}, \quad f_2 = \frac{1}{Y_t} + \frac{1}{Y_c}\,, \tag{4.94}$$

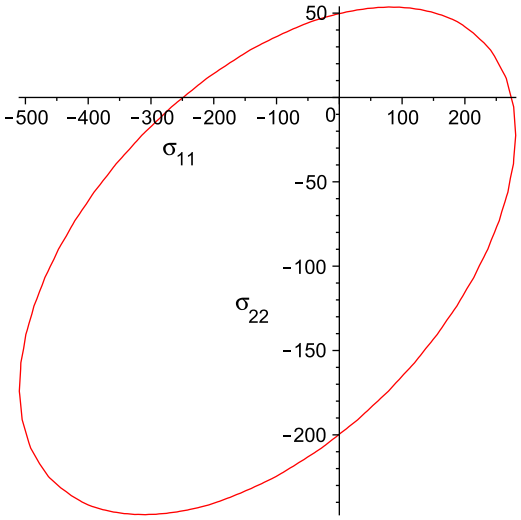

Figure 4.15: The Tsai-Wu failure function in stress-space.

where F_{12}^* is a coefficient, mainly considered to be empiric but by default taken as $F_{12}^* = -0.5$. To give an idea of the criterion, the contour is plotted for a typical CFRP UD ply (X_t = 275MPa, X_c = 250MPa, Y_t = 50MPa, Y_c = 200MPa, S = 50MPa) in Fig.(4.15). Notice the strength corresponding at the contour-axis intersections. This failure envelope should be, as can be verified from the figure, a convex elliptical contour that describes the material strengths accurately. However, this failure criterion does not distinguish the different failure mechanisms of the composite ply but is a accurate fit of the experimental values.

4.1.7 Environmental effects

During operation the pressure hull can suffer from various environmental effects such as oxidation, moisture absorption and temperature related degradation. Although widely applied in marine structures, moisture absorption in the matrix of a composite can cause critical material degradation. Moisture acts like a plasticizer, which softens the matrix and lowers the glass transition temperature [38]. Ultimately, the matrix dominated properties of the composite, such as (interlaminar) shear strength and compression strength can be affected by the absorption. Also, the stiffness of the composite can be altered. It is found [38] that the effect of degradation for the initial Young's modulus given by

$$E_c = V_f E_f + V_m E_m \,, \tag{4.95}$$

can be described with the rule of mixtures:

$$E_c^* = V_f E_f + V_m E_m^* - \alpha E_f V_f W_c \,, \tag{4.96}$$

where E is the Young's modulus with subscript c, f, m denoting the composite, fiber and matrix. The asterisk (*) is used to indicate the degraded entities. The same notation is used for the volume fraction V and α is an empirical constant belonging to the type of reinforcement and coupling agent and W is the composite moisture content by weight. It is found that this formula, rewritten for a [0/90] laminate, correlates very closely to experimental results with $\alpha = 3$ for carbon fiber.

As mentioned already, the initial properties in strength are also degraded due to moisture effects. In [38] an formula is mentioned that describes this retention, i.e.

$$\sigma_c^* = \sigma_f \left(V_f + V_m \beta \frac{E_m^*}{E_f} \right) - \alpha \sigma_f V_f W_c \,, \tag{4.97}$$

where σ denotes the strengths either for the composite or the constituents and β is an empirical factor belonging to the coupling agent and the type of reinforcement.

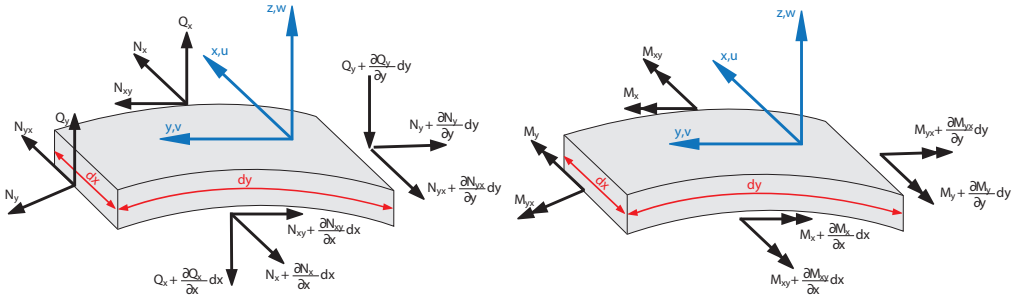

Figure 4.16: A differential cylindrical shell element with force (a) and moment equilibrium (b)

4.2 Buckling of composite cylinders

Analogous to the conventional pressure hull, the collapse of a pressure hull is mainly related to material failure and buckling effects. In the next a linearized buckling theory is elaborated that describes buckling of externally pressurized shells. The equilibrium equations concerning the forces and moments in a differential cylindrical shell element as graphically illustrated in Fig.(4.16) of the Flügge model [44] are

$$\begin{aligned}
\frac{\partial N_x}{\partial x}+\frac{\partial N_{xy}}{\partial y}-p\left(r\frac{\partial^2 u}{\partial y^2}+\frac{r}{2}\frac{\partial^2 u}{\partial x^2}-\frac{\partial w}{\partial x}\right) &= 0\,,\\
\frac{\partial N_{xy}}{\partial x}+\frac{\partial N_y}{\partial y}+\frac{1}{r}\frac{\partial M_y}{\partial y}+\frac{1}{r}\frac{\partial M_{xy}}{\partial x}-p\left(r\frac{\partial^2 v}{\partial y^2}+\frac{r}{2}\frac{\partial^2 v}{\partial x^2}+\frac{\partial w}{\partial x}\right) &= 0\,,\\
\frac{\partial^2 M_x}{\partial x^2}+2\frac{\partial^2 M_{xy}}{\partial x\partial y}+\frac{\partial^2 M_y}{\partial y^2}-\frac{N_y}{r}-p\left(\frac{\partial u}{\partial x}-\frac{\partial v}{\partial y}+r\frac{\partial^2 w}{\partial y^2}+\frac{r}{2}\frac{\partial^2 w}{\partial x^2}\right) &= 0\,.
\end{aligned} \tag{4.98}$$

In these equations N_i is the acting force per unit length and M_i is the moment per unit length in the i-th direction. The displacements u,v and w refer to the axial, circumferential and radial direction, respectively. It is important to note that the radius r is measured between the axis of symmetry and the the mid-shell surface.
The kinematic relations are

$$\begin{aligned}
\varepsilon_x^0 &= \frac{\partial u}{\partial x}\,, & \varepsilon_y^0 &= \frac{\partial v}{\partial y}+\frac{w}{r}\,, & \gamma_{xy}^0 &= \frac{\partial u}{\partial y}+\frac{\partial v}{\partial x}\,,\\
\kappa_x &= -\frac{\partial^2 w}{\partial x^2}\,, & \kappa_y &= -\frac{\partial^2 w}{\partial y^2}+\frac{w}{r^2}\,, & \kappa_{xy} &= -2\frac{\partial^2 w}{\partial x\partial y}-\frac{1}{r}\frac{\partial u}{\partial y}+\frac{1}{r}\frac{\partial v}{\partial x}\,,
\end{aligned} \tag{4.99}$$

where the superscripted 0 indicates the mid-surface. The proposed solutions for the displacements are

$$\begin{aligned}
u &= U\cos(\alpha x)\cos(\beta y)\,,\\
v &= V\sin(\alpha x)\sin(\beta y)\,,\\
w &= W\sin(\alpha x)\cos(\beta y)\,,
\end{aligned} \tag{4.100}$$

where

$$\begin{aligned} \alpha &= \frac{m\pi}{L}\,, \\ \beta &= \frac{n}{r}\,. \end{aligned} \tag{4.101}$$

In Eq.4.100 the variables U,V and W are the displacement amplitudes. For Eq.4.101 the cylinders length is denoted by L, $m = 1, 2, 3...$ is the number of buckling half-waves in the axial direction and $n = 1, 2, 3...$ is the number of full-waves around the circumference.
If the proposed solution (Eq.4.100) is substituted into the kinematic relations (Eq.4.99) and the result is used in the equilibrium equations, a system of homogeneous equations can be established, i.e:

$$\begin{bmatrix} a_{11} & a_{12} & a_{13} \\ & a_{22} & a_{23} \\ & & a_{33} \end{bmatrix} \begin{bmatrix} U \\ V \\ W \end{bmatrix} = \begin{bmatrix} 0 \\ 0 \\ 0 \end{bmatrix}\,, \tag{4.102}$$

where for a symmetric and balanced laminate with the assumption that the bending twisting terms D_{16} and D_{26} are relatively small compared to other D_{ij} terms:

$$\begin{aligned} a_{11} &= -A_{11}\alpha^2 - A_{66}\beta^2 + pr\beta^2 + \tfrac{1}{2}\,pr\alpha^2\,, \\ a_{12} &= \alpha\,\beta\,\left(A_{12} + A_{66}\right)\,, \\ a_{13} &= \alpha\tfrac{1}{r}\left(A_{12} + pr\right)\,, \\ a_{22} &= -\tfrac{1}{2L^2r^2}\left(2A_{66}m^2\pi^2r^2 + 2A_{22}n^2L^2 + 2D_{66}m^2\pi^2 - 2prn^2L^2 - pr^3m^2\pi^2\right)\,, \\ a_{23} &= -\tfrac{n}{r^4L^2}\left(A_{22}r^2L^2 + D_{12}m^2\pi^2r^2 + D_{22}L^2n^2 + D_{22}L^2 + 2D_{66}m^2\pi^2r^2 - pr^3L^2\right)\,, \\ a_{33} &= -\tfrac{1}{2L^4r^4}(4D_{12}m^2\pi^2n^2L^2r^2 + 2D_{22}n^4L^4 + 8D_{66}m^2\pi^2n^2L^2r^2 + 2D_{11}m^4\pi^4r^4 \\ &\quad + 2D_{12}m^2\pi^2L^2r^2 + 2A_{22}L^4r^2 - 2pr^3L^4n^2 - pr^5L^2m^2\pi^2)\,. \end{aligned} \tag{4.103}$$

The homogeneous system could be abbreviated as:

$$\mathbf{A}\boldsymbol{\delta} = \mathbf{0}\,, \tag{4.104}$$

where the solution of this system for the external pressure p is found when

$$\det \mathbf{A} = 0\,. \tag{4.105}$$

In general, this equation has to be evaluated for a range of m and n in order to identify the lowest buckling pressure. By writing Eq.(4.105) in a polynomial form of pressure p one obtains the following:

$$\det \mathbf{A} = c_3p^3 + c_2p^2 + c_1p + c_0 = 0\,, \tag{4.106}$$

with the constants c_i defined in Appendix D, for the sake of briefness.

4.3 Composite design and weight minimization techniques

A higher level description of a laminate with the use of lamination parameters is given in Section (4.3.1). Furthermore, the utilization of lamination parameters for a laminate optimization is also performed in this section. Optimization of composite laminates in a FE context with these lamination parameters is treated in Section (4.3.2).

4.3.1 Laminate optimization with the use of lamination parameters

As indicated earlier in the treated classical laminate theory in Section (4.1.2), the laminate stiffness matrix governs the relation between the generalized strains and stresses as

$$\left\{ \begin{array}{c} \mathbf{N} \\ \mathbf{M} \end{array} \right\} = \left[\begin{array}{cc} \mathbf{A} & \mathbf{B} \\ \mathbf{B} & \mathbf{D} \end{array} \right] \left\{ \begin{array}{c} \boldsymbol{\varepsilon}^0 \\ \boldsymbol{\kappa} \end{array} \right\}, \tag{4.107}$$

where the in-plane stiffness is $\mathbf{A}$, the coupling stiffness is $\mathbf{B}$ and out-of-plane stiffness is denoted by $\mathbf{D}$. Note that $\mathbf{B} = \mathbf{0}$ for a symmetric lay-up with respect to the midplane. The components of these stiffness tensors can be expressed in lamination parameters ξ and material invariants U as follows:

$$\left\{ \begin{array}{c} A_{11} \\ A_{22} \\ A_{12} \\ A_{66} \\ A_{16} \\ A_{26} \end{array} \right\} = h \left[\begin{array}{ccccc} 1 & \xi_1 & \xi_2 & 0 & 0 \\ 1 & -\xi_1 & \xi_2 & 0 & 0 \\ 0 & 0 & -\xi_2 & 1 & 0 \\ 0 & 0 & -\xi_2 & 0 & 1 \\ 0 & \xi_3/2 & \xi_4 & 0 & 0 \\ 0 & \xi_3/2 & -\xi_4 & 0 & 0 \end{array} \right] \left\{ \begin{array}{c} U_1 \\ U_2 \\ U_3 \\ U_4 \\ U_5 \end{array} \right\}, \tag{4.108}$$

$$\left\{ \begin{array}{c} B_{11} \\ B_{22} \\ B_{12} \\ B_{66} \\ B_{16} \\ B_{26} \end{array} \right\} = \frac{h^2}{4} \left[\begin{array}{ccccc} 0 & \xi_5 & \xi_6 & 0 & 0 \\ 0 & -\xi_5 & \xi_6 & 0 & 0 \\ 0 & 0 & -\xi_6 & 0 & 0 \\ 0 & 0 & -\xi_6 & 0 & 0 \\ 0 & \xi_7/2 & \xi_8 & 0 & 0 \\ 0 & \xi_7/2 & -\xi_8 & 0 & 0 \end{array} \right] \left\{ \begin{array}{c} U_1 \\ U_2 \\ U_3 \\ U_4 \\ U_5 \end{array} \right\}, \tag{4.109}$$

$$\left\{ \begin{array}{c} D_{11} \\ D_{22} \\ D_{12} \\ D_{66} \\ D_{16} \\ D_{26} \end{array} \right\} = \frac{h^3}{12} \left[\begin{array}{ccccc} 1 & \xi_9 & \xi_{10} & 0 & 0 \\ 1 & -\xi_9 & \xi_{10} & 0 & 0 \\ 0 & 0 & -\xi_{10} & 1 & 0 \\ 0 & 0 & -\xi_{10} & 0 & 1 \\ 0 & \xi_{11}/2 & \xi_{12} & 0 & 0 \\ 0 & \xi_{11}/2 & -\xi_{12} & 0 & 0 \end{array} \right] \left\{ \begin{array}{c} U_1 \\ U_2 \\ U_3 \\ U_4 \\ U_5 \end{array} \right\}, \tag{4.110}$$

with the lamination parameters defined as

$$\begin{array}{lcll} \xi_{[1,2,3,4]} & = & \xi^{A}_{[1,2,3,4]} & = & \frac{1}{2}\int_{-1}^{1}[cos(2\theta(\bar{z})), cos(4\theta(\bar{z})), sin(2\theta(\bar{z})), sin(4\theta(\bar{z}))]\ \mathrm{d}\bar{z}, \\ \xi_{[5,6,7,8]} & = & \xi^{B}_{[1,2,3,4]} & = & \int_{-1}^{1}[cos(2\theta(\bar{z})), cos(4\theta(\bar{z})), sin(2\theta(\bar{z})), sin(4\theta(\bar{z}))]\ \bar{z}\,\mathrm{d}\bar{z}, \\ \xi_{[9,10,11,12]} & = & \xi^{D}_{[1,2,3,4]} & = & \frac{3}{2}\int_{-1}^{1}[cos(2\theta(\bar{z})), cos(4\theta(\bar{z})), sin(2\theta(\bar{z})), sin(4\theta(\bar{z}))]\ \bar{z}^2\,\mathrm{d}\bar{z}. \end{array} \tag{4.111}$$

The orientation of the plies is a function of the normalized thickness i.e. $\theta(\bar{z})$. Note that this normalized thickness is $\bar{z} = (2/h)z$. Where h is the thickness and z is the thickness coordinate. The material parameters can be expressed as

$$\begin{array}{lcl} U_1 & = & \left(3Q_{11} + 3Q_{22} + 2Q_{12} + 4Q_{66}\right)/8, \\ U_2 & = & \left(Q_{11} - Q_{12}\right)/2, \\ U_3 & = & \left(Q_{11} + Q_{22} - 2Q_{12} - 4Q_{66}\right)/8, \\ U_4 & = & \left(Q_{11} + Q_{22} + 6Q_{12} - 4Q_{66}\right)/8, \\ U_5 & = & \left(Q_{11} + Q_{22} - 2Q_{12} + 4Q_{66}\right)/8. \end{array} \tag{4.112}$$

In this equation $\mathbf{Q}$ is the reduced stiffness matrix. For an unidirectional ply the indices can be expressed as function of material parameters by

$$\begin{array}{lcl} Q_{11} & = & E_{11}^2/(E_{11} - E_{22}\nu_{12}^2), \\ Q_{22} & = & E_{11}E_{22}/(E_{11} - E_{22}\nu_{12}^2), \\ Q_{12} & = & \nu_{12}Q_{22}, \\ Q_{66} & = & G_{12}. \end{array} \tag{4.113}$$

Where E_{11} and E_{22} correspond to the Young's modulus in the fiber and transverse direction, respectively. Other in-plane properties are ν_{12} which is the Poisson's modulus and G_{12} as the shear modulus.

Originally, the lamination parameters first appeared in the work of Miki [45] and Miki & Sugiyama [46]. Because the lamination parameters are coupled by trigonometric relations, Miki defined feasible regions between some of these parameters. For an orthotropic laminate using two in-plane or out-of-plane lamination parameters he defined the feasible region to be:

$$2(\xi_1^j)^2 - 1 \leq \xi_2^j, \tag{4.114}$$

where $j = A, D$. Fukunaga & Sekine [47] extended these regions to a formulation of the four in-plane or for out-of-plane lamination parameters, i.e:

$$\begin{array}{c} 2(1+\xi_2^2)(\xi_3^j)^2 - 4\xi_1^j\xi_3^j\xi_4^j + (\xi_4^j)^2 - (\xi_2^j - 2(\xi_1^j)^2 + 1)(1 - \xi_2^j) \leq 0\,, \\ (\xi_1^j)^2 + (\xi_3^j)^2 \leq 1\,, \end{array} \tag{4.115}$$

where $j = A, D$. Later, Diaconu et al. [48] derived a feasible region of lamination parameters that describes the connection between in-plane, coupling and out-of-plane lamination parameters:

$$\begin{aligned} 4(\xi_i^A + 1)(\xi_i^D + 1) &\leq (\xi_i^A + 1)^4 + 3(\xi_i^B)^2 \,, \\ 4(\xi_i^A - 1)(\xi_i^D - 1) &\leq (\xi_i^A - 1)^4 + 3(\xi_i^B)^2 \,, \end{aligned} \tag{4.116}$$

where $i = 1, .., 4$. Apart from the previously treated regions, much research is performed on this topic and feasible regions are only known for specific parameters or restrictions of the laminate.

[49] showed the relation between the four lamination parameters governing the laminate stiffness and a method to determine the laminate configurations corresponding to the lamination parameters. Mathematical programming is used to obtain the optimal laminate configurations for a maximum buckling load. In their work they considered a buckling optimization problem of an orthotropic laminated cylindrical shell. Because their work is highly relevant in the light of the present thesis, a similar approach is elaborated in the next.

A generalized symmetric and balanced laminate is considered Section 4.1.3. Because the laminate is symmetric, the **B** coupling stiffness matrix vanishes. This means that the constitutive equation changes into:

$$\left\{ \begin{array}{c} \mathbf{N} \\ \mathbf{M} \end{array} \right\} = \left[\begin{array}{cc} \mathbf{A} & \mathbf{0} \\ \mathbf{0} & \mathbf{D} \end{array} \right] \left\{ \begin{array}{c} \boldsymbol{\varepsilon}^0 \\ \boldsymbol{\kappa} \end{array} \right\}, \tag{4.117}$$

Note that for simplicity the bending-twisting coupling terms D_{16} and D_{26} are neglected. The result of this assumption and since $\mathbf{B} = \mathbf{0}$, the description of **A** and **D** can be simplified into:

$$\left\{ \begin{array}{c} A_{11} \\ A_{22} \\ A_{12} \\ A_{66} \end{array} \right\} = h \left[\begin{array}{ccccc} 1 & \xi_1 & \xi_2 & 0 & 0 \\ 1 & -\xi_1 & \xi_2 & 0 & 0 \\ 0 & 0 & -\xi_2 & 1 & 0 \\ 0 & 0 & -\xi_2 & 0 & 1 \end{array} \right] \left\{ \begin{array}{c} U_1 \\ U_2 \\ U_3 \\ U_4 \\ U_5 \end{array} \right\}, \tag{4.118}$$

$$\left\{ \begin{array}{c} D_{11} \\ D_{22} \\ D_{12} \\ D_{66} \end{array} \right\} = \frac{h^3}{12} \left[\begin{array}{ccccc} 1 & \xi_9 & \xi_{10} & 0 & 0 \\ 1 & -\xi_9 & \xi_{10} & 0 & 0 \\ 0 & 0 & -\xi_{10} & 1 & 0 \\ 0 & 0 & -\xi_{10} & 0 & 1 \end{array} \right] \left\{ \begin{array}{c} U_1 \\ U_2 \\ U_3 \\ U_4 \\ U_5 \end{array} \right\}. \tag{4.119}$$

It is important to note that the description of the laminate stiffness has dropped from 12 to 4 lamination parameters, being:

$$\begin{array}{rcl} \xi_{[1,2]} = \xi^A_{[1,2]} & = & \frac{1}{2} \int_{-1}^{1} [cos(2\theta(\bar{z})), cos(4\theta(\bar{z}))] \, \mathrm{d}\bar{z} \,, \\ \xi_{[9,10]} = \xi^D_{[1,2]} & = & \frac{3}{2} \int_{-1}^{1} [cos(2\theta(\bar{z})), cos(4\theta(\bar{z}))] \, \bar{z}^2 \, \mathrm{d}\bar{z} \,. \end{array} \tag{4.120}$$

ξ_1^*	ξ_2^*	ξ_9^*	ξ_{10}^*
-0.173	-0.163	-0.858	-0.853

Table 4.1: The target lamination parameters ξ_i^* for the found optimum of 12.02 MPa

The material invariants U_i are calculated with the engineering constants

$$\begin{array}{rclrcl} \mathrm{E}_{11} & = & 129 \quad [\mathrm{GPa}]\,, & \mathrm{E}_{22} & = & 8.5 \quad [\mathrm{GPa}]\,, \\ \nu_{12} & = & 0.32 \quad [-]\,, & \mathrm{G}_{12} & = & 3.74 \quad [\mathrm{GPa}]\,, \end{array} \tag{4.121}$$

which are in the standard range of a carbon-epoxy UD laminate. The considered cylinder has a geometry with dimensions similar to the *L510-No18* specimen from MacKay [50], that is

$$L \;=\; 510\ [mm]\,, \quad h \;=\; 13\ [mm]\,, \quad r \;=\; 116.5\ [mm]\,. \tag{4.122}$$

The first goal is to find the target lamination parameters belonging to a composite cylinder that is prone to buckling. To be able to do this, the earlier treated Flügge model in Section (4.2) is used to describe the critical pressure. With the previous defined constants, the coefficients a_{ij} of matrix $\mathbf{A}$ in Eq.(4.105) are only a function of the lamination parameters $\xi_1^A, \xi_2^A, \xi_1^D, \xi_2^D$ and the pressure p for a given m and n. A small computer programme is written to investigate the behavior of the critical pressure as a function of the lamination parameters. For $m = 1$ and $n = 3$ an impression of the critical pressure found by the computer programme is displayed in Fig.(4.17).

Next, this model is coupled to an optimization algorithm which is able to find the global optimum of this convex domain. A suitable optimizer for this non-linear convex optimization problem is the interior point algorithm which is implemented in the *MATLAB fmincon* optimizer. The result of this optimization i.e. the target lamination parameters, are listed in Table 4.1. As indicated, the optimum is found at 12.02 MPa, which has a strong global character as it is found for different starting points.

At this point, with knowledge of the target lamination parameters, the corresponding lay-up has to be found. This lay-up could for instance be found by using a optimization algorithm which fits the lay-up lamination parameters to the target values. However, most practical composite laminates are restricted to some discrete sets of ply orientation angles such as $0°, 90°$ and $\pm 45°$ because of the availability of test data for structural verification [51]. Yamazaki [52] proposed that for this two level procedure, which is at top level described by the search for the optimal lamination parameters, a genetic algorithm (GA) is used to search for the matching lay-up. Although GAs are not known for computational efficiency, good performance is found for this combinatorial stacking sequence problem. The author is aware of these algorithms but in the present thesis the lay-up is fitted by a total combinatorial approach that is comparable to a

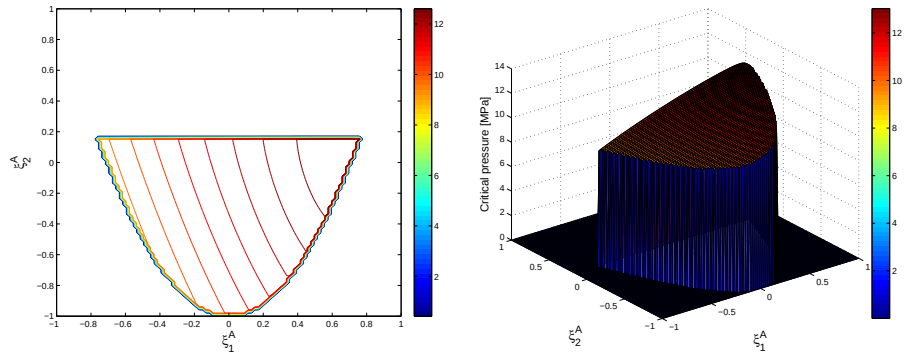

(a) Contours of p^{cr} for $(\xi_1^D, \xi_2^D) = (-1, 0)$ (b) Surface of p^{cr} for $(\xi_1^D, \xi_2^D) = (-1, 0)$

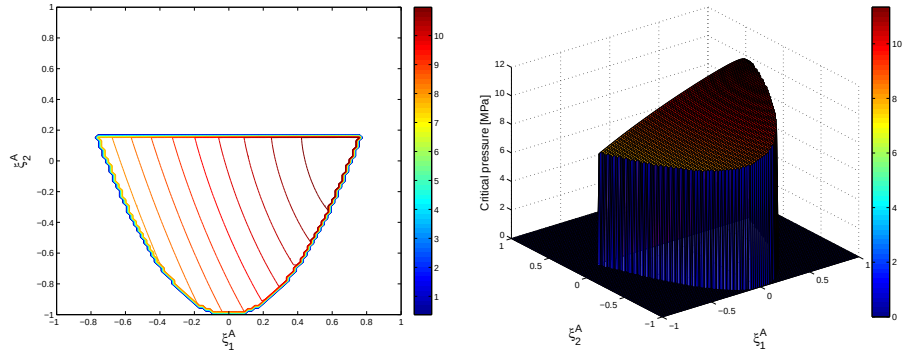

(c) Contours of p^{cr} for $(\xi_1^D, \xi_2^D) = (0, 0)$ (d) Surface of p^{cr} for $(\xi_1^D, \xi_2^D) = (0, 0)$

Figure 4.17: The response of the critical pressure p^{cr} for various choices of lamination parameters ξ_1^A, ξ_2^A at fixed out-of-plane parameters with $(\xi_1^D, \xi_2^D) = (-1, 0)$ in (a),(b) and with $(\xi_1^D, \xi_2^D) = (0, 0)$ in (c),(d)

brute force method. In this method a basis vector is used that consists of the considered ply angles to generate a n-dimensional grid, where n refers to the number of plies in the laminate. With all possible lay-ups generated, guidelines are checked for each lay-up via conditional statements and for the feasible lay-ups the lamination parameters are calculated, with the help of Eq.(4.108),(4.109) and (4.110), which can in this case be written as a finite set, i.e.:

$$\xi_{[1,2,3,4]} = \xi^A_{[1,2,3,4]} = \frac{1}{2}\sum_{k=1}^{N} \left[cos2\theta_k, cos4\theta_k, sin2\theta_k, sin4\theta_k\right] \left(\bar{z}_k - \bar{z}_{k-1}\right), \tag{4.123}$$

$$\xi_{[5,6,7,8]} = \xi^B_{[1,2,3,4]} = \frac{1}{2}\sum_{k=1}^{N} \left[cos2\theta_k, cos4\theta_k, sin2\theta_k, sin4\theta_k\right] \left(\bar{z}_k^2 - \bar{z}_{k-1}^2\right), \tag{4.124}$$

$$\xi_{[9,10,11,12]} = \xi^D_{[1,2,3,4]} = \frac{1}{2}\sum_{k=1}^{N} \left[cos2\theta_k, cos4\theta_k, sin2\theta_k, sin4\theta_k\right] \left(\bar{z}_k^3 - \bar{z}_{k-1}^3\right), \tag{4.125}$$

where N is the number of plies and $\bar{z}$ is the normalized thickness coordinate. The difference between the target and these lamination parameter is checked such that the lay-up(s) with the

Ply count n	**Laminate**	$\boldsymbol{\Delta\xi}$	$\mathbf{P}_{cr}$
8	$[90\ 90\ 0\ 0]^s$	4.83	8.66 MPa
12	$[45\ -45\ -45\ 90\ 45\ 0]^s$	0.66	8.80 MPa
16	$[45\ -45\ 90\ -45\ 90\ 45\ 0\ 0]^s$	0.59	8.86 MPa
20	$[45\ -45\ 90\ -45\ 45\ 90\ -45\ 45\ 0\ 0]^s$	0.54	8.75 MPa
24	$[90\ -45\ 45\ 45\ -45\ 45\ -45\ -45\ 45\ 90\ 0\ 0]^s$	0.56	8.68 MPa

Table 4.2: The found laminates for different ply counts n accompanied by the error $\Delta\xi$ and corresponding critical pressure P_{cr}

Ply count n	**Laminate**	$\boldsymbol{\Delta\xi'}$	$\mathbf{P}_{cr}$
8	$[90\ 90\ 0\ 0]^s$	2.37	8.66 MPa
12	$[90\ 90\ 90\ 0\ 0\ 0]^s$	2.37	8.66 MPa
16	$[90\ 90\ 45\ -45\ -45\ 0\ 45\ 0]^s$	1.74	9.27 MPa
20	$[90\ 90\ 90\ -45\ 45\ 0\ 45\ 0\ 0\ -45]^s$	1.74	9.13 MPa
24	$[90\ 90\ 90\ 90\ -45\ 45\ 0\ 45\ 0\ -45\ 0\ 0]^s$	1.69	9.32 MPa

Table 4.3: The found laminates for different ply counts n accompanied by the modified error $\Delta\xi'$ and corresponding critical pressure P_{cr}

least error is returned. Table 4.2 lists the resulting lay-up for this process for some values of ply count n. From this table, the results for different lay-ups is shown a varying number of plies in a lay-up. In this table, the error is defined as

$$\Delta\xi = \sum_{i=1}^{12} \left(\xi_i - \xi_i^*\right)^2 , \tag{4.126}$$

which is the squared difference between the estimated lamination parameters ξ_i and the target parameters ξ_i^*. From the table it can be seen that the pressure found by evaluation of the laminate corresponding to the least error is at around 72-74% of the target. Furthermore, a decrease in error does not mean, for this particular problem, that a higher pressure is found. But since this error treats all lamination parameters with the same importance (or weight factor), which does not correspond to the nature of the Flügge model where this can be illustrated in terms of derivatives

$$\left[\frac{\partial P(\boldsymbol{\xi}^*)}{\partial \boldsymbol{\xi}_{(1,2,9,10)}}\right] \quad = \quad [-2.5 \quad -0.8 \quad 4.9 \quad 1.6] , \tag{4.127}$$

where $P(\xi_j^*)$ is the pressure at the target. By appliance of weight factors with magnitudes corresponding to the derivatives in Eq.(4.127) to the terms in Eq.(4.126), Table (4.3) is constructed. With this new definition of error it is observed that the response has improved. Furthermore, it can be seen that the found laminates for the increasing ply count develop more in a structured way than the random behavior observed in Table (4.2).

4.3.2 FE optimization of composites and composite sandwich pressure hulls

The use of lamination parameters is also suitable in a finite element (FE) description of the pressure hull. [53] determined optimal stacking sequences for laminate panels using a two-stage optimization method. For practical applications the ply orientations were limited to a finite set of angles. With a assumed number of plies, optimal balanced laminates were obtained in this method. For a pressure hull, an analogous approach is elaborated in the following. At the first stage of the optimization the target lamination parameters need to be found. This higher-level description of the model gives an indication of the entire design domain and the global optimum. Furthermore, the FE model, which is computational intensive, is only evaluated for different lamination parameters subjected to the constraints treated in the previous section. If the target lamination parameters are found, these parameters are estimated by a combinatorial search of laminate stacking sequences at the second stage of optimization. These estimations are relatively small calculations. Therefore, this two-stage approach reduces the computation time tremendously. The details of the first stage are treated in the next.

At first, the sectional stiffness matrix is constructed by the lamination (design) parameters ξ_i^j. Subsequently the FE model is evaluated and sectional membrane strains and curvature changes can be inquired. Also, a linear buckling analysis can be evaluated to obtain the linear buckling pressure. A simple failure criterion for the composite cannot be applied because there is no lay-up defined. In order to indicate material failure, a suitable (conservative) failure criterion developed by IJsselmuiden et al. [54], deduced from the Tsai-Wu failure criterion [43], predicts material failure in the defined section without an established lay-up. The failure criterion yields:

$$4u_6^2 I_2^2 - 4u_6 u_1 I_2^2 + 4\left(1 - u_2 I_1 - u_3 I_1^2\right)(u_1 - u_6) + (u_4 + u_5 I_1)^2 = 0\,, \tag{4.128}$$

$$u_1^2 I_2^4 - I_2^2 (u_4 + u_5 I_1)^2 - 2u_1 I_2^2 \left(1 - u_2 I_1 - u_3 I_1^2\right) + \left(1 - u_2 I_1 - u_3 I_1^2\right)^2 = 0\,, \tag{4.129}$$

where the strain invariants for volumetric strain is I_1 and the maximum shear strain I_2 are given by

$$\begin{aligned} I_1 &= \varepsilon_x + \varepsilon_y\,, \\ I_2 &= \sqrt{\left(\tfrac{\varepsilon_x - \varepsilon_y}{2}\right)^2 + \varepsilon_{xy}^2}\,. \end{aligned} \tag{4.130}$$

The coefficients u_i are

$$\begin{aligned} u_1 &= G_{11} + G_{22} - 2G_{12}\,, \\ u_2 &= (G_1 + G_2)/2\,, \\ u_3 &= (G_{11} + G_{22} - 2G_{12})/4\,, \\ u_4 &= G_1 - G_2\,, \\ u_5 &= G_{11} - G_{22}\,, \\ u_6 &= G_{66}\,, \end{aligned} \tag{4.131}$$

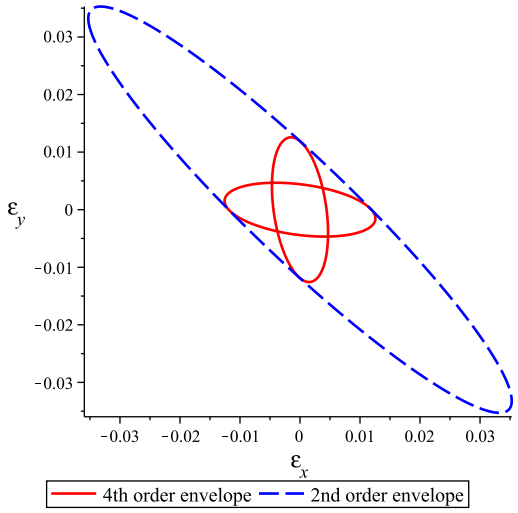

Figure 4.18: Impression of the Tsai-Wu failure criterion envolopes for high strength carbon-epoxy

where

$$\begin{aligned} G_{11} &= Q_{11}^2 F_{11} + Q_{12}^2 F_{22} + 2F_{12} Q_{11} Q_{12}\,, \\ G_{22} &= Q_{22}^2 F_{11} + Q_{12}^2 F_{22} + 2F_{12} Q_{22} Q_{12}\,, \\ G_{1} &= Q_{11} F_1 + Q_{12} F_2\,, \\ G_{2} &= Q_{12} F_1 + Q_{22} F_2\,, \\ G_{12} &= Q_{11} Q_{12} F_{11} + Q_{12} Q_{22} F_{22} + F_{12} Q_{12}^2 + F_{12} Q_{11} Q_{22}\,, \\ G_{66} &= 4 Q_{66}^2 F_{66}\,. \end{aligned} \tag{4.132}$$

In this equation $\mathbf{Q}$ is the reduced stiffness matrix and the coefficients of the Tsai-Wu failure criterion are denoted by F_{ij} and F_k. The latter are given given by:

$$\begin{aligned} F_{11} &= \frac{1}{X_T X_C}\,, \\ F_{22} &= \frac{1}{Y_T Y_C}\,, \\ F_{1} &= \frac{1}{X_T} - \frac{1}{X_C}\,, \\ F_{2} &= \frac{1}{Y_T} - \frac{1}{Y_C}\,, \\ F_{12} &= -\frac{1}{2\sqrt{X_T X_C Y_T Y_C}}\,, \\ F_{66} &= \frac{1}{S^2}\,, \end{aligned} \tag{4.133}$$

where the strength in fiber direction for an UD-ply in tension is X_T and X_C for compression, the transverse strengths in tension and compression are denoted by Y_T and Y_C, respectively. The shear strength is given by S.

In order to understand this failure criterion, it has to be clear that the first criterion Eq.(4.128) is a second order equation with respect to the strains, while the second criterion Eq.(4.129) is of the fourth order. The failure criterion which is represented by both equations, is graphically shown in Fig.(4.18) for a high strength carbon-epoxy composite in strain space. It can be observed from this figure that the fourth order envelope is the critical envelope, since it is forms the inner strain envelope. Therefore, the so called safe region is given by the common area of the two ellipses belonging to the fourth order envelope. It is important to note that the critical envelope is a material property.

In a linear elastic description of the composite, a strength constraint suitable to the present description is developed by IJsselmuiden et al. [54]. It is practical to use in optimization and uses a safety factor λ which is defined as

$$\lambda = \frac{b}{a} \tag{4.134}$$

where a is the distance between the origin and an arbitrary point P in strain space i.e. $(\varepsilon_x, \varepsilon_y) = (0,0)$ and $(\varepsilon_x, \varepsilon_y) = (P_x, P_y)$. The distance b is defined as the length between the origin and a point on the critical failure envelope P^* which is in the direction of P. The strain invariants that are initially described in Eq.(4.130), belonging to point P^* are now defined in similar fashion:

$$\begin{aligned} I_1^* &= \lambda I_1 \,, \\ I_2^* &= \lambda I_2 \,. \end{aligned} \tag{4.135}$$

With this description of the strain invariants Eq.(4.128) and Eq.(4.129) can be reformulated for the critical state, hence

$$\begin{aligned} 4u_6^2 \left(\lambda I_2\right)^2 - 4u_6 u_1 \left(\lambda I_2\right)^2 + 4\left(1 - u_2 \lambda I_1 - u_3 \left(\lambda I_1\right)^2\right)\left(u_1 - u_6\right) \\ + \left(u_4 + u_5 \lambda I_1\right)^2 = 0 \,, \end{aligned} \tag{4.136}$$

$$\begin{aligned} u_1^2 \left(\lambda I_2\right)^4 - \left(\lambda I_2\right)^2 \left(u_4 + u_5 \lambda I_1\right)^2 - 2u_1 \left(\lambda I_2\right)^2 \left(1 - u_2 \lambda I_1 - u_3 \left(\lambda I_1\right)^2\right) \\ + \left(1 - u_2 \lambda I_1 - u_3 \left(\lambda I_1\right)^2\right)^2 = 0 \,. \end{aligned} \tag{4.137}$$

The next step is to express these equations in terms of λ:

$$a_{12}\lambda^2 + a_{11}\lambda + a_{10} = 0 \,, \tag{4.138}$$

$$a_{24}\lambda^4 + a_{23}\lambda^3 + a_{22}\lambda^2 + a_{21}\lambda + a_{20} = 0 \,, \tag{4.139}$$

where Eq.(4.138) corresponds to Eq.(4.136) and Eq.(4.139) to Eq.(4.137). The coefficients a_{ij} are given by

$$\begin{aligned}
a_{10} &= u_4^2 + 4u_1 - 4u_6\,, \\
a_{11} &= 4u_2 I_1 u_6 - 4u_2 I_1 u_1 + 2u_4 u_5 I_1\,, \\
a_{12} &= -4u_3 {I_1}^2 u_1 + 4u_3 {I_1}^2 u_6 + 4{u_6}^2 {I_2}^2 - 4u_6 u_1 {I_2}^2 + {u_5}^2 {I_1}^2\,, \\
a_{20} &= 1\,, \\
a_{21} &= -2u_2 I_1\,, \\
a_{22} &= -{I_2}^2 {u_4}^2 - 2u_3 {I_1}^2 + {u_2}^2 {I_1}^2 - 2u_1 {I_2}^2\,, \\
a_{23} &= 2u_1 {I_2}^2 u_2 I_1 - 2{I_2}^2 u_4 u_5 I_1 + 2u_2 {I_1}^3 u_3\,, \\
a_{24} &= 2u_1 {I_2}^2 u_3 {I_1}^2 + {u_1}^2 {I_2}^4 - {I_2}^2 {u_5}^2 {I_1}^2 + {u_3}^2 {I_1}^4\,,
\end{aligned} \tag{4.140}$$

which are functions of the strain invariants I_1, I_2 and coefficients u_i which were treated in Eq.(4.131). For a given material under known strain state, the failure constraint can be calculated by finding the solutions of Eq.(4.138) and Eq.(4.139). The smallest absolute real root among the six root solution for λ is the active critical safety factor for failure, i.e. the corresponding λ for the critical envelope belonging to the strain state. [54] formulated the strength constraint as

$$\frac{1}{\lambda_c^2} - 1 \leq 0, \tag{4.141}$$

where λ_c is the active critical safety factor. However, before this strength constraint is useable for the whole laminate, the strain within the laminate has to be defined. An assumption is made that

$$\boldsymbol{\varepsilon}(x, y, z) = \boldsymbol{\varepsilon}^0(x, y) + z\boldsymbol{\kappa}(x, y), \tag{4.142}$$

which is similar to Eq.(4.31). As a result, the strength constraint of Eq.(4.141) can be either critical at the top or bottom surface of the laminate, i.e. $z = \pm h/2$ with h representing the laminate thickness. IJsselmuiden and coworkers [54] described that this result may seem paradoxical at first because it is well known that the most critical point through the thickness of a composite need not be one of the extreme fibers. But since the formulation of the failure criterion is regardless to the ply orientation this result is expected. Hence this failure criterion is conservative with in particular for bending dominated problems.

Having the strength constraint defined, together with the linear buckling pressure, a optimization procedure can be constructed for the composite pressure hull. It has to be mentioned that the treated method can be utilized on composite sandwich pressure hulls as long as the effect of core failure and face wrinkling effects are also described in additional constraints. For both models, a logical objective function can be either the buckling pressure or the weight of the pressure hull. As described previously, the strength of the structure forms the constraint and the lamination parameters are the design variables at this first optimization stage. With a optimal solution for the lamination parameters found, i.e. target lamination parameters, the second (and last) stage of the optimization procedure is started. Since the lamination parameters are

simple sequential functions of the desired finite set of ply orientations and thicknesses of the laminate, evaluation of this procedure is computational efficient. Hence, the method presented in Section 4.3.1 can be used to fit an actual laminate to the desired target values.

4.4 Conclusion

The mechanical basics of a composite material are treated and techniques to gather engineering constants at ply level are shown. But as composite laminates mostly consists of multiple stacked plies that vary in orientation the ply description is not appropriate. Therefore, the classical laminate theory is elaborated. As an important note this theory neglects through-the-thickness shear deformations, which cannot be neglected for all laminates. Furthermore, in the search of an actual laminate, the most appropriate lay-up guidelines are presented and applied throughout this work.

However, composite materials bring more complexity in the light of failure and strength prediction. Most important failure mechanisms are shown for a composite laminate and for sandwich structures. The used formulae for strength and failure criteria are treated and, of course, applied in the present thesis. Apart from material failure, buckling effects can dominate the collapse of a composite cylinder. A linearized buckling theory is elaborated which is used as a basic model in the subsequent section.

A higher level approach for a laminate description in terms of lamination parameters is elaborated. The advantage of these parameters is demonstrated for an analytic linearized description of a composite cylinder prone to buckling. It turns out that this approach is very appropriate and an indication of the global optimum is easily found. Since this optimum is formulated in terms of the (target) lamination parameters, an actual laminate needs to be found. The proposed method for this fitting problem selects the most appropriate lay-up which also is in accordance with the laminate guidelines.

The use of lamination parameters in a FE context is outlined. The missing link turns out to be a constraint that indicates material failure. The Tsai-Wu based failure criterion in the context of a lamination parameter approach, deduced by IJsselmuiden et al. [54] is the answer for this problem. It is demonstrated that it is a conservative failure criterion since it is regardless to the ply orientations in the potential laminate.

Chapter 5

FE modeling, analysis and weight minimization of pressure hulls

In this chapter the majority of the topics treated earlier are applied. For the stiffened cylinder, which is the reference and is described in Section (5.1), an experimentally tested cylinder is modeled in FE. Different analyzes are performed and results are compared to the experiment. With the FE model defined, weight minimization is performed. With the experience of this model and description in terms of lamination parameters, a FE composite cylinder is modeled in Section (5.2). Target lamination parameters are found for the maximization of the critical buckling load and weight minimization. Corresponding lay-ups are presented. At last, a composite sandwich FE model is created and described in Section (5.3). Similar optimizations as in the previous section are performed and results are presented.

5.1 Stiffened cylinder FE analysis and optimization

In this chapter a stiffened cylinder is modeled. This is a proven pressure hull concept (see Section (3.2)) and understanding the mechanics up to the collapse pressure is paramount. Hence, a FE model is created that predicts this collapse pressure. This model is based on an experiment with an aluminium stiffened cylinder subjected to external pressure described by MacKay [50]. Ultimately, with the geometry defined in a parametric manner, weight minimization is performed in Section (5.1.6).

5.1.1 Experiment

MacKay [50] describes collapse tests on twelve small-scale ring-stiffened aluminium cylinders. Out-of-circularity (OOC) in the critical collapse mode was applied by mechanically deforming the specimens. MacKay studied the effect of corrosion damage on the specimens' stability. Half of the specimens was subjected to artificial damage, while the other half was still intact. The

Figure 5.1: Typical internally stiffened cylinder of MacKay's test series [50]

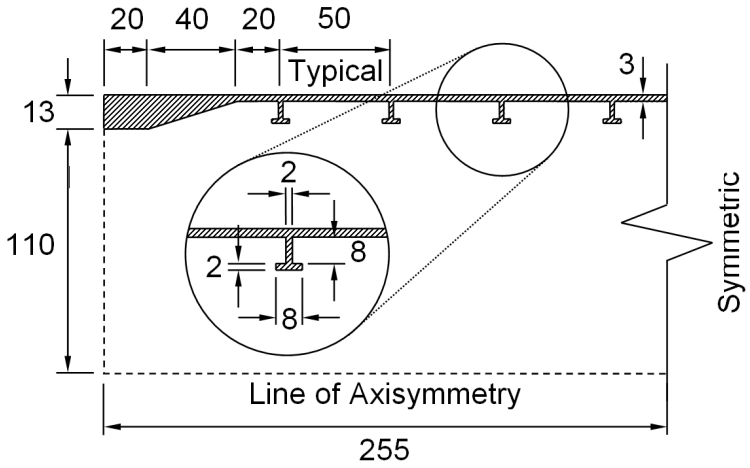

Figure 5.2: Design dimensions of the test specimen, figure is adapted from [50]

L510-No-18 cylinder which is one of MacKay's intact specimens (in the following referred to as the test specimen), is described in the next. Ultimately, the specimen is modeled in FE and validation of the model is performed with the specimen's test results.

5.1.2 Geometry

The nominal axisymmetric geometry of the test specimen is CNC machined from 6082-T6 aluminium alloy tubing. An impression of such a typical test specimen is given in Fig.(5.1). As illustrated in Fig.(5.2), the cylinder is stiffened by eight internal T-section ring stiffeners. Dimensions of the specimen are chosen such that the cylinders would fail in a overall elasto-plastic collapse of the shell and stiffeners. This means that the stiffeners are small in terms of bending stiffness compared to the shell. The end sections of the shell are thick and the transition to the thin mid-shell is tapered. This prevents undesired end bay failures and gives enough material

Maximum radial eccentricity[a] (mm)			Maximum Fourier Amplitude[b] (mm)				
Outward	Inward	Average	$n = 2$	$n = 3$	$n = 4$	$n = 5$	$n = 6$
0.337	0.503	0.399	0.023	0.366	0.022	0.023	0.090

Table 5.1: List of measured eccentricites and Fourier decomposition for the outer shell radii of the specimen L510-No-18
a. Outward and inward eccentricity are based on the absolute maximum values of the positive and negative deviation, respectively, from the mean outer shell radius for all axial measurement locations. The average eccentricities are computed at each axial measurement location and taken as half the difference between the maximum outward and inward eccentricities. The listed maximum average eccentricity is the maximum of all average eccentricities.
b. Maxiumum Fourier amplitudes, based on decomposition of outer shell radii at all axial measurement locations, are reported. Fourier amplitudes for $n > 6$ are negligible.

	Young's modulus [GPa]	Poisson's ratio [-]	Yield strength (elastic limit) [MPa]	Tensile strength [MPa]	Compressive strength [MPa]	Elongation at break [%]
L510-No-18	57.2	-	305.1	328.0	-	11.7
Handbook	70-74	0.325-0.335	240-290	280-340	295-326	5-11

Table 5.2: Engineering properties AA 6082-T6: measurements on the specimen [50] and handbook values [55]

to secure the end caps with bolts, as described by MacKay.
The specimen is subjected to a mechanical deformation with the purpose to leave a dominating ($n = 3$, $m = 1$) mode. This mode shape is the most critical for collapse of the test specimen. The resulting OOCs are measured and listed in Tab.(5.1). Note that these measurements were made with the earlier described chord gauge. From Tab.(5.1) it is easily seen that the critical collapse mode $n = 3$ dominates.

5.1.3 Material

As mentioned earlier in this chapter, the test specimen is made from AA-6082-T6 aluminium alloy. MacKay performed tensile tests on the alloy and showed that anisotropic material behavior was present. He suggested that this would be related to the extrusion process for the aluminium tubing, which preferentially align the grain structure in the axial direction. The engineering properties for the test specimen, accompanied by the typical handbook values [55] are listed in Tab.(5.2). It has to be mentioned that the Young's modulus is significantly lower than the typical handbook value of 70 to 74 GPa. MacKay indicated that the measured value could be incorrect due to the fact that only one extensometer was used instead of the typical number of two. Any unwanted bending effects could not be measured and therefore the results can differ from the true material behavior.

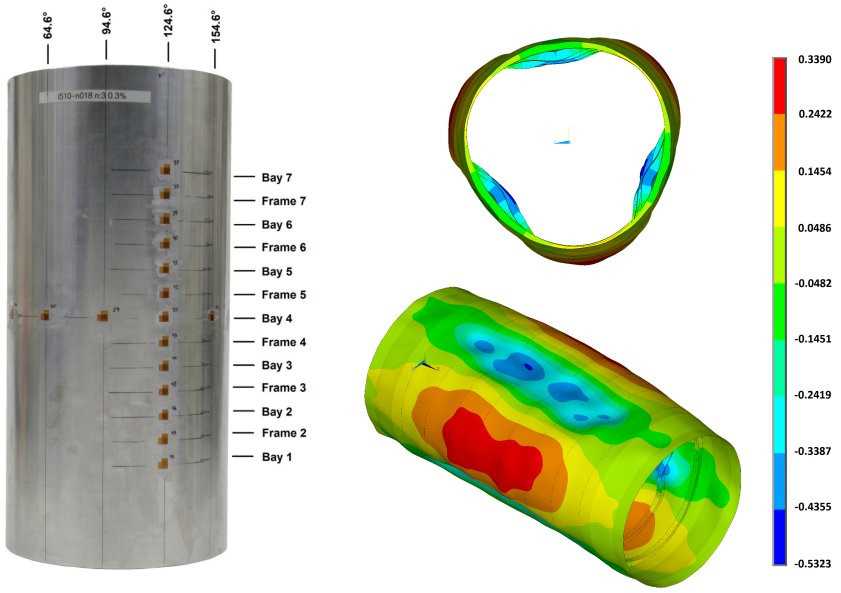

(a) (b)

Figure 5.3: Picture of the specimen with the strain gauge instrumentation in (a) and a graphical visualized OOC model (b) both adapted from [50]

5.1.4 Strain gauge plan

The instrumentation consists of uni-axial linear strain gauges (Vishay Micro-Measurements gauge designated CEA-13-250UW-350) together with bi-axial 90° stacked rosettes (Vishay Micro-Measurements gauge designated CEA-13-125WT-350). The accuracy of these gauges is around 0.5% of the reported value. The tabular instrumentation plan of the test specimen is listed in Appendix E.1.

In short, there are twelve uni-axial gauges fixed to each of the two central-right stiffeners (i.e. Frames 4 and 5) at 30° increments about the circumference. Additionally, twelve bi-axial gauges were fixed to the outside of the shell mid-way between the two central ring-stiffeners in Bay 4 at 30° increments about the circumference. Lastly, a row of thirteen bi-axial gauges are located at the outer shell along the length of the cylinder at each mid-bay and and ring stiffener location, starting at Bay 1. To illustrate this, a picture of the the test specimen is shown in Fig.(5.3a).

5.1.5 FE model

The test specimen is modeled with finite elements (FE) in *Abaqus/CAE*. The general idea behind this approach is to achieve a similar behavior in the FE model as in the test specimen's experiment. In order to get to this point, certain phases is terms of modeling have to be completed.
First, a linear elastic FE model (Section 5.1.5) is created with shell elements. Appropriate

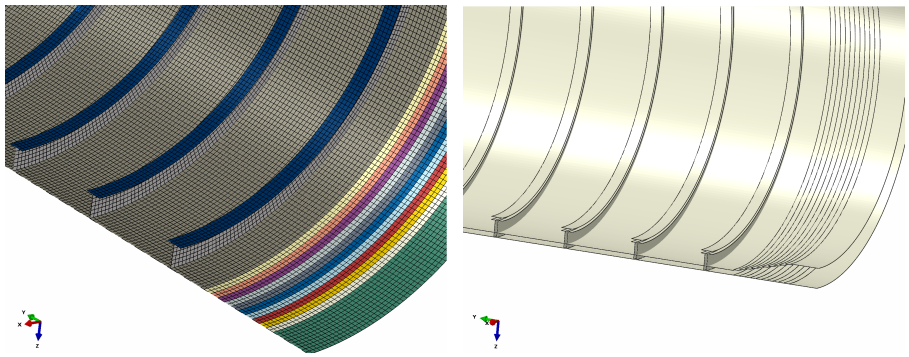

(a) Details of the mesh (b) Rendered thickness of shell elements

Figure 5.4: Close-up of the mesh for the stiffened cylinder cross section

loads and boundary conditions have to be applied. The initial measured stiffness of the test specimen has to be more or less the same as this linear elastic FE model. In order to make a comparison, the strain gauge readings are compared with strain gauges modeled in FE. Second, a linear buckling analysis is performed in Section 5.1.5. Mode shapes and buckling loads have to be extracted. If correct boundary conditions are applied, the critical buckling mode with $n = 3$ has to be found. Third, a non-linear material model needs to be created to imitate the true material behavior. With this model and accounting for large-displacements, a non-linear buckling analysis has to be performed (see Section 5.1.5). Because the specimen is sensitive to imperfections, these have to be modeled according to measurements that are already listed in Tab.(5.1). The non-linear material model has to be implemented. Further, FE strain gauges have to be modeled in order to compare the output with the experiment.

Linear elastic model

The linear elastic FE model consists of shell elements and is comparable to the FE model treated in [50]. It has to be noted that the general mesh size is equal to 2 mm. This mesh is illustrated in Fig.(5.4a), with the colors corresponding to specific sections. The tapered section of the shell is created by a stepwise (linear) change in thickness. An overview of the model is shown in Fig.(5.4b). It can be seen from the figure that the end plates are not modeled. Instead of that, appropriate boundary conditions are applied to simulate the end plates. As [50] described, "quasi-clamped" boundary conditions are applied whereby out-of-plane bending is prevented at the cylinder ends, while end-warping is allowed. The external pressure is applied as an uniform pressure of 10 MPa at the outer shell surface. As a result from the missing end plates, an axial force on a reference point which is coupled to the shell's end section represents the pressure axial component of the pressure. At the opposite end section the axial displacement is equal to zero. The rigid body modes are prevented by locking the tangential displacement at two node pairs. The thick end plates are modeled with the same "quasi clamped" boundary condition at the axial outer shell location of the inner end plate surface. The aluminium is modeled with a handbook Young's modulus of 70GPa.

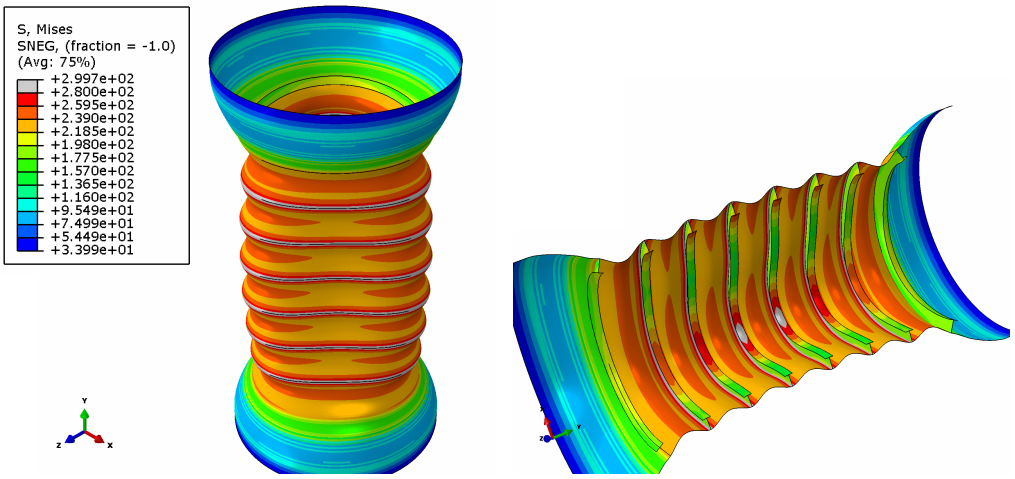

Figure 5.5: The von Mises stress distribution in the linear elastic model at 8 MPa

The results are compared via strain gauge readings. The strain gauges are modeled as a linear connector with zero stiffness between two reference points that are constrained to the corresponding outer surface of the shell elements. The reference points follow the displacement of the facing and the change in length will be measured for the connector. This method is a proven concept and widely applied in the aerospace industry. The results are shown in Appendix E.2. The match with the experiments for the initial slope of the readings is shown in Appendix E.4. The initial response for the majority of the gauges is very comparable to the experimental measured values. Some of the longitudinal strain gauge array show a moderate match with the test results, this behavior is discussed later in Section (5.1.5).

It is important to note that the model has an imperfect geometry, the critical n=3 mode is added (as initial geometric deviations of the nodes corresponding to the values listed in Table(5.1)) with an *Abaqus/Standard* *IMPERFECTION command at the model's input file. In order to add this mode to the geometry, an linear buckling analysis has to be performed and a *NODE FILE command has to be added to the model's input file. This linear buckling analysis is treated in the next section.

In Fig.(5.5) the von Mises stress is illustrated for the outer shell surface and the stiffened cylinder interior. In the grey colored contour area the von Mises stress is higher than the (assumed) typical handbook strength value of 280 MPa. With the applied 8 MPa it can be clearly seen that yielding takes place at this pressure. To be more precise, first yielding occurs at the outer shell when 7.5 MPa uniform pressure is applied.

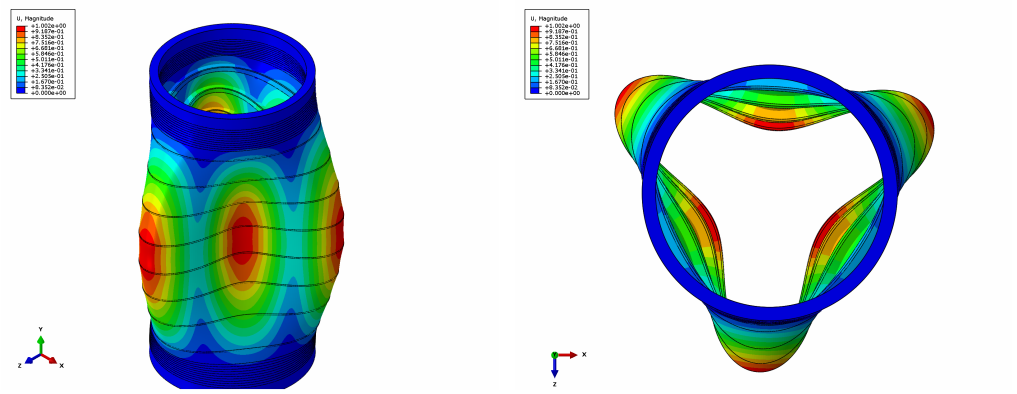

Figure 5.6: Illustration of the lowest eigenvalue ($n = 3$, $m = 1$)

	Mode			
	n=3, m=1	**n=4, m=1**	**n=4, m=2**	**n=8, m=7**
Eigenvalue [MPa]	15.1	20.3	22.8	23.5

Table 5.3: Found eigenvalues for the test specimen a the linear buckling analysis

Linear buckling analysis

Since the test specimen is prone to buckling it is essential to perform a buckling analysis. Additionally, the imperfection needed in the linear elastic and non-linear buckling analysis can be extracted in this process. This FE model is in the initial configuration the same as in the linear elastic model described in Section (5.1.5). A linear buckling analysis is performed and the first found mode shape, which has the lowest buckling load, is illustrated in Fig.(5.6). To be complete the found values and mode shapes are listed in Table (5.3). As expected a typically large pressure is found as buckling load compared to the experiment. To be complete, the mode shapes belonging to the other eigenvalues are graphically shown in Appendix F. With the knowledge of the previous section it is easily demonstrated that yielding occurs at a lower pressure than the first linear buckling mode. Hence, the expected collapse of the imperfect pressure with an nonlinear material model will be around this lower pressure. This is also a result of the previously described approach of Johnson-Ostenfeld in Section (3.3). Therefore, it is important to implement a more realistic model that accounts for material yielding and geometrical imperfections. This approach is elaborated in the next.

Non linear buckling FE model

A non-linear buckling analysis is performed to accurately describe the test specimen. This Section describes the aspects of the model and this analysis. First, the boundary conditions are the same as in the previously treated linear elastic FE model. Additionally, the geometry is not axi-symmetric but the critical $n = 3$ mode shape imperfection is added to imitate the imperfect test specimen. The amplitude of this imperfection is the same as in the experiment, which was

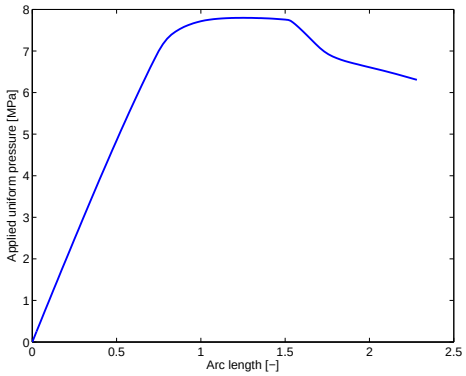

Figure 5.7: Applied pressure as a function of the arc length

already listed in Table (5.1) as the Fourier amplitude for this mode. The non-linear material behavior of the AA-6082-T6 aluminium alloy is characterized with a (typical handbook) tensile yield strength of 280 MPa. Furthermore, the strain hardening modulus is 350 MPa. The implemented material model is a bilinear material model with an initial (handbook) Young's modulus of 70 GPa. As before, the strain gauges are modeled and the output can be compared with the experimental gauges. The readings are compared to the experimental values and graphically plotted in Appendix E.3. Furthermore, an arc length method is used as a step method. To attain good convergence a maximum arc length of 0.025 is used for an applied pressure at 10 MPa.

The results of the FE strain gauge readings are compared to the experiment. An indication of output matches is listed in Appendix E.4. After inspection of these readings, the collapse pressure is found to be 7.8 MPa. The collapse pressure is conveniently close to the measured value in the experiment, i.e. 7.71 MPa [50]. As in the linear elastic model, the readings are compared to the experimental values. Good correspondence is found for the majority of the FE readings. Again, in the longitudinal strain gauge array there is a moderate match. These discrepancies could originate from various simplifications in the FE model. Residual stress that occurs after mechanically applying the $n = 3$ mode shape imperfection changes the local displacement behavior. Other imperfections, such as higher modes or local dents (see Fig.(5.3b) for an impression) that are present in the model can be the origin of this error. The local behavior that governs the strain gauges could also change if these modes are also added to the FE model. Other effects can have influence on the strain gauges, e.g. the anisotropic behavior which is found in samples from the cylinders.

Because the collapse is clearly caused by the initiation of material yielding, the elastic or plastic condition of the model is visualized with a so-called yield flag in Fig.(5.8). As can be seen from Fig.(5.8a), first yielding occurs at the centermost stiffener flanges (frames 4 and 5) at an arc length of 0.7. From Fig.(5.7) one can observe that this arc length corresponds to a pressure of

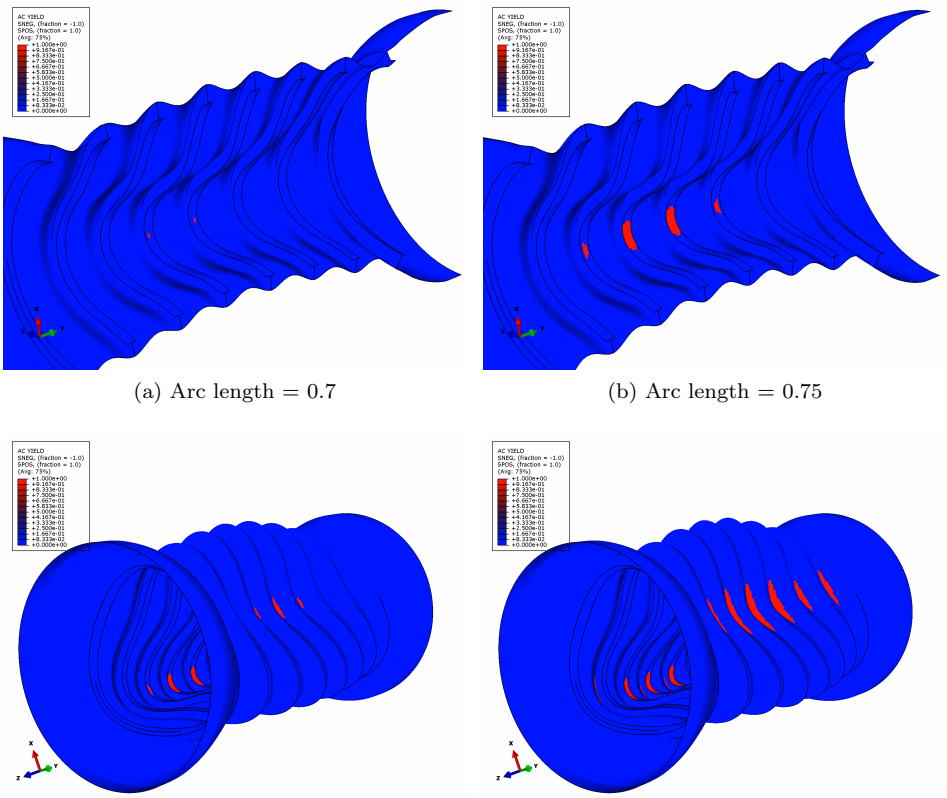

(a) Arc length = 0.7

(b) Arc length = 0.75

(c) Arc length = 0.75

(d) Arc length = 0.8

Figure 5.8: The contour plot of the red yielding flag at different arc lengths

6.6 MPa. This plasticity extends when the arc length is increased to 0.75, at an equivalent 7 MPa the outer shell starts to yield at the inter-frame locations, see Fig.(5.8c) for a complete impression. In Fig.(5.8d) the equivalent pressure is 7.3 MPa and first yielding occurs at the stiffener webs. Material yielding was also observed in the experimental model. It has to be noted that the found yield pressures were, according to MacKay [50], predicted by assuming that the as-tested cylinders were in a stress-relieved condition; that is, the effect of residual stresses that necessarily arose during application of OOC were neglected. As such, the reported yield pressures may be greater or less than the actual yield pressures, depending on the interaction of the residual stresses with the applied load. However, by comparing the yielding locations and relative values of the yield pressure it is found that the test specimen also shows first yielding at the centermost stiffener flanges and outer shell yielding at a slightly higher pressure.

5.1.6 Optimization the FE model

The previously treated FE model is constructed by means of scripting. With this scripting interface for *Abaqus/Standard* which is written in the language *Python*, modeling can easily be made parametric. This opens the possibility to see how dimensional changes in the geometry

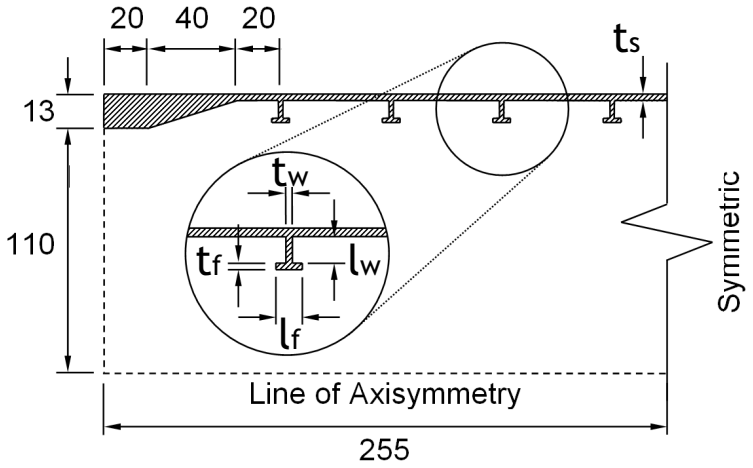

Figure 5.9: Design dimensions of the test specimen in terms of design variables, figure is adapted from [50] but customized

alter the collapse strength. Of course, the weight of the structure can change during this process and this should not be neglected. In order to see the potential of this conventional design, the parametric model is subjected to an optimization that has the purpose to minimize the structural weight while keeping the performance with respect to collapse on the same level. The optimization problem therefore yields

$$\begin{array}{ll} \text{minimize} & W^*\left(t_s, t_w, t_f, l_w, l_f, N^s\right) \\ \text{subject to} & \text{Eq.(5.2) and Eq.(5.3)} \\ \text{design variables} & \{t_s, t_w, t_f, l_w, l_f, N^s\} \end{array} \tag{5.1}$$

where the unit weight W^* is defined as the weight in [kg] per [mm] unit length, neglecting the tapered and thick end sections. The design parameters t_s, t_w and t_f are the thickness of the shell, stiffener web and flange, respectively. The radially measured length of the stiffener web and the length of the stiffener flange in axial direction are denoted by l_w and l_f. To be complete, these dimensions are shown in Fig.(5.9). The last design parameter is the number of stiffeners N_s. It has to be noted that the stiffeners are evenly distributed between the two stiffeners near the end sections. For the constraints, the von Mises stress in the material in the static analysis has to be satisfy the condition

$$\sqrt{\left[\frac{(\sigma_1-\sigma_2)^2+(\sigma_2-\sigma_3)^2+(\sigma_3-\sigma_1)^2}{2}\right]}-\sigma_y \leq 0\,, \tag{5.2}$$

and the critical pressure from the linear buckling analysis ($P_{cr,le}$) has to be larger or equal than in the reference model ($P^*_{cr,le}$), i.e:

$$P^*_{cr,le} - P_{cr,le} \leq 0\,. \tag{5.3}$$

Material	Objective	Optimal design variables						Constraint values	
	W^*	t_s	t_w	t_f	l_w	l_f	N^s	Eq.(5.2)	Eq.(5.3)
	[kg/mm]	[mm]	[mm]	[mm]	[mm]	[mm]	[-]	[MPa]	[MPa]
AA-6082-T6	6.52E-3	2.31	0.91	2.06	8.63	5.63	18	−9.9E-4	−1.1E-2
HY80	9.9E-2	1.41	0.115	0.49	8.63	5.56	28	−3.45	−3.08
Ti-6Al-4V	6.57E-3	1.36	0.44	2.06	7.00	3.37	19	−7.5	−6.5E-2

Table 5.4: Results of the optimization process of the conventional stiffened cylinder for the reference aluminium alloy (AA-6082-T6), the commonly applied high-yield steel (HY80) and titanium alloy (Ti-6Al-4V)

with of course the absolute value of the external pressures $P_{cr,le}$ and $P^*_{cr,le}$.

Because of the present formulation, i.e. five continuous design variables and one integer design variable, a suitable solver for this optimization problem is a so-called mixed-integer global optimizer that can deal with this discontinuity. *MIDACO* optimization software [56] is capable to solve such problems. The routine, which is originally written in *Fortran77*, has direct *C* translation which can be called from *Matlab* [57] via a gateway function in the form of a *MEX* file. The mixed-integer optimizer from *MIDACO* is used to solve the optimization problem.

The results of this optimization are listed in Table (5.4). Also, a convergence curve is provided in Fig.(5.10) which shows that the unit weight, which is the objective function, lowers quickly to the found optimum. It has to be noted that all constraints are satisfied. The material failure constraint i.e. the von Mises stress is active at the optimum. To be complete, the model in optimal form is displayed in Fig.(5.12a) and Fig.(5.12b). The von Mises stress at an external pressure of 10 MPa is plotted in Fig.(5.12c) and Fig.(5.12d) the critical mode shape for the linear buckling analysis is shown in Fig.(5.12e) and Fig.(5.12f). As a result of inspection the critical von Mises stress is found to be located at the inside of the shell near the stiffener webs. With the knowledge that the original model had a unit weight of 7.73E-3 kg/mm, it can be said that the optimization caused an impressive 15% weight reduction while keeping the same strength in terms of yielding and buckling with respect to the reference model.

The current optimization is also applied at an FE model with material properties belonging to the widely applied HY80 steel. The properties used for stiffness and strength are given in tabular format in Appendix C. In this appendix one can observe the difference in specific strength for HY80 steel and the reference aluminium 6082-T6, which is about 20% higher for the aluminium. Furthermore, the specific stiffness is only 1.4% higher for steel. With this in mind, the same mixed-integer weight minimization is performed and the result indicates the expected: An unit weight optimum of 9.9E-3 kg/mm is found, which is 50% heavier than the optimized reference model. As such, titanium (Ti-6Al-4V, see Appendix C) is evaluated. This material shows a 75% higher specific strength but a 5% lower specific stiffness. Hence the found optimum of 6.57E-3

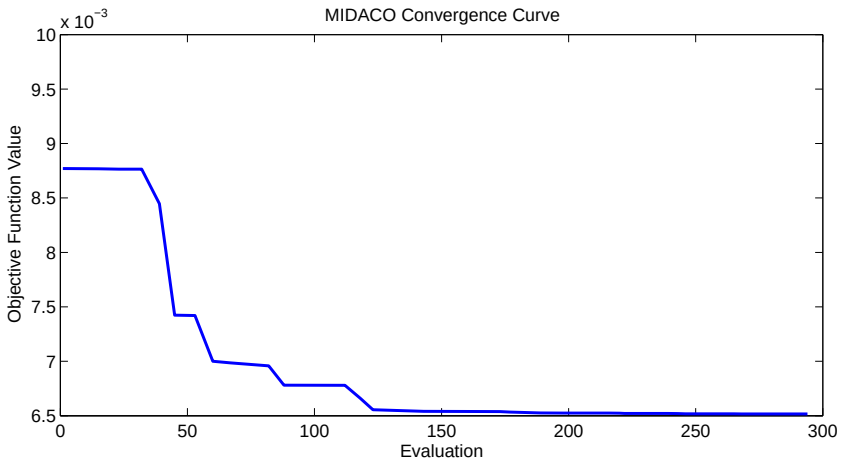

Figure 5.10: The automatically generated convergence plot of the mixed-integer optimization process for the unit weight minimization of the stiffened pressure hull

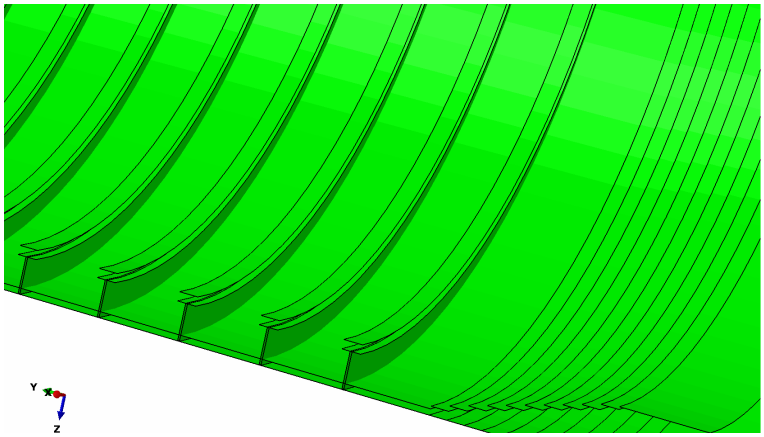

Figure 5.11: The titanium hull in its optimal design

kg/mm unit weight is more or less the same as the reference optimum. The optimization results of HY80 and the titanium hull are listed in Table (5.4) An impression of the optimal design for the titanium hull is given in Fig.(5.11).

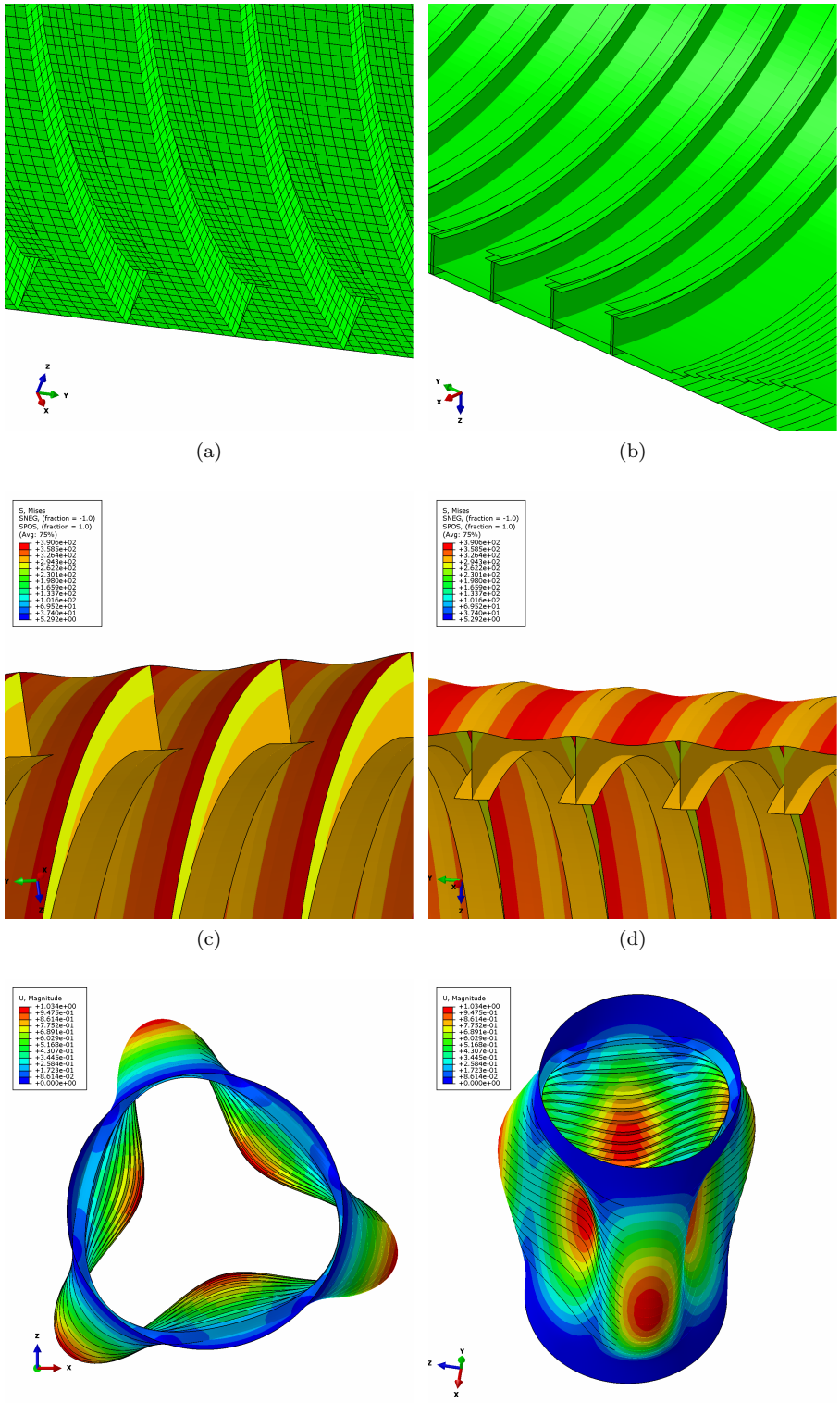

Figure 5.12: Impression of the found optimal stiffened model with the mesh in (a), the rendered shell thicknesses in (b), the von Mises stress distribution at 10 MPa external pressure in (c) and (d), the critical buckling mode shape in (e) and (f).

5.2 Optimization of a composite pressure hull using lamination parameters

As a start, Section (5.2.1) describes the general procedure for a optimization of a composite laminate pressure hull FE model. The FE model itself is described in Section (5.2.2) and the optimization is performed in Section (5.2.3).

5.2.1 General procedure

At this stage, the approach outlined and described in Section.(4.3.2) is used to optimize a composite pressure hull. The first of the two-stage optimization process is schematically shown in Fig.(5.13). As illustrated the lamination parameters, which are the design variables are passed via the *Python* scripting interface to *Abaqus/Standard*. Because the total lay-up thickness needs to be defined in order to evaluate the FE model, this is also written to a data file by *MATLAB*. The FE model is evaluated with the sectional stiffness matrix. The details of this implementation are provided in the next.

An *Abaqus/Standard* user subroutine (*UGENS*) is used to define the shell section stiffness for the FE analysis. The advantage of this subroutine which is written in the *Fortran 90* language, is that the mechanical behavior the shell section can be defined in terms of generalized section quantities. The ABD matrix which is a function of the lamination parameters, governs the relation between the sectional membrane forces, bending moments and the membrane strains and curvature changes. Consequently, this matrix is implemented in the subroutine.

The FE analysis of the model is analogous to the validated stiffened shell model (Section 5.1), i.e. a linear buckling analysis to extract the eigenvalues (i.e. linear buckling load) and a static analysis with a uniformly applied external pressure of 10 MPa. In addition, similar boundary conditions and loads are applied. In order to perform the analysis the composite section thickness and transverse shear moduli are needed. The latter quantities are calculated as described in [58]:

$$K_{11}^{ts} = K_{22}^{ts} = \left(\tfrac{1}{6}(D_{11} + D_{22}) + \tfrac{1}{3}D_{33}\right) Y\,, \quad K_{12}^{ts} = 0 \tag{5.4}$$

where Y is the initial scaling modulus which is equal to unity and D_{ij} are components of the section stiffness matrix.

The section membrane strain and curvature changes of the mid-plane (that is the reference plane in this case) are requested as output of the static analysis. The material failure criterion, which is the Tsai-Wu strength constraint described in Section.(4.3.2), is evaluated with these quantities at the top- and bottommost section points of the shell. Together with the lowest eigenvalue found in the linear buckling analysis, these failure criterion values are returned to the optimizer.

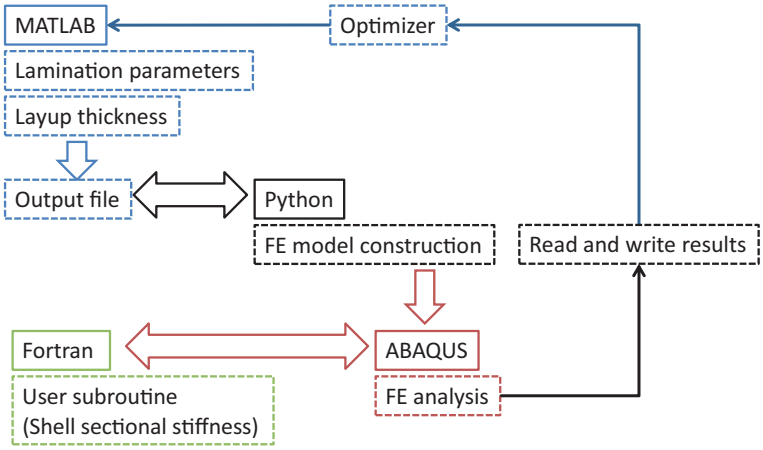

Figure 5.13: Simplified overview of the FE optimization procedure using lamination parameters

It is important to note that because of the gross size of the procedure, the model needs to be validated. By evaluation of a similar FE model for a set of non-trivial lay-ups, the FE model is evaluated and the sectional stiffness matrix are extracted. Perfect correspondence is found for the FE model that is constructed by lamination parameters.

The *MATLAB* algorithm *fmincon*, which is a constrained nonlinear optimization algorithm, is used as an optimizer. It is capable to find a optimum for multi-variable functions. The interior-point algorithm is selected because it is capable to find the optimum in nonlinear convex function. It has to be mentioned that numerical experience seems to indicate that the feasible and strength-constrained domain is indeed convex or nearly so [54]. Implementation of user defined constraint functions is possible, in order to specify the desired design domain. The used constraints are feasible regions of the lamination parameters and material failure, both described in Section.(4.3.2). As a first step, the objective is chosen to be the maximization of the linear buckling pressure. The lay-up thickness and hence the weight of the pressure hull is constant.

5.2.2 FE model description

The main idea behind the construction of this FE model is to adapt most of the features from the reference model, i.e. the previously treated stiffened cylinder FE model, since good correspondence between this model and the experiment. This choice is made since there is no information about an existing model and/or experiments for the composite cylinder. Hence, the dimensions are the same for the outer shell radius and cylinder length. Boundary conditions are also similar. The only difference is that the thick end sections of the *L510-No18* are not modeled. Instead, a single wall thickness is applied to the whole model, which can ultimately

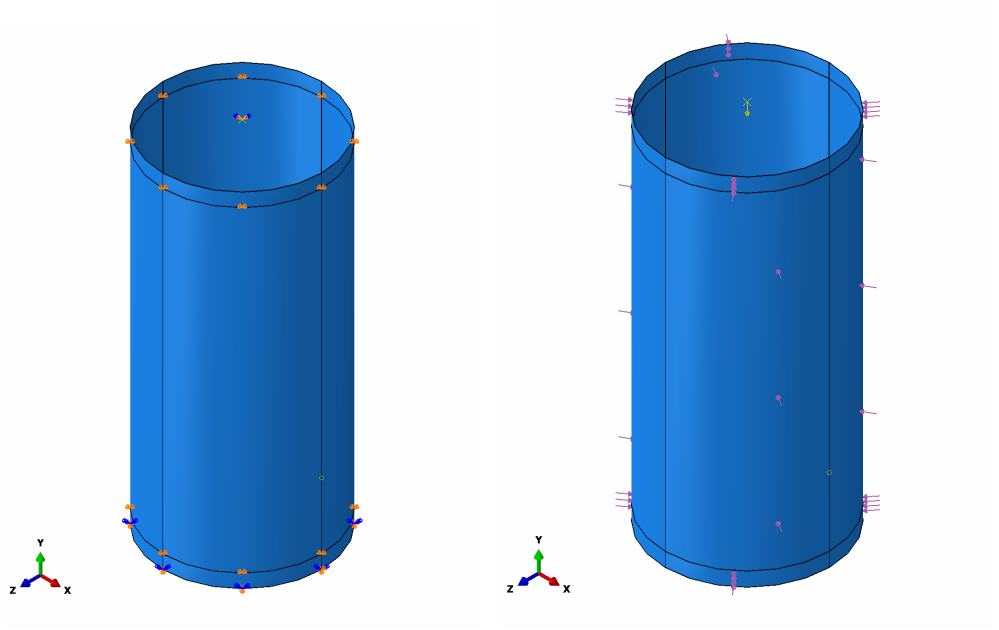

(a) (b)

Figure 5.14: Impression of FE composite cylinder model with the boundary conditions in (a) and the applied loads in (b)

be used as a design variable for the optimization process. The consequence of this choice is that stresses will occur at the boundary conditions. Because the thicker and tapered end section of the reference model, these stresses are diminished. However, in the present thin single walled specimen these stresses will be higher. By assuming that the far field stresses are crucial and by neglecting these stresses, this effect is omitted. Because an end section has to be designed such that these boundary stresses will not occur, e.g. in the reference model, this is a valid choice. A side effect of this choice is that the model will be conservative with respect to the reference model. Boundary conditions are applied at the cylinder ends and at the thick side of the tapered section. Furthermore, the reference model still has an increased stiffness due to this tapered section and a smaller characteristic buckling length.

An impression of the geometry, the boundary conditions and loads is given in Fig.(5.14). As said before, no changes in boundary conditions or loads are made with respect to the reference model. It has to be noted that no imperfections are modeled because of the lack of experimental data. The mesh of the model consists of 10 mm *S4* elements which are fully integrated, general-purpose, finite-membrane-strain shell elements. The element's membrane response is treated with an assumed strain formulation that gives accurate solutions to in-plane bending problems, is not sensitive to element distortion, and avoids parasitic locking. These elements are of course more computational intensive than the reduced integration elements but a greater solution accuracy is obtained for prone to membrane- or bending-mode hourglassing [58].

Thickness	**Lamination parameters**				**Critical pressure**	**Unit weight**
h [mm]	ξ_1	ξ_2	ξ_9	ξ_{10}	P_{cr} [MPa]	[kg/mm]
4	-0.111	-0.133	0.655	0.618	5.27	4.71 E-3
6	0.134	0.094	0.838	0.781	12.99	7.01 E-3
8	0.368	0.355	0.937	0.932	27.96	9.27 E-3

Table 5.5: Result of the critical pressure maximization process with target lamination parameters for specific choices of laminate thickness h

As noted before the mechanical behavior of the shell section is defined by an *UGENS* user subroutine. To activate this general shell section behavior the **SHELL GENERAL SECTION* keyword in the input file is needed. Now, the subroutine is called at the beginning of the increments in all integration points. At the end of the increment it returns the section stiffness matrix of the shell section and the forces and moments per unit length of the shells surface.

5.2.3 Optimization

With the procedure and FE model described, the optimization to obtain the target lamination parameters is elaborated in the next. In general, for a maximization of the linear buckling pressure P_{cr} the optimization problem can be stated as

$$\begin{array}{ll} \text{maximize} & P_{cr}\left(\xi_1, \xi_2, \xi_9, \xi_{10}\right) \\ \text{subject to} & \text{Eq.(4.114) - Eq.(4.116) and Eq.(4.141)} \\ \text{design variables} & \{\xi_1, \xi_2, \xi_9, \xi_{10}\} \end{array} \tag{5.5}$$

First, the ply properties belong to a AS4 carbon fiber/3501-6 epoxy UD composite and are given in Table(C.5). By taking h as the lay-up thickness, the FE model can be defined in terms of the lamination parameters. The found target lamination parameters are provided in Table 5.5. The active constraint in all considered cases is the lamination feasible domain restriction in Eq.(4.116). Furthermore, if one directly compares the unit weight of the stiffened cylinder, being the weight per unit length in axial direction for a characteristic mid-section which is equal to 7.33E-3 kg/mm, one can observe the potential of the 6 mm cylinder in terms of weight. The second stage, which is the search for the most appropriate lay-up is treated in the next.

Analogous to the approach outlined in Section 4.3.1, the construction of a lay-up is performed via a combinatorial fitting of the target lamination parameters with the eye for laminate guidelines. The result for the experiments is displayed in Table 5.5. Again, the minimized error is not the simple squared difference but the derivatives at the target is calculated, as discussed in Section 4.3.1. The Tsai-Wu failure criterion is checked for all lay-ups in Table (5.6) and as expected, all laminates are intact. Furthermore, it can be observed from the table that the lay-ups do not change between range of thicknesses. This is a result of the definition of the error

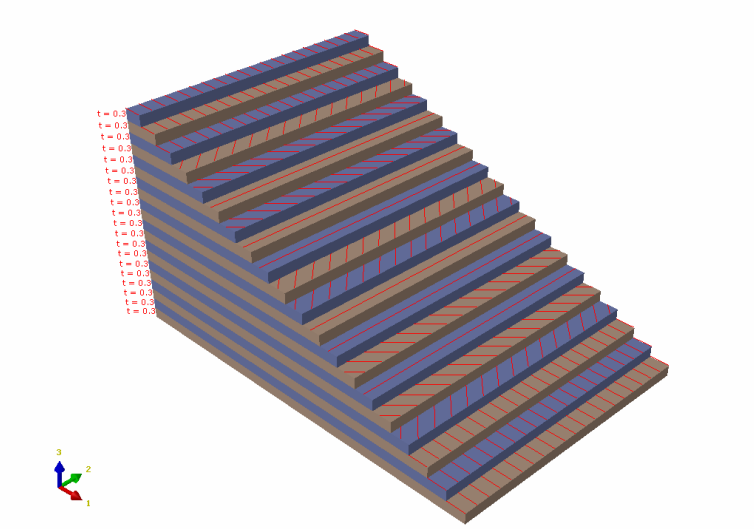

Figure 5.15: Graphical illustration of the found 6 mm laminate with 20 plies

that is minimized throughout the laminate selection fitting process. Note that the ^{s} indicates a symmetric laminate e.g. [0 90]^s=[0 90 90 0].

If one compares the results to the found optimum in critical buckling pressure in terms of lamination parameters, one will see that laminates with a high amount of plies are closer to the this pressure than the lower numbers as there are more degrees of freedom in the fitting process. Of course, this is expected but one has to remember that laminate guidelines can influence this behavior. Notice that the for the found laminates the critical linear buckling pressure can reach values up to an impressive 97% of the target design.

From the target lamination parameter results, which were listed in Table (5.5), it is easily observed that the found optimal design of 6.52E-3 kg/mm for the stiffened conventional pressure hull is a better choice than the more heavy composite cylinder. Since the critical pressure of the stiffened specimen in the linear buckling analysis was 15.1 MPa. However, for deep depth regimes material failure is the critical collapse mechanism and roles are reversed.

Thickness	**Ply count** n	**Laminate**	$\mathbf{\Delta\xi}$	$\mathbf{P}_{cr}$
4 mm	12	$[\text{-45 45 45 0 -45 90}]^s$	0.862	3.38 MPa
4 mm	16	$[\text{0 0 -45 45 45 90 -45 90}]^s$	0.069	4.94 MPa
4 mm	20	$[\text{0 0 0 -45 45 90 45 90 90 -45}]^s$	0.053	4.97 MPa
4 mm	24	$[\text{0 0 0 0 45 -45 90 -45 90 45 90 90}]^s$	0.064	4.99 MPa
6 mm	12	$[\text{-45 45 45 0 -45 90}]^s$	2.512	9.26 MPa
6 mm	16	$[\text{0 0 -45 45 45 90 -45 90}]^s$	0.42	12.215 MPa
6 mm	20	$[\text{0 0 0 -45 45 90 45 90 90 -45}]^s$	0.351	12.44 MPa
6 mm	24	$[\text{0 0 0 0 45 -45 90 -45 90 45 90 90}]^s$	0.292	12.64 MPa
8 mm	12	$[\text{-45 45 45 0 -45 90}]^s$	14.520	18.14 MPa
8 mm	16	$[\text{0 0 -45 45 45 90 -45 90}]^s$	3.119	25.05 MPa
8 mm	20	$[\text{0 0 0 -45 45 90 45 90 90 -45}]^s$	2.279	25.70 MPa
8 mm	24	$[\text{0 0 0 0 45 -45 90 -45 90 45 90 90}]^s$	1.744	26.26 MPa

Table 5.6: The found laminates for different ply counts n and thicknesses h accompanied by the modified error $\Delta\xi$ and corresponding critical pressure P_{cr}. An impression of the 6 mm 20 ply laminate is shown in Fig.(5.15)

5.3 Optimization of a composite sandwich pressure hull using FE

The FE model of a composite sandwich pressure hull is described together with the general procedure for analysis in Section (5.3.1). Optimization is performed in Section (5.3.2).

5.3.1 General procedure and FE model

The general approach to find an optimal composite sandwich structure is very similar to the previously treated composite pressure hull, in Section (5.2). But as the core adds a new feature to the model, the FE model is slightly changed. The model is created such that the skins can consist of different composite laminates. As such, the thickness of each skin can also be used as design variable. As in the previous, *S4* shell elements are used to model these skins. The core is modeled with *C3D8I* continuum elements. These are first-order incompatible mode elements that are enhanced by incompatible modes to improve their bending behavior. In addition to the standard degrees of freedom, incompatible deformation modes are added internally to the elements to eliminate the parasitic shear stresses that cause the response of normal first order displacement elements to be too stiff in bending. Furthermore, the artificial stiffening caused by the Poisson's effect in bending is eliminated with these modes [58]. An impression of the mesh that has a global seed of 10 mm, is given in Fig.(5.16). The used modeling technique in *Abaqus/CAE* is to apply so-called skin layers at the inner and outer facings of the solid elements. As a result from this approach, the reference plane for the laminates are not at the shell mid-plane. Hence, the material is translated and therefore the translated sectional stiffness matrix i.e. Eq.(4.60) is used to describe the sectional mechanical behavior.

Analogous to the previously discussed composite cylinder, validity of the model is cross-checked by evaluation of a similar FE model for a set of non-trivial lay-ups. The FE model is evaluated and the sectional stiffness matrix are extracted. Perfect correspondence is found for the FE model that is constructed by lamination parameters.

Core failure is captured by a three dimensional formulation of the Tsai-Wu criterion:

$$\begin{aligned} &F_{11}\sigma_{11}^2 + F_{22}\sigma_{22}^2 + F_{33}\sigma_{33}^2 + 2F_{12}\sigma_{11}\sigma_{22} + 2F_{13}\sigma_{11}\sigma_{33} + 2F_{23}\sigma_{22}\sigma_{33} \\ &+F_{44}\sigma_{23}^2 + F_{55}\sigma_{13}^2 + F_{66}\sigma_{12}^2 + f_1\sigma_{11} + f_2\sigma_{22} + f_3\sigma_{33} \leq 1\,, \end{aligned} \tag{5.6}$$

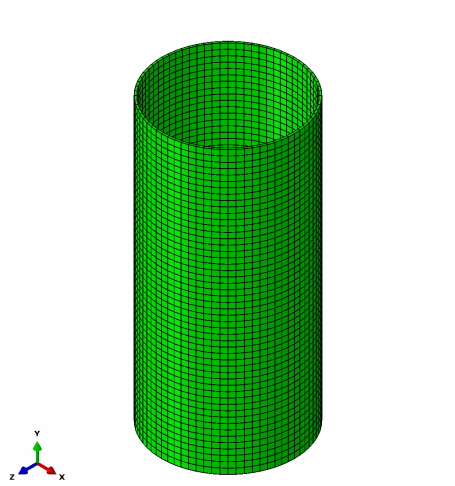

Figure 5.16: Overview of the sandwich mesh, note that the continuum elements are clearly visible while the shell elements are situated at the cylinder inner and outer face

with

$$\begin{aligned}
F_{11} &= \frac{1}{X_t X_c}, & F_{22} &= \frac{1}{Y_t Y_c}, & F_{33} &= \frac{1}{Z_t Z_c} \\
F_{44} &= \frac{1}{Q_{yz}^2} & F_{55} &= \frac{1}{Q_{xz}^2} & F_{66} &= \frac{1}{Q_{xy}^2}, \\
F_{12} &= \frac{-1}{2\sqrt{X_t X_c Y_t Y_c}}, & F_{13} &= \frac{-1}{2\sqrt{X_t X_c Z_t Z_c}}, & F_{23} &= \frac{-1}{2\sqrt{Y_t Y_c Z_t Z_c}}, \\
f_1 &= \frac{1}{X_t} - \frac{1}{X_c}, & f_2 &= \frac{1}{Y_t} - \frac{1}{Y_c}, & f_3 &= \frac{1}{Z_t} - \frac{1}{Z_c}
\end{aligned} \tag{5.7}$$

where the Z refers to the out-of-plane direction and the Q_{ij} refers to the shear strength in the ij-plane. Other values are already described in Section 4.1.6.

Face wrinkling effects are captured with the maximum compressive stress formula for a sandwich with orthotropic cores Eq.(4.83). In-plane sectional forces in the laminate and the engineering constants of the laminates, i.e. according to [30]:

$$E_x^0 = \frac{A_{11}A_{22} - A_{12}^2}{hA_{22}}, \quad E_y^0 = \frac{A_{11}A_{22} - A_{12}^2}{hA_{11}}, \quad \nu_{xy}^0 = \frac{A_{12}}{A_{22}}, \quad G_{xy}^0 = \frac{A_{66}}{h}, \tag{5.8}$$

are used to determine the ultimate wrinkling stress of the sandwich faces.

For honeycomb cores the local face dimpling effect is captured with Eq.(4.85). The largest compressive strength found among all section points is divided by the laminate thickness. Both constraints are constructed with this conservative measure of stress and are applied in fiber and transverse direction. Furthermore, the Tsai-Wu failure criterion in terms of strain components is used to indicate material failure at the skins.

Thicknesses			Lamination parameters				Unit weight
h_{fi} [mm]	h_{fo} [mm]	h_c [mm]	ξ_1	ξ_2	ξ_9	ξ_{10}	[kg/mm]
1.66	1.51	7.77	0.218	0.043	0.287	0.031	4.47 E-3

Table 5.7: Result of the weight minimization process with target lamination parameters and thicknesses

Since the weight is in the following, the buckling strength has to be at least at the same level as the reference, i.e:

$$P_{cr}^{*} - P_{cr} \leq 0 \tag{5.9}$$

5.3.2 Optimization

For simplicity the considered sandwich has two equal orientated lay-ups with different thicknesses. When the core thickness is also taken as a design variable, minimization of the unit weight W^* can be stated as the following optimization problem:

$$\begin{array}{ll} \text{minimize} & W^{*}\left(h_{fi}, h_{fo}, h_c\right) \\ \text{subject to} & \text{Eq.(4.114) - Eq.(4.116), Eq.(4.141), Eq(5.6),} \\ & \text{Eq.(4.83), Eq.(4.85) and Eq.(5.9)} \\ \text{design variables} & \{\xi_1, \xi_2, \xi_9, \xi_{10}, h_{fi}, h_{fo}, h_c\} \end{array} \tag{5.10}$$

Where the unit weight is influenced by the thickness of the inner and outer laminate facing, h_{fi} and h_{fo} respectively. Because of the computational intensive description of the sandwich model a single optimization is performed. Target values for lamination parameters are listed in Table (5.7). With the fitting procedure, the lay-ups are found and presented in Table (5.8).

As the results in Table (5.7) indicate, a tremendous decrease in structural weight is possible. In fact, with this target design a weight saving of 31% can be realized. The target design satisfies all constraints. A margin of 0.37 MPa for the critical linear buckling pressure is reserved and the material failure constraints show that the external pressure could be increased with 10%. Since there is a relatively small margin in linear buckling pressure, the linear buckling constraint for fitted laminates is not satisfied. This can be observed from Table (5.8). Of course, instead of a further search for a more appropriate laminate, a simple but not so elegant solution is to increase the thicknesses. In this way, a design is found which has a little more weight than the target. The details of this design are listed in Table (5.9). This design is closely investigated and all constraints are satisfied, including of course the critical linear buckling pressure constraint. As the thicknesses are changed, the unit weight increases with 4.5% with respect to the target. Moreover, this sandwich designs offers a total weight reduction up to 28% with respect to the optimized reference design treated in Section (5.1.6).

Thickness			Laminate	Error	Unit weight	Critical pressure
$\mathbf{h}_c$ [mm]	$\mathbf{h}_{fi}$ [mm]	$\mathbf{h}_{fo}$ [mm]		$\boldsymbol{\Delta\xi}$ [–]	$\mathbf{W}^*$ [kg/mm]	$\mathbf{P}_{cr}$ [MPa]
7.77	1.66	1.51	$[-45\ 45\ 45\ 0\ -45\ 90]^s$	0.146	4.47E-3	12.87
7.77	1.66	1.51	$[-45\ 45\ 0\ 45\ 0\ -45\ 90\ 90]^s$	0.125	4.47E-3	14.258
7.77	1.66	1.51	$[0\ 0\ 90\ 45\ -45\ 90\ -45\ 0\ 90\ 45]^s$	0.126	4.47E-3	14.378
7.77	1.66	1.51	$[0\ 90\ 0\ 0\ -45\ 45\ 45\ 90\ -45\ -45\ 45\ 90]^s$	0.124	4.47E-3	14.307

Table 5.8: The laminates that satisfy all constraints accompanied by the unit weight, critical linear buckling pressure P_{cr}, for different ply counts n, core thickness h_c, inner and outer facing thicknesses h_{fi} and h_{fo}

Thickness			Laminate	Unit weight	Critical pressure
$\mathbf{h}_c$ [mm]	$\mathbf{h}_{fi}$ [mm]	$\mathbf{h}_{fo}$ [mm]		$\mathbf{W}^*$ [kg/mm]	$\mathbf{P}_{cr}$ [MPa]
7.77	1.75	1.60	$[0\ 0\ 90\ 45\ -45\ 90\ -45\ 0\ 90\ 45]^s$	4.67E-3	15.135 MPa

Table 5.9: The laminate that satisfies all constraints and with an equal critical pressure in the linear buckling analysis accompanied by the unit weight, critical linear buckling pressure P_{cr}, for different ply counts n, core thickness h_c, inner and outer facing thicknesses h_{fi} and h_{fo}

For the sake of completeness, the total optimization procedure is presented in Appendix G. In short, the optimization is called from the *MATLAB main.m* file. The *fmincon* solver is calls the objective function (*objectiveFunction.m*) and the user defined constraint function (*confun.m*). Within the objective function, *Abaqus/Standard* is called with so-called system commands, which of course vary between operating systems. The present system commands can be used in a Linux operating system. At first, the sandwich model in constructed with the *Python* programmed *createSandwich2.py* script. Subsequently, the input file for the FE analysis is modified with another *Python* script called *inputFileModify_sandwich.py* to be able to use the user subroutine *UGENS* for the sectional description. The modified input file called with this subroutine (*ugens_v1.f*) and results are gathered via the *Python* scripting interface with *readOutput_sandwich3.py*. Of course, the constraints are checked with this information. Now, the objective and constraints are passed back to the *fmincon* solver, which will evaluate the previous until convergence is satisfied within the predetermined tolerances.

5.4 Conclusion

As an analogy for the first part of this work, the cylindrical stiffened pressure hull is taken as a reference and is modeled with FE. In an approach to stay in touch with the actual mechanics in such a structure, a pressure hull specimen described by MacKay [50] with comprehensive experimental data is modeled. For the geometry of the specimen, which on purpose deviates from the nominal geometry, the most critical mode shape ($n = 3$) is captured in a linear buckling analysis and later on added to the FE geometry. Of course, the mode shape has an amplitude corresponding to the Fourier decomposition found in [50], which is by far the largest among all amplitudes. With this geometry and a plasticity model for the used material, a non-linear buckling analysis is evaluated. Strain gauge readings of the experiment are compared with output from the strain gauges modeled in FE. Good correspondence is found for the majority of the gauges.

The potential of this conventional model is investigated with a minimization of the structural unit weight. A suitable optimizer was able to find an optimum that satisfies all constraints within the given tolerance. The unit weight was reduced an impressive 15%; maintaining the same strength in terms of yielding and buckling with respect to the reference.

For the composite pressure hull the framework described in Section 4.3.2 is used to form a FE model. The major advantage of this sectional formulation with lamination parameters is a tremendous decrease in calculation time for the FE analysis. As a result, the model can be used in an optimization procedure. Maximization of the linear buckling pressure is first treated and target lamination parameters are found. A combinatorial fitting procedure is subsequently performed to find the most suitable lay-up for different numbers of plies within the laminate. As an addition, a weight minimization procedure which is comparable to the approach outlined in Section 5.1.6, i.e. the reference model, is adopted. Results showed that the optimized stiffened reference model is still a better choice in the search for lightweight design in the considered depth regime. It has to be mentioned that the used FE model for the composite pressure hull is conservative, which is in advantage of the reference model. This conservatism is used in for instance the absence of tapered end sections and in the failure function.

The FE modeling of the sandwich pressure hull is very similar to the previously treated composite hull. But as the sandwich structure has a core that needs to be described accurately, the framework has to be modified for these changes. Again, optimization is performed for the description with lamination parameters for the two skin facings. Again, modeling is performed on a conservative level, and unwanted numerical effects as shear locking are prevented. Results for the weight minimization in terms of target lamination parameters, core and face thicknesses are found with satisfaction of all constraints. Lay-ups are found at the second stage of optimization which show good correspondence with the found optimum. In fact, a 28% weight reduction compared to the optimized stiffened pressure hull is demonstrated with the found design.

Chapter 6

Conclusions and Recommendations

6.1 Lightweight pressure hull design

In general, a submarine is a weight-sensitive structure in which the buoyancy and weight have to reach an equilibrium state. For a given enveloped volume, reducing the structural weight of the submarine has positive effects, e.g. larger payload capability, increase of engine size or even additional structural reinforcement which can ultimately result in even larger depths [12]. The appliance of lightweight materials in pressure hulls holds the key for the gain in performance increase. It is observed that composite materials are promising lightweight candidates. Hence, it is important to investigate such a lightweight composite pressure hull, the related mechanics, the methods in design and compare the new properties with the conventional pressure hull as a reference.

The conventional internally stiffened cylindrical steel pressure hull is found to be 15% heavier than the composite hull and over 2 times heavier when compared to the sandwich hull. This is very promising in terms of performance. As a typical third of the submarine structural weight is occupied by the conventional pressure hull. This means that there is at least 16% of the submarine weight available for extra payload and for instance extra structural reinforcements. Of course it should be remembered that this is only in case of the considered specimen and loads. The effect of e.g. imperfections, fatigue and required load cases has to be investigated. But as there is weight budget left for structural reinforcements, the composite and sandwich hull are still promising candidates.

6.2 Composite pressure hulls

As indicated, the mechanical behavior of a composite material needs to be known before such materials are applied in a pressure hull. The mechanical basics of a composite material are treated and techniques to gather engineering constants at ply level are shown. But as composite laminates mostly consists of multiple stacked plies that vary in orientation the ply description is not appropriate. Therefore the classical laminate theory is elaborated. As an important note this theory neglects through-the-thickness shear deformations, which cannot be neglected for all laminates. Furthermore, in the search of an actual laminate, the most appropriate lay-up guidelines are presented and applied throughout this work.

However, composite materials bring more complexity in the light of failure and strength prediction. Most important failure mechanisms are shown for a composite laminate and for sandwich structures. Descriptions for the onset of failure in terms of analytical formulae, so-called failure criteria, are found to be highly usable to indicate material failure.

A higher level approach for a laminate description in terms of lamination parameters offers a powerful tool when the global optimum in terms of resistance for, say a composite specimen prone to buckling, needs to be assessed for any possible laminate. Since this optimum is formulated in terms of so-called target lamination parameters, an actual laminate needs to be found that is sufficiently close to this target. The proposed method for this fitting problem selects the most appropriate lay-up in accordance with laminate design guidelines.

6.3 FE modeling of pressure hulls

The cylindrical stiffened pressure hull is taken as a reference and elaborated in a FE analysis. In an approach to stay in touch with the actual mechanics in such a structure, a pressure hull specimen described by MacKay [50] with comprehensive experimental data is modeled. For the geometry of the specimen, which on purpose deviates from the nominal geometry, the most critical mode shape ($n = 3$) is captured in a linear buckling analysis and later on added to the FE geometry. With this geometry and a plasticity model for the applied material, a non-linear buckling analysis is evaluated. Strain gauge readings of the experiment are compared with output from the strain gauges modeled in this FE analysis. Good correspondence is found for the majority of the gauges and the collapse pressure. For the considered specimen an thorough weight optimization showed that a reduction of 15% is feasible without a decrease in collapse pressure.

Lessons learned in the process of FE modeling for the stiffened pressure hull are applied in the foundation of a composite pressure hull. For the used FE application, i.e. *Abaqus*, the lamination parameter formulation of the material is implemented via a sectional description of the

material. The user subroutine *UGENS* opens the possibility use such a description for a material.

The use of lamination parameters in a FE context is outlined. The missing link turns out to be a constraint that indicates material failure. The Tsai-Wu based failure criterion in the context of a lamination parameter approach, proposed by IJsselmuiden et al. [48] is the answer for this problem. It is demonstrated that this is a conservative failure criterion since it is regardless to the ply orientations in the potential laminate.

The FE modeling of the composite sandwich pressure hull is very similar to the previously treated composite hull. But as the sandwich structure has a core material that needs to be described accurately, the framework used for the description of a single laminated composite cylinder has to be slightly modified for these changes.

6.4 Weight minimization of composite FE models

The major advantage of this sectional formulation with lamination parameters is the tremendous decrease in calculation time for the FE analysis. As a result, the model can be used in an optimization procedure and target lamination parameters are easily found. A computational extensive combinatorial fitting procedure on the target lamination parameters is subsequently performed to find the most suitable lay-up for different numbers of plies within the laminate.

Weight minimization for a FE model of the composite cylindrical pressure hull which is subjected to constraints related to material failure and buckling effects is found to be convenient when lamination parameters are used. Compared to the reference model, it is shown that for the considered depth regime the optimized reference model is still superior to the composite FE model. However, it is important to note that the composite FE model is described in a conservative manner.

The weight minimization for the composite sandwich model is performed with a sectional description in terms of lamination parameters for the two skin layers. The core brings some extra complexity to the model when compared to the single laminated cylinder. The use of lamination parameters provides computational profit in calculation time. As for the composite model, results for the optimization in terms of target lamination parameters are found with satisfaction of all constraints. In this search for a minimal structural weight it is lay-ups are found at the second stage of optimization which show good correspondence with the found optimum. In fact, a weight reduction up to 28%, with respect to the optimized stiffened pressure hull, is demonstrated with the found lay-up sandwich design.

For the considered shallow water depth regime, calculations have shown that the sandwich-structured composite pressure hull performs better than the composite monocoque pressure

hull, in terms of weight. Because the collapse for the monocoque is buckling dominated, this result is expected as the sandwich hull has more bending stiffness. For deeper depths the need of a core material diminishes because the collapse is dominated by material failure. Eventually, when depths are increased, the sandwich will converge to a monocoque for the optimum in unit weight.

6.5 Recommendations for future work

Validation of the composite and composite sandwich FE models has to be performed. In order to do this, experimental models have to be produced and accurate measurements have to be performed, similar to MacKay's [29] specimens of conventional pressure hulls. In this context, the material properties have to be gathered from experiments. Additionally, the effect of residual stresses due to curing of the laminate should be estimated and modeled in an FE context to get an accurate description. The geometry of such a test specimen has to be carefully designed. The end sections can potentially be a source of failure due to the increase of radial stiffness. Hence, the specimen should be designed such that failure initiates at the mid-section which is, as an important note, also the design philosophy in MacKay's work.

With these test specimens designed and tested, knowledge is gained about shell to end section transitions. A straightforward next step would be to design a whole pressure hull, that is for instance, including the end domes and bulkheads. It should be noted that these design problems can be solved with the present use of lamination parameters. Specific areas that need other mechanical properties can in this context be seen as laminates with different lamination parameters. Extreme care has to be taken for these discontinuities in the sandwich cylinder. Existing design solutions for these transitions have to be assessed.

The FE part of this work is deduced from small-scale pressure hull specimens. Likewise, the found results correspond to this small-scale. It is important to note that scale effects can influence the mechanical behavior or collapse on a full-scale (or larger-scale). Scale effects can for instance appear in the strength of the applied material. A statistical approach as the Weibull theory is commonly used to investigate the effect of size on strength. Hence, the correspondence with realistic full-scale models has to be investigated and an extrapolation to such a model is not straightforward.

Since the present thesis focusses only at the resistance against the external hydrostatic pressure, more load cases need to be investigated. The mechanical performance that arises from operational requirements, e.g. in terms of fatigue life and impact, cannot be neglected in the further design procedure.

The sectional description in terms of lamination parameters needs to be further explored in

terms of the feasible region. The more accurately these regions are defined, the more precise the global optimum (target) refers to an actual laminate design. The effect of development (and possible changes) in the formulation of feasible regions for lamination parameters should be taken into account for future research.

The application of composites instead steel in the conventional hull with internal stiffeners should be investigated for shallow depths. This design could potentially provide a larger gross interior volume than the proposed sandwich hull. For an actual design, the stiffeners should be modeled with sets of lamination parameters. In this way, the presented framework for optimization can be utilized to design such a structure with minimized weight.

Acknowledgements

The author gratefully acknowledges the helpful support and advise provided by Prof.dr.ir. Fred van Keulen and Dr.ir. John R. MacKay in his Master's Thesis process.

Bibliography

[1] R. Burcher and L. Rydill, *Concepts in submarine design.* Cambridge University Press, 1994.

[2] T. P. C. Staff, *Steel Boats, Iron Men: History of the U.S. Submarine Force.* Turner Publishing Company, 1994.

[3] W. Stevens and A. Westcott, *A history of sea power.* G. H. Doran company, 1920.

[4] P. Walker, *Engineers of Independence: A Documentary History of the Army Engineers in the American Revolution, 1775-1783.* University Press of the Pacific, 2002.

[5] "Battle of the atlantic." Technical Intelligence from Allied C.I., SRH-25, vol. 4.

[6] J. Schlemm, "U-boat types: Type xxi." Date of access: 19-7-2012.

[7] D. Walsh, "The bathyscaph trieste," Research report 1096, U.S. Navy Electronics Laboratory, 1962.

[8] R. O'Rourke, *The United States Navy: Current Issues and Background.* Nova Science Publishers, 2003.

[9] C. Prins, P. Breen, D. Simons, J. Wilgenhof, J. Reijmers, E. Jansen, and A. van Koersel, "Reach - a submerged remote sensing reconnaissance system," tech. rep., Dutch Underwater Knowledge Centre, 2008.

[10] N. Polmar and J. Noot, *Submarines of the Russian and Soviet Navies, 1718-1990.* Naval Institute Press, 1991.

[11] D. Haynes, "Composite materials for submarine pressure hulls," Master's thesis, University college london, 1999.

[12] C.S. and Smith, "Design of submersible pressure hulls in composite materials," *Marine Structures*, vol. 4, no. 2, pp. 141 – 182, 1991.

[13] C.-J. Moon, I.-H. Kim, B.-H. Choi, J.-H. Kweon, and J.-H. Choi, "Buckling of filament-wound composite cylinders subjected to hydrostatic pressure for underwater vehicle applications," *Composite Structures*, vol. 92, no. 9, pp. 2241 – 2251, 2010. ¡ce:title¿Fifteenth International Conference on Composite Structures¡/ce:title¿.

[14] C. Ross, "A conceptual design of an underwater vehicle," *Ocean Engineering*, vol. 33, no. 16, pp. 2087 – 2104, 2006.

[15] Derek and Graham, "Buckling of thick-section composite pressure hulls," *Composite Structures*, vol. 35, no. 1, pp. 5 – 20, 1996. ¡ce:title¿Stability of Composite Structures¡/ce:title¿.

[16] J. Tucker, "Glass reinforced plastic submersibles," *Trans. NEC Inst. Engrs. and Shipbuilders*, vol. 95, no. 2, pp. 48 – 59, 1979.

[17] T. Messager, M. Pyrz, B. Gineste, and P. Chauchot, "Optimal laminations of thin underwater composite cylindrical vessels," *Composite Structures*, vol. 58, no. 4, pp. 529 – 537, 2002.

[18] C.-C. Liang, H.-W. Chen, and C.-Y. Jen, "Optimum design of filament-wound multilayer-sandwich submersible pressure hulls," *Ocean Engineering*, vol. 30, no. 15, pp. 1941 – 1967, 2003.

[19] C. Smith, *Design of marine structures in composite materials*. Elsevier Science Publishers, 1990.

[20] J. Gao, W. Sun, and K. Morino, "Mechanical properties of steel fiber-reinforced, high-strength, lightweight concrete," *Cement and Concrete Composites*, vol. 19, no. 4, pp. 307 – 313, 1997.

[21] W. Flugge, "Stress problems in pressurized cabins," Tech. Rep. NACA TN 2612, National Advisory Committee for Aeronautics, 1952.

[22] J. MacKay, *Experimental and Numerical Modeling in support of a Structural Design Framework for Submarine Pressure Hulls based on Nonlinear Finite element Collapse Predictions*. PhD thesis, Delft University of Technology, 2012.

[23] P. Radha and K. Rajagopalan, "Ultimate strength of submarine pressure hulls with failure governed by inelastic buckling," *Thin-Walled Structures*, vol. 44, pp. 309–313, 2006.

[24] W. Nash, *Hydrostatically loaded structures*. Elsevier Science Publishers, 1995.

[25] M. A. Krenzke and R. D. Short, "Graphical method for determining maximum stresses in ring-stiffened cylinders under external hydrostatic pressure," tech. rep., Defense Technical Information Center, 1998.

[26] J. Arbocz and J. Hol, "Collapse of axially compressed cylindrical shells with random imperfections," *Thin-Walled Structures*, vol. 23, no. 1-4, pp. 131 – 158, 1995.

[27] S. Kendrick, "Shape imperfections in cylinders and spheres: Their importance in design and methods of measurement," *The Journal of Strain Analysis for Engineering Design*, vol. 12, no. 2, pp. 117–122, 1977.

[28] S. Kendrick, *The Stress analysis of pressure vessels and pressure vessel components.* Pergamon Press, 1970.

[29] J. MacKay, "Structural analysis and design of pressure hulls: the state of the art and future trends," tech. rep., Defence R&D Canada - Atlantic, 2007.

[30] A. Nijhof, *Vezelversterkte kunststoffen: mechanica en ontwerp.* VSSD, 2005.

[31] R. Jones, *Mechanics of composite materials.* Taylor and Francis, 1975.

[32] R. Förster and S. Knappe, W., "Experimentelle und theoretische untersuchungen zur rißbildungsgrenze an zweischichtigen wickelrohren aus GFK unter innendruck," *Kunststoffe*, vol. 8, no. 61, 1971.

[33] H. Schneider, "Experimentelle und theoretische betrachtungen zur ermittlung von elastizitätskenngrößen von CFK laminaten," 1981. DGLR Vortrag Nr. 81 058.

[34] A. Puck, "Zur beansprung und verformung von GFK - mehrschichtenverbund bauelementen," *Kunststoffe*, vol. 4, no. 57, 1967.

[35] J. Reddy, *A refined shear deformation theory for the analysis of laminated plates.* National Aeronautics and Space Administration, Scientific and Technical Information Branch, 1986.

[36] J. Bailie, R. Ley, and A. Pasricha, "A summary and review of composite laminate design guidelines," Tech. Rep. NAS1-19347, NASA, 1997.

[37] A. Orifici, *Degradation Models for the Collapse Analysis of Composite Aerospace Structures.* PhD thesis, RMIT University, 2007.

[38] ESTEC, "Esa pss-03-203," Noordwijk, the Netherlands, 1994.

[39] V. K. Srivastava and S. Lal, "Mechanical properties of e-glass fibre reinforced nylon 6/6 resin composites," *Journal of Materials Science*, vol. 26, pp. 6693–6698, 1991. 10.1007/BF00553694.

[40] N. F. Dow and B. W. Rosen, "Evaluations of filament-reinforced composites for aerospace structural applications," Tech. Rep. NASA-CR-207, NASA, 1965.

[41] R. Marissen, "Vezelversterkte kunststoffen vervolgcursus." Delft University of Technology Lecture Notes wb1430B, 1994.

[42] ESTEC, "Ecss-e-hb-32-20 part 3a," Noordwijk, The Netherlands, 2011.

[43] S. Tsai and E. Wu, "A general theory of strength for anisotropic materials," *Journal of composite materials*, vol. 5, no. 58, 1971.

[44] W. Flügge, *Stresses in shells.* Springer-Verlag, 1973.

[45] M. Miki, "Material design of composite laminates with required in-plane elastic properties," *Progress in Science and Engineering of Composites (Proc. ICCMIV)*, pp. 1725–1731, 1982.

[46] M. Miki and Y. Sugiyama, "Optimum design of laminated composite plates using lamination parameters," in *Proceedings of AIAA 32nd Structures, Structural dynamics and Materials Conference*, pp. 275–283, 1991.

[47] H. Fukunaga and H. Sekine, "Stiffness design method of symmetric laminates using lamination parameters," *AIAA Journal*, vol. 30, pp. 2791–2793, 1992.

[48] C. G. Diaconu, M. Sato, and H. Sekine, "Buckling characteristics and layup optimization of long laminated composite cylindrical shells subjected to combined loads using lamination parameters," *Composite Structures*, vol. 58, no. 4, pp. 423 – 433, 2002.

[49] H. Fukunaga and G. Vanderplaats, "Stiffness optimization of orthotropic laminated composites using lamination parameters," *AIAA Journal*, vol. 29, pp. 641–646, 1991.

[50] J. MacKay, "Experimental investigation of the strength of damaged pressure hulls - phases 5 & 6," tech. rep., Defence R&D Canada - Atlantic, 2011.

[51] A. Todoroki and R. T. Haftka, "Stacking sequence optimization by a genetic algorithm with a new recessive gene like repair strategy," *Composites Part B: Engineering*, vol. 29, no. 3, pp. 277 – 285, 1998.

[52] K. Yamazaki, "Two-level optimization technique of composite laminate panels by genetic algorithms," *AIAA-96-1539-CP*, pp. 1882–1887, 1996.

[53] K. Yamazaki, "Two-level optimization technique of composite laminate panels by genetic algorithm," *AIAA-96-1539-CP*, 1996.

[54] S. IJsselmuiden, M. Abdalla, and Z. Gürdal, "Implementation of strength-based failure criteria in the lamination parameter design space," *AIAA Journal*, vol. 46, pp. 1826–1834, 2008.

[55] "Ces edupack." Granta Design Limited, Cambridge.

[56] M. Schlüter, "Global optmization software for mixed integer nonlinear programming," *http://www.midaco-solver.com*, 2009.

[57] "Matlab, r2010b." the MathWorks, Inc., http://www.mathworks.com, 2010.

[58] "Abaqus 6.10 online documentation." Dassault Systèmes, 2010.

[59] J. Blachut and P. Smith, "Buckling of multi-segment underwater pressure hull," *Ocean Engineering*, vol. 35, no. 2, pp. 247 – 260, 2008.

[60] G. Pahl and W. Beitz, "Engineering design, a systematic approach," 2007.

[61] "Submarine sytem requirements." Submarine structures, part 1, Australian Defence Force, DEF(AUST)5000, 2009.

[62] "Hy-80, sa-197," 1966. Engineering Alloys Digest, Inc., ASM International, 1966.

[63] "Hy-100, sa-255," 1970. Engineering Alloys Digest, Inc., ASM International, 1970.

[64] "Hy-130 and hy-140(t), sa-280," 1972. Engineering Alloys Digest, Inc., ASM International, 1972.

[65] C. Harper, *Handbook of materials for product design.* McGraw-Hill, 2001.

[66] P. Soden, M. Hinton, and A. Kaddour, "Lamina properties, lay-up configurations and loading conditions for a range of fibre-reinforced composite laminates," *Composites Science and Technology*, vol. 58, no. 7, pp. 1011 – 1022, 1998.

Appendix A

Basic pressure hull concepts

A.1 Geometrical pressure hull concepts

In the following an overview is given of existing pressure hull geometries. The discussed concepts can later be used as ingredients for concept generation.

Sphere

The ideal shape of a pressure vessel subject to uniform hydrostatic pressure is a sphere. The sphere is ideal due to the efficient stress and strain situation in the material. Efficiency in a way that stresses and strains are equally distributed throughout the material. For submarines that are designed only to withstand the external pressure, a sphere may be a suitable shape. But in terms of hydrodynamics, as mentioned earlier, a slender body is required to lower the form drag forces.

Tear shaped shell

The most streamlined form of a submerged body is tear or needle shaped. For a submarine that has to be the most efficient in traveling underwater, one has to adopt this form. Unfortunately this shape causes a lot of bending effects in the material, unlike the spherical form, especially at the front and aft of the shell. It can be said that if the submarine is created for shallow water purposes only, the tear shaped form of the hull could be advantageous.

Right circular cylinder

In order to make a compromise between the spherical ideal pressure withstanding shape and the streamlined tear drop shape, a cylindrical form is a fitting option. The stresses in the cylinder are distributed such that the circumferential part is two times as large as the axial part, which is less efficient than the sphere. Also, there are bending effects at the front and the aft of the cylindrical shell in the dome-cylinder transition region. On the other hand, the

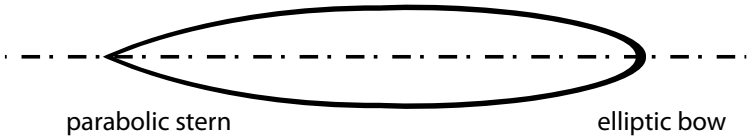

Figure A.1: Hydrodynamic efficient forms

Figure A.2: Example of a cylindrical pressure hull

sphere is not quite as efficient in volumetric efficiency, i.e. the possibility to fill the internal space. Full occupation of the internal space by the interior is a difficult task since the sphere is doubly curved. The cylinder has a single curvature which increases the volumetric efficiency. The hydrodynamic shape, which is optimal for $(L/D = 6)$, is streamlined.

Shaped circular cylinder

A smooth diametrically varying shaped circular cylinder is desired if the form drag has to be lowered. This idea can be seen as a step in the tear shaped form, from the right circular cylinder point of view. In cases that the pressure hull outside is actually the outside of the whole submarine, this shape is desired [1].

Corrugated cylinder

The idea to use corrugated cylinders as a pressure hull is proposed by Ross in [14]. In view of the manufacturability of the submarine this shape, as shown in Fig.(A.4) can ease the production of the whole. Due to the repeatedness of the segments the efficiency in production can be increased. The segments itself can also be changed in shape. Ross proposed conical segments, while spherical segments can potentially be more efficient in terms of stress distribution. [59] showed that in fact, the spherical segments perform good in terms of collapse strength. An impression of the spherical segments is given in Fig.(A.5).

A.2 Concept generation

Pahl [60] describes the steps to enhance the process of conceptual design. The approach is as follows: By identifying the essential problems in designing a pressure hull through abstraction the first step is made in concept generation. Subsequently the main and subfunctions have to be established. With these functions a set of appropriate working principles is created. From here a basic solution path is created to describe the principle solutions i.e. the concept.

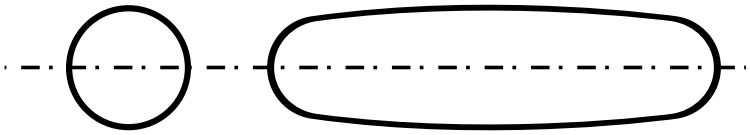

Figure A.3: The right circular cylinder (top) and the shaped circular cylinder (bottom)

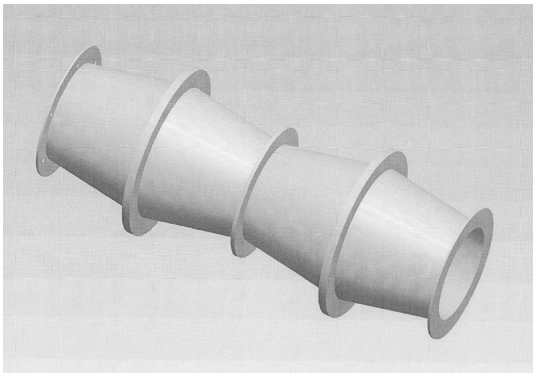

Figure A.4: The corrugated cylinder as presented in [14]

Concept related requirements and functions

In order to generate pressure hull concepts and to get a clear view on the philosophy concerned with the different concepts, the pressure hull is considered to be a system with (at first) the following requirements:

1 General

F 1.1 Provide internal space

F 1.2 Resist hydrostatic pressure

The most important boundary conditions are listed in the next.

1 Performance

B 1.1 Lower the acoustic signature

B 1.2 Lower the magnetic signature

2 Costs

B 2.1 Lower the operational costs

B 2.2 Lower fabrication costs

Search for solutions

Previously a list of main functions and boundary conditions is established. With this information the search for solutions is started. From F 1.1 and F 1.2 a set of solutions is found:

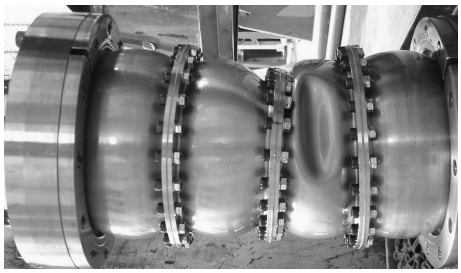

Figure A.5: The corrugated flanged sphere cylinder as presented in [59]

[S 1] Sphere

[S 2] Cylinder

With the given functions the perfect solution would be a sphere [S 1]. The stress in the plane induced by the external pressure is the same in both directions. As a result the (isotropic) hull material is used in an effective way. A cylinder [S 2] with end closures is also a solution, but the 2:1 (circumferential to axial) stress relation is less efficient than the sphere. To optimize this efficiency the following solutions are found:

[S 3] Ring stiffened cylinder

[S 4] Cylinder with anisotropic skin

[S 5] Corrugated cylinder

[S 6] Thick-walled cylinder

By adding material in the circumferential direction and maintaining the amount in the axial direction, the stress relation can be equalized to a 1:1 situation. This is positive with respect to the material efficiency. The found solutions with this philosophy are listed above. The first solution, the ring stiffened cylinder [S 3], is a proven concept. Due to the use of ring stiffeners in the circumferential direction the (mean) stress in the circumferential direction can be lowered. In this way the stress relation can be 1:1. The stiffeners can have different appearances. Different appearances can be for instance the internal placement of the stiffeners in the cylinder. In this case the interface between the hull and the stiffeners is loaded in compression. Second, a known solution is the external stiffened cylinder. The interface is now loaded in tension.
The use of an anisotropic material [S 4] that is tailored such that the direction and magnitude of the stresses correspond to the strength of the material can be a very efficient solution. Composites are known for their anisotropic behavior. Hence, it is important to mention composite as a potential candidate. To give an example, a filament wound composite cylinder would be appropriate. The desired anisotropic behavior can be obtained by filament winding in the axial direction and in the hoop direction, with the amount of a higher amount of fibers in the hoop direction.
The solution for the function to resist the hydrostatic pressure F 1.2 does not only concern hull

strength only. The collapse of a pressure hull can also take place due to buckling, especially for thin walled structures which are used in small depths. To increase the amount of resistance against buckling the following solutions are found: A corrugated cylinder [S 5] is known to be very resistant to lateral buckling.
Another way to avoid the buckling regime is to thicken the hull. That is why a thick-walled pressure hull [S 6] can be suitable. A proven solution is for instance a sandwich structure. Different skin and core types can be applied. Additionally the anisotropic behavior can also be imitated by the use of a composite skin.

[S 7] Noise damping skin materials

[S 8] Streamlined hull

[S 9] Non-ferromagnetic skin materials

[S 10] Hull with dimensions L/D=6

[S 11] Modular hull sections

In the next the listed boundary conditions are treated. In an approach to lower the acoustic signature B 1.1 the hull material must have good damping properties [S 7]. The reduction due to isolation of the acoustic signature, with steel as reference, can be achieved with composites and sandwich structures. These materials have good noise damping properties compared to steel. Sound produced internally by for instance machinery can be silenced to improve stealth.
Another approach to lower the acoustic signature is to minimize the hydrodynamic noise. This noise is generated in transit due to the perturbation of water caused by the outside of the hull. A streamlined body will minimize this noise [S 8]. An example is the tear-shaped hull Fig.A.1.
The magnetic signature B 1.2 refers to the ferromagnetic property of the hull material. There are only a few substances that are ferromagnetic, and the only relevant examples here are iron and nickel. To increase stealth, the magnetic signature should be lowered. The main solution for this is to construct in non-ferromagnetic materials [S 9].
Additionally, boundary conditions for costs are also mentioned. The most relevant costs during operation arise when the submarine powers the engine in transit. Obviously, the drag on the hull has to minimized in order to decrease the amount of power. The application of a streamlined hull is therefore also a suitable solution here. But for a given volume, it is already mentioned that the drag is the lowest for $(L/D = 6)$. Hence, this optimal shape is a good solution in lowering the desired engine propulsion power [S 10].
The second cost related boundary condition concerns the fabrication costs. Apart from the material costs of the hull, there are labor costs. The fabrication of a steel main hull structure is described by [1]: The usual procedure is to assemble the plating and frames into lengths of two to three meters of the hull and these are known as hoops. Some of the hoops will be cylindrical, others will have slight conicality and others near the stern may have quite marked conical shaping to them. It is now common practice to have some form of very large mandrel on

which the whole hoop section can be rotated to allow hand-down welding on both internal and external welds of the hull. The next stage of fabrication is to join the cylindrical hoops together with cones and domes and some of the external structure to form a few major sub-assemblies of the hull say, three or four major assemblies. After the internal fitting out process the hull is joined together. If the creation of the major sub-assemblies of the hull is performed in fewer steps or even automated the costs on labor could be decreased. For instance, when a machine produces modular main hull section that is later joined together with other modular sections [S 11], the amount of time and labor of the hull fabrication process could potentially drop.

Appendix B

General Requirements

An small part of a general requirements list for military purposes, excerpted from [61], is listed in the following.

1 Performance

1.1 The considered loading on the structure is the following:

R 1.1.1 Hydrostatic and hydrodynamic pressure

R 1.1.2 Pressure/load induced by the interior

R 1.1.3 Pressure/load due to operational equipment

R 1.1.4 Shock pressure loads and accelerations

R 1.1.5 Rolling and pitching motions

R 1.1.6 Bottoming and docking

1.2 Shock load design guidance:

R 1.2.1 Avoid large difference in stiffness of adjoining members

R 1.2.2 Avoid use of unsymmetrical stiffening

2 Materials

2.1 The materials proposed for the pressure hull structure should meet the following criteria regarding the mechanical properties.

R 2.1.1 High yield strength

R 2.1.2 High toughness levels

R 2.1.3 Ability to withstand extreme deformation at high strain rates

R 2.1.4 Low susceptibility to stress corrosion cracking

R 2.1.5 Resistance to high stress low cycle fatigue

R 2.1.6 Resistance to corrosion or loss of properties at environmental extremes

Appendix C

Hull materials

In this section an overview is given on materials that are capable to be applied in the pressure hull. Not only the resistance to external pressure is of great importance but also withstanding the exposed environment. The environment could for instance cause oxidation for some metals. Specific properties as acoustic and magnetic signatures are important for naval applications. In the following the most important traits of the selected materials are summed up. Apart from that, each material is outlined for the following features:

- Structural properties (Young's modulus, compressive/tensile/yield strength, density, failure strain)
- Approximate price per unit mass
- Operating temperatures
- Fatigue strength after 10^7 cycles
- Fracture toughness
- Fabrication properties
- Environmental durability (Flammability, salt water resistance, water absorption after 24h)

With the help of a material selection software package, CES Edupack [55], different property diagrams are made in order to visualize the mechanical properties and to create a pre-selection of materials. In the process of material selection, this software turns out to be a powerful tool.

C.1 Selected materials

Because lightweight design is paramount, ranking materials in the present thesis is performed on a specific mechanical property basis. By doing this for all materials, envelopes for material families are easily created. By creation of such envelopes for the Youngs modulus and compressive strength a combined envelope is created. The result is shown in Fig.(C.1). In this figure, it

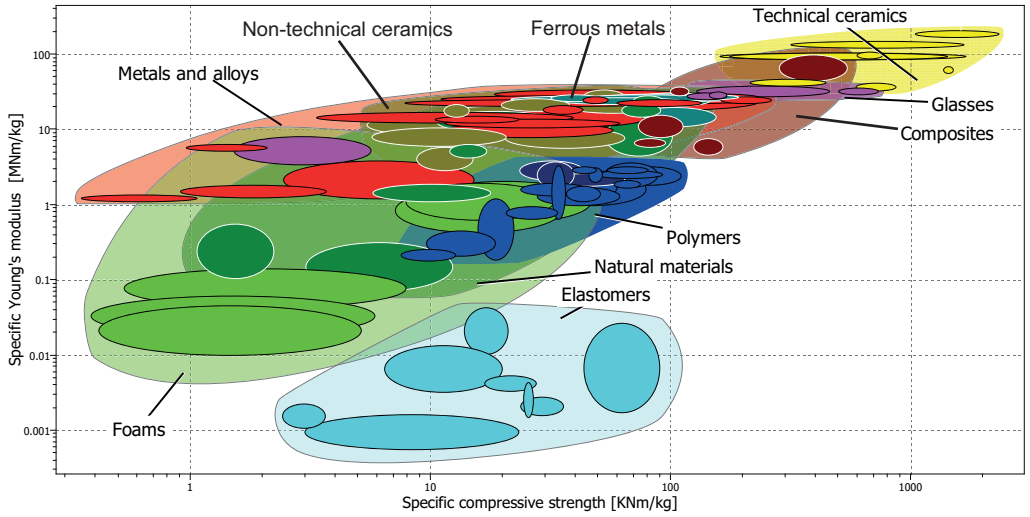

Figure C.1: The specific strength versus specific Youngs modulus chart. The illustration is created with [55]

is easily seen that the technical ceramics are the best choice when one only wants high specific compressive strength and stiffness. But, since other mechanical properties as fracture toughness are important, construction of a hull in technical ceramics is not the best choice. With the assumption that a potential hull material has to have similar or better properties in fracture and fatigue strength as the conventional hull material, i.e. high strength steel, a new diagram is constructed in Fig.(C.2). The characteristics of this small but suitable selection of materials is treated in the next.

C.2 Metals

The most common choice for a pressure hull materials are metals and especially high strength steel [1]. A more exotic choice is utilized in the Russian Alfa class; titanium alloys are used to reach great performance in speed and diving depth.

C.2.1 Steel

High strength steels are the most suitable among the ferrous metals for submarine applications. HY80 is the most commonly used of the high strength steels [14]. Note that the HY refers to high yield and the 80 is the yield strength in ksi, i.e. in thousands of psi) According to [62] HY-80 is a low carbon, nickel, chromium, molybdenum allay steel exhibiting moderate strength combined with excellent ductility at tall expected service temperatures. It can be readily welded to form tough weldments. This steel was developed as a high yield strength material with excellent low temperature impact properties. It performs good under dynamic loading, shows an high resistance to crack propagation and joints welded according proper procedures can be made

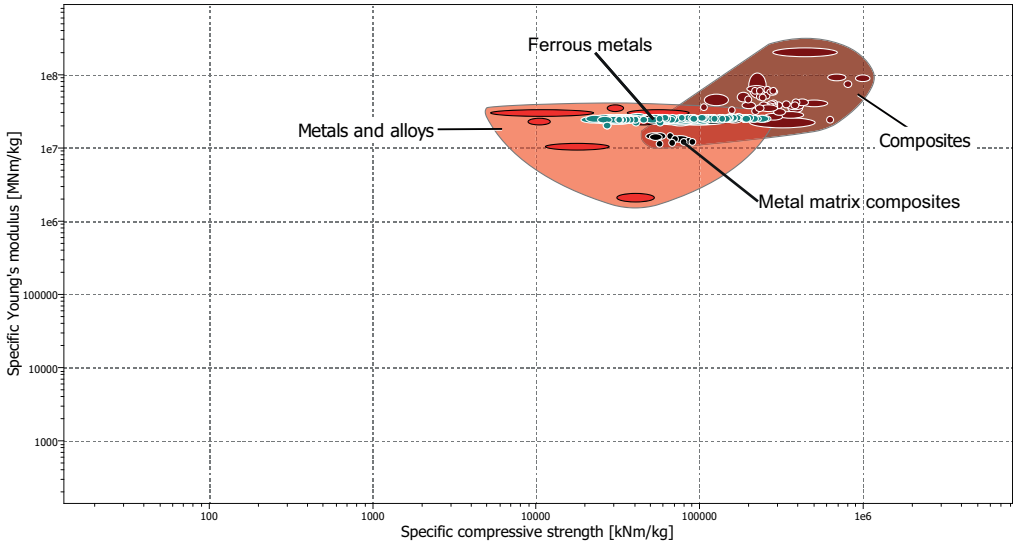

Figure C.2: The specific strength versus specific Youngs modulus chart. The illustration is created with [55]

to approach prime plate in strength and toughness. The HY100 steel performs similar to the HY80 but its composition and heat treatment have been adjusted to achieve a higher yield strength. It can be welded readily with existing processes to form weldments which are tough enough to withstand repeated shock loading without failure. It provides great resistance to crack initiation and propagation, even at low temperatures [63]. For higher strength steels e.g. HY130, associated problems in welding, control of pre-heat and post-weld cooling makes fabrication difficult especially for large structures. The main advantages of steel are its ductility, high modulus and that the material is inexpensive and readily available [11]. An overview of relevant mechanical properties is provided in Table (C.1). Note that these steels are subject to temper embrittlement. Stress relief treatments of heavy welded sections can result in such embrittlement due to the time spent during cooling in the temperature 560°C to 400°C [64].

The corrosive behavior of steel is the general disadvantage. Moreover, the magnetic property and the brittleness at low temperatures are potential show stoppers.

C.2.2 Titanium alloys

Titanium alloys are known for their high (specific) compressive and tensile strength. Also these alloys are non-magnetic and show superior corrosion resistance. The primary disadvantages of titanium are the high material cost and the problems in welding [11] and machining. Titanium alloys are fully resistant to seawater, up to 315° C (i.e. steam) [65]. Table (C.2) shows the properties of typical titanium alloys.

Name	Steel HY-80	Steel HY-100	Steel HY-130
Density $[kg/m^3]$	7700 - 7800	7700 - 7800	7700 - 7800
Price $[EUR/kg]$	N/A	N/A	N/A
Youngs modulus $[GPa]$	200 - 207	200 - 207	200 - 207
Compressive strength $[MPa]$	710 - 720	N/A	N/A
Strength to weight ratio $[KNm/kg]$	92 - 92	N/A	N/A
Tensile yield strength $[MPa]$	552 - 690	690 - 827	896 - 1034
Tensile strength $[MPa]$	710 - 720	N/A	N/A
Fatigue strength $n = 10^7$ $[MPa]$	280 - 315	N/A	N/A
Fracture toughness $[MPa\sqrt{m}]$	66 - 95	N/A	N/A
Elongation $[\%strain]$	19 - 20	18 - 18	18 - 18
Service temperature $[°C]$	-35 - 470	N/A	N/A
CO_2 footprint, Primary production $[kg/kg]$	2.36 - 2.61	N/A	N/A
Flammability	Non-Flammable	Non-Flammable	Non-Flammable
Salt water	N/A	N/A	N/A
UV Radiation (sun)	Excellent	Excellent	Excellent
Recylcle	Yes	Yes	Yes
Magnetic	Yes	Yes	Yes

Table C.1: List of different types of Steel [55]

Name	Titanium,Ti-6Al-4V	Titanium, Ti-5Al-2.5Sn-0.5Fe
Density $[kg/m^3]$	4410 - 4450	4460 - 4510
Price $[EUR/kg]$	42 - 46.1	35.6 - 39.2
Youngs modulus $[GPa]$	110 - 119	107 - 112
Compressive strength $[MPa]$	848 - 1080	600 - 896
Strength to weight ratio $[KNm/kg]$	192 - 243	135 - 199
Tensile yield strength $[MPa]$	786 - 910	758 - 862
Tensile strength $[MPa]$	862 - 1200	793 - 945
Fatigue strength $n = 10^7$ $[MPa]$	529 - 566	410 - 450
Fracture toughness $[MPa\sqrt{m}]$	84 - 107	93 - 100
Elongation $[\%strain]$	10 - 14	6 - 10
Service temperature $[°C]$	-273 - 350	-273 - 530
CO_2 footprint, Primary production $[kg/kg]$	38.8 - 42.9	36.6 - 40.4
Flammability	Non-Flammable	Non-Flammable
Salt water	Excellent	Excellent
UV Radiation (sun)	Excellent	Excellent
Recylcle	Yes	Yes
Magnetic	No	No

Table C.2: List of different types of Titanium [55]

Name	Aluminum, 6082-T6	Aluminum, 5086-O	Aluminum, 7075-T6
Density $[kg/m^3]$	2640 - 2730	2640 - 2670	2770 - 2830
Price $[EUR/kg]$	2.10 - 2.31	1.85 - 2.03	1.84 - 2.03
Youngs modulus $[GPa]$	70 - 74	70 - 73.6	69 - 76
Compressive strength $[MPa]$	295 - 326	97 - 200	393 - 530
Strength to weight ratio $[KNm/kg]$	110 - 119	37 - 75	142 - 187
Tensile yield strength $[MPa]$	240 - 290	97 - 107	359 - 530
Tensile strength $[MPa]$	280 - 340	241 - 266	359 - 530
Fatigue strength $n = 10^7$ $[MPa]$	90 - 100	125 - 135	152 - 168
Fracture toughness $[MPa\sqrt{m}]$	33 - 35	27 - 37	30 - 33
Elongation $[\%strain]$	5 - 11	14 - 18	2 - 10
Service temperature $[°C]$	-273 - 110	-273 - 130	-273 - 130
CO_2 footprint, Primary production $[kg/kg]$	12 - 13.3	11.4 - 12.6	11.4 - 12.6
Flammability	Non-Flammable	Non-Flammable	Non-Flammable
Salt water	Acceptable	Acceptable	Acceptable
UV Radiation (sun)	Excellent	Excellent	Excellent
Recylcle	Yes	Yes	Yes
Magnetic	No	No	No

Table C.3: List of different types of Aluminum [55]

C.2.3 Aluminium alloys

The second lightest of all metals with a density of about one-third of steel is aluminum. Aluminium alloys are commonly used in shipbuilding. Furthermore, the material is non-magnetic and has a good strength to weight ratio. However, aluminium reacts to oxygen very rapidly, but formation of this tough oxide skin prevents further oxidation of the metal. Aluminium is not prone to brittle fracture at low temperatures and has a higher strength and toughness at low temperatures [65]. Unfortunately, a structural loss of strength is developed for temperatures above 200° C. Aluminium is also characterized by poor fatigue life properties [11]. Note that these and other properties are listed in Table (C.3) for a few commonly used aluminium alloys.

C.3 Composites

Composites are made up of two or more individual materials referred to as constituents. In the case of two constituents one material embeds the other and hence it is called matrix (or resin). The other constituent functions as reinforcement for this matrix. The shape of the reinforcement plays an important role for mechanical performance. Composites with fibrous reinforcements are known to show excellent mechanical properties. In the present work, composites with a fibrous reinforcement are considered and the word composite refers to these composite materials. In the next, the most appropriate composite materials for a pressure hull are evaluated.

Name	Polyester/E-Glass fiber, woven cloth, .5	Polyester/E-Glass fiber, chopped roving	Epoxy/E-Glass fiber,.45 Quasi-isotropic	Epoxy/S-Glass fiber, UD composite, .5 Quasi-isotropic
Density $[kg/m^3]$	1600 - 2000	1700 - 2100	1750 - 1970	1840 - 1970
Price $[EUR/kg]$	27.3 - 30.1	3.22 - 3.54	23.2 - 25.5	18.2 - 20
Youngs modulus $[GPa]$	14.1 - 31	6.3 - 13.8	21 - 21.8	23.9 - 24.2
Compressive strength $[MPa]$	172 - 345	103 - 207	207 - 257	301 - 312
Strength to weight ratio $[KNm/kg]$	108 - 173	61 - 99	118 - 130	164 - 158
Tensile yield strength $[MPa]$	166 - 276	82.4 - 166	207 - 304	117 - 121
Tensile strength $[MPa]$	207 - 345	103 - 207	207 - 304	117 - 121
Fatigue strength $n = 10^7$ $[MPa]$	82.8 - 138	41.2 - 82.8	41.3 - 91.1	23.3 - 36.3
Fracture toughness $[MPa\sqrt{m}]$	10.7 - 20.9	6.6 - 11.4	6.12 - 29.9	6.12 - 32.7
Elongation $[\%strain]$	1 - 2	1 - 5	0.85 - 0.95	0.44 - 0.48
Service temperature $[°C]$	-27 - 172	-27 - 172	-73 - 140	-28 - 140
CO_2 footprint, Primary production $[kg/kg]$	14.9 - 16.5	7.13 - 7.88	7.46 - 8.25	13.4 - 14.8
Water absorption after 24h [%]	0.05 - 0.5	0.01 - 1	0.0456 - 0.078	0.0456 - 0.078
Flammability	Highly flammable	Highly flammable	Slow-burning	Slow-burning
Salt water	Excellent	Excellent	Excellent	Excellent
UV Radiation (sun)	Good	Good	Fair	Fair
Recylcle	No	No	No	No
Magnetic	No	No	No	No

Table C.4: List of different types of GFRP [55]

C.3.1 Glass fiber reinforced plastic

The most widely used fiber for commodity composites is fiberglass [65]. The most common type of glass fibers is E-Glass. A rather high strength in combination with low stiffness and cost are the main properties of these glass fibers [19]. The relatively high compressive strength and their relative inexpensiveness has led to their selection for use in underwater deep diving applications. Electric properties of glass-reinforced composites allowed their use as radomes and other applications that require high dielectric strength [65]. Properties of typical glass fiber reinforced plastics (GFRP or GRP) are listed in Table (C.4).

C.3.2 Carbon fiber reinforced plastic

Carbon/graphite fibers have demonstrated the widest variety of strengths and moduli. Additionally, in terms of specific mechanical properties, carbon fiber reinforced plastics (CFRPs)

Name	Epoxy/HS carbon fiber, UD composite, 0.6 Quasi-isotropic	Epoxy/carbon fiber SMC	AS4 carbon fiber/3501-6 epoxy, UD composite 0.6
Density $[kg/m^3]$	1550 - 1580	1400 - 1700	1550
Price $[EUR/kg]$	29.4 - 32.3	15.1 - 16.6	N/A
Youngs modulus $[GPa]$	49.7 - 60.1	69 - 150	126
Compressive strength $[MPa]$	542 - 657	207 - 276	1480
Strength to weight ratio $[KNm/kg]$	350 - 416	148 - 162	954
Tensile yield strength $[MPa]$	249 - 356	221 - 276	N/A
Tensile strength $[MPa]$	249 - 356	276 - 345	1950
Fatigue strength $n = 10^7$ $[MPa]$	137 - 231	109 - 142	N/A
Fracture toughness $[MPa\sqrt{m}]$	137 - 231	9.45 - 28.4	N/A
Elongation $[\%strain]$	0.32 - 0.35	0.5 - 2	1.38
Service temperature $[°C]$	-73 - 140	-73 - 166	N/A
CO_2 footprint, Primary production $[kg/kg]$	16.4 - 18.1	16.4 - 18.1	N/A
Water absorption after 24h [%]	0.036 - 0.0525	1.45 - 1.76	N/A
Flammability	Slow-burning	Self-extinguishing	N/A
Salt water	Excellent	Excellent	N/A
UV Radiation (sun)	Good	Good	N/A
Recylcle	No	No	N/A
Magnetic	No	No	N/A

Table C.5: List of different types of CFRP [55] for Epoxy/HS and SMC, [66] for the data belonging to the AS4/3501-6 UD composite

are superior to GRP and titanium. It has to be noted that, analogous to GRP, degradation of mechanical properties occurs when CFRPs are exposed to UV light. Furthermore, for different resin systems mechanical properties can be reduced due to moisture effects. Properties of typical CFRPs are listed in Table (C.5).

C.3.3 Metal matrix composite

This special type of composite is a more futuristic than the previously treated materials. Since the production is not sufficiently large and prices are too high for pressure hull applications [11], these metal matrix composites (MMCs) are only treated shortly. As can be observed from Table (C.6) that this expensive composite material has excellent mechanical properties.

C.4 Sandwich structures

The sandwich materials treated here consist of a core material, sandwiched between two skin layers. The core, which shows a relatively lower stiffness than the skin layers, connects the two skins in order to increase the bending stiffness. In the present work, skin layers of FRP are considered. Also, a selection of appropriate cores is made and treated in the next section.

Name	MMC, Al 6061-SCS-2 Cross-Ply	MMC, Al/Nextel 610 fiber .65 composite, Quasi-isotropic
Density $[kg/m^3]$	2840 - 2850	3400 - 3400
Price $[EUR/kg]$	1270 - 1480	5470 - 6230
Youngs modulus $[GPa]$	135 - 140	158 - 179
Compressive strength $[MPa]$	1460 - 1530	361 - 405
Strength to weight ratio $[KNm/kg]$	514 - 537	106 - 119
Tensile yield strength $[MPa]$	260 - 645	183 - 252
Tensile strength $[MPa]$	673 - 723	183 - 252
Fatigue strength $n = 10^7$ $[MPa]$	454 - 488	91.6 - 126
Fracture toughness $[MPa\sqrt{m}]$	11 - 16	7 - 16
Elongation $[\%strain]$	0.7 - 1	0.1 - 0.16
Service temperature $[°C]$	-273 - 270	-273 - 290
CO_2 footprint, Primary production $[kg/kg]$	953 - 1050	3070 - 3400
Flammability	Non-Flammable	Non-Flammable
Salt water	Acceptable	Acceptable
UV Radiation (sun)	Excellent	Excellent
Recylcle	No	No
Magnetic	No	No

Table C.6: List of different types of MMC

C.4.1 Core materials

Since sandwich cores are in general lightweight materials, airy matter as honeycomb and foam materials are commonly applied. Table (C.7) gives an overview of the mechanical properties of typical core materials. it has to be noted that through-the-thickness properties are listed in this table.

Name	Alumina foam (99.8perc)(1.2)	End-grain balsa (0.22)	Aluminum 5052 honeycomb (0.198)	PVC cross-linked foam (0.400)
Density $[kg/m^3]$	1180 - 1220	210 - 257	194 - 202	390 - 410
Price $[EUR/kg]$	25.7 - 38.8	5.24 - 7.08	12.3 - 20.5	9.11 - 18.2
Youngs modulus $[GPa]$	17.1 - 34.2	0.193 - 0.236	0.0403 - 0.0446	0.46 - 0.48
Compressive strength $[MPa]$	77 - 85	6.67 - 8.15	17.4 - 19.2	10.5 - 12
Strength to weight ratio $[KNm/kg]$	65 - 70	32 - 32	90 - 95	27 - 29
Tensile yield strength $[MPa]$	57.8 - 63.8	0.916 - 1.12	0.336 - 0.372	10.5 - 12
Tensile strength $[MPa]$	57.8 - 63.8	1.05 - 1.28	0.392 - 0.44	10.9 - 12.4
Fatigue strength $n = 10^7$ $[MPa]$	46.2 - 51	N/A	N/A	8.4 - 9.6
Fracture toughness $[MPa\sqrt{m}]$	0.177 - 0.197	N/A	N/A	0.0735 - 0.0792
Elongation $[\%strain]$	0.17 - 0.37	N/A	N/A	3 - 5
Service temperature $[°C]$	-273 - 1800	-191 - 147	-69.5 - 130	-200 - 92
CO_2 footprint, Primary production $[kg/kg]$	6.53 - 7.22	0.405 - 0.494	11.4 - 12.6	3.55 - 3.93
Water absorption after 24h [%]	0.5 - 1	180 - 220	0.001 - 0.002	0.688 - 0.713
Flammability	Non-flammable	Highly-flammable	Non-flammable	Self-extinguishing
Salt water	Excellent	Limited use	Acceptable	Excellent
UV Radiation (sun)	Excellent	Good	Excellent	Good
Recylcle	No	No	Yes	No
Magnetic	No	No	No	No

Table C.7: List of different types of core materials [55]

Appendix D

Coefficients of homogeneous buckling system

In order to be complete, the coefficients c_i belonging to Eq.(4.106) which is described in Section 4.2 are:

$$
\begin{aligned}
c_0 \;=\; & -\frac{1}{r^6}[-A_{11}\alpha^2\beta^2{D_{22}}^2 - 2A_{66}\beta^6{D_{22}}^2r^2 - A_{66}\beta^8{D_{22}}^2r^4 \\
& - \alpha^4r^4A_{66}{A_{12}}^2 - \alpha^4r^2D_{66}{A_{12}}^2 + \alpha^4r^4{A_{12}}^2D_{12}\beta^2 \\
& - 2A_{11}\alpha^2\beta^4{D_{22}}^2r^2 - A_{11}\alpha^2\beta^6{D_{22}}^2r^4 + A_{11}\alpha^6r^2D_{66}D_{12} \\
& + A_{11}\alpha^4r^2D_{66}A_{22} + A_{11}\alpha^8r^6A_{66}D_{11} + A_{11}\alpha^6r^4A_{66}D_{12} \\
& + A_{11}\alpha^4r^4A_{66}A_{22} + A_{11}\alpha^8r^4D_{66}D_{11} - A_{11}\alpha^6\beta^2{D_{12}}^2r^4 \\
& + A_{66}\beta^8r^6A_{22}D_{22} - A_{66}\beta^6r^4A_{22}D_{22} - A_{66}\beta^4{D_{12}}^2\alpha^4r^4 \\
& - 2A_{66}\beta^4A_{22}r^2D_{22} + 4\alpha^4\beta^2r^4D_{66}{A_{12}}^2 - \alpha^2\beta^6r^6{A_{12}}^2D_{22} \\
& - \alpha^6\beta^2r^6{A_{12}}^2D_{11} - 2\alpha^4\beta^4r^6{A_{12}}^2D_{12} - 4\alpha^4\beta^4r^6{A_{12}}^2D_{66} \\
& + 2\alpha^2\beta^2r^2D_{22}{A_{12}}^2 + \alpha^2r^4{A_{12}}^2D_{22}\beta^4 - A_{66}\beta^4{D_{22}}^2 \\
& + A_{11}\alpha^2r^6A_{22}\beta^6D_{22} - A_{11}\alpha^2r^4A_{22}\beta^4D_{22} - 2A_{11}\alpha^2\beta^2A_{22}r^2D_{22} \\
& - 3A_{11}\alpha^4r^2D_{66}D_{22}\beta^2 + 2A_{11}\alpha^6r^6A_{66}D_{12}\beta^2 + A_{11}\alpha^4r^6A_{66}D_{22}\beta^4 \\
& + A_{11}\alpha^4r^4A_{66}D_{22}\beta^2 + 4A_{11}\alpha^6r^6A_{66}D_{66}\beta^2 + 2A_{11}\alpha^4r^6A_{22}\beta^4D_{12} \\
& + 4A_{11}\alpha^4r^6A_{22}\beta^4D_{66} + A_{11}\alpha^6r^6A_{22}\beta^2D_{11} - A_{11}\alpha^4r^4A_{22}\beta^2D_{12} \\
& - 2A_{11}\alpha^6r^4D_{66}D_{12}\beta^2 - 3A_{11}\alpha^4r^4D_{66}D_{22}\beta^4 - 4A_{11}\alpha^4\beta^2A_{22}r^4D_{66} \\
& - 2A_{11}\alpha^4\beta^2D_{12}r^2D_{22} - 2A_{11}\alpha^4\beta^4D_{12}r^4D_{22} + A_{66}\beta^2r^2D_{66}\alpha^4D_{12} \\
& + A_{66}\beta^2r^2D_{66}\alpha^2A_{22} + A_{66}\beta^2r^4D_{66}\alpha^6D_{11} - 3A_{66}\beta^4r^2D_{66}\alpha^2D_{22} \\
& + 2A_{66}\beta^6r^6A_{22}D_{12}\alpha^2 + 4A_{66}\beta^6r^6A_{22}D_{66}\alpha^2 + A_{66}\beta^4r^6A_{22}D_{11}\alpha^4 \\
& - A_{66}\beta^4r^4A_{22}D_{12}\alpha^2 - 2A_{66}\beta^4r^4D_{66}\alpha^4D_{12} - 3A_{66}\beta^6r^4D_{66}\alpha^2D_{22} \\
& - 4A_{66}\beta^4A_{22}r^4D_{66}\alpha^2 - 2A_{66}\beta^4D_{12}\alpha^2r^2D_{22} - 2A_{66}\beta^6D_{12}\alpha^2r^4D_{22} \\
& - 2\alpha^2\beta^6r^6A_{12}A_{66}D_{22} - 2\alpha^6\beta^2r^6A_{12}A_{66}D_{11} + 4\alpha^4\beta^2r^4A_{66}D_{66}A_{12} \\
& + 2\alpha^2\beta^2r^2A_{66}D_{22}A_{12} - 4\alpha^4\beta^4r^6A_{12}A_{66}D_{12} - 8\alpha^4\beta^4r^6A_{12}A_{66}D_{66}],
\end{aligned}
\tag{D.1}
$$

$$
\begin{aligned}
c_1 \;=\; & -\frac{1}{2}\frac{1}{r^6}[4A_{66}\alpha^4 r^4 D_{12}\beta^2 + 4A_{66}\alpha^2 r^4 D_{22}\beta^4 - 2A_{11}\alpha^2 r^7 A_{22}\beta^4 \\
& + 4A_{11}\alpha^2\beta^2 A_{22} r^5 + 4A_{11}\alpha^2\beta^2 D_{22} r^3 + 4A_{11}\alpha^2\beta^4 D_{22} r^5 \\
& - 2A_{11}\alpha^4 r^7 A_{66}\beta^2 - A_{11}\alpha^4 r^7 A_{22}\beta^2 + 6A_{11}\alpha^4 r^5 D_{66}\beta^2 \\
& + 4A_{11}\alpha^4\beta^2 D_{12} r^5 - 9A_{66}\beta^2 r^5 D_{66}\alpha^4 - A_{66}\beta^4 r^7 A_{22}\alpha^2 \\
& + 6A_{66}\beta^4 r^5 D_{66}\alpha^2 + 4A_{66}\beta^4 D_{12}\alpha^2 r^5 - 4\alpha^2\beta^2 r^3 A_{12} D_{22} \\
& - 4\alpha^2\beta^2 r^5 A_{66} A_{22} - 4\alpha^2\beta^2 r^3 A_{66} D_{22} - 4\alpha^2\beta^2 r^5 A_{66} A_{12} \\
& + 4\alpha^2\beta^2 r^4 A_{66} A_{22} - 4\alpha^2\beta^4 r^5 A_{12} D_{22} - 4\alpha^4\beta^2 r^5 A_{12} D_{12} \\
& - 8\alpha^4\beta^2 r^5 A_{12} D_{66} + 2\alpha^4\beta^2 r^7 A_{12} A_{66} + 4\alpha^2\beta^4 r^7 A_{12} A_{66} \\
& + 4\alpha^2\beta^6 r^6 A_{12} D_{22} + 4\alpha^6\beta^2 r^6 A_{12} D_{11} - 4\alpha^2\beta^4 r^5 A_{66} D_{22} \\
& - 4\alpha^4\beta^2 r^5 A_{66} D_{12} + 4\alpha^2\beta^6 r^6 A_{66} D_{22} + 4\alpha^6\beta^2 r^6 A_{66} D_{11} \\
& - 8\alpha^4\beta^2 r^4 D_{66} A_{12} - 4\alpha^2\beta^2 r^2 D_{22} A_{12} + 8\alpha^4\beta^4 r^6 A_{12} D_{12} \\
& + 16\alpha^4\beta^4 r^6 A_{12} D_{66} + 8\alpha^4\beta^4 r^6 A_{66} D_{12} + 16\alpha^4\beta^4 r^6 A_{66} D_{66} \\
& + 4\alpha^4 r^5 A_{12} A_{66} + 4\alpha^4 r^3 A_{12} D_{66} - A_{11}\alpha^6 r^7 A_{66} - A_{11}\alpha^6 r^5 D_{66} \\
& - 2A_{66}\beta^6 r^7 A_{22} + 4A_{66}\beta^4 A_{22} r^5 + 4A_{66}\beta^4 D_{22} r^3 + 4A_{66}\beta^6 D_{22} r^5 \\
& + \alpha^4\beta^2 r^7 A_{12}^2 + 2\alpha^2\beta^4 r^7 A_{12}^2 - 4\alpha^2\beta^2 r^5 A_{12}^2],
\end{aligned}
\tag{D.2}
$$

$$
\begin{aligned}
c_2 \;=\; & -\frac{1}{2}\frac{1}{r^6}[4\,\alpha^4\beta^2 r^5 D_{12} + 4\,\alpha^2\beta^4 r^5 D_{22} + 4\,\alpha^2\beta^2 r^6 A_{66} + 8\,\alpha^4\beta^2 r^5 D_{66} \\
& - 2\,\alpha^2\beta^2 r^4 A_{22} + 4\,\alpha^2\beta^2 r^6 A_{12} + 4\,\alpha^2\beta^2 r^5 A_{22} - 2\,\alpha^6\beta^2 r^6 D_{11} \\
& + 4\,\alpha^2\beta^2 r^5 A_{12} - 2\,A_{11}\,\alpha^2\beta^2 r^6 - 2\,\alpha^2\beta^4 r^4 D_{22} + 4\,\alpha^2\beta^2 r^3 D_{22} \\
& - 4\,\alpha^2\beta^4 r^7 A_{12} - 4\,\alpha^2\beta^4 r^7 A_{66} - 2\,A_{66}\,\beta^4 r^6 - 2\,\alpha^4\beta^2 r^7 A_{12} \\
& - 2\,\alpha^4 r^4 D_{66} - 2\,\alpha^4\beta^2 r^4 D_{12} - 2\,\alpha^2\beta^6 r^6 D_{22} - 2\,\alpha^4 r^6 A_{66} \\
& - 4\,\alpha^4\beta^4 r^6 D_{12} - 8\,\alpha^4\beta^4 r^6 D_{66} - 2\,\alpha^2 r^6 A_{22}\,\beta^2 - 2\,\alpha^4\beta^2 r^7 A_{66}],
\end{aligned}
\tag{D.3}
$$

$$
c_3 \;=\; -\frac{1}{2}\frac{1}{r^6}[-4\alpha^2\beta^2 r^6 + \alpha^4\beta^2 r^7 + 2\alpha^2\beta^4 r^7]. \tag{D.4}
$$

Appendix E

Strain gauge results

E.1 Strain gauge locations

This Section lists the description and location of the used strain gauges for the L510-No18.

Strain Gauge ID	Description	Location		
		Axial (mm)	Radial (mm)	Circumferential (deg)
L510-No18-13	Flange-Frame-4	230.0	110.0	4.6
L510-No18-24	Flange-Frame-4	230.0	110.0	34.6
L510-No18-23	Flange-Frame-4	230.0	110.0	64.6
L510-No18-22	Flange-Frame-4	230.0	110.0	94.6
L510-No18-21	Flange-Frame-4	230.0	110.0	124.6
L510-No18-20	Flange-Frame-4	230.0	110.0	154.6
L510-No18-19	Flange-Frame-4	230.0	110.0	184.6
L510-No18-18	Flange-Frame-4	230.0	110.0	214.6
L510-No18-17	Flange-Frame-4	230.0	110.0	244.6
L510-No18-16	Flange-Frame-4	230.0	110.0	274.6
L510-No18-15	Flange-Frame-4	230.0	110.0	304.6
L510-No18-14	Flange-Frame-4	230.0	110.0	334.6

Table E.1: Locations of the uni-axial strain gauges for L510-No18 at frame 4

Strain Gauge ID	Description	Location		
		Axial (mm)	Radial (mm)	Circumferential (deg)
L510-No18-01	Flange-Frame-5	280.0	110.0	4.6
L510-No18-12	Flange-Frame-5	280.0	110.0	34.6
L510-No18-11	Flange-Frame-5	280.0	110.0	64.6
L510-No18-10	Flange-Frame-5	280.0	110.0	94.6
L510-No18-09	Flange-Frame-5	280.0	110.0	124.6
L510-No18-08	Flange-Frame-5	280.0	110.0	154.6
L510-No18-07	Flange-Frame-5	280.0	110.0	184.6
L510-No18-06	Flange-Frame-5	280.0	110.0	214.6
L510-No18-05	Flange-Frame-5	280.0	110.0	244.6
L510-No18-04	Flange-Frame-5	280.0	110.0	274.6
L510-No18-03	Flange-Frame-5	280.0	110.0	304.6
L510-No18-02	Flange-Frame-5	280.0	110.0	334.6

Table E.2: Locations of the uni-axial strain gauges for L510-No18 at frame 5

Strain Gauge ID	Description	Location		
		Axial (mm)	Radial (mm)	Circumferential (deg)
L510-No18-25	Outside Shell-Mid-Bay-4	255.0	123.0	4.6
L510-No18-36	Outside Shell-Mid-Bay-4	255.0	123.0	34.6
L510-No18-35	Outside Shell-Mid-Bay-4	255.0	123.0	64.6
L510-No18-34	Outside Shell-Mid-Bay-4	255.0	123.0	94.6
L510-No18-33	Outside Shell-Mid-Bay-4	255.0	123.0	124.6
L510-No18-32	Outside Shell-Mid-Bay-4	255.0	123.0	154.6
L510-No18-31	Outside Shell-Mid-Bay-4	255.0	123.0	184.6
L510-No18-30	Outside Shell-Mid-Bay-4	255.0	123.0	214.6
L510-No18-29	Outside Shell-Mid-Bay-4	255.0	123.0	244.6
L510-No18-28	Outside Shell-Mid-Bay-4	255.0	123.0	274.6
L510-No18-27	Outside Shell-Mid-Bay-4	255.0	123.0	304.6
L510-No18-26	Outside Shell-Mid-Bay-4	255.0	123.0	334.6
L510-No18-48	Outside Shell-Mid-Bay-1	105.0	123.0	124.6
L510-No18-47	Outside Shell-Fr-2	130.0	123.0	124.6
L510-No18-46	Outside Shell-Mid-Bay-2	155.0	123.0	124.6
L510-No18-45	Outside Shell-Fr-3	180.0	123.0	124.6
L510-No18-44	Outside Shell-Mid-Bay-3	205.0	123.0	124.6
L510-No18-43	Outside Shell-Fr-4	230.0	123.0	124.6
L510-No18-42	Outside Shell-Fr-5	280.0	123.0	124.6
L510-No18-41	Outside Shell-Mid-Bay-5	305.0	123.0	124.6
L510-No18-40	Outside Shell-Fr-6	330.0	123.0	124.6
L510-No18-39	Outside Shell-Mid-Bay-6	355.0	123.0	124.6
L510-No18-38	Outside Shell-Fr-7	380.0	123.0	124.6
L510-No18-37	Outside Shell-Mid-Bay-7	405.0	123.0	124.6

Table E.3: Locations of the bi-axial strain gauges on the outer shell surface for L510-No18

E.2 Linear elastic strain gauge readings

This appendix shows the strain gauge readings for the internally stiffened conventional pressure hull experiment (EXP) and the linear elastic FE analysis. Note that channel A is the circumferential direction and C the longitudinal direction.

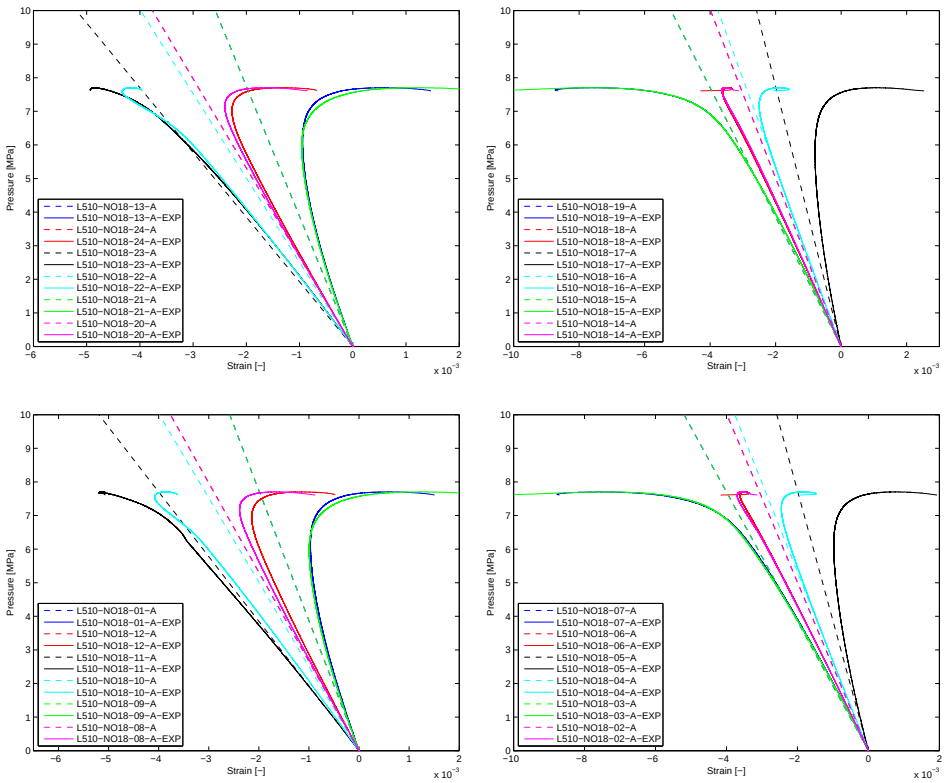

Figure E.1: Linear elastic FE analysis and experimental strain gauge readings

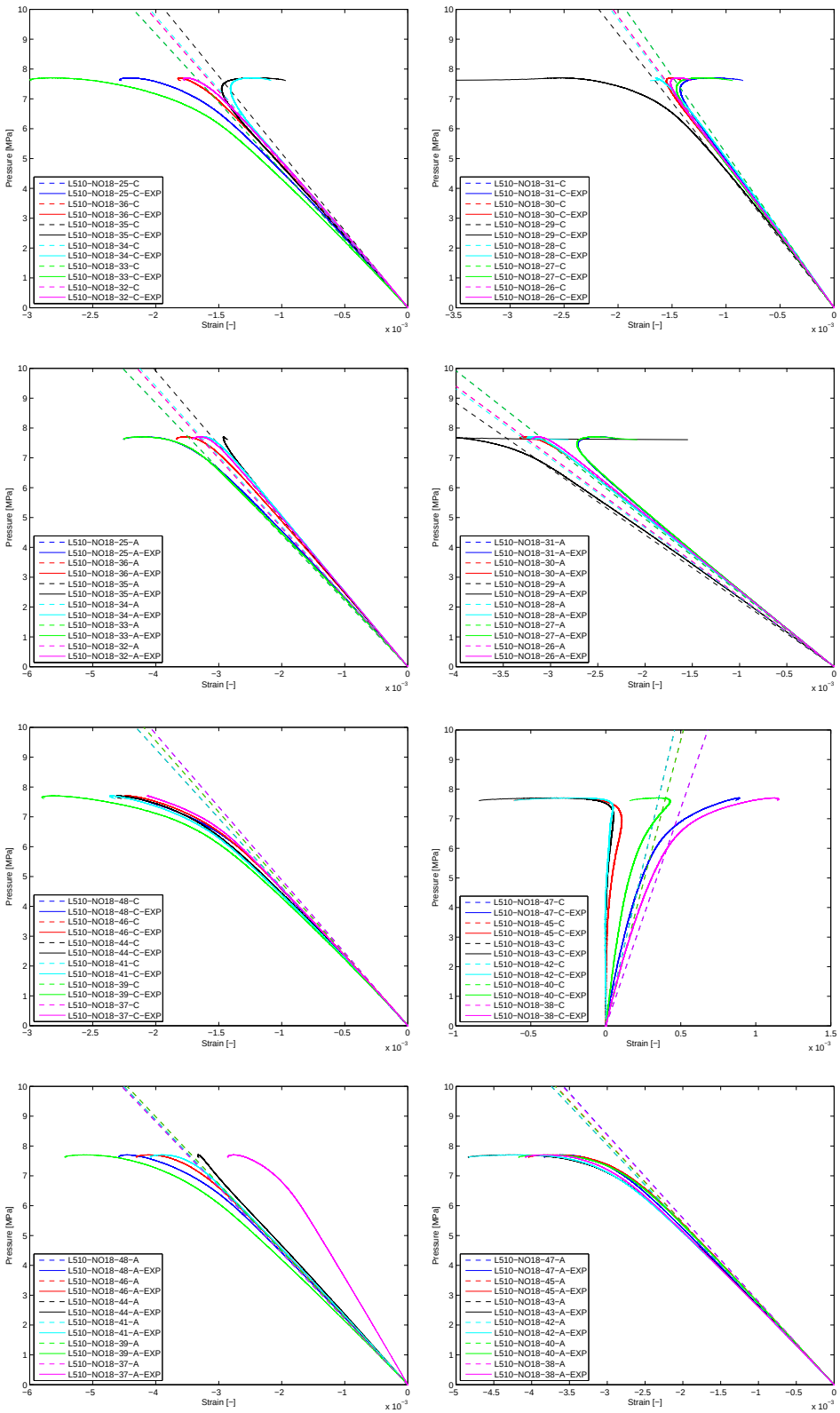

Figure E.2: Linear elastic FE analysis and experimental strain gauge readings

E.3 Non-linear buckling strain gauge readings

This appendix shows the strain gauge readings for the internally stiffened conventional pressure hull experiment (EXP) and the non-linear buckling FE analysis. Note that channel A is the circumferential direction and C the longitudinal direction.

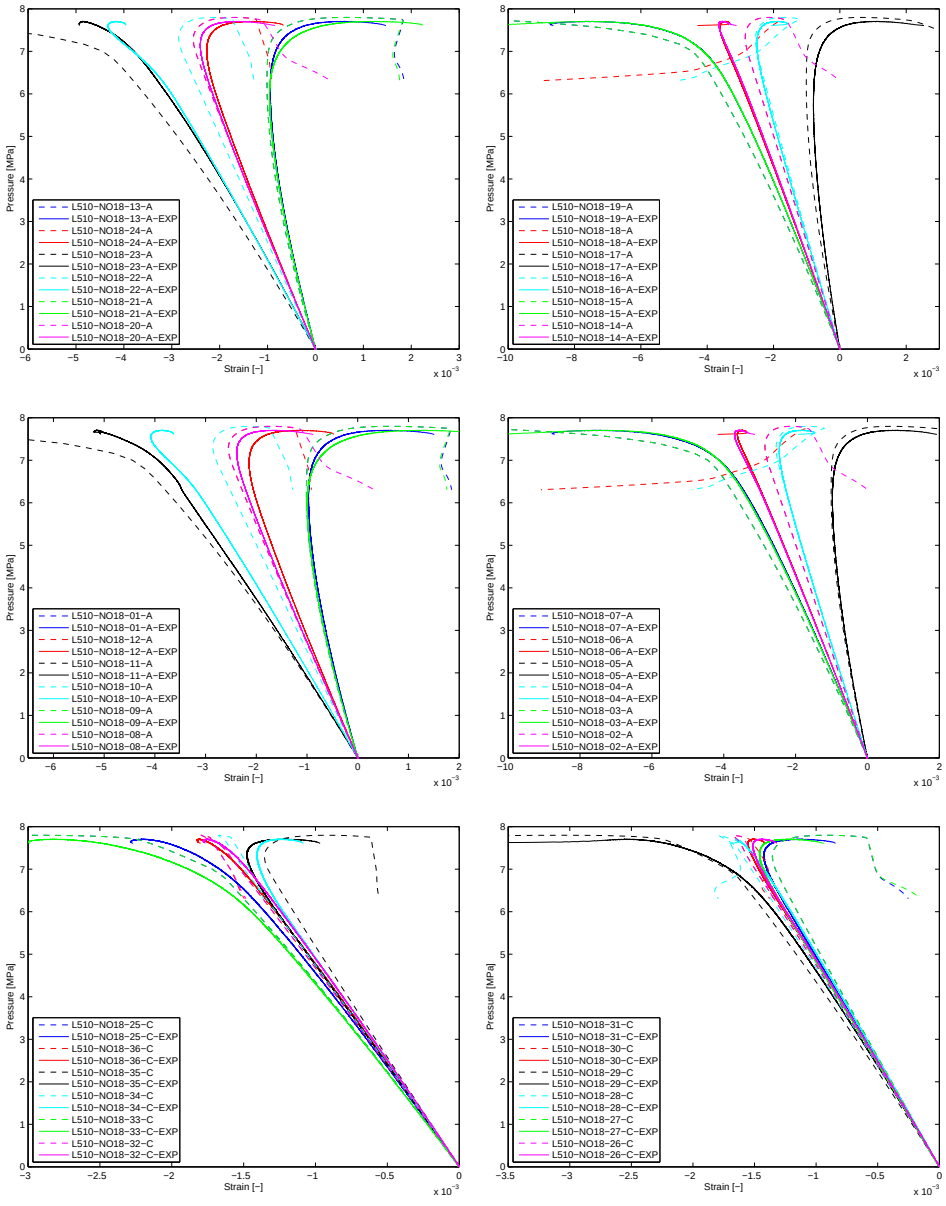

Figure E.3: Non-linear buckling FE analysis and experimental strain gauge readings

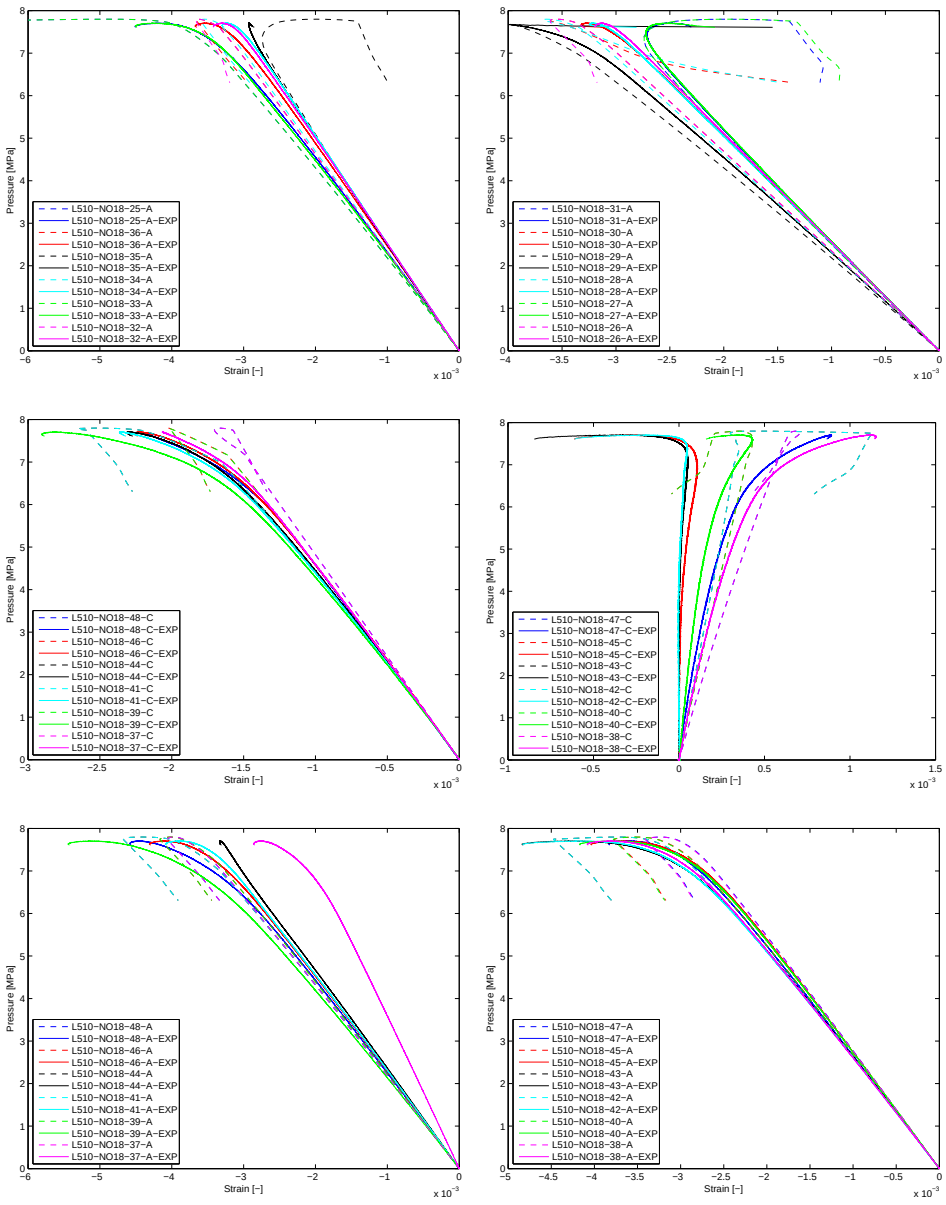

Figure E.4: Non-linear buckling FE analysis and experimental strain gauge readings

E.4 Strain gauge results

Strain Gauge ID	Description	Initial slope	Match
L510-No18-13	Flange-Frame-4	GOOD	GOOD
L510-No18-24	Flange-Frame-4	GOOD	GOOD
L510-No18-23	Flange-Frame-4	GOOD	GOOD
L510-No18-22	Flange-Frame-4	GOOD	MODERATE
L510-No18-21	Flange-Frame-4	GOOD	GOOD
L510-No18-20	Flange-Frame-4	GOOD	GOOD
L510-No18-19	Flange-Frame-4	GOOD	GOOD
L510-No18-18	Flange-Frame-4	GOOD	GOOD
L510-No18-17	Flange-Frame-4	GOOD	GOOD
L510-No18-16	Flange-Frame-4	GOOD	GOOD
L510-No18-15	Flange-Frame-4	GOOD	GOOD
L510-No18-14	Flange-Frame-4	GOOD	GOOD
L510-No18-01	Flange-Frame-5	GOOD	GOOD
L510-No18-12	Flange-Frame-5	GOOD	GOOD
L510-No18-11	Flange-Frame-5	GOOD	GOOD
L510-No18-10	Flange-Frame-5	GOOD	MODERATE
L510-No18-09	Flange-Frame-5	GOOD	GOOD
L510-No18-08	Flange-Frame-5	GOOD	GOOD
L510-No18-07	Flange-Frame-5	GOOD	GOOD
L510-No18-06	Flange-Frame-5	GOOD	GOOD
L510-No18-05	Flange-Frame-5	GOOD	GOOD
L510-No18-04	Flange-Frame-5	GOOD	GOOD
L510-No18-03	Flange-Frame-5	GOOD	GOOD
L510-No18-02	Flange-Frame-5	GOOD	GOOD

Table E.4: Uni-axial strain gauge matches for the non-linear FE analysis with respect to the experimentally measured values

Strain Gauge ID	Description	Initial slope	Match
L510-No18-25-A	Outside Shell-Mid-Bay-4	GOOD	GOOD
L510-No18-36-A	Outside Shell-Mid-Bay-4	GOOD	GOOD
L510-No18-35-A	Outside Shell-Mid-Bay-4	GOOD	GOOD
L510-No18-34-A	Outside Shell-Mid-Bay-4	GOOD	GOOD
L510-No18-33-A	Outside Shell-Mid-Bay-4	GOOD	GOOD
L510-No18-32-A	Outside Shell-Mid-Bay-4	GOOD	GOOD
L510-No18-31-A	Outside Shell-Mid-Bay-4	GOOD	GOOD
L510-No18-30-A	Outside Shell-Mid-Bay-4	GOOD	GOOD
L510-No18-29-A	Outside Shell-Mid-Bay-4	GOOD	GOOD
L510-No18-28-A	Outside Shell-Mid-Bay-4	GOOD	GOOD
L510-No18-27-A	Outside Shell-Mid-Bay-4	GOOD	GOOD
L510-No18-26-A	Outside Shell-Mid-Bay-4	GOOD	GOOD
L510-No18-48-A	Outside Shell-Mid-Bay-1	GOOD	GOOD
L510-No18-47-A	Outside Shell-Fr-2	GOOD	GOOD
L510-No18-46-A	Outside Shell-Mid-Bay-2	GOOD	GOOD
L510-No18-45-A	Outside Shell-Fr-3	GOOD	GOOD
L510-No18-44-A	Outside Shell-Mid-Bay-3	GOOD	MODERATE
L510-No18-43-A	Outside Shell-Fr-4	GOOD	GOOD
L510-No18-42-A	Outside Shell-Fr-5	GOOD	GOOD
L510-No18-41-A	Outside Shell-Mid-Bay-5	GOOD	GOOD
L510-No18-40-A	Outside Shell-Fr-6	GOOD	GOOD
L510-No18-39-A	Outside Shell-Mid-Bay-6	MODERATE	MODERATE
L510-No18-38-A	Outside Shell-Fr-7	GOOD	GOOD
L510-No18-37-A	Outside Shell-Mid-Bay-7	MODERATE	MODERATE

Table E.5: Bi-axial strain gauge matches for the non-linear FE analysis with respect to the experimentally measured values. These are the results for the circumferential direction (i.e. channel A).

Strain Gauge ID	Description	Initial slope	Match
L510-No18-25-C	Outside Shell-Mid-Bay-4	GOOD	GOOD
L510-No18-36-C	Outside Shell-Mid-Bay-4	GOOD	GOOD
L510-No18-35-C	Outside Shell-Mid-Bay-4	GOOD	GOOD
L510-No18-34-C	Outside Shell-Mid-Bay-4	GOOD	GOOD
L510-No18-33-C	Outside Shell-Mid-Bay-4	GOOD	GOOD
L510-No18-32-C	Outside Shell-Mid-Bay-4	GOOD	GOOD
L510-No18-31-C	Outside Shell-Mid-Bay-4	GOOD	GOOD
L510-No18-30-C	Outside Shell-Mid-Bay-4	GOOD	GOOD
L510-No18-29-C	Outside Shell-Mid-Bay-4	GOOD	GOOD
L510-No18-28-C	Outside Shell-Mid-Bay-4	GOOD	GOOD
L510-No18-27-C	Outside Shell-Mid-Bay-4	GOOD	GOOD
L510-No18-26-C	Outside Shell-Mid-Bay-4	GOOD	GOOD
L510-No18-48-C	Outside Shell-Mid-Bay-1	GOOD	GOOD
L510-No18-47-C	Outside Shell-Fr-2	GOOD	MODERATE
L510-No18-46-C	Outside Shell-Mid-Bay-2	GOOD	GOOD
L510-No18-45-C	Outside Shell-Fr-3	MODERATE	MODERATE
L510-No18-44-C	Outside Shell-Mid-Bay-3	GOOD	GOOD
L510-No18-43-C	Outside Shell-Fr-4	MODERATE	MODERATE
L510-No18-42-C	Outside Shell-Fr-5	MODERATE	MODERATE
L510-No18-41-C	Outside Shell-Mid-Bay-5	GOOD	GOOD
L510-No18-40-C	Outside Shell-Fr-6	MODERATE	MODERATE
L510-No18-39-C	Outside Shell-Mid-Bay-6	MODERATE	MODERATE
L510-No18-38-C	Outside Shell-Fr-7	MODERATE	MODERATE
L510-No18-37-C	Outside Shell-Mid-Bay-7	GOOD	MODERATE

Table E.6: Bi-axial strain gauge matches for the non-linear FE analysis with respect to the experimentally measured values. These are the results for the longitudinal direction (i.e. channel C).

Appendix F

Buckling mode shapes

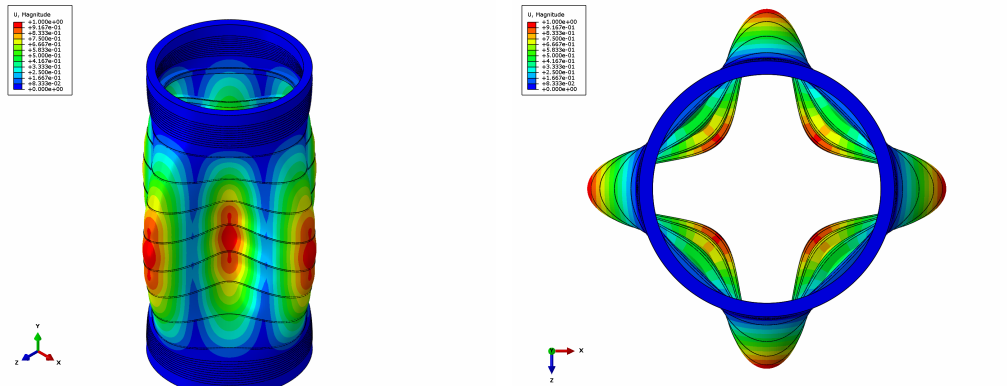

Figure F.1: Illustration of the second lowest eigenvalue ($n = 4$, $m = 1$)

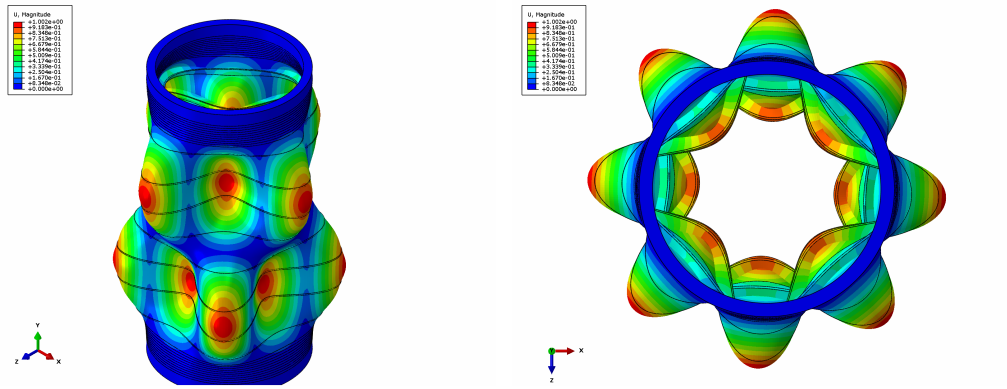

Figure F.2: Illustration of the third lowest eigenvalue ($n = 4$, $m = 2$)

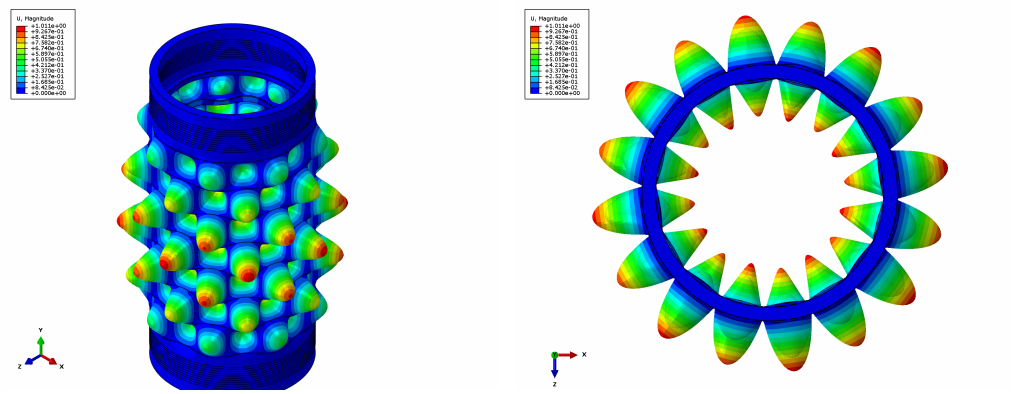

Figure F.3: Illustration of the fourth lowest eigenvalue ($n = 8$, $m = 7$)

Appendix G

Scripts

In this appendix, the complete script of the sandwich optimization framework is given, including the FE model generation. As an important note, the mother-file is the main.m *MATLAB* file which is treated first.

```
%find target lamination parameters - optimization main file
%Note: written in Matlab
%Copyright - Stanley I. Wong - 2012
clear all; clc; close all; format long;
global props data Xn Xdat
diary on

data  = [];
props = [];
flags = [];

%%%%%%%%%%%%%%%%%%%%%%%%%%%%%%%%%%%%%%%%%%%%%%%%%%%%%%%%%%%%%%%%%%%%%%%%%%%%
% Process control panel %%%%%%%%%%%%%%%%%%%%%%%%%%%%%%%%%%%%%%%%%%%%%%%%%%%%
%%%%%%%%%%%%%%%%%%%%%%%%%%%%%%%%%%%%%%%%%%%%%%%%%%%%%%%%%%%%%%%%%%%%%%%%%%%%
data.refSkinIn = 'top';          %check this from the cae (refplane)
data.refSkinOut = 'bottom';      %check this from the cae (refplane)

data.L = 510;                    % cylinder length
data.r_out=123;                  % cylinder outer radius
data.extPressure=8.0;           % external pressure for static analysis
data.minBucklingPressure=15.1; % minimal required buckling pressure
data.minThicknessConstraint = 1e-3;
data.maxThicknessConstraint = 13;

data.fileCaseName  = 'case_sandwich.dat';% written in initPropsWrite
data.filePropsName = 'props_sandwich.dat';% written in initPropsWrite
data.fileCorePropsName = 'props_core.dat';
data.fileABDNameSkinIn   = 'ABDskinIn.dat';% written in createABDfromLP
data.fileABDNameSkinOut   = 'ABDskinOut.dat';% written in createABDfromLP
data.fileTSNameSkinIn    = 'TSskinIn.dat'; % written in calcTransverseShearModuli
```

```
data.fileTSNameSkinOut    = 'TSskinOut.dat';

%%%%%%%%%%%%%%%%%%%%%%%%%%%%%%%%%%%%%%%%%%%%%%%%%%%%%%%%%%%%%%%%%%%%%%%%
% Set initial design variables %%%%%%%%%%%%%%%%%%%%%%%%%%%%%%%%%%%%%%%%%
%%%%%%%%%%%%%%%%%%%%%%%%%%%%%%%%%%%%%%%%%%%%%%%%%%%%%%%%%%%%%%%%%%%%%%%%
data.eval.counter = 0;
data.optimizer.flag = 'OBJ';

%temp. symmetry condition (determination of design variables)
Xn = [1 2 9 10];
%temporary: define bounds
lb = [-1 -1 -1 -1]; ub= [1 1 1 1];
disp('MAKE SURE LB & UB ARE OK!')

%initial lamination parameters:
X1i =    0.336297570631182;
X2i =    0.157014356779905;
X9i =    0.890557917363859;
X10i=    0.283363339099736;

X1o =    X1i;
X2o =    X2i;
X9o =    X9i;
X10o=    X10i;
%initial thicknesses:
hSkinIn  = 2.79; %note: weight < 3.6453 kg
hSkinOut = 2.79;
hCore    = 7.42-4;

X0i = [X1i X2i 0 0 0 0 0 0 X9i X10i 0 0];

X0o = [X1o X2o 0 0 0 0 0 0 X9o X10o 0 0];

X0=[X0i X0o hSkinIn hSkinOut hCore]; %length = 27!
  % [1-12, 13-24, 25, 26, 27]

Xdat=[];
for i = 1:length(X0)
    eval(['X',num2str(i),'=X0(',num2str(i),');']);
    eval(['Xdat.X',num2str(i),'=X0(',num2str(i),');']);
end

%set fmincon options
options=optimset('Algorithm','interior-point','TolFun',1e-3,'MaxIter',5000,...
    'DiffMinChange',1e-3,'ScaleProblem','none','MaxFunEvals',5000,...
    'TolCon',1e-6,'TolX',1e-6,'FinDiffType','central','SubproblemAlgorithm','cg'
        ,...
    'FunValCheck','on');

%Create a flexible way to determine design variables
tmpStr='';
```

```
for i=1:length(Xn)
    if i<length(Xn)
        space=' ';
    else
        space='';
    end
    tmpStr=[tmpStr 'X' num2str(Xn(i)) space];
end
tmpStr=['Xopt = [' tmpStr '];'];
eval(tmpStr);
%%%%%%%%%%%%%%%%%%%%%%%%%%%%%%%%%%%%%%%%%%%%%%%%%%%%%%%%%%%%%%%%%%%%%%%
% Obtain material information %%%%%%%%%%%%%%%%%%%%%%%%%%%%%%%%%%%%%%%%%
%%%%%%%%%%%%%%%%%%%%%%%%%%%%%%%%%%%%%%%%%%%%%%%%%%%%%%%%%%%%%%%%%%%%%%%
data.hCore = hCore; %also in objective
data.hSkinIn = hSkinIn; %etc
data.hSkinOut = hSkinOut; %etc
[props,data] = initPropsWrite(props,data); %etc
data  = materialInvariants(data,props);  %etc
%%%%%%%%%%%%%%%%%%%%%%%%%%%%%%%%%%%%%%%%%%%%%%%%%%%%%%%%%%%%%%%%%%%%%%%
% Run optimization %%%%%%%%%%%%%%%%%%%%%%%%%%%%%%%%%%%%%%%%%%%%%%%%%%%%
%%%%%%%%%%%%%%%%%%%%%%%%%%%%%%%%%%%%%%%%%%%%%%%%%%%%%%%%%%%%%%%%%%%%%%%
[x,fval,flag,output,lambda] = fmincon(@objectiveFunction,Xopt,[],[],[],[],lb,ub,
    @confun,options);
%Show the converged values, if existing:
if flag >=1
  disp('The converged values are:')
  x'
  fval
end
```

scripts/main.m

```
function objective = objectiveFunction(Xopt)
%Objective function for the sandwich optimization
%Note: written in Matlab
%Copyright - Stanley I. Wong - 2012
global props data Xn Xdat
disp('started with objective function')
Xopt
%React at the history flag of the model
%Do not evalute objectiveFunction again, to save time!
if strcmp(data.optimizer.flag,'XOBJ')
    %objective=-data.history(data.eval.counter).criticalPressure;
    objective=data.history(data.eval.counter).totalWeight;
    data.history(data.eval.counter).status.XOBJ=1;
    data.optimizer.flag = 'OBJ';
else
    if strcmp(data.optimizer.flag,'XCON')
        data.optimizer.flag = 'XOBJ';
        data.history(data.eval.counter+1).status.XCONXOBJ=1;
    else
```

```
        data.optimizer.flag = 'OBJ';
        data.history(data.eval.counter+1).status.XCONOBJ=1;
    end
    for i=1:length(fieldnames(Xdat)) %X1 to X27
        eval(['X' num2str(i) '= Xdat.X' num2str(i) ';']);
    end
    tmpLengthOld=1;
    for i=1:length(Xn)
        eval(['tmpLength = length(X' num2str(Xn(i)) ');'])
        tmpLength=tmpLength+tmpLengthOld;
        eval(['X' num2str(Xn(i)) '= Xopt(tmpLengthOld:tmpLength-1);'])
        tmpLengthOld=tmpLength;
    end
    %temp symmetry condition:
    X0 = [X1 X2 X3 X4 X5 X6 X7 X8 X9 X10 X11 X12 X1 X2 X3 X4 X5 X6 X7 X8 X9 X10
        X11 X12 X25 X25 X27];

    data.hCore = X27;
    data.hSkinIn = X25;
    data.hSkinOut = X26;

    [props,data] = initPropsWrite(props,data);
    data  = materialInvariants(data,props);

    %now for inner skin:
    data.refSkin =  data.refSkinIn;
    data.hSkin = data.hSkinIn;
    data.fileABDNameSkin = data.fileABDNameSkinIn;
    data.fileTSNameSkin = data.fileTSNameSkinIn;

    data = createABDfromLP_sandwich(X0,props,data);
    data = calcTransverseShearModuli_sandwich(data);

    data.ABDSkinIn = data.ABDSkin;
    data.factorPosDefSkinIn = data.factorPosDefSkin;


    %now for outer skin:
    data.refSkin =  data.refSkinOut;
    data.hSkin = data.hSkinOut;
    data.fileABDNameSkin = data.fileABDNameSkinOut;
    data.fileTSNameSkin = data.fileTSNameSkinOut;

    data = createABDfromLP_sandwich(X0,props,data);
    data = calcTransverseShearModuli_sandwich(data);

    data.ABDSkinOut = data.ABDSkin;
    data.factorPosDefSkinOut = data.factorPosDefSkin;

    %From here the ABAQUS model is evaluated:
    %Generate model with the help of the python scripting interface for ABAQUS:
```

```
    system('abq6101 cae noGUI=createSandwich2.py')

    system('abq6101 cae noGUI=inputFileModify_sandwich.py')

    %Evalute model, for linear buckling pressure and static analysis:
    system('yes | abq6101 job=myInputFile_python_sandwich user=ugens_v1.f cpu=12
        inter')
    %Obtain results with the help of python:
    system('echo "Done with evaluation, now post-processing"')
    system('abq6101 cae noGUI=readOutput_sandwich3.py')
    disp('READY WITH FE ANALYSIS')

    criticalPressure = importdata('buckle.dat');

    data.eval.counter = data.eval.counter + 1

    data.history(data.eval.counter).Xopt0 = Xopt;
    data.history(data.eval.counter).XoptX0  = [data.factorPosDefSkinIn*X0(1:12)
        data.factorPosDefSkinOut*X0(13:24) X0(25:27)];
    data.history(data.eval.counter).factorPosDefSkinIn =data.factorPosDefSkinIn;
    data.history(data.eval.counter).factorPosDefSkinOut =data.factorPosDefSkinOut
        ;
    data.history(data.eval.counter).criticalPressure =criticalPressure;

    [totalWeight,unitWeight] = calcMassSandwich(data,props);
    data.history(data.eval.counter).totalWeight = totalWeight;
    data.history(data.eval.counter).unitWeight = unitWeight;

    %objective=-criticalPressure;
    objective=totalWeight;
    disp(sprintf('>> objective = %f',objective))
    disp('evaluated objective function')
end
```

scripts/objectiveFunction.m

```
function [c, ceq] = confun(Xopt)
%Constraint function for the sandwich optimization
%Note: written in Matlab
%Copyright - Stanley I. Wong - 2012
global props data Xn Xdat

%Check the flag of the optimization model,
%redirect to objective function if not evaluated yet
if strcmp(data.optimizer.flag,'CON') || strcmp(data.optimizer.flag,'XOBJ')
    data.optimizer.flag = 'XCON';
    objective = objectiveFunction(Xopt);
    data.history(data.eval.counter).status.XCON=1;
else
    data.optimizer.flag = 'CON';
    data.history(data.eval.counter).status.CON=1;
```

```
end
disp('started with constraints')
for i=1:length(fieldnames(Xdat)) %X1 to X27
    eval(['X' num2str(i) '= Xdat.X' num2str(i) ';']);
end
tmpLengthOld=1;
for i=1:length(Xn)
    eval(['tmpLength = length(X' num2str(Xn(i)) ');'])
    tmpLength=tmpLength+tmpLengthOld;
    eval(['X' num2str(Xn(i)) '= Xopt(tmpLengthOld:tmpLength-1);'])
    tmpLengthOld=tmpLength;
end
%temp. symmetry condition:
X0 = [X1 X2 X3 X4 X5 X6 X7 X8 X9 X10 X11 X12 X1 X2 X3 X4 X5 X6 X7 X8 X9 X10 X11
    X12 X25 X25 X27];
xi0 = X0(1:24);
xi=[data.factorPosDefSkinIn*xi0(1:12) data.factorPosDefSkinOut*xi0(13:end)];
c=[];
ceq=[];

for num = [0] %temp. symmetry condition:
    %-----------------------------------------%
    % check constraints and nonlinear constraints
    %-----------------------------------------%
    % First rough constraint:  -1< xi <1 :
    %-----------------------------------------%
    j=1+num;
    c(end+1) =  xi(j) - 1;
    c(end+1) = -xi(j) - 1;
    j=2+num;
    c(end+1) =  xi(j) - 1;
    c(end+1) = -xi(j) - 1;
    j=9+num;
    c(end+1) =  xi(j) - 1;
    c(end+1) = -xi(j) - 1;
    j=10+num;
    c(end+1) =  xi(j) - 1;
    c(end+1) = -xi(j) - 1;
    %-----------------------------------------%
    % Parabola-type:
    %-----------------------------------------%
    %for A (From Miki @ Bloomfield)
    j=1+num;
    c(end+1)=2*xi(j)^2-1-xi(j+1);
    j=8+num;
    c(end+1)=2*xi(j)^2-1-xi(j+1);

    %-----------------------------------------%
    % In and out of plane (Diaconu et al.)
    %-----------------------------------------%
    %for A (B) and D (From Diaconu @ Bloomfield)
```

```
    j=1+num;
    c(end+1)=( (xi(j)-1)^4 + 3*(xi(4+j))^2 )-( 4*(xi(8+j)-1) * (xi(j)-1) );
    j=2+num;
    c(end+1)=( (xi(j)-1)^4 + 3*(xi(4+j))^2 )-( 4*(xi(8+j)-1) * (xi(j)-1) );
    j=1+num;
    c(end+1)=( (xi(j)+1)^4 + 3*(xi(4+j))^2 )-( 4*(xi(8+j)+1) * (xi(j)+1) );
    % j=4;
    j=2+num;
    c(end+1)=( (xi(j)+1)^4 + 3*(xi(4+j))^2 )-( 4*(xi(8+j)+1) * (xi(j)+1) );
end

%INNER SKIN
stuff = importdata('outputSkinIn.csv',',');
ref = 'top';
h = data.hSkinIn;
%%%%%%%%%%%%%%%%%%%%%%%%%%%%%%%%%%%%%%%%%%%%%%%%%%%%%%%%%%%%%%%%%%%%%%%
%format of output.csv:
%elementlabel,SE1,SE2,SE6,SE3,SE4,SE5,SK2,SK1,SK3
% SE1= Direct membrane strain in local 1-direction.
% SE2= Direct membrane strain in local 2-direction.
% SE6= Strain in the thickness direction.
% SE3= Shear membrane strain in local 1-2 plane.
% SE4= Transverse shear strain in the local 1-direction.
% SE5= Transverse shear strain in the local 2-direction.
% SK2= Curvature change about local 1-axis.
% SK1= Curvature change about local 2-axis.
% SK3= Surface twist in local 1-2 plane.
%%%%%%%%%%%%%%%%%%%%%%%%%%%%%%%%%%%%%%%%%%%%%%%%%%%%%%%%%%%%%%%%%%%%%%%
Ex  = stuff(:,2);
Ey  = stuff(:,3);
Exy = stuff(:,5);
Kx  = stuff(:,8); %rate of change of slope in x-direction
Ky  = stuff(:,9); %rate of change of slope in y-direction
Kxy = stuff(:,10);%amount of bending in the x-direction along the y-axis (i.e.
    twisting)
Nx  = stuff(:,11);
Ny  = stuff(:,12);
Nxy = stuff(:,13);
%determine strains for in and outer planes:
if strcmp(ref,'mid')
    zmin = -h/2;
    zmax = h/2;
elseif strcmp(ref,'top')
    zmin = -h;
    zmax =  0;
elseif strcmp(ref,'bot')
    zmin = 0;
    zmax = h;
end
%the local strain is described as:
%epsilon[x y xy] = epsilon0(x,y)+z*kappa(x,y)
```

```
%inner surface:
epsXzmin = Ex+zmin.*Kx;
epsYzmin = Ey+zmin.*Ky;
epsXYzmin= Exy+zmin.*Kxy;
I1Zmin = epsXzmin+epsYzmin;
I2Zmin = sqrt( ((epsXzmin.^2-epsYzmin.^2)./2)+epsXYzmin.^2);
ffZmin = zeros(length(I1Zmin),1);
for i = 1:length(I1Zmin) %number of elements..
    ff = failureFunctionTsaiWuLP([I1Zmin I2Zmin],data.u);
    ffZmin(i) = ff;
end

c(end+1) = max(ffZmin);

%outer surface:
epsXzmax = Ex+zmax.*Kx;
epsYzmax = Ey+zmax.*Ky;
epsXYzmax= Exy+zmax.*Kxy;
I1Zmax = epsXzmax+epsYzmax;
I2Zmax = sqrt( ((epsXzmax.^2-epsYzmax.^2)./2)+epsXYzmax.^2);
ffZmax = zeros(length(I1Zmax),1);
for i = 1:length(I1Zmax) %number of elements.. should not be different than the
    former
    ff = failureFunctionTsaiWuLP([I1Zmax I2Zmax],data.u);
    ffZmax(i) = ff;
end
c(end+1) = max(ffZmax);

%face wrinkling:
A11 = data.ABDskinIn(1,1);
A22 = data.ABDskinIn(2,2);
A12 = data.ABDskinIn(1,2);
A66 = data.ABDskinIn(3,3);
D11 = data.ABDskinIn(4,4);
D22 = data.ABDskinIn(5,5);
D12 = data.ABDskinIn(4,5);
D66 = data.ABDskinIn(6,6);
Ex0 = (A11*A22-A12^2)/(h*A22);
Ey0 = (A11*A22-A12^2)/(h*A11);
nu120 = A12/A22;
nu210 = nu120/Ex0*Ey0;
Gxy0 = A66/h;
S = props.core.cellSize;
a = S/sqrt(3);
b = S;
Ec = props.core.E11;
Ef = Ex0;
tf = h;
vf = sqrt(props.nu12*props.nu21);
tc = data.hCore;
Q = 0.5; %safety factor
```

```
sFW = Q*sqrt(Ec*Ef*tf/((1-vf^2)*tc));
c(end+1) = -(min(Nx)/h)/sFW -1; %constraint face wrinkling (1-dir)
Ef = Ey0;
sFW = Q*sqrt(Ec*Ef*tf/((1-vf^2)*tc));
c(end+1) = -(min(Ny)/h)/sFW -1; %constraint face wrinkling (2-dir)

%dimpling stress:
Kd = pi^2*(D11/D22*(b/a)^2+8/3*(D12*2*D66)/D22+16/3*(a/b)^2);
sD = Kd*D22/(tf*b^2)
c(end+1) = -(min(Nx)/h)/sD -1; %constraint dimpling (1-dir)
c(end+1) = -(min(Ny)/h)/sD -1; %constraint dimpling (2-dir)

%OUTER SKIN
stuff = importdata('outputSkinOut.csv',',');
ref = 'bot'; %i.e. bot mid or top
h = data.hSkinOut;
%%%%%%%%%%%%%%%%%%%%%%%%%%%%%%%%%%%%%%%%%%%%%%%%%%%%%%%%%%%%%%%%%%%%%%%
%format of output.csv:
%elementlabel,SE1,SE2,SE6,SE3,SE4,SE5,SK2,SK1,SK3
% SE1= Direct membrane strain in local 1-direction.
% SE2= Direct membrane strain in local 2-direction.
% SE6= Strain in the thickness direction.
% SE3= Shear membrane strain in local 1-2 plane.
% SE4= Transverse shear strain in the local 1-direction.
% SE5= Transverse shear strain in the local 2-direction.
% SK2= Curvature change about local 1-axis.
% SK1= Curvature change about local 2-axis.
% SK3= Surface twist in local 1-2 plane.
%%%%%%%%%%%%%%%%%%%%%%%%%%%%%%%%%%%%%%%%%%%%%%%%%%%%%%%%%%%%%%%%%%%%%%%
Ex  = stuff(:,2);
Ey  = stuff(:,3);
Exy = stuff(:,5);
Kx  = stuff(:,8); %rate of change of slope in x-direction
Ky  = stuff(:,9); %rate of change of slope in y-direction
Kxy = stuff(:,10);%amount of bending in the x-direction along the y-axis (i.e.
    twisting)
Nx  = stuff(:,11);
Ny  = stuff(:,12);
Nxy = stuff(:,13);
%determine strains for in and outer planes:
if strcmp(ref,'mid')
    zmin = -h/2;
    zmax = h/2;
elseif strcmp(ref,'top')
    zmin = -h;
    zmax =  0;
elseif strcmp(ref,'bot')
    zmin = 0;
    zmax = h;
end
%the local strain is described as:
```

```
%epsilon[x y xy] = epsilon0(x,y)+z*kappa(x,y)
%inner surface:
epsXzmin = Ex+zmin.*Kx;
epsYzmin = Ey+zmin.*Ky;
epsXYzmin= Exy+zmin.*Kxy;
I1Zmin = epsXzmin+epsYzmin;
I2Zmin = sqrt( ((epsXzmin.^2-epsYzmin.^2)./2)+epsXYzmin.^2);
ffZmin = zeros(length(I1Zmin),1);
for i = 1:length(I1Zmin) %number of elements
    ff = failureFunctionTsaiWuLP([I1Zmin I2Zmin],data.u);
    ffZmin(i) = ff;
end

c(end+1) = max(ffZmin);

%outer surface:
epsXzmax = Ex+zmax.*Kx;
epsYzmax = Ey+zmax.*Ky;
epsXYzmax= Exy+zmax.*Kxy;
I1Zmax = epsXzmax+epsYzmax;
I2Zmax = sqrt( ((epsXzmax.^2-epsYzmax.^2)./2)+epsXYzmax.^2);
ffZmax = zeros(length(I1Zmax),1);
for i = 1:length(I1Zmax) %number of elements
    ff = failureFunctionTsaiWuLP([I1Zmax I2Zmax],data.u);
    ffZmax(i) = ff;
end

c(end+1) = max(ffZmax);

%face wrinkling:
A11 = data.ABDskinOut(1,1);
A22 = data.ABDskinOut(2,2);
A12 = data.ABDskinOut(1,2);
A66 = data.ABDskinOut(3,3);
D11 = data.ABDskinOut(4,4);
D22 = data.ABDskinOut(5,5);
D12 = data.ABDskinOut(4,5);
D66 = data.ABDskinOut(6,6);
Ex0 = (A11*A22-A12^2)/(h*A22);
Ey0 = (A11*A22-A12^2)/(h*A11);
nu120 = A12/A22;
nu210 = nu120/Ex0*Ey0;
Gxy0 = A66/h;
S = props.core.cellSize;
a = S/sqrt(3);
b = S;
Ec = props.core.E11;
Ef = Ex0;
tf = h;
vf = sqrt(props.nu12*props.nu21);
tc = data.hCore;
```

```
Q = 0.5; %safety factor
sFW = Q*sqrt(Ec*Ef*tf/((1-vf^2)*tc));
c(end+1) = -(min(Nx)/h)/sFW -1; %constraint face wrinkling (1-dir)
Ef = Ey0;
sFW = Q*sqrt(Ec*Ef*tf/((1-vf^2)*tc));
c(end+1) = -(min(Ny)/h)/sFW -1; %constraint face wrinkling (2-dir)

%dimpling stress:
Kd = pi^2*(D11/D22*(b/a)^2+8/3*(D12*2*D66)/D22+16/3*(a/b)^2);
sD = Kd*D22/(tf*b^2)
c(end+1) = -(min(Nx)/h)/sD -1; %constraint dimpling (1-dir)
c(end+1) = -(min(Ny)/h)/sD -1; %constraint dimpling (2-dir)


if props.core.threeD
    Xt=props.core.XT;
    Xc=props.core.XC;
    Yt=props.core.YT;
    Yc=props.core.YC;
    Zt=props.core.ZT;
    Zc=props.core.ZC;
    Q12 = props.core.Q12;
    Q13 = props.core.Q13;
    Q23 = props.core.Q23;

    F11 = 1/(Xt*Xc);
    F22 = 1/(Yt*Yc);
    F33 = 1/(Zt*Zc);
    F1  = 1/Xt - 1/Xc;
    F2  = 1/Yt - 1/Yc;
    F3  = 1/Zt - 1/Zc;
    F12 = -1/(2*sqrt(Xt*Xc*Yt*Yc));
    F13 = -1/(2*sqrt(Xt*Xc*Zt*Zc));
    F23 = -1/(2*sqrt(Yt*Yc*Zt*Zc));
    F44 = 1/(Q12^2);
    F55 = 1/(Q13^2);
    F66 = 1/(Q23^2);
else
    %EXTRACT CORE:
    XT = props.core.XT;
    XC = props.core.XC;
    YT = props.core.YT;
    YC = props.core.YC;
    Q  = props.core.Q;

    F11 = 1./(XT*XC);
    F22 = 1./(YT*YC);
    F1  = 1./XT - 1./XC;
    F2  = 1./YT - 1./YC;
    F12 = -1./(2.*sqrt(XC*XT*YC*YT));
    F66 = 1./(Q^2);
```

```
end
stuff = importdata('outputCore.csv');
maxTsaiWuIndices = find(stuff.data(:,end) == max(stuff.data(:,end))); %last
    column is the tsai-wu
maxTsaiWu = max(stuff.data(:,end));
if maxTsaiWu > 1
    disp('BEWARE: material failure is active!')
end
stresses = stuff.data(maxTsaiWuIndices,2:end-1);
tsaiWu = zeros(size(stresses,1),1);
lambdaCoeffMat = zeros(size(stresses,1),3);
lambdaRootsMat = [];
for i = 1:size(stresses,1)
    if props.core.threeD
        S11 = stresses(i,1);
        S22 = stresses(i,2);
        S33 = stresses(i,3);
        S12 = stresses(i,4);
        S13 = stresses(i,5);
        S23 = stresses(i,6);
        tsaiWu(i)=F11*S11^2 +F22*S22^2 +F33*S33^2+...
            F44*S12^2+F55*S13^2+F66*S23^2+...
            F1*S11 + F2*S22 + F3*S33+...
            2.*F12*S11*S22+ 2.*F13*S11*S33+ 2.*F23*S22*S33;
    else
        S11 = stresses(i,1);
        S22 = stresses(i,2);
        S12 = stresses(i,3);
        tsaiWu(i) = F11*S11^2 +F22*S22^2 +F66*S12^2+F1*S11 + F2*S22 +2.*F12*S11*
            S22;
        lambdaCoeffVec = [-1; (F1*S11 + F2*S22); (F11*S11^2 + F22*S22^2 + 2*F12*
            S11*S22 + F66*S12^2)]';
        lambdaCoeffMat(i,:) =lambdaCoeffVec;
        lambdaRootsMat(i,:) = roots(fliplr(lambdaCoeffVec));
    end
end

%Note that the tsai-Wu is double checked
error = max([tsaiWu-stuff.data(maxTsaiWuIndices,end)]);
if error > 1e-8
    disp('check tsaiWu')
    data.error.tsaiWu1 = tsaiWu;
    data.error.tsaiWu2 =stuff.data(maxTsaiWuIndices,end);
    eof
end

if props.core.threeD
    maxMatPressure=data.extPressure/(1-max(tsaiWu));
else
    tmp =[];
    for i = 1:size(lambdaRootsMat,1)
```

```
        tmp(end+1)=max(lambdaRootsMat(i,:));
    end

    if min(tmp) <= 0
        disp('check roots')
        eof
    else
        smallestPositiveRoot = min(tmp);
    end
    maxMatPressure = data.extPressure*smallestPositiveRoot;
end

c(end+1) = -maxMatPressure+data.extPressure;
disp(sprintf('Failure [Core %f],[SkinOut %f],[SkinIn %f] ',c(end),c(end-1),c(end
    -2)))
c(end+1) = -data.history(data.eval.counter).criticalPressure+data.
    minBucklingPressure;

%Thickness Constraints
hC = data.hCore;
hSi = data.hSkinIn;
hSo = data.hSkinOut;
c(end+1) = (hC+hSi+hSo)-data.maxThicknessConstraint;
c'
data.history(data.eval.counter).c = c;
disp('confunction evaluated!!')
```

scripts/confun.m

```
function [props,data] = initPropsWrite(props,data)
%write the material properties to file and save in structurals
%Note: written in Matlab
%Copyright - Stanley I. Wong - 2012
%AS4 fiber/3501-6 epoxy
props.E11   = 126e3;          %[MPa]
props.E22   = 11e3;         %[MPa]
props.nu12  = 0.28;           %[-]
props.nu21  = props.nu12/props.E11*props.E22;  %[-]
props.G12   = 6.6e3;        %[MPa]
props.XT    = 1950;         %[MPa]
props.XC    = 1480;         %[MPa]
props.YT    = 48;         %[MPa]
props.YC    = 200;        %[MPa]
props.Q     = 79;         %[MPa]
props.rho   = 1.55E+3;    %[kg/m^3]

% aluminium 5056 honeycomb (0.147) (3D description)
props.core.threeD = 1;
props.core.E11   = 3280;        %[MPa]% out-of-plane
props.core.E22   = 19.1;        %[MPa]% W-dir
props.core.E33   = 5.96;        %[MPa]% L-dir
```

```
props.core.nu12  = 0.001;        %[-]
props.core.nu13  = 0.001;        %[-]
props.core.nu23  = 0.01;         %[-] checked via orthocheck
props.core.G12   = 328;          %[MPa]
props.core.G13   = 758;          %[MPa]
props.core.G23   = 6;          %[MPa]
props.core.XT    = 11.8;         %[MPa]
props.core.XC    = 11.8;         %[MPa]
props.core.YT    = 0.25;         %[MPa]
props.core.YC    = 0.25;         %[MPa]
props.core.ZT    = 0.92;         %[MPa]
props.core.ZC    = 0.92;         %[MPa]
props.core.Q12   = 3.93;         %[MPa]
props.core.Q13   = 6.42;         %[MPa]
props.core.Q23   = 0.1;          %[MPa]
props.core.rho   = 147;    %[kg/m^3]
props.core.cellSize = 1.588      %[mm]

%note that for the core the axes are:
% 1 = out of plane
% 2 = circumferential
% 3 = longitudinal

% FOR I/O these values are written to a props file:
outputFormat2='%21.14e ';
file1 = fopen(data.filePropsName,'w');

fprintf(file1,outputFormat2,props.E11);
fprintf(file1,outputFormat2,props.E22);
fprintf(file1,outputFormat2,props.nu12);
fprintf(file1,outputFormat2,props.nu21);
fprintf(file1,outputFormat2,props.G12);
fprintf(file1,outputFormat2,props.XT);
fprintf(file1,outputFormat2,props.XC);
fprintf(file1,outputFormat2,props.YT);
fprintf(file1,outputFormat2,props.YC);
fprintf(file1,outputFormat2,props.Q);
fprintf(file1,outputFormat2,data.hSkinIn);
fprintf(file1,outputFormat2,data.hSkinOut);
fclose(file1);

% FOR I/O these values are written to a case file:
outputFormat2='%21.14e ';
file1 = fopen(data.fileCaseName,'w');

fprintf(file1,outputFormat2,data.L);
fprintf(file1,outputFormat2,data.r_out);
fprintf(file1,outputFormat2,data.hCore);
fprintf(file1,outputFormat2,data.hSkinIn);
fprintf(file1,outputFormat2,data.hSkinOut);
fprintf(file1,outputFormat2,data.extPressure);
```

```
fclose(file1);

% FOR I/O these values are written to a core props file:
outputFormat2='%21.14e ';
file1 = fopen(data.fileCorePropsName,'w');

fprintf(file1,outputFormat2,props.core.E11);
fprintf(file1,outputFormat2,props.core.E22);
fprintf(file1,outputFormat2,props.core.E33);
fprintf(file1,outputFormat2,props.core.nu12);
fprintf(file1,outputFormat2,props.core.nu13);
fprintf(file1,outputFormat2,props.core.nu23);
fprintf(file1,outputFormat2,props.core.G12);
fprintf(file1,outputFormat2,props.core.G13);
fprintf(file1,outputFormat2,props.core.G23);
fprintf(file1,outputFormat2,props.core.XT);
fprintf(file1,outputFormat2,props.core.XC);
fprintf(file1,outputFormat2,props.core.YT);
fprintf(file1,outputFormat2,props.core.YC);
if props.core.threeD
    fprintf(file1,outputFormat2,props.core.ZT);
    fprintf(file1,outputFormat2,props.core.ZC);
    fprintf(file1,outputFormat2,props.core.Q12);
    fprintf(file1,outputFormat2,props.core.Q13);
    fprintf(file1,outputFormat2,props.core.Q23);
else
    fprintf(file1,outputFormat2,props.core.Q);
end
fclose(file1);
```

scripts/initPropsWrite.m

```
function data = materialInvariants(data,props)
%Calculate the material invaraints and save in structural
%Note: written in Matlab
%Copyright - Stanley I. Wong - 2012
%-----------------------------------------%
% read props
%-----------------------------------------%
E11  = props.E11;
E22  = props.E22;
nu12 = props.nu12;
G12  = props.G12;
XT   = props.XT;
XC   = props.XC;
YT   = props.YT;
YC   = props.YC;
S    = props.Q;
%-----------------------------------------%
% construct reduced stiffness matrix
%-----------------------------------------%
```

```
Q11 = E11^2/(E11-E22*nu12^2);
Q22 = E11*E22/(E11-E22*nu12^2);
Q12 = nu12*Q22;
Q66 = G12;
Q = [Q11 Q12 0;...
    Q12 Q22 0;...
    0 0 Q66];
data.Q = Q;

%----------------------------------------%
% construct material invariant vector
%----------------------------------------%
U1=(3*Q11+3*Q22+2*Q12+4*Q66)/8;
U2=(Q11-Q12)/2;
U3=(Q11+Q22-2*Q12-4*Q66)/8;
U4=(Q11+Q22+6*Q12-4*Q66)/8;
U5=(Q11+Q22-2*Q12+4*Q66)/8;
U=[U1;U2;U3;U4;U5];
data.U = U;

F=[];
F(11)=0.1e1 / XT / XC;
F(22)=0.1e1 / YT / YC;
F(1)=0.1e1 / XT - 0.1e1 / XC;
F(2)=0.1e1 / YT - 0.1e1 / YC;
F(12)=-(XT * XC * YT * YC) ^ (-0.1e1 / 0.2e1) / 0.2e1;
F(66)=0.1e1 / S ^ 2;

u=[];
u(1)=Q(1,1) ^ 2 * F(11) + Q(1,2) ^ 2 * F(22) +...
2 * F(12) * Q(1,1) * Q(1,2) + Q(1,2) ^ 2 * F(11) +...
Q(2,2) ^ 2 * F(22) + 2 * F(12) * Q(1,2) * Q(2,2) -...
2 * Q(1,1) * Q(1,2) * F(11) - 2 * Q(1,2) * Q(2,2) * F(22)...
- 2 * F(12) * Q(1,2) ^ 2 - 2 * F(12) * Q(1,1) * Q(2,2);

u(2)=Q(1,1) * F(1) / 0.2e1 + Q(1,2) * F(2) / 0.2e1 +...
Q(1,2) * F(1) / 0.2e1 + Q(2,2) * F(2) / 0.2e1;

u(3)=Q(1,1) ^ 2 * F(11) / 0.4e1 +...
Q(1,2) ^ 2 * F(22) / 0.4e1 +...
F(12) * Q(1,1) * Q(1,2) / 0.2e1 +...
Q(1,2) ^ 2 * F(11) / 0.4e1 + Q(2,2) ^ 2 * F(22) / 0.4e1 +...
F(12) * Q(1,2) * Q(2,2) / 0.2e1 +...
Q(1,1) * Q(1,2) * F(11) / 0.2e1 +...
Q(1,2) * Q(2,2) * F(22) / 0.2e1 +...
F(12) * Q(1,2) ^ 2 / 0.2e1 +...
F(12) * Q(1,1) * Q(2,2) / 0.2e1;

u(4)=Q(1,1) * F(1) + Q(1,2) * F(2) -...
Q(1,2) * F(1) - Q(2,2) * F(2);

```

```
u(5)=Q(1,1) ^ 2 * F(11) + Q(1,2) ^ 2 * F(22) +...
2 * F(12) * Q(1,1) * Q(1,2) - Q(1,2) ^ 2 * F(11) -...
Q(2,2) ^ 2 * F(22) - 2 * F(12) * Q(1,2) * Q(2,2);

u(6)=4 * Q(3,3) ^ 2 * F(66);
data.u = u; %save in structural
```

scripts/materialInvariants.m

```
#This script creates a composite sandwich cylinder
#Note: written in Python, for ABAQUS
#Copyright - Stanley I. Wong - 2012
from part import *
from material import *
from section import *
from assembly import *
from step import *
from interaction import *
from load import *
from mesh import *
from job import *
from sketch import *
from visualization import *
from connectorBehavior import *
from Numeric import *
import regionToolset
####$$$$$$####$$$$$$#### MY LITTLE TUI ####$$$$$$####$$$$$$####
caeName='myCae'
jobName='Job-1-sandwich'
writeJob=True
writeCAE=True
meshSize = 10.0
#################################################################
#case file read
case_vars = []
f = open('case_sandwich.dat','r')
for line in f:
  tmp = line.split()
  for value in tmp:
      case_vars.append(float(value))
f.close()

cylinderLength = case_vars[0]
cylinderOuterRadius = case_vars[1]
coreThickness  = case_vars[2]
skinInThickness = case_vars[3]
skinOutThickness = case_vars[4]
externalPressure = case_vars[5]
#other variables
coreOutRadius = cylinderOuterRadius - skinOutThickness
coreInRadius = coreOutRadius - coreThickness
```

```
coreMidRadius = (coreOutRadius+coreInRadius)/2.
cylinderInnerRadius = cylinderOuterRadius - coreThickness - skinOutThickness -
    skinInThickness
pert = 1e-3 #for geometry searching
################################################################
#CREATE CORE MATERIAL AND SKIN (DUMMY) MATERIAL
#for the lamination parameters this is overwritten:
props_skin = []
f = open('DUMMYmaterial_props.dat','r')
for line in f:
  tmp = line.split()
  props_skin.append(float(tmp[0]))
f.close()
props_core = []
f = open('props_core.dat','r')
for line in f:
  tmp = line.split()
  for value in tmp:
      props_core.append(float(value))
f.close()

#props for skin (a) #THIS IS A DUMMY
skinMaterialName='skinMaterial'
E1a   = props_skin[0]
E2a   = props_skin[1]
E3a   = props_skin[2]
nu12a = props_skin[3]
nu13a = props_skin[4]
nu23a = props_skin[5]
G12a  = props_skin[6]
G13a  = props_skin[7]
G23a  = props_skin[8]
#props for core (b)
coreMaterialName='coreMaterial'
E1b   = props_core[0]
E2b   = props_core[1]
E3b   = props_core[2]
nu12b = props_core[3]
nu13b = props_core[4]
nu23b = props_core[5]
G12b  = props_core[6]
G13b  = props_core[7]
G23b  = props_core[8]
if len(props_core) <> 18:
    print 'Something going on with core props'
    z = 1/0 #LET IT CRASH!
##other (dummy) properties
opt_vars = []
f = open('DUMMYopt_vars.dat','r')
for line in f:
  tmp = line.split()
```

```
  opt_vars.append(float(tmp[0]))
f.close()

nPlySkinIn = int(opt_vars[2])
nPlySkinOut = int(opt_vars[3])
plyThicknessArrayIn = []
for i in range(4,4+nPlySkinIn):
  plyThicknessArrayIn.append(opt_vars[i])
  iTmp = i
plyThicknessArrayOut= []
for i in range(iTmp+1,iTmp+1+nPlySkinOut):
  plyThicknessArrayOut.append(opt_vars[i])
  iTmp = i
plyOriArrayIn = []
for i in range(iTmp+2,iTmp+2+nPlySkinIn):
  plyOriArrayIn.append(opt_vars[i])
  iTmp = i
plyOriArrayOut = []
for i in range(iTmp+1,iTmp+1+nPlySkinOut):
  plyOriArrayOut.append(opt_vars[i])
  iTmp = i


##################################################################
#PRESETS
myModel  = 'Model-1'
myPart   = 'Part-1'
mySketch = '__profile__'

loadPressure=externalPressure
session.journalOptions.setValues(recoverGeometry=INDEX)
session.journalOptions.setValues(replayGeometry=INDEX)
##################################################################
#create sketch
mdb.models[myModel].ConstrainedSketch(name=mySketch, sheetSize=1000.0)
mySketch = mdb.models[myModel].sketches[mySketch]
mySketch.ConstructionLine(point1=(0.0, -500.0), point2=(0.0, 500.0))
mySketch.rectangle(point1=(coreInRadius, 0.0), point2=(coreOutRadius,
    cylinderLength))
mdb.models[myModel].Part(name=myPart, dimensionality=THREE_D, type=
    DEFORMABLE_BODY)
mdb.models[myModel].parts[myPart].BaseSolidRevolve(sketch=mySketch, angle=360.0,
    flipRevolveDirection=OFF)
del mdb.models[myModel].sketches['__profile__']
partName = mdb.models[myModel].parts[myPart]

##################################################################
#DATUMS
xzPlaneOffsetBase=partName.DatumPlaneByPrincipalPlane(offset=20.0, principalPlane
    =XZPLANE)
```

```
xzPlaneOffsetTop=partName.DatumPlaneByPrincipalPlane(offset=cylinderLength-20.0,
    principalPlane=XZPLANE)
xyPlane=partName.DatumPlaneByPrincipalPlane(offset=0.0, principalPlane=XYPLANE)
yzPlane=partName.DatumPlaneByPrincipalPlane(offset=0.0, principalPlane=YZPLANE)
xzPlane=partName.DatumPlaneByPrincipalPlane(offset=0.0, principalPlane=XZPLANE)
##############################################################
#CREATE SETS IN PART
setFaceCoreIn='Set-Face-Core-In'
faceNumber=partName.faces.getClosest(coordinates=([0.0,0.0,cylinderInnerRadius],)
    )[0][0].index
partName.Set(faces=partName.faces[faceNumber:faceNumber+1], name=setFaceCoreIn)

setFaceCoreOut='Set-Face-Core-Out'
faceNumber=partName.faces.getClosest(coordinates=([0.0,0.0,cylinderOuterRadius],)
    )[0][0].index
partName.Set(faces=partName.faces[faceNumber:faceNumber+1], name=setFaceCoreOut)

setFaceCoreTop='Set-Face-Core-Top'
faceNumber=partName.faces.getClosest(coordinates=([0.0,cylinderLength,
    coreMidRadius],))[0][0].index
partName.Set(faces=partName.faces[faceNumber:faceNumber+1], name=setFaceCoreTop)

setFaceCoreBase='Set-Face-Core-Base'
faceNumber=partName.faces.getClosest(coordinates=([0.0,0.0,coreMidRadius],))
    [0][0].index
partName.Set(faces=partName.faces[faceNumber:faceNumber+1], name=setFaceCoreBase)

setCellCore='Set-Cell-Core'
partName.Set(cells=partName.cells[0:1], name=setCellCore)
##############################################################
#CREATE SURFACE IN PART
partName.Surface(name='Surf-1', side1Faces=partName.sets['Set-Face-Core-Out'].
    faces)

##############################################################
#CREATE MATERIALS
modelName=mdb.models[myModel]
modelName.Material(name=skinMaterialName)
mdb.models[myModel].materials[skinMaterialName].Elastic(\
    table=((E1a, E2a, E3a,\
    nu12a, nu13a, nu23a,\
    G12a, G13a, G23a), ), type=ENGINEERING_CONSTANTS)
modelName.Material(name=coreMaterialName)
modelName.materials[coreMaterialName].Elastic(\
    table=((E1b, E2b, E3b,\
    nu12b, nu13b, nu23b,\
    G12b, G13b, G23b), ), type=ENGINEERING_CONSTANTS)

#create orientations
partName.DatumPointByCoordinate(coords=(0.0, 0.0,-coreMidRadius))#!mod
indexVertex=partName.vertices.getClosest([(0.,0.,1.)])[0][0].index
```

```
partName.DatumCsysByThreePoints(coordSysType=
    CYLINDRICAL, name='Datum csys-1', origin=(0.0, 0.0, 0.0), point1=
    partName.vertices[indexVertex], point2=
    partName.datums[max(partName.datums.keys())])
datumID=partName.features['Datum csys-1'].id
layupOrientation = partName.datums[datumID]

##create skins
skinCoreOut = 'Skin-Core-Out'
partName.Skin(faces=partName.sets[setFaceCoreOut].faces, name=skinCoreOut)
skinCoreIn = 'Skin-Core-In'
partName.Skin(faces=partName.sets[setFaceCoreIn].faces, name=skinCoreIn)

#create layup
myLayupIn='CompositeLayup-In'
tmpFaces = partName.sets[setFaceCoreIn].faces
region = regionToolset.Region(skinFaces=((skinCoreIn,tmpFaces),))
partName.CompositeLayup(description='',
    elementType=SHELL, name=myLayupIn, offsetType=TOP_SURFACE,
    symmetric=False, thicknessAssignment=FROM_SECTION)
partName.compositeLayups[myLayupIn].Section(
    integrationRule=SIMPSON, poissonDefinition=DEFAULT, preIntegrate=OFF,
    temperature=GRADIENT, thicknessType=UNIFORM, useDensity=OFF)
partName.compositeLayups[myLayupIn].ReferenceOrientation(
    additionalRotationType=ROTATION_NONE, angle=0.0, axis=AXIS_1, fieldName='',
    localCsys=partName.datums[datumID], orientationType=GLOBAL)
partName.compositeLayups[myLayupIn].orientation.setValues(orientationType=SYSTEM,
    localCsys=layupOrientation)

for i in range(0,nPlySkinIn):
  partName.compositeLayups[myLayupIn].CompositePly(additionalRotationField='',
      additionalRotationType=ROTATION_NONE, angle=plyOriArrayIn[i],axis=AXIS_3,
      material=skinMaterialName, numIntPoints=3,orientationValue=0.0,
      orientationType=SPECIFY_ORIENT,plyName='Ply-'+str(i+1+nPlySkinOut)+'-Shell'
      , region=region,suppressed=False,thickness=plyThicknessArrayIn[i],
      thicknessType=SPECIFY_THICKNESS)

myLayupOut='CompositeLayup-Out'
tmpFaces = partName.sets[setFaceCoreOut].faces
region = regionToolset.Region(skinFaces=((skinCoreOut,tmpFaces),))
partName.CompositeLayup(description='',
    elementType=SHELL, name=myLayupOut, offsetType=BOTTOM_SURFACE,
    symmetric=False, thicknessAssignment=FROM_SECTION)
partName.compositeLayups[myLayupOut].Section(
    integrationRule=SIMPSON, poissonDefinition=DEFAULT, preIntegrate=OFF,
    temperature=GRADIENT, thicknessType=UNIFORM, useDensity=OFF)
partName.compositeLayups[myLayupOut].ReferenceOrientation(
    additionalRotationType=ROTATION_NONE, angle=0.0, axis=AXIS_1, fieldName='',
    localCsys=partName.datums[datumID], orientationType=GLOBAL)
partName.compositeLayups[myLayupOut].orientation.setValues(orientationType=SYSTEM
    ,localCsys=layupOrientation)
```

```
for i in range(0,nPlySkinOut):
  partName.compositeLayups[myLayupOut].CompositePly(additionalRotationField='',
      additionalRotationType=ROTATION_NONE, angle=plyOriArrayOut[i],axis=AXIS_3,
      material=skinMaterialName, numIntPoints=3,orientationValue=0.0,
      orientationType=SPECIFY_ORIENT,plyName='Ply-'+str(i+1+nPlySkinOut)+'-Shell'
      , region=region,suppressed=False,thickness=plyThicknessArrayOut[i],
      thicknessType=SPECIFY_THICKNESS)


myLayupCore='CompositeLayup-Core'
partName.CompositeLayup(description='', elementType=SOLID, name=myLayupCore,
    symmetric=False, thicknessAssignment=FROM_SECTION)
partName.compositeLayups[myLayupCore].Section(
    integrationRule=SIMPSON, poissonDefinition=DEFAULT, preIntegrate=ON,
    temperature=GRADIENT, thicknessType=UNIFORM, useDensity=OFF)
partName.compositeLayups[myLayupCore].ReferenceOrientation(
    additionalRotationType=ROTATION_NONE, angle=0.0, axis=AXIS_1, fieldName='',
    localCsys=partName.datums[datumID], orientationType=GLOBAL)
partName.compositeLayups[myLayupCore].orientation.setValues(orientationType=
    SYSTEM,localCsys=layupOrientation,stackDirection=STACK_3)
partName.compositeLayups[myLayupCore].CompositePly(additionalRotationField='',
    additionalRotationType=ROTATION_NONE, angle=0.0, axis=AXIS_3, material=
    coreMaterialName, numIntPoints=3, orientationType=ANGLE_0,plyName='Ply-Core',
     region=partName.sets['Set-Cell-Core'],suppressed=False, thickness=3.0,
    thicknessType=SPECIFY_THICKNESS)

flipNormalRegions = partName.sets[setFaceCoreIn]
partName.flipNormal(regions=flipNormalRegions)

# partitioning
#CREATE PARTITION, EXTRA SETS

partName.PartitionCellByDatumPlane(datumPlane=
    partName.datums[xzPlaneOffsetBase.id], cells=
    partName.cells[0:len(partName.cells)])
partName.PartitionCellByDatumPlane(datumPlane=
    partName.datums[xzPlaneOffsetTop.id], cells=
    partName.cells[0:len(partName.cells)])

edgeNumber1=partName.edges.getClosest(coordinates=([pert,20.0,coreMidRadius],))
    [0][0].index
edgeNumber2=partName.edges.getClosest(coordinates=([-pert,20.0,coreMidRadius],))
    [0][0].index
edgeNumber3=partName.edges.getClosest(coordinates=([pert,20.0,-coreMidRadius],))
    [0][0].index
edgeNumber4=partName.edges.getClosest(coordinates=([-pert,20.0,-coreMidRadius],))
    [0][0].index

setEdgeBaseOffset='Set-Edge-Base-Offset'
partName.Set(edges=partName.edges[edgeNumber1:edgeNumber1+1]+\
    partName.edges[edgeNumber2:edgeNumber2+1]+\
```

```
    partName.edges[edgeNumber3:edgeNumber3+1]+\
    partName.edges[edgeNumber4:edgeNumber4+1]\
    , name=setEdgeBaseOffset)

edgeNumber=partName.edges.getClosest(coordinates=([0.0,cylinderLength-20.0,
    coreMidRadius],))[0][0].index
edgeNumber1=partName.edges.getClosest(coordinates=([pert,cylinderLength-20.0,
    coreMidRadius],))[0][0].index
edgeNumber2=partName.edges.getClosest(coordinates=([-pert,cylinderLength-20.0,
    coreMidRadius],))[0][0].index
edgeNumber3=partName.edges.getClosest(coordinates=([pert,cylinderLength-20.0,-
    coreMidRadius],))[0][0].index
edgeNumber4=partName.edges.getClosest(coordinates=([-pert,cylinderLength-20.0,-
    coreMidRadius],))[0][0].index

setEdgeTopOffset='Set-Edge-Top-Offset'
partName.Set(edges=partName.edges[edgeNumber1:edgeNumber1+1]+\
    partName.edges[edgeNumber2:edgeNumber2+1]+\
    partName.edges[edgeNumber3:edgeNumber3+1]+\
    partName.edges[edgeNumber4:edgeNumber4+1]\
    , name=setEdgeTopOffset)


partName.PartitionCellByDatumPlane(datumPlane=
    partName.datums[yzPlane.id], cells=
    partName.cells[0:len(partName.cells)])
partName.PartitionCellByDatumPlane(datumPlane=
    partName.datums[xyPlane.id], cells=
    partName.cells[0:len(partName.cells)])

## midSection:
# 5 times sqrt(r_out*t_max) ~= 200
# Thus for a given mesh size the partition needs to be:
charLength = 5.*sqrt(cylinderOuterRadius*13.0)
nElementsBending = charLength/int(meshSize)+1
partitionYmin = float(meshSize)*nElementsBending
partitionYmax = cylinderLength-partitionYmin

xzPlaneOffsetBendingBase=partName.DatumPlaneByPrincipalPlane(offset=partitionYmin
    , principalPlane=XZPLANE)
xzPlaneOffsetBendingTop=partName.DatumPlaneByPrincipalPlane(offset=partitionYmax,
     principalPlane=XZPLANE)
partName.PartitionCellByDatumPlane(datumPlane=
    partName.datums[xzPlaneOffsetBendingBase.id], cells=
    partName.cells[0:len(partName.cells)])
partName.PartitionCellByDatumPlane(datumPlane=
    partName.datums[xzPlaneOffsetBendingTop.id], cells=
    partName.cells[0:len(partName.cells)])

i1 = partName.faces.findAt((((cylinderOuterRadius-skinOutThickness)*cos(pi/4.0),
    cylinderLength/2.0,(cylinderOuterRadius-skinOutThickness)*sin(pi/4.0),))).
```

```
    index
f1 = partName.faces[i1:i1+1]
i2 = partName.faces.findAt((((cylinderOuterRadius-skinOutThickness)*cos(pi/4.0+pi
    /2.0),cylinderLength/2.0,(cylinderOuterRadius-skinOutThickness)*sin(pi/4.0+pi
    /2.0),))).index
f2 = partName.faces[i2:i2+1]
i3 = partName.faces.findAt((((cylinderOuterRadius-skinOutThickness)*cos(pi/4.0+pi
    ),cylinderLength/2.0,(cylinderOuterRadius-skinOutThickness)*sin(pi/4.0+pi),))
    ).index
f3 = partName.faces[i3:i3+1]
i4 = partName.faces.findAt((((cylinderOuterRadius-skinOutThickness)*cos(pi/4.0+pi
    *1.5),cylinderLength/2.0,(cylinderOuterRadius-skinOutThickness)*sin(pi/4.0+pi
    *1.5),))).index
f4 = partName.faces[i4:i4+1]

partName.Set(skinFaces=(('Skin-Core-Out', f1),('Skin-Core-Out', f2),('Skin-Core-
    Out', f3),('Skin-Core-Out', f4) ), name='Set-Skin-Out-Mid')

i1 = partName.faces.findAt((((cylinderOuterRadius-skinOutThickness-coreThickness)
    *cos(pi/4.0),cylinderLength/2.0,(cylinderOuterRadius-skinOutThickness-
    coreThickness)*sin(pi/4.0),))).index
f1 = partName.faces[i1:i1+1]
i2 = partName.faces.findAt((((cylinderOuterRadius-skinOutThickness-coreThickness)
    *cos(pi/4.0+pi/2.0),cylinderLength/2.0,(cylinderOuterRadius-skinOutThickness-
    coreThickness)*sin(pi/4.0+pi/2.0),))).index
f2 = partName.faces[i2:i2+1]
i3 = partName.faces.findAt((((cylinderOuterRadius-skinOutThickness-coreThickness)
    *cos(pi/4.0+pi),cylinderLength/2.0,(cylinderOuterRadius-skinOutThickness-
    coreThickness)*sin(pi/4.0+pi),))).index
f3 = partName.faces[i3:i3+1]
i4 = partName.faces.findAt((((cylinderOuterRadius-skinOutThickness-coreThickness)
    *cos(pi/4.0+pi*1.5),cylinderLength/2.0,(cylinderOuterRadius-skinOutThickness-
    coreThickness)*sin(pi/4.0+pi*1.5),))).index
f4 = partName.faces[i4:i4+1]

partName.Set(skinFaces=(('Skin-Core-In', f1),('Skin-Core-In', f2),('Skin-Core-In'
    , f3),('Skin-Core-In', f4) ), name='Set-Skin-In-Mid')

i1 = partName.cells.findAt((((coreMidRadius)*cos(pi/4.0),cylinderLength/2.0,(
    coreMidRadius)*sin(pi/4.0),))).index
c1 = partName.cells[i1:i1+1]
i2 = partName.cells.findAt((((coreMidRadius)*cos(pi/4.0+pi/2.0),cylinderLength
    /2.0,(coreMidRadius)*sin(pi/4.0+pi/2.0),))).index
c2 = partName.cells[i2:i2+1]
i3 = partName.cells.findAt((((coreMidRadius)*cos(pi/4.0+pi),cylinderLength/2.0,(
    coreMidRadius)*sin(pi/4.0+pi),))).index
c3 = partName.cells[i3:i3+1]
i4 = partName.cells.findAt((((coreMidRadius)*cos(pi/4.0+pi*1.5),cylinderLength
    /2.0,(coreMidRadius)*sin(pi/4.0+pi*1.5),))).index
c4 = partName.cells[i4:i4+1]
partName.Set(cells=((c1),(c2),(c3),(c4) ), name='Set-Core-Mid')
```

```
#create mesh
#assign mesh controls
partName.setElementType(elemTypes=(ElemType(elemCode=S4R, elemLibrary=STANDARD,
    secondOrderAccuracy=OFF, hourglassControl=ENHANCED),),regions=(partName.skins
    [skinCoreOut].faces,))
partName.setElementType(elemTypes=(ElemType(elemCode=S4R, elemLibrary=STANDARD,
    secondOrderAccuracy=OFF, hourglassControl=ENHANCED),),regions=(partName.skins
    [skinCoreIn].faces,))
partName.setElementType(elemTypes=(ElemType(elemCode=C3D8R, elemLibrary=STANDARD,
    kinematicSplit=AVERAGE_STRAIN, secondOrderAccuracy=OFF,hourglassControl=
    ENHANCED, distortionControl=DEFAULT),),regions=(partName.sets[setCellCore].
    cells,))

#seed
partName.seedPart(deviationFactor=0.1, size=meshSize)
partName.generateMesh()

##############################################################
#CREATE ASSEMBLY
mdb.models[myModel].rootAssembly.DatumCsysByDefault(CARTESIAN)
assName=mdb.models[myModel].rootAssembly
mdb.models[myModel].rootAssembly.Instance(dependent=ON, name=myPart+'-1',
    part=partName)
iName=assName.instances[myPart+'-1']
myInstance=myPart+'-1'

##############################################################
#CREATE STEP
modelName.StaticStep(initialInc=1.0, maxInc=1.0, name='Step-1',
    nlgeom=ON, previous='Initial')

##############################################################
#CREATE BCs

modelName.YsymmBC(createStepName='Initial', name='BC-Base-Ysymm', region=
    assName.instances[myInstance].sets[setFaceCoreBase])
modelName.DisplacementBC(amplitude=UNSET, createStepName='Initial',
    distributionType=UNIFORM, fieldName='', fixed=OFF, localCsys=None, name=
    'BC-Top-Offset-XZ', region=iName.sets[setEdgeTopOffset],
    u1=0.0, u2=UNSET, u3=0.0, ur1=UNSET, ur2=UNSET, ur3=UNSET)
modelName.DisplacementBC(amplitude=UNSET, createStepName='Initial',
    distributionType=UNIFORM, fieldName='', fixed=OFF, localCsys=None, name=
    'BC-Base-Offset-XZ', region=iName.sets[setEdgeBaseOffset],
    u1=0.0, u2=UNSET, u3=0.0, ur1=UNSET, ur2=UNSET, ur3=UNSET)
modelName.DisplacementBC(amplitude=UNSET, createStepName='Initial',
    distributionType=UNIFORM, fieldName='', fixed=OFF, localCsys=None, name=
    'BC-Base-XZ', region=iName.sets[setFaceCoreBase],
    u1=0.0, u2=UNSET, u3=0.0, ur1=UNSET, ur2=UNSET, ur3=UNSET)

tmpIndex1=partName.vertices.findAt(coordinates=(0.,0.,-coreOutRadius),).index
```

```
tmpIndex2=partName.vertices.findAt(coordinates=(0.,0.,coreOutRadius),).index
modelName.DisplacementBC(amplitude=UNSET, createStepName='Initial',
    distributionType=UNIFORM, fieldName='', localCsys=None, name='BC-Base-X',
    region=Region(
    vertices=assName.instances[myInstance].vertices[tmpIndex1:tmpIndex1+1]+\
    assName.instances[myInstance].vertices[tmpIndex2:tmpIndex2+1])
    , u1=SET, u2=UNSET, u3=UNSET, ur1=UNSET, ur2=UNSET, ur3=UNSET)
tmpIndex1=partName.vertices.findAt(coordinates=(-coreOutRadius,0.,0.),).index
tmpIndex2=partName.vertices.findAt(coordinates=(coreOutRadius,0.,0.),).index
modelName.DisplacementBC(amplitude=UNSET, createStepName='Initial',
    distributionType=UNIFORM, fieldName='', localCsys=None, name='BC-Base-Z',
    region=Region(
    vertices=assName.instances[myInstance].vertices[tmpIndex1:tmpIndex1+1]+\
    assName.instances[myInstance].vertices[tmpIndex2:tmpIndex2+1])
    , u1=UNSET, u2=UNSET, u3=SET, ur1=UNSET, ur2=UNSET, ur3=UNSET)

#############################################################
#CREATE UNIFORM PRESSURE
modelName.Pressure(amplitude=UNSET, createStepName='Step-1',
    distributionType=UNIFORM, field='', magnitude=loadPressure, name='Load-1',
        region=
    assName.instances[myInstance].surfaces['Surf-1'])
mdb.models['Model-1'].steps['Step-1'].setValues(minInc=2e-06, timePeriod=1.0)
#############################################################
#CREATE AXIAL FORCE
refPoint=assName.ReferencePoint(point=(0.0, cylinderLength+10.0, 0.0))
loadAxial=-(cylinderOuterRadius**2*pi)*loadPressure
modelName.Coupling(controlPoint=Region(referencePoints=(assName.referencePoints[
    refPoint.id], )), couplingType=KINEMATIC, influenceRadius=WHOLE_SURFACE,
    localCsys=None, name='Constraint-RP', surface=Region(faces=iName.sets[
    setFaceCoreTop].faces), u1=ON, u2=ON, u3=ON, ur1=ON, ur2=OFF, ur3=ON)
modelName.ConcentratedForce(cf2=loadAxial, createStepName='Step-1',
    distributionType=UNIFORM, field='', localCsys=None, name='Load-2', region=
    Region(referencePoints=( assName.referencePoints[refPoint.id], )))
#############################################################
#EXTRA BC FOR RP
refPointNumber=assName.referencePoints.items(refPoint)[0][0]
modelName.DisplacementBC(amplitude=UNSET, createStepName='Initial',\
    distributionType=UNIFORM, fieldName='', localCsys=None, name='BC-RP-XZ-rXrZ',
        region=Region(referencePoints=(\
    assName.referencePoints[refPointNumber],\
    )), u1=SET, u2=UNSET, u3=SET, ur1=SET, ur2=UNSET, ur3=SET)
#############################################################
#FIELD OUTPUT REQUESTS
#WHOLE MODEL
#COMPOSITE LAYUP
modelName.FieldOutputRequest(createStepName='Step-1',
    layupLocationMethod=SPECIFIED, layupNames=(myInstance+'.'+myLayupIn, ),
    name='F-Output-Skin-In', outputAtPlyBottom=False, outputAtPlyMid=False,
    outputAtPlyTop=True, rebar=EXCLUDE, variables=('SE','U','RF','CF','SF','TF','
        SDV'))
```

```
424 modelName.FieldOutputRequest(createStepName='Step-1',
        layupLocationMethod=SPECIFIED, layupNames=(myInstance+'.'+myLayupOut, ),
426     name='F-Output-Skin-Out', outputAtPlyBottom=True, outputAtPlyMid=False,
        outputAtPlyTop=False, rebar=EXCLUDE, variables=('SE','U','RF','CF','SF','TF',
            'SDV'))
428 modelName.FieldOutputRequest(createStepName='Step-1',
        layupLocationMethod=SPECIFIED, layupNames=(myInstance+'.'+myLayupCore, ),
430     name='F-Output-Core', outputAtPlyBottom=False, outputAtPlyMid=True,
        outputAtPlyTop=False, rebar=EXCLUDE, variables=('S', 'E'))
432 modelName.fieldOutputRequests['F-Output-Core'].setValues(
        layupLocationMethod=ALL_LOCATIONS)
434 ##############################################################
    #LINEAR BUCKLING ANALYSIS
436 modelName.BuckleStep(name='Step-2', numEigen=1, previous='Initial',
        vectors=30, maxIterations=3000)
438 modelName.steps['Step-1'].setValues(nlgeom=OFF)
    modelName.Pressure(amplitude=UNSET, createStepName='Step-2',\
440     distributionType=UNIFORM, field='', magnitude=1.0, name='Load-3', region=\
        assName.instances[myInstance].surfaces['Surf-1'])
442 forceRP = -cylinderOuterRadius**2.0*pi
    modelName.ConcentratedForce(cf2=forceRP, createStepName=
444     'Step-2', distributionType=UNIFORM, field='', localCsys=None, name='Load-4'
        , region=Region(referencePoints=(
446     mdb.models['Model-1'].rootAssembly.referencePoints[6], )))

448 ##############################################################
    #OUTPUT CREATE JOB, INPUT FILE AND CAE
450 mdb.Job(atTime=None, contactPrint=OFF, description='', echoPrint=OFF,
        explicitPrecision=SINGLE, getMemoryFromAnalysis=True, historyPrint=OFF,
452     memory=90, memoryUnits=PERCENTAGE, model=myModel, modelPrint=ON,
        multiprocessingMode=DEFAULT, name=jobName, nodalOutputPrecision=SINGLE,
454     numCpus=1, queue=None, scratch='', type=ANALYSIS, userSubroutine='',
        waitHours=0, waitMinutes=0)
456
    #write input
458 if writeJob:
      mdb.jobs[jobName].writeInput()
460 if writeCAE:
      mdb.saveAs(pathName=caeName + '.cae')
462 print 'done!!'
```

scripts/createSandwich2.py

```
1 #Modify the sandwich input file for the given values
  #Note: written in Python, for ABAQUS
3 #Copyright - Stanley I. Wong - 2012
  from abaqus import *
5 from abaqusConstants import *
  from viewerModules import *
7 from math import *
  from Numeric import *
```

```
from LinearAlgebra import *
# inputs: (formats are for writing)
inputFile    = 'Job-1-sandwich.inp' #blank inputfile
newInputFile= 'myInputFile_python_sandwich.inp'
elementSetSkinIn  = 'CompositeLayup-In-1'
elementSetSkinOut = 'CompositeLayup-Out-1'
nstatev     = 6
orientationSkinIn = 'Ori-2'
orientationSkinOut = 'Ori-3'


dataFileSkinIn= 'ABDskinIn.dat'
dataFileSkinOut= 'ABDskinOut.dat'
dataFormat1='%32.16e '
dataFormat2='%21.14e '

propsFile = 'props_sandwich.dat'
propsFormat = '%21.14e '

transverseShearFileSkinIn='TSskinIn.dat'
transverseShearFileSkinOut='TSskinOut.dat'
transverseShearFormat='%21.14e '

# ----------------------------------------------------------------#
# READ ALL DATA FILES CREATED BY MATLAB :
# ----------------------------------------------------------------#

#read ABD matrix created by matlab (inner skin)
f = open(dataFileSkinIn,'r')
lines = f.readlines()
f.close()

ABDskinIn = zeros((6,6),'d')
i = -1
for line in lines:
    i+=1
    row = line.split()
    j=-1
    for index in row:
  j+=1
  ABDskinIn[i,j] = float(index)

#read ABD matrix created by matlab (outer skin)
f = open(dataFileSkinOut,'r')
lines = f.readlines()
f.close()

ABDskinOut = zeros((6,6),'d')
i = -1
for line in lines:
    i+=1
```

```
    row = line.split()
    j=-1
    for index in row:
  j+=1
  ABDskinOut[i,j] = float(index)


#read props used in matlab
f = open(propsFile,'r')
lines = f.readlines()
f.close()
nprops = len(lines[0].split())
props = zeros((nprops),'d')
row = lines[0].split()
i = -1
for index in row:
    i+=1
    props[i] = float(index)

#needed properties (maybe things like strength on a later stage):
hSkinIn  = props[nprops-2]
hSkinOut = props[nprops-1]
#read transverse shear moduli (in)
f = open(transverseShearFileSkinIn,'r')
lines = f.readlines()
f.close()
nTS = len(lines[0].split())
TSskinIn = zeros((nTS),'d')
row = lines[0].split()
i = -1
for index in row:
    i+=1
    TSskinIn[i] = float(index)
#read transverse shear moduli (out)
f = open(transverseShearFileSkinOut,'r')
lines = f.readlines()
f.close()
nTS = len(lines[0].split())
TSskinOut = zeros((nTS),'d')
row = lines[0].split()
i = -1
for index in row:
    i+=1
    TSskinOut[i] = float(index)

#-----------------------------------------------------------------#
# prepare lines to write
#-----------------------------------------------------------------#
#shell general section:
nABDvalues = 36
nProps2Write = 1+nABDvalues #i.e. {h,ABD(i,j)}
```

```
SGSskinIn =[]
commentLine='**Section: General Shell (ABD) passed to be created by UGENS\n'
SGSskinIn.append(commentLine)
s1 = '*Shell General Section, '
s2 = 'elset='+elementSetSkinIn+', '
s3 = 'user, '
s4 = 'variables='+str(nstatev)+', '
s5 = 'properties='+str(nProps2Write)+', '
s6 = 'orientation='+orientationSkinIn+', '
s7 = 'controls=EC-1'+'\n'
SGSskinIn.append(s1+s2+s3+s4+s5+s6+s7) #LINE1: header
#LINE2: only the thickness:
SGSskinIn.append(str(hSkinIn)+' \n')
#LINE(3 : 7) : ABD values

tmpStr = ''
count = -1
for i in range(0,6):
    for j in range(0,6):
  count+=1
  if (count == 8) or ((i ==5) and (j==5)):
      if ((i==5) and (j==5)):
    tmpStr=tmpStr+str(ABDskinIn[i,j])+' '
    tmpStr=tmpStr+'\n'
    SGSskinIn.append(tmpStr)
      else:
    count=0
    tmpStr=tmpStr+'\n'
    SGSskinIn.append(tmpStr)
    tmpStr=''
  if (count==7):
      tmpStr=tmpStr+str(ABDskinIn[i,j])+' '
  else:
      tmpStr=tmpStr+str(ABDskinIn[i,j])+', '


#transverse shear stiffness:
t1 = '*TRANSVERSE SHEAR STIFFNESS\n'
SGSskinIn.append(t1)
tmpStr = ''
count = 0
for index in TSskinIn:
    count+=1
    if (count < len(TSskinIn)):
  tmpStr=tmpStr+str(index)+', '
    else:
  tmpStr=tmpStr+str(index)+' \n'
SGSskinIn.append(tmpStr)
SGSskinOut =[]

commentLine='**Section: General Shell (ABD) passed to be created by UGENS\n'
```

```
SGSskinOut.append(commentLine)
s1 = '*Shell General Section, '
s2 = 'elset='+elementSetSkinOut+', '
s3 = 'user, '
s4 = 'variables='+str(nstatev)+', '
s5 = 'properties='+str(nProps2Write)+', '
s6 = 'orientation='+orientationSkinOut+', '
s7 = 'controls=EC-1'+'\n'
SGSskinOut.append(s1+s2+s3+s4+s5+s6+s7) #LINE1: header
SGSskinOut.append(str(hSkinOut)+' \n')
#LINE(3 : 7) : ABD values

tmpStr = ''
count = -1
for i in range(0,6):
    for j in range(0,6):
  count+=1
  if (count == 8) or ((i ==5) and (j==5)):
      if ((i==5) and (j==5)):
    tmpStr=tmpStr+str(ABDskinOut[i,j])+' '
    tmpStr=tmpStr+'\n'
    SGSskinOut.append(tmpStr)
      else:
    count=0
    tmpStr=tmpStr+'\n'
    SGSskinOut.append(tmpStr)
    tmpStr=''
  if (count==7):
      tmpStr=tmpStr+str(ABDskinOut[i,j])+' '
  else:
      tmpStr=tmpStr+str(ABDskinOut[i,j])+', '

#transverse shear stiffness:
t1 = '*TRANSVERSE SHEAR STIFFNESS\n'
SGSskinOut.append(t1)
tmpStr = ''
count = 0
for index in TSskinOut:
    count+=1
    if (count < len(TSskinOut)):
  tmpStr=tmpStr+str(index)+', '
    else:
  tmpStr=tmpStr+str(index)+' \n'
SGSskinOut.append(tmpStr)

# ------------------------------------------------------------#
# Write values in ori. input file (created by createSandwich2.py)
# ------------------------------------------------------------#
#first copy the input file and search for the correct lines
f = open(inputFile,'r')
lines = f.readlines()
```

```
f.close()
flag = False
stopFor = False
count=-1


for line in lines:
    count+=1
    if line[0:32] == '** Section: CompositeLayup-Out-1':
  nLineTop = count
  flag = True
    if (flag):
  if (line[0:13] == '*Orientation,'):
      nLineBot = count+1
      stopFor = True
    if (stopFor):
  break

# writing part
nLinesInpOld  = len(lines)
nLinesNewData = len(SGSskinOut)
nLinesRemove  = nLineBot-nLineTop
nLinesInpNew  = nLinesInpOld + nLinesNewData - nLinesRemove
f = open(newInputFile,'w')
count = -1
subCount =-1
flag=False
for i in range(0,nLinesInpNew):
    if (count<nLineTop-1):
  count+=1
  f.write('%s'%(lines[count]))
    if (count>=nLineTop-1) and (count<nLineTop+nLinesNewData) and (subCount<
        nLinesNewData-1):
  subCount+=1
  print '>>subcount = '+str(subCount)
  f.write('%s'%(SGSskinOut[subCount]))
    if (subCount==nLinesNewData-1):
  count+=nLinesRemove
  break
for i in range(count,nLinesInpOld):
    f.write('%s'%lines[i])
f.close()

#first copy the input file and search for the correct lines
f = open(newInputFile,'r')
lines = f.readlines()
f.close()
flag = False
stopFor = False
count=-1
```

```
for line in lines:
    count+=1
    if line[0:31] == '** Section: CompositeLayup-In-1':
  nLineTop = count
  flag = True
    if (flag):
  if (line[0:9] == '*End Part'):
      nLineBot = count+1
      stopFor = True
    if (stopFor):
  break

# writing part
nLinesInpOld  = len(lines)
nLinesNewData = len(SGSskinIn)
nLinesRemove  = nLineBot-nLineTop
nLinesInpNew  = nLinesInpOld + nLinesNewData - nLinesRemove
f = open(newInputFile,'w')
count = -1
subCount =-1
flag=False
for i in range(0,nLinesInpNew):
    if (count<nLineTop-1):
  count+=1
  f.write('%s'%(lines[count]))
    if (count>=nLineTop-1) and (count<nLineTop+nLinesNewData) and (subCount<
        nLinesNewData-1):
  subCount+=1
  print '>>subcount = '+str(subCount)
  f.write('%s'%(SGSskinIn[subCount]))
    if (subCount==nLinesNewData-1):
  count+=nLinesRemove
  break
for i in range(count,nLinesInpOld):
    f.write('%s'%lines[i])
f.close()
print 'done with input file modification'
```

scripts/inputFileModify_sandwich.py

```
      subroutine UGENS(ddndde,force,statev,sse,spd,pnewdt,stran,dstran,
     1 tss,time,dtime,temp,dtemp,predef,dpred,cename,ndi,nshr,nsecv,
     2 nstatv,props,jprops,nprops,njprop,coords,celent,thick,dfgrd,curv,
     3 basis,noel,npt,kstep,kinc,kit,linper)
c
      include 'aba_param.inc'
c
      character*80 cename
      DIMENSION ddndde(nsecv,nsecv),force(nsecv),statev(nstatv),
     1 stran(nsecv),dstran(nsecv),tss(2),time(2),predef(*),
     2 dpred(*),props(*),jprops(*),coords(3),dfgrd(3,3),
```

```
12      3 curv(2,2),basis(3,3)
        real*8 ABD(6,6)
14      integer counter
        parameter (zero=0.0d0, half=0.5d0, one=1.0d0)
16      !-----------------------------------------------------!
        ! DESCRIPTION                                         !
18      !-----------------------------------------------------!
        ! This is a FORTRAN file that describes the sectional
20      ! material behavior of a material, given a ABD matrix
        ! Copyright - Stanley I. Wong - 2012
22      !-----------------------------------------------------!
        ! PROPS                                               !
24      !-----------------------------------------------------!
        !
26      ! ABD(1,1)          = props(1)  - Stiffness matrix index
        ! ABD(1,2)          = props(2)  - ...
28      ! ...               = props(..) - ...
        ! ABD(2,1)          = props(7)  - ...
30      ! ...               = props(..) - ...
        ! ABD(6,6)          = props(36) - ...
32      !-----------------------------------------------------!
        ! STATE VARIABLES                                     !
34      !-----------------------------------------------------!
        !
36      ! force-i per unit length    = statev(i=1..3)
        ! moment-j per unit length   = statev(3+j=1..3)
38      !-----------------------------------------------------!
        ! Define variables
40      !-----------------------------------------------------!
        counter=0
42      do i = 1,6
          do j = 1,6
44            counter = counter+1
              ABD(i,j) = props(counter)
46        end do
        end do
48
        !-----------------------------------------------------!
50      !DEFINE DDNDDE
        !-----------------------------------------------------!
52      if (nsecv.eq.4) then
          write(*,*) 'ERROR: nsecv == 4'
54        call XIT
        else if (nsecv.eq.6) then
56        ddndde = ABD
        end if
58
        !-----------------------------------------------------!
60      !UPDATE FORCES AND MOMENTS
        !-----------------------------------------------------!
62      if(linper.eq.0)then
```

```
       do i=1,nsecv
64      do j=1,nsecv
          force(i) = force(i) + ddndde(i,j)*dstran(j)
66      end do
       end do
68    else
       do i=1,nsecv
70      do j=1,nsecv
          force(i) = ddndde(i,j)*stran(j)
72      end do
       end do
74    endif

76    !------------------------------------------------------------!
      !DEFINE STATE VARIABLES
78    !------------------------------------------------------------!
      do i=1,nsecv
80      statev(i) = force(i)
      end do
82    RETURN
      END
```

scripts/ugens.f

```
#Read the output of the evaluated sandwich cylinder calculation
2 #Write stresses and Tsai-Wu failure criteria to csv files
#Note: written in Python, for ABAQUS
4 #Copyright - Stanley I. Wong - 2012
from Numeric import *
6 from odbAccess import *
jobName='myInputFile_python_sandwich'
8 myPart='PART-1'
myStep='Step-1'
10 myBuckleStep='Step-2'
myInstance=myPart+'-1'
12 fileName = 'buckle.dat'
corePropsFile ='props_core.dat'
14
#read core props that are used in matlab
16 f = open(corePropsFile,'r')
lines = f.readlines()
18 f.close()
nprops = len(lines[0].split())
20 props = zeros((nprops),'d')
row = lines[0].split()
22 i = -1
for index in row:
24     i+=1
    props[i] = float(index)
26 if nprops == 18:
    Q23 = props[nprops-1]
```

```
    Q13 = props[nprops-2]
    Q12 = props[nprops-3]
    ZC  = props[nprops-4]
    ZT  = props[nprops-5]
    YC  = props[nprops-6]
    YT  = props[nprops-7]
    XC  = props[nprops-8]
    XT  = props[nprops-9]
    threeD = 1
else:
    Q = props[nprops-1]
    YC = props[nprops-2]
    YT = props[nprops-3]
    XC = props[nprops-4]
    XT = props[nprops-5]
    threeD = 0
#for the Tsai-Wu criterion:
if threeD == 0:
    F11 = 1./(XT*XC)
    F22 = 1./(YT*YC)
    F33 = 1./(ZT*ZC)
    F1  = 1./XT - 1./XC
    F2  = 1./YT - 1./YC
    F12 = -1./(2.*sqrt(XC*XT*YC*YT))
    F66 = 1./(Q**2)
if threeD == 1:
    F11 = 1./(XT*XC)
    F22 = 1./(YT*YC)
    F33 = 1./(ZT*ZC)
    F1  = 1./XT - 1./XC
    F2  = 1./YT - 1./YC
    F3  = 1./ZT - 1./ZC
    F12 = -1./(2.*sqrt(XT*XC*YT*YC))
    F13 = -1./(2.*sqrt(XT*XC*ZT*ZC))
    F23 = -1./(2.*sqrt(YT*YC*ZT*ZC))
    F44 = 1./(Q12**2)
    F55 = 1./(Q13**2)
    F66 = 1./(Q23**2)

#partial set names:
elSetNameSkinIn  = 'SET-SKIN-IN-MID'
elSetNameSkinOut  = 'SET-SKIN-OUT-MID'
elSetNameCore   = 'SET-CORE-MID'

#output files
fileNameSkinOut ='outputSkinOut.csv'
fileNameSkinIn  ='outputSkinIn.csv'
fileNameCore    ='outputCore.csv'

#open the database
odb = session.openOdb(name=jobName+'.odb')
```

```
# READ BUCKLING PRESSURE
bucklingPressure = float(odb.steps[myBuckleStep].frames[1].description.split()
    [-1])
file = open(fileName,'w')
file.write('%21.14e' %(bucklingPressure))
file.close()
print 'Buckling pressure is written to file'


#READ SECTION STRAINS (see abaqus documentation 26.6.7)
#first get subsets
setSkinIn  =  odb.rootAssembly.instances['PART-1-1'].elementSets[elSetNameSkinIn]
setSkinOut =  odb.rootAssembly.instances['PART-1-1'].elementSets[elSetNameSkinOut
    ]
setCore    =  odb.rootAssembly.instances['PART-1-1'].elementSets[elSetNameCore]

fileSkinIn  = open(fileNameSkinIn,'w')
fileSkinOut = open(fileNameSkinOut,'w')
fileCore    = open(fileNameCore,'w')

datSEskinIn  = odb.steps[myStep].frames[-1].fieldOutputs['SE'].getSubset(region=
    setSkinIn).values
datSKskinIn  = odb.steps[myStep].frames[-1].fieldOutputs['SK'].getSubset(region=
    setSkinIn).values
datSFskinIn  = odb.steps[myStep].frames[-1].fieldOutputs['SF'].getSubset(region=
    setSkinIn).values
datSEskinOut = odb.steps[myStep].frames[-1].fieldOutputs['SE'].getSubset(region=
    setSkinOut).values
datSKskinOut = odb.steps[myStep].frames[-1].fieldOutputs['SK'].getSubset(region=
    setSkinOut).values
datSFskinOut = odb.steps[myStep].frames[-1].fieldOutputs['SF'].getSubset(region=
    setSkinOut).values
datScore     = odb.steps[myStep].frames[-1].fieldOutputs['S'].getSubset(region=
    setCore).values

if (len(datScore)/5 <> len(datSKskinOut)) or (len(datSEskinIn) <> len(
    datSEskinOut)):
    zz = 1/0 #cause an error!
for i in range(0,len(datSEskinIn)):
    datE=datSEskinIn[i]
    datK=datSKskinIn[i]
    datF=datSFskinIn[i]
    SE1=datE.data[0] # Direct membrane strain in local 1-direction.
    SE2=datE.data[1] # Direct membrane strain in local 2-direction.
    SE6=datE.data[2] # Strain in the thickness direction.
    SE3=datE.data[3] # Shear membrane strain in local 1-2 plane.
    SE4=datE.data[4] # Transverse shear strain in the local 1-direction.
    SE5=datE.data[5] # Transverse shear strain in the local 2-direction.
    SK2=datK.data[0] # Curvature change about local 1-axis.
    SK1=datK.data[1] # Curvature change about local 2-axis.
```

```
    SK3=datK.data[2] # Surface twist in local 1-2 plane.
    SF1=datF.data[0] # Membrane force in local 1-direction
    SF2=datF.data[1] # Membrane force in local 2-direction
    SF6=datF.data[2] # Membrane shear force in 1-2 plane
    elLbl=datE.elementLabel
    fileSkinIn.write('%21.14e,%21.14e,%21.14e,%21.14e,%21.14e,%21.14e,%21.14e
        ,%21.14e,%21.14e,%21.14e,%21.14e,%21.14e,%21.14e,\n' %(float(elLbl),SE1,
        SE2,SE6,SE3,SE4,SE5,SK2,SK1,SK3,SF1,SF2,SF6))

    datE=datSEskinOut[i]
    datK=datSKskinOut[i]
    datF=datSFskinOut[i]
    SE1=datE.data[0] # Direct membrane strain in local 1-direction.
    SE2=datE.data[1] # Direct membrane strain in local 2-direction.
    SE6=datE.data[2] # Strain in the thickness direction.
    SE3=datE.data[3] # Shear membrane strain in local 1-2 plane.
    SE4=datE.data[4] # Transverse shear strain in the local 1-direction.
    SE5=datE.data[5] # Transverse shear strain in the local 2-direction.
    SK2=datK.data[0] # Curvature change about local 1-axis.
    SK1=datK.data[1] # Curvature change about local 2-axis.
    SK3=datK.data[2] # Surface twist in local 1-2 plane.
    SF1=datF.data[0] # Membrane force in local 1-direction
    SF2=datF.data[1] # Membrane force in local 2-direction
    SF6=datF.data[2] # Membrane shear force in 1-2 plane
    elLbl=datE.elementLabel
    fileSkinOut.write('%21.14e,%21.14e,%21.14e,%21.14e,%21.14e,%21.14e,%21.14e
        ,%21.14e,%21.14e,%21.14e,%21.14e,%21.14e,%21.14e,\n' %(float(elLbl),SE1,
        SE2,SE6,SE3,SE4,SE5,SK2,SK1,SK3,SF1,SF2,SF6))

fileSkinIn.close()
fileSkinOut.close()
if threeD:
    for i in range(0,len(datScore)):
  datS=datScore[i]
  des = datS.sectionPoint.description
  if des[0]<>'S':
      des = ','+des
  S11=datS.data[0] # normal stress in 1 direction
  S22=datS.data[1] # normal stress in 2 direction
  S33=datS.data[2] # normal stress in 3 direction
  S12=datS.data[3] # shear stress in 12 plane
  S13=datS.data[4] # shear stress in 13 plane
  S23=datS.data[5] # shear stress in 23 plane
  tsaiWu3D = F11*S11**2 +F22*S22**2 +F33*S33**2 +\
    F44*S12**2+F55*S13**2+F66*S23**2+\
    F1*S11 + F2*S22 + F3*S33+\
    2.*F12*S11*S22+ 2.*F13*S11*S33+ 2.*F23*S22*S33
  elLbl=datS.elementLabel
  fileCore.write('%s,%21.14e,%21.14e,%21.14e,%21.14e,%21.14e,%21.14e,%21.14e
      ,%21.14e\n' %(des,float(elLbl),S11,S22,S33,S12,S13,S23,tsaiWu3D))
    fileCore.close()
```

```
166 else:
        for i in range(0,len(datScore)):
168   datS=datScore[i]
      des = datS.sectionPoint.description
170   if des[0]<>'S':
          des = ','+des
172   S11=datS.data[0] # normal stress in 1 direction
      S22=datS.data[1] # normal stress in 2 direction
174   S12=datS.data[3] # shear stress in 12 plane
      elLbl=datS.elementLabel
176   tsaiWu = F11*S11**2 +F22*S22**2 +F66*S12**2+F1*S11 + F2*S22 +2.*F12*S11*S22
      fileCore.write('%s,%21.14e,%21.14e,%21.14e,%21.14e,%21.14e,\n' %(des,float(
          elLbl),S11,S22,S12,tsaiWu))
178     fileCore.close()
    odb.close()
180 print "Three Dimensions = "+str(threeD)
```

scripts/readOutput_sandwich3.py

```
1  function data = createABDfromLP_sandwich(xi0,props,data)
   %Create the (translated) ABD matrix for the sandwich model
3  %Note: written in Matlab
   %Copyright - Stanley I. Wong - 2012
5  factorPosDef = 1; %initiate factor
   stepSizeFactor = 1e-5;
7  h    = data.hSkin;
   %-refers to top, + bottom
9  if strcmp(data.refSkin,'top')
       transCoeff = -0.5*h;
11 elseif strcmp(data.refSkin,'bottom')
       transCoeff = 0.5*h;
13 end

15 % calculate material invariants
   E11  = props.E11;
17 E22  = props.E22;
   nu12 = props.nu12;
19 G12  = props.G12;

21 Q11 = E11^2/(E11-E22*nu12^2);
   Q22 = E11*E22/(E11-E22*nu12^2);
23 Q12 = nu12*Q22;
   Q66 = G12;
25
   U1=(3*Q11+3*Q22+2*Q12+4*Q66)/8;
27 U2=(Q11-Q22)/2;
   U3=(Q11+Q22-2*Q12-4*Q66)/8;
29 U4=(Q11+Q22+6*Q12-4*Q66)/8;
   U5=(Q11+Q22-2*Q12+4*Q66)/8;
31 U=[U1;U2;U3;U4;U5];
   data.U = U;
```

```
33
%set up translated ABD matrix
35 Axi = zeros(6,5);
Bxi = zeros(6,5);
37 Dxi = zeros(6,5);
converged = 0;
39 while not(converged) %do while not(ABD=positive definite)
    xi=factorPosDef*xi0;
41  Axi(1,1)=1; Axi(2,1)=1; Axi(3,4)=1; Axi(4,5)=1;
    Axi(1,2)=xi(1);
43  Axi(1,3)=xi(2);
    Axi(2,2)=-xi(1);
45  Axi(2,3)=xi(2);
    Axi(3,3)=-xi(2);
47  Axi(4,3)=-xi(2);
    Axi(5,2)=xi(3)/2;
49  Axi(5,3)=xi(4);
    Axi(6,2)=xi(3)/2;
51  Axi(6,3)=-xi(4);
    Avec=(data.hSkin)*Axi*data.U;
53  A = [Avec(1) Avec(3) Avec(5);...
        Avec(3) Avec(2) Avec(6);...
55      Avec(5) Avec(6) Avec(4)];

57  Bxi(1,2)=xi(5);
    Bxi(1,3)=xi(6);
59  Bxi(2,2)=-xi(5);
    Bxi(2,3)=xi(6);
61  Bxi(3,3)=-xi(6);
    Bxi(4,3)=-xi(6);
63  Bxi(5,2)=xi(7)/2;
    Bxi(5,3)=xi(8);
65  Bxi(6,2)=xi(7)/2;
    Bxi(6,3)=-xi(8);
67  Bvec=(data.hSkin^2)/4*Bxi*data.U;
    B = [Bvec(1) Bvec(3) Bvec(5);...
69      Bvec(3) Bvec(2) Bvec(6);...
        Bvec(5) Bvec(6) Bvec(4)];
71


73  Dxi(1,1)=1; Dxi(2,1)=1; Dxi(3,4)=1; Dxi(4,5)=1;
    Dxi(1,2)=xi(9);
75  Dxi(1,3)=xi(10);
    Dxi(2,2)=-xi(9);
77  Dxi(2,3)=xi(10);
    Dxi(3,3)=-xi(10);
79  Dxi(4,3)=-xi(10);
    Dxi(5,2)=xi(11)/2;
81  Dxi(5,3)=xi(12);
    Dxi(6,2)=xi(11)/2;
83  Dxi(6,3)=-xi(12);
```

```
    Dvec=(data.hSkin^3)/12*Dxi*data.U;
    D = [Dvec(1) Dvec(3) Dvec(5);...
        Dvec(3) Dvec(2) Dvec(6);...
        Dvec(5) Dvec(6) Dvec(4)];

    ABDnoError = [A B;B' D];
    if min(eig(ABDnoError)) > 0
        converged = 1; %matrix is positive definite
    else
        factorPosDef = factorPosDef-stepSizeFactor;
    end
end
ABD = ABDnoError;

ABD_trans = zeros(6);
ABD_trans(1:3,1:3) = ABD(1:3,1:3);
ABD_trans(1:3,4:6) = transCoeff*ABD(1:3,1:3)+ABD(1:3,4:6);
ABD_trans(4:6,1:3) = ABD_trans(1:3,4:6)';
ABD_trans(4:6,4:6) = transCoeff^2*ABD(1:3,1:3)+2*transCoeff*ABD(1:3,4:6)+ABD
    (4:6,4:6);

ABD = ABD_trans;

% FOR I/O the ABD is written to a file:
outputFormat2='%21.14e ';
file1 = fopen(data.fileABDNameSkin,'w'); %fileABDName is defined in the main file
for i=1:6
    for j=1:6
        fprintf(file1,outputFormat2,ABD(i,j));
    end
    fprintf(file1,'\n');
end
fclose(file1);

data.factorPosDefSkin=factorPosDef; %very important quantity
data.ABDSkin = ABD;
```

scripts/createABDfromLP_sandwich.m

```
function data = calcTransverseShearModuli_sandwich(data)
%Calculate the transverse shear moduli for the sandwich model
%Note: written in Matlab
%Copyright - Stanley I. Wong - 2012
TS = zeros(3,1);
D = data.ABDSkin;
%For a general shell with a given section stiffness,
%the transverse shear moduli are given by:
%TS(1)=TS(2)=(1/6*(D(1,1)+D(2,2))+1/3*D(3,3))*Y

%according to Abaqus documentation:
%(@ 26.6.4 Shell section behavior)
```

```
%the default value of Y is:
Y = 1;
TS(1) = (1/6*(D(1,1)+D(2,2))+1/3*D(3,3))*Y;
TS(2) = TS(1);

% FOR I/O these values are written to a file:
% outputFormat1='%32.16e ';
outputFormat2='%21.14e ';
file1 = fopen(data.fileTSNameSkin,'w');
fprintf(file1,outputFormat2,TS(1));
fprintf(file1,outputFormat2,TS(2));
fprintf(file1,outputFormat2,TS(3));
fclose(file1);
data.TS=TS;
```

scripts/calcTransverseShearModuli_sandwich.m

```
function ff = failureFunctionTsaiWuLP(Iv,u)
%Calculate the material failure constraint for a
%section that is defined by lamination parameters
%Note: written in Matlab
%Copyright - Stanley I. Wong - 201
%coefficients for the failure function:
a=[];
a(10)=u(4) ^ 2 + 4 * u(1) - 4 * u(6);
a(11)=-4 * u(2) * Iv(1) * (u(1) - u(6)) + 2 * u(4) * u(5) * Iv(1);
a(12)=4 * u(6) ^ 2 * Iv(2) ^ 2 - 4 * u(3) * Iv(1) ^ 2 * (u(1) - u(6)) - 4 * u(6)
    * u(1) * Iv(2) ^ 2 + u(5) ^ 2 * Iv(1) ^ 2;
a(20)=1;
a(21)=-2 * u(2) * Iv(1);
a(22)=-2 * u(3) * Iv(1) ^ 2 + u(2) ^ 2 * Iv(1) ^ 2 - Iv(2) ^ 2 * (u(4) ^ 2 + 2 *
    u(1));
a(23)= 2 * u(2) * Iv(1) ^ 3 * u(3) - Iv(2) ^ 2 * (2 * u(4) * u(5) * Iv(1) - 2 * u
    (1) * u(2) * Iv(1));
a(24)=u(1) ^ 2 * Iv(2) ^ 4 - Iv(2) ^ 2 * (u(5) ^ 2 * Iv(1) ^ 2 - 2 * u(1) * u(3)
    * Iv(1) ^ 2) + u(3) ^ 2 * Iv(1) ^ 4;

EQ1=roots([a(12) a(11) a(10)]);
EQ2=roots([a(24) a(23) a(22) a(21) a(20)]);
realRootsEQ1=EQ1(find(imag(EQ1)==0));
realRootsEQ2=EQ2(find(imag(EQ2)==0));
answerTry1=min(realRootsEQ1(find(realRootsEQ1>0)));
answerTry2=min(realRootsEQ2(find(realRootsEQ2>0)));
lambda = min(answerTry1,answerTry2);

r = 1/(lambda^2);
ff = r-1; %If intact, this ff is smaller or equal to 0
```

scripts/failureFunctionTsaiWuLP.m

```
function [totalWeight,unitWeight] = calcMassSandwich(data,props)
```

```
%Calculate the mass of the cylinder
%Note: written in Matlab
%Copyright - Stanley I. Wong - 2012
hC = data.hCore;  %[mm]
hSi = data.hSkinIn; %[mm]
hSo = data.hSkinOut;  %[mm]
rhoS = props.rho;   %[kg/m^3]
rhoC = props.core.rho;  %[kg/m^3]

L = data.L;     %[mm]
R = data.r_out;   %[mm]

%mid-planes for the three different layers
rMidOut  = R-0.5*hSo;
rMidCore = R-hSo-0.5*hC;
rMidIn   = R-hSo-hC-0.5*hSi;

%perimeters:
pOut = 2*pi*rMidOut;
pCore = 2*pi*rMidCore;
pIn = 2*pi*rMidIn;

factor = 1/(1000^3); % [m^3 to mm]

%unitWeights:
unitWeightOut = pOut*factor*hSo*rhoS;
unitWeightCore = pCore*factor*hC*rhoC;
unitWeightIn = pIn*factor*hSi*rhoS;

unitWeight  = unitWeightOut+unitWeightCore+unitWeightIn; % weight per unit length
     [kg/mm]
totalWeight = unitWeight*L; % total weight [kg]
```

scripts/calcMassSandwich.m